

**EDUCATION IS NOT ONLY THE LEARNING OF FACTS,
IT'S RATHER
THE TRAINING OF THE MIND TO THINK.**

- Albert Einstein



Vienna University of Technology
Technische Universität Wien



DIPLOMA THESIS

Click Chemistry mediated Cell Uptake – towards triggered Auger Therapy

conducted at the
Institute of Applied Synthetic Chemistry | E163
Technical Chemistry (066 490)

under supervision of
Projectass. Dipl.-Ing. Dr.techn. Christoph **Denk**,

under Co-supervision of
Univ. Prof. Dr.med. Thomas L. **Mindt**,
(Ludwig Boltzmann Institute Applied Diagnostics | General Hospital, Vienna)

under the group management of
Univ.Ass. Dipl.-Ing. Dr.techn. Hannes **Mikula**

and headed by
Univ. Prof. Dipl.-Ing. Dr.techn. Johannes **Fröhlich**

by
Josef **Balla**, BSc



Vienna, 04.06.2019

autograph signature

Ich erkläre hiermit eidesstattlich, dass ich die Arbeit selbständig angefertigt, keine anderen als die angegebenen Hilfsmittel benutzt und alle aus ungedruckten Quellen, gedruckter Literatur oder aus dem Internet im Wortlaut oder im wesentlichen Inhalt übernommenen Formulierungen und Konzepte gemäß den Richtlinien wissenschaftlicher Arbeiten zitiert und durch Fußnoten gekennzeichnet bzw. mit genauer Quellenangabe kenntlich gemacht habe. Diese schriftliche Arbeit wurde noch an keiner Stelle vorgelegt.

Ort, Datum

Unterschrift (Verfasser)

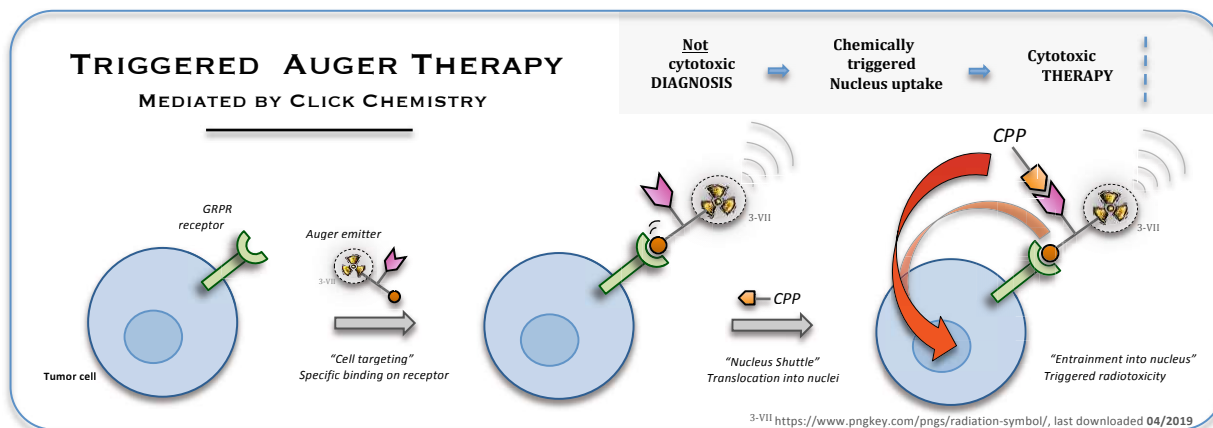
ABSTRACT

Within nuclear medicine various diseases are diagnosed or even treated by administering radiopharmaceuticals. Commonly used radioisotopes are alpha-, beta- as well as gamma-emitters. Whereas traditional radiotherapy is relying on external beam radiation, the radioactivity in the course of nuclear medicine applications is administered to the patient.

In terms of treating oncologic diseases, diagnostic radionuclides offer the possibility to address and thus detect tumor cells in a very specific manner, since administered “radiotracers” circulate in the whole body. Therefore, also a small collection of cancer cells (micrometastasis), descending from original tumor and spreading to other parts of the body, is detectable.

In particular, Auger electron emitters as radiation source have emerged to possess appropriate characteristics regarding radiotoxicity at specific sites. Due to low range of Auger electrons in tissue, the emitters must be located at the nucleus for cytotoxic effects – This allows advanced targeting strategies that might reduce effects in off-target-tissues.

The range of their radiation is less than the size of a single cell, which is why radiotoxicity is not occurring until the radioactive species is transferred into the nucleus. So the engineering challenge is to have Auger emitter-based therapeutics ended up within the targeted cells, for gaining a high biological efficiency. Within this thesis, a Cell Uptake strategy has been considered to verify the accessibility of Auger emitting radioisotopes for both, diagnosis and therapy mode.

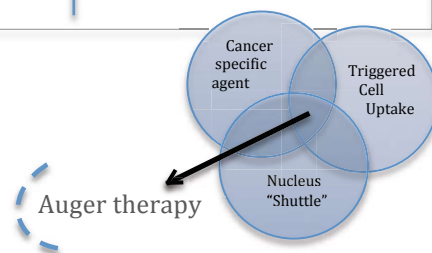


Cell targeting via specific, extracellular binding of a radiolabeled peptide on diseased cells is achieved by binding to a GRPR receptor. Diagnosis using SPECT (or other imaging modalities) is possible. Due to the extracellular location of the emitter no therapeutic effect is achieved. This would allow physician to monitor tumor-targeting of the radiolabeled agent. As the tumor targeting species is additionally modified with a bioorthogonal tag (“click tag”), bioorthogonal ligation with a cell penetrating peptide [CPP] shall lead to translocation into the cell nucleus of affected cells, thus turning the diagnostic agent into effective therapeutic.

Within this thesis, important steps towards **triggered Auger therapy** were taken by modification of peptides with appropriate “click tags” and fluorescent probes. The exceptionally fast bioorthogonal click chemistry reaction between 1,2,4,5-tetrazines and *trans*-cyclooctenes [TCOs] was chosen to mediate nucleus uptake by ligating TAT-peptide as nucleus shuttle to the pre-accumulated targeting agent.

The proof of concept has been evaluated in the course of *in vitro* assays. Fluorescent microscopy has provided the feasibility to visualize the just mentioned concept, with the aid of BODIPY fluorescent agent.

Auger/ γ -emitter extracellular	Auger/ γ -emitter within nucleus
<ul style="list-style-type: none"> • low radiation dose • low radiation induced damage • diagnostic application 	<ul style="list-style-type: none"> • high radiation induced damage • DNA strand breaks • therapeutic application



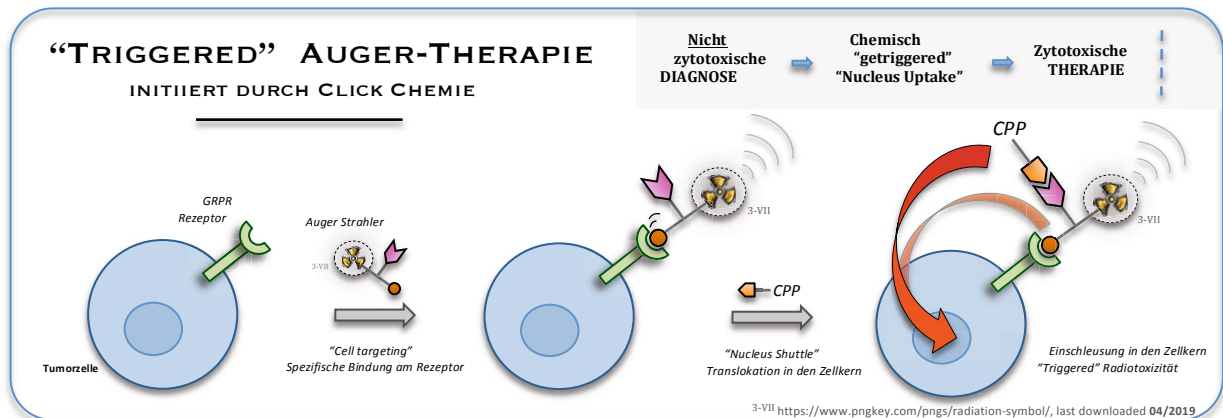
KURZFASSUNG

In der Nuklearmedizin werden mittels Verabreichung diverser Radiopharmazeutika unterschiedliche Krankheiten diagnostiziert beziehungsweise auch behandelt. Die üblicherweise eingesetzten Radioisotope sind demnach Alpha-, Beta- sowie Gamma-Strahler. Während die traditionelle Strahlentherapie (Radiotherapie) auf externer Strahlenanregung basiert, wird die Radioaktivität im Rahmen der nuklearmedizinischen Anwendungen dem Patienten verabreicht.

Im Falle von Behandlungen onkologischer Krankheiten eröffnen diagnostische Radionuklide die Möglichkeit, Tumorzellen anzupeilen und somit zu detektieren. Dies geschieht auf sehr spezifische Art und Weise, nachdem die verabreichten "Radiotracer" im gesamten menschlichen Körper zirkulieren. Daher ist eine kleine Ansammlung von Krebszellen (Mikrometastase), die vom ursprünglichen Tumor abstammt und sich in andere Körperregionen ausbreitet, detektierbar.

Im Speziellen sind Auger-Elektronen Strahler als Strahlungsquelle aufgekommen, die geeignete Charakteristika bezüglich spezifischer Radiotoxizität aufweisen. Aufgrund der geringen Reichweite von Auger Elektronen im Gewebe, müssen die Radionuklide jedoch in den Zellkern eingeschleust werden, um letztlich zytotoxische Effekte zu erreichen – Dies erlaubt weiterentwickelte "tumor targeting" Strategien, welche die Effekte an "Off-target"-Gewebszellen reduzieren sollen.

Die Reichweite der Strahlung ist geringer als die Größe einer einzelnen Zelle, weshalb die Radiotoxizität erst dann vorliegt, sobald die radioaktive Spezies in den Zellkern vordringt. Somit besteht die technische Herausforderung darin, die Augerstrahlungsbasierten Therapeutika in die "targeted"-Zellen einzuschleusen, um eine hohe biologische Aktivität zu erzielen. Im Rahmen dieser Arbeit wurde eine „Cell Uptake“-Strategie angestrebt, um die Zugänglichkeit der Auger emittierenden Radioisotope für sowohl diagnostische Zwecke als auch für therapeutische Anwendungen zu beurteilen.

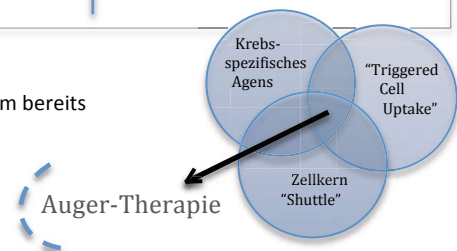


Das "targeting" krankhafter Zellen durch spezifische, extrazelluläre Bindung eines radiomarkierten Peptids wird mittels Bindung an einem GRPR Tumorrezeptor erreicht. Bildgebungsverfahren wie beispielsweise SPECT ermöglichen anschließend eine Diagnose. Aufgrund des extrazellulär gelegenen Strahlers wird kein therapeutischer Effekt erreicht. Dies würde Medizinerinnen zunächst erlauben, radiomarkierte "tumor targeting" Verbindungen nachzuverfolgen. Nachdem die "tumor targeting" Spezies zusätzlich mit einem bioorthogonalen "tag" ("Click tag") modifiziert ist, soll eine bioorthogonale Ligation mit einem zellpenetrierenden Peptid [CPP] zur Translokation in den Zellkern der betroffenen Krebszellen führen, und somit das diagnostische Agens in ein effektives Therapeutikum umwandeln.

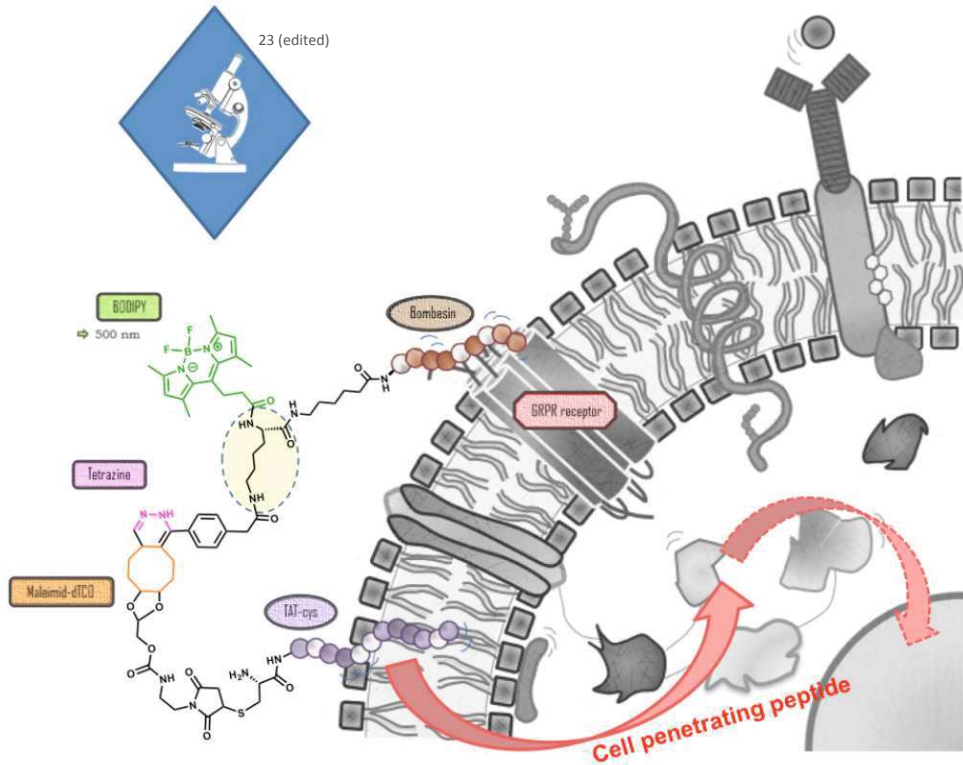
Während dieser Arbeit wurden wichtige Schritte zur **"triggered" Auger-Therapie** gemacht, indem Peptide mit entsprechenden "Click tags" und Fluoreszenzkomponenten modifiziert wurden. Die außergewöhnlich schnelle bioorthogonale Click-Chemie Reaktion zwischen 1,2,4,5-Tetrazinen und *trans*-Cyclooctenen [TCOs] wurde gewählt, um den "Nucleus Uptake" durch Ligation des TAT Peptids als "Nucleus Shuttle" mit dem bereits akkumulierten, "targeting" Peptid zu initiieren.

Der "Proof of Concept" wurde im Zuge der *in vitro* Untersuchungen evaluiert. Dabei wurde das Konzept am Fluoreszenzmikroskop mit Hilfe von BODIPY als Fluoreszenzfarbstoff visualisiert.

Auger/ γ -Strahler extrazellulär	Auger/ γ -Strahler im Zellkern
<ul style="list-style-type: none"> • geringe Strahlendosis • geringe Schäden durch Strahlung • diagnostische Anwendung 	<ul style="list-style-type: none"> • hohe Schäden durch Strahlung • DNA-Strang Zerstörung • therapeutische Anwendung



THESIS ILLUSTRATION



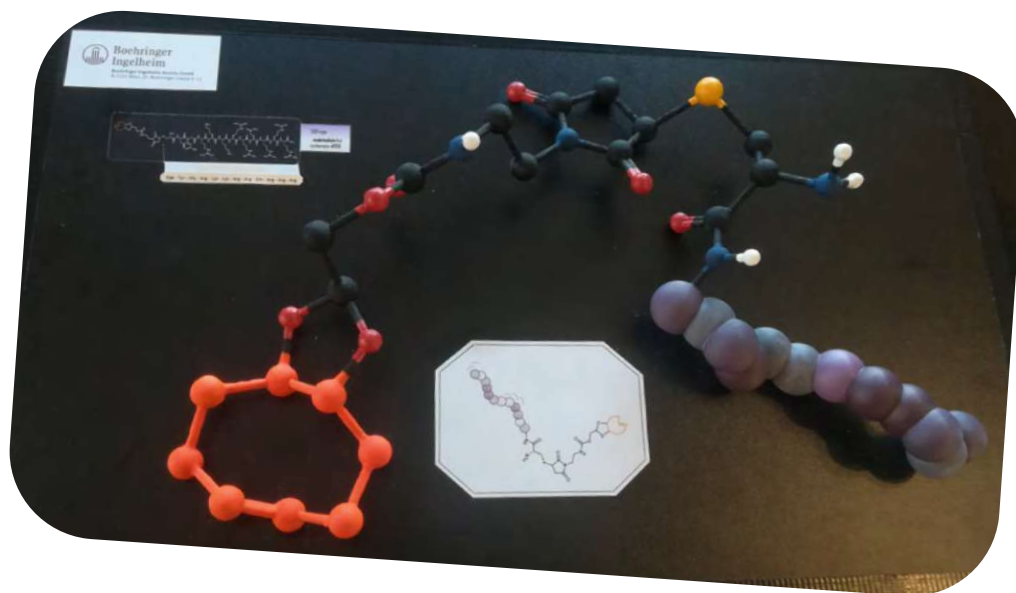
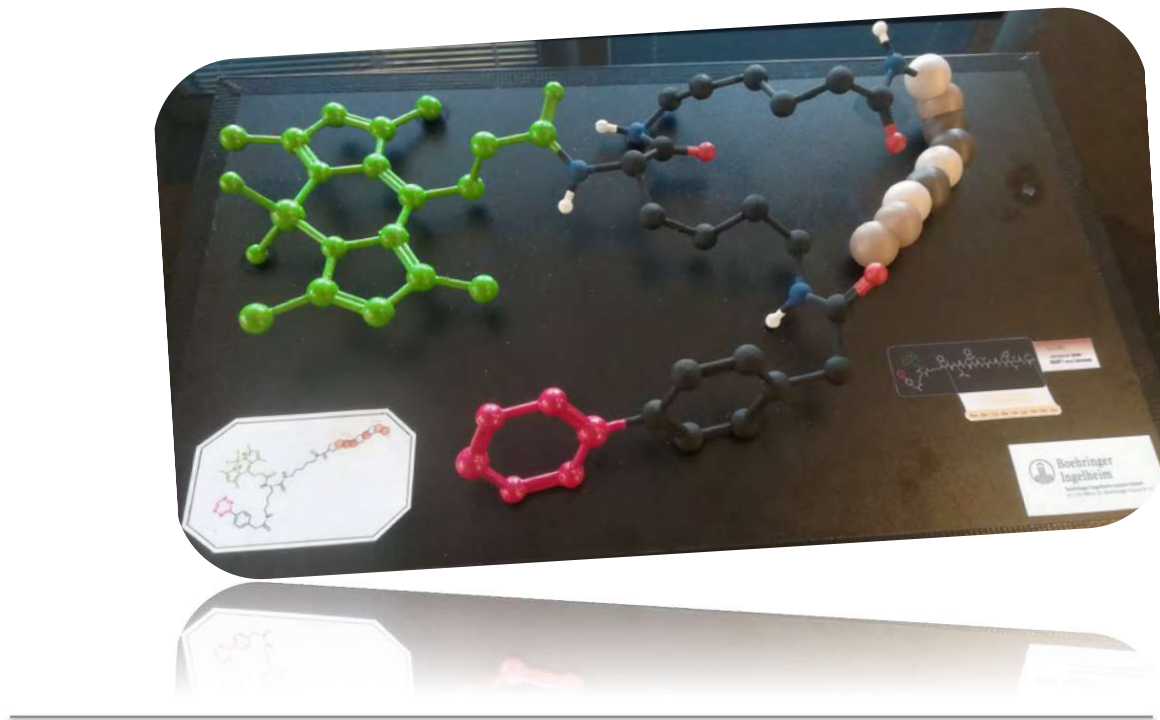
²³ <https://www.kisspng.com/png-optical-microscope-clip-art-black-and-white-art-de-191880/>, last downloaded 05/2019



Ludwig Boltzmann Institute
Applied Diagnostics

...based on idea of **Prof. Mindt, Thomas**

| Ludwig Boltzmann Institute, Vienna



■ Kornigg, Stefan & Peinsipp, Christoph | 3D-print engineers

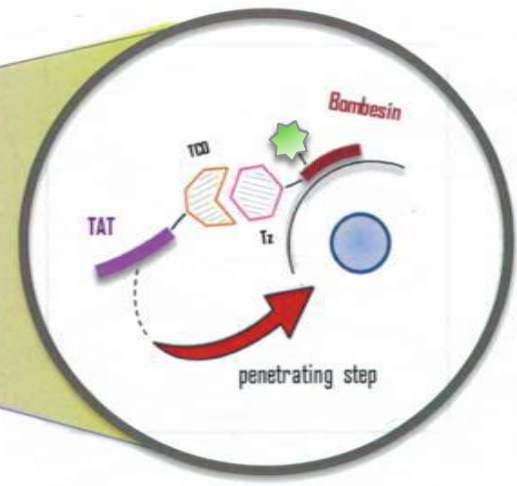
■ Peric-Simov, Biljana | Design

■ Fuchs, Julian | Modelling



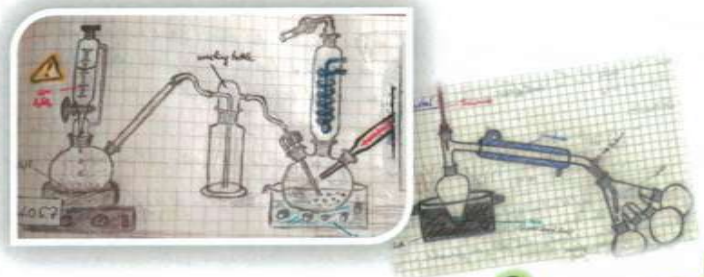


CLICK CHEMISTRY MEDIATED CELL UPTAKE



...TOWARDS TRIGGERED AUGER THERAPY





Chemical COMICS

made by

Josef Balla, TU Vienna

E163 | Institute of Applied Synthetic Chemistry



Starting here with...



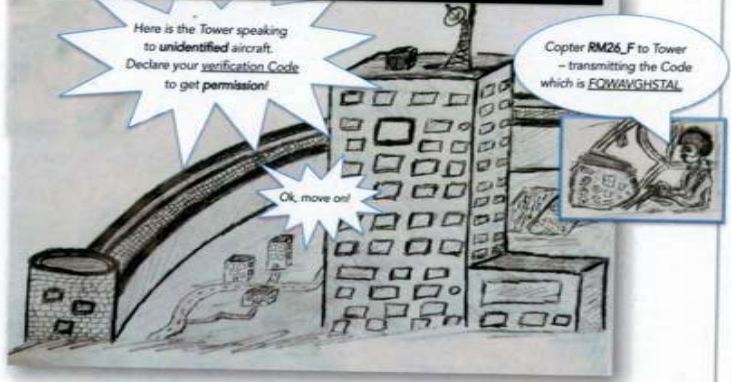
Mission C-104(18,19)/T1 - eliminate the tumor!



Hacking program named Bombesin - online.
/[Module No SG25-148E_LMH02JB/A]

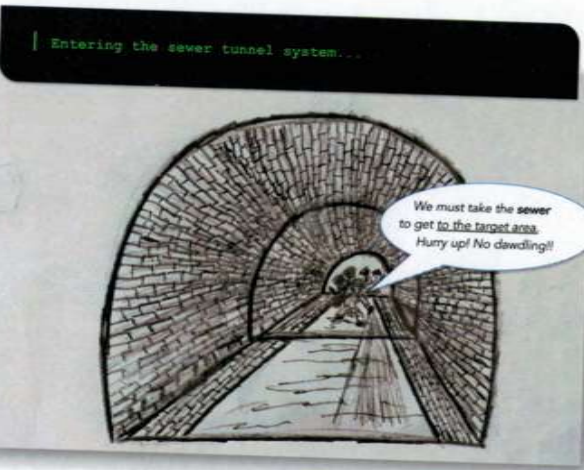


Code announcement - access granted!



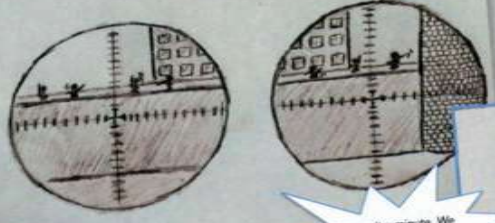
Auger Electron Special Unit (AESU-T1) on board...





We must take the sewer to get to the target area. Hurry up! No dawdling!!

No getting ahead through the wall /cell membrane...



Just wait a minute. We arranged some friends from older days!



Sir, it's too secure. We can't go ahead!

Auscultating with stethoscope - applied successfully!



Ok, now... so - R...mmhm... now - R...again - R...Q...R...K...K...R...G...Y...C. Give it a 10!

CRACK

Arrival of partners (TAT team) from older days - linked together





The END

Additional Information/Explanation...



The Helicopter as well as the military Truck, each stands for a **syringe** which is used for **administering** the tumor targeting bio-chemical compounds.

With the aid of the hacking program named Bombesin that is in place of - as the name implies - a **peptide bombesin** analoga, the **attaching** on the target, a hostile city, is successful - so having the scene depicting a **tumor cell** with it's cell membrane and the extracellular docking [by means of announcing the Code which is the **amino acid sequence**]. At this point there is no getting through the previously mentioned **cell mebrane** which is represented by a great wall in the comic story.

The Bombesin/Auger electron special unit (AESU) and the TAT team are friends from older days which makes them able to **get combined** again via communication [reaction of Tetrazine & TCO] very easily and fast. This kind of linkage and it's properties can be directly referred to **Click Chemistry** reactions that are furthermore **bioorthogonal** (*no disturbing of any metabolic processes in living system*).

Gaining the support of the TAT team, both end up within the hostile city [tumor] by overpowering the wall [cell membrane] in reaching the sewer tunnel first and subsequent entering the Code (amino acid sequence) at the steel-reinforced door for getting in, standing for the ability of doing a **cell penetrating step**.

As the Bombesin/Auger electron special unit (AESU) is now successfully **transferred** even into the core building (nucleus) with the help of friends from the TAT team that knows how to get in the hostile city [tumor cell], they can finally install C4-explosives wich are depicting the **Auger electrons** that are capable of **destroying** tumor cells by **high radioactivity** [explosion].

The Crystal represents the **heart**, the **vital energy**, of the tumor cell.

I

II

III

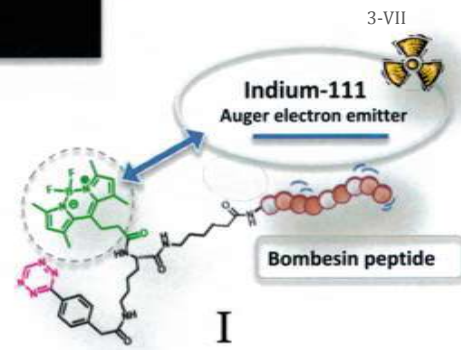
IV

Summed-up Parallels...

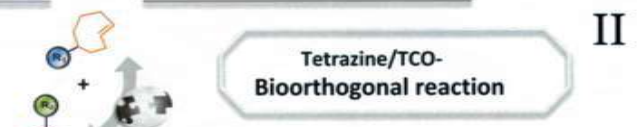
■ „Docking“ of peptide Bombesin specifically on bombesin **GRPR receptors** of tumor cells, extracellularly.

Therefore hacking program → **Bombesin**

↻ ensures transmission of Code. → Amino acid sequence

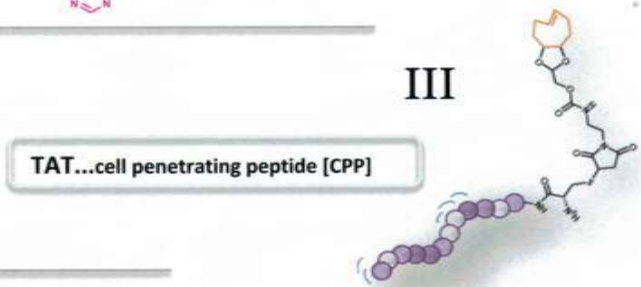


■ Arriving of TAT-Team to get linked together → **Click Chemistry reaction**



■ Entering the Code at steel-reinforced door → Amino acid sequence

↻ to get through the wall (cell membrane).



■ Installing of C4-explosives → **Auger electrons**

↻ in the core (cell nucleus) and target area (cell).





Die approbierte gedruckte Originalversion dieser Diplomarbeit ist an der TU Wien Bibliothek verfügbar
The approved original version of this thesis is available in print at TU Wien Bibliothek. | **ix**

ACKNOWLEDGEMENT

First of all, I want to thank the Head of Institute, Univ. Professor Johannes Fröhlich for the opportunity to conduct my diploma thesis at the Institute of Applied Synthetic Chemistry in the FGHF research group. I'm gonna move on to special thanks to my supervisor Project Assistant Christoph Denk, who supported me over the whole year during my work on such a versatile and at once fascinating topic, as well as to Univ. Assistant Hannes Mikula being the group manager.

A further big thank you goes to the great collaboration with the Ludwig Boltzmann Institute of Applied Diagnostics situated at the General Hospital in Vienna, mentioned by name, to Senior Scientist Jens Cardinale, together with Postdoctoral Fellow Marie Brandt, and to the Head of Imaging Biomarkers, Professor Thomas Mindt being the originator of this enthralling as well as promising strategy.

Moreover, I'm obligated to huge appreciation for Assistant Professor Christian Hametner, for doing particular NMR measurements and also giving great support in analysis. I am also in accurate awareness of the support from my colleagues, especially from my bench neighbour and PhD student Stefan Kronister, PhD student Thomas Kader and Diploma students Patrick Keppel together with Nik Poremba for introducing me to or helping me out a lot in the laboratories.

Concerning all my personal background, my whole family, involving my parents, my sisters and my brothers deserve my highest gratefulness. Thank you all for having such a great time together and learning from each other while growing up. I'm looking forward to the time to come, because I deeply have to say, you are royally backing me up. I will always keep the following saying in mind, which is "Don't forget where you come from, where your roots are, which is where you belong." I'm very proud being a part of you!

It has been one of the turning points in my life, when I have met you, my beloved Lisa. With these words I'm also saying thank you in the most loving kind I'm up to, for being on my side, properly for allowing me to be on your side, and spending hours together in debonair and at the same time insightful way. I really appreciate your response while taking me into timeless account. You definitely make my life joyful, which is why I'm beneficially expecting good times, spending with you, to come. At this point, I wanna thank my parents-in-law and brother-in-law as well for admitting me in their home with such naturalness.

Conclusively, a major, honourable gratitude to all my relatives, closer friends and soccer club players for the time we spent with each other we are having no regrets about.

ABBREVIATIONS

Alongside typical chemical element symbols and diverse SI units, the following abbreviations have been used, including many common ones.

Ar	argon
Boc	<i>tert</i> - <u>butoxycarbonyl</u> group, protecting group
BODIPY	<u>boron-dipyrromethene</u> , (4,4-difluoro-4-bora-3a,4a-diaza-s-indacene, propionic acid)
brine	sodium chloride [NaCl], saturated aqueous solution
CCO	<i>cis</i> -cyclooctene
CuAAC	<u>copper catalysed Alkine-Azide cycloaddition</u>
cys	cysteine
DA	Diels-Alder (reaction)
DCM	dichloromethane, CH ₂ Cl ₂
DIPEA	diisopropylethylamine, <i>i</i> -Pr ₂ NEt
DMF	<i>N,N</i> -dimethylformamide, (CH ₃) ₂ NCHO
DMSO	dimethyl sulfoxide, (CH ₃) ₂ SO
dTCO	<u>dioxolyl-trans-cyclooctene</u>
EDG	electron donating group
EE	ethyl acetate, CH ₃ COOEt
EtOAc	ethyl acetate, CH ₃ COOEt
EtOH	ethanol
Et ₂ O	diethyl ether
EWG	electron withdrawing group
FA	formic acid, CHOOH
HAc	acetic acid, CH ₃ COOH
HBTU	(2-(1H-Benzotriazol-1-yl)-1,1,3,3-tetramethyluronium-hexafluorophosphat), coupling agent
¹ H ₄ -cycle	3,11,17,18-tetraazatricyclo[11.3.1.15,9]octadeca-1(17),5,7,9(18),13,15-hexaene
HCl	hydrochloric acid / hydrogen chloride gas
HOMO	highest occupied molecular orbital
(HP)LC-MS	(high-pressure) liquid chromatography – mass spectrometer

H ₂ O	water, dest.
H ₂ SO ₄	sulphuric acid
IEDDA	inverse electron demand Diels-Alder (reaction)
K ₂ CO ₃	potassium carbonate, basic salt
LiAlH ₄	lithium aluminium hydride
LC	liquid chromatography
LUMO	lowest unoccupied molecular orbital
MeCN	acetonitrile, CH ₃ CN
MeOH	methanol
MgSO ₄	magnesium sulphate, drying agent
Ms	mesyl group, <u>meth</u> ylsulfonyl, leaving group
NaHCO ₃ , sat	sodium hydrogen carbonate, saturated aqueous solution
NaNO ₂	sodium nitrite, oxidising agent
NaOH	sodium hydroxide
NHS	<u>N</u> -hydroxysuccinimide[yl], (CH ₂ CO) ₂ NOH
NH ₄ Cl	ammonium chloride salt
NMR	nuclear magnetic resonance
NP	normal phase
PBS	phosphate buffer saline
PE	petroleum ether (n-hexane, n-pentane, ...)
PNP	<i>para</i> -nitrophenol
RP	reversed phase
rt	room temperature
SPAAC	<u>s</u> train promoted <u>A</u> lkyne- <u>A</u> zide <u>c</u> ycloaddition
TAT	<u>T</u> ransactivator of <u>T</u> ranscription [peptide]
TBAF	<u>t</u> etra <u>b</u> utylammonium <u>f</u> luoride, <i>n</i> -Bu ₄ NF
TCEP	<u>t</u> ris(2- <u>c</u> arboxy <u>e</u> thyl)phosphine, (EtCOOH) ₃ P
TCO	<i>trans</i> -cyclooctene
TEA	triethylamine, NEt ₃
TEG	tetraethylene glycol

TFA	trifluoroacetic acid
THF	tetrahydrofuran, (CH ₂) ₄ O
TLC	thin layer chromatography
TMS	trimethylsilyl group, protecting group
Ts	tosyl group, 4-toluenesulfonyl, leaving group
^{Ts} N ₄ -cycle	3,11-Bis-tosyl-3,11,17,18-tetraazatricyclo[11.3.1.15,9]octadeca-1(17),5,7,9(18),13,15-hexaene (“pyridinophane”)
TSTU	<i>N,N,N',N'</i> -Tetramethyl- <i>O</i> -(<i>N</i> -succinimidyl)uroniumtetrafluorborat, coupling agent
Tz	tetrazine

GENERAL EXPLANATORY NOTES

Literature References

The literature references are denoted as Arabic numerals in square brackets, whereas figure references as well as literature related to them are quoted in Arabic numerals without square brackets, accordingly. Figure references of thesis parts *Scheme* as well as *Materials & Methods* are correlated with Roman numerals.

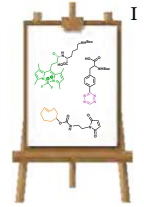
Substance Identification

All compounds that are already described and known by literature are numbered in bold Arabic numerals. On the contrary, the compounds that have been synthesized for the purposes of this work are signalled with bold Roman numerals. In addition, the substances that were not able to be formed or isolated as desired products (ref. to Scheme | failed reactions) are not numbered and thus are not shown in experimental part (**chapter 4**).

Nomenclature

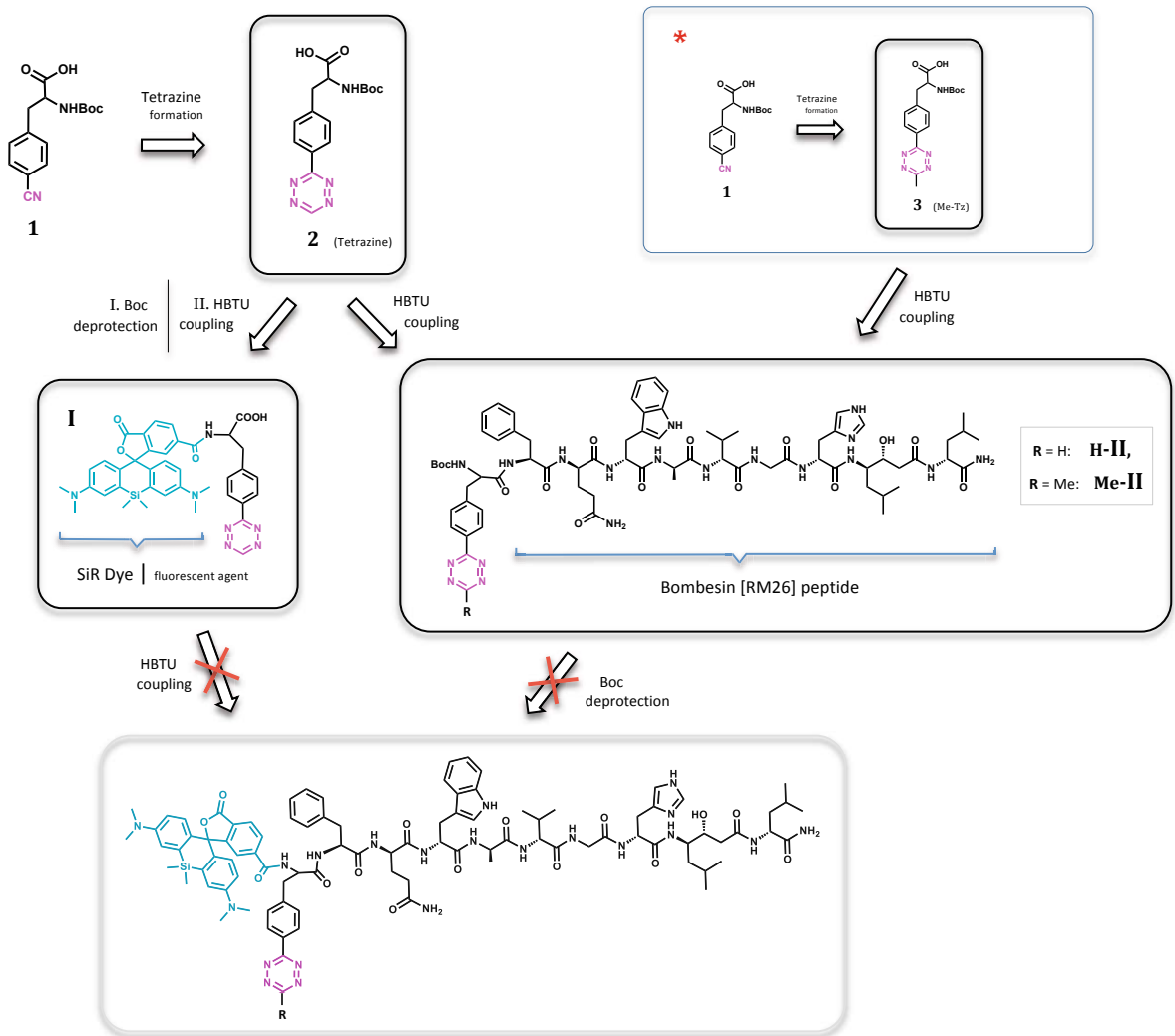
The nomenclature of chemical compounds that are not known by literature is referred to the rules of Chemical Abstracts, all searched at SciFinder platform. All other substances, reagents and solvents that are described in literature are written either in common, or trade or even simplified term names.

SCHEMES



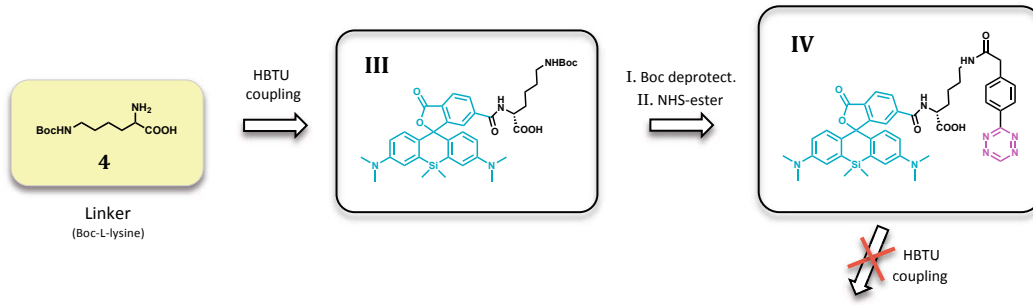
Modifying tumor targeting carrier molecules

I. STRATEGY

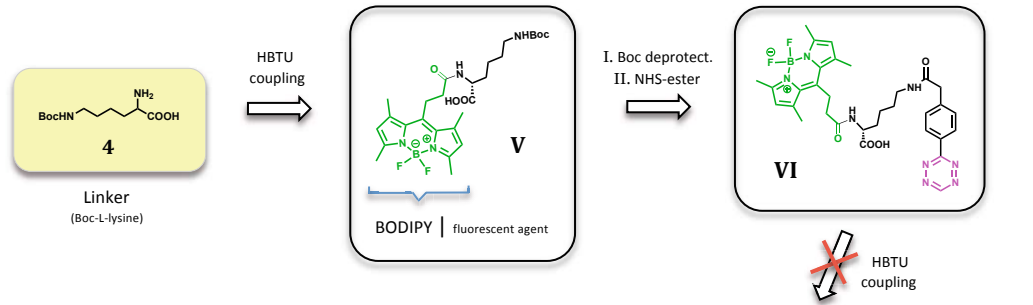


* The strategy concerning the initial formation of bombsin-tetrazine coupling product, described via the path on the right hand side, was additionally carried out for Me-Tetrazine derivative!

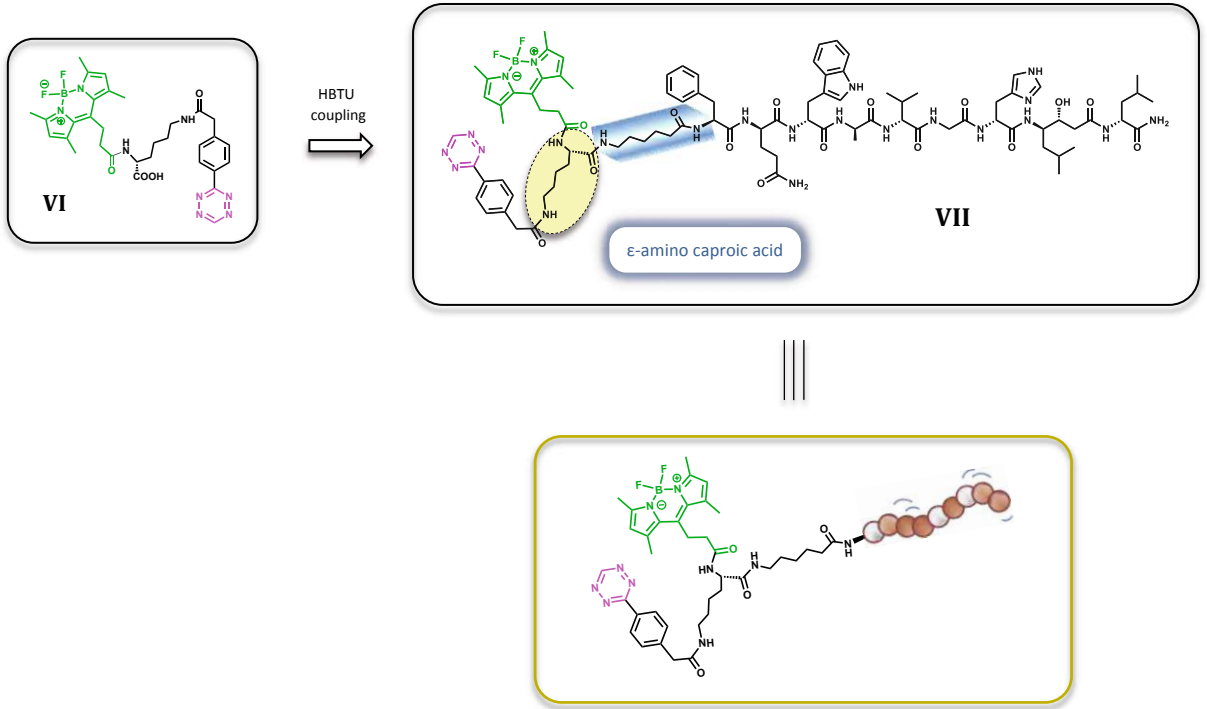
II. STRATEGY



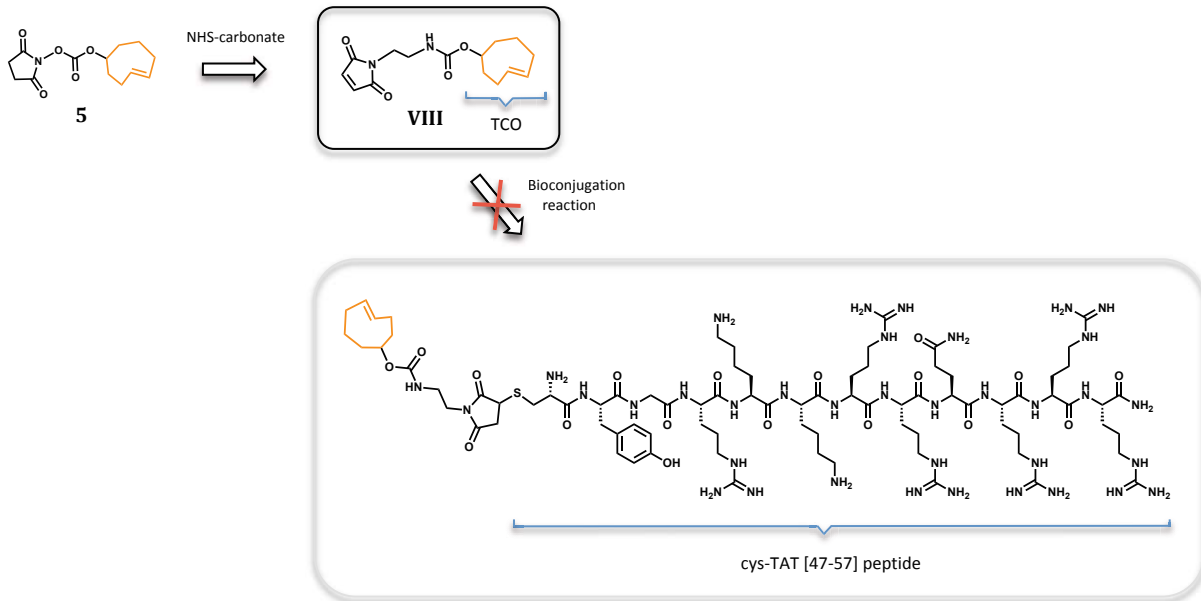
CHANGE OF
FLUORESCENT AGENT



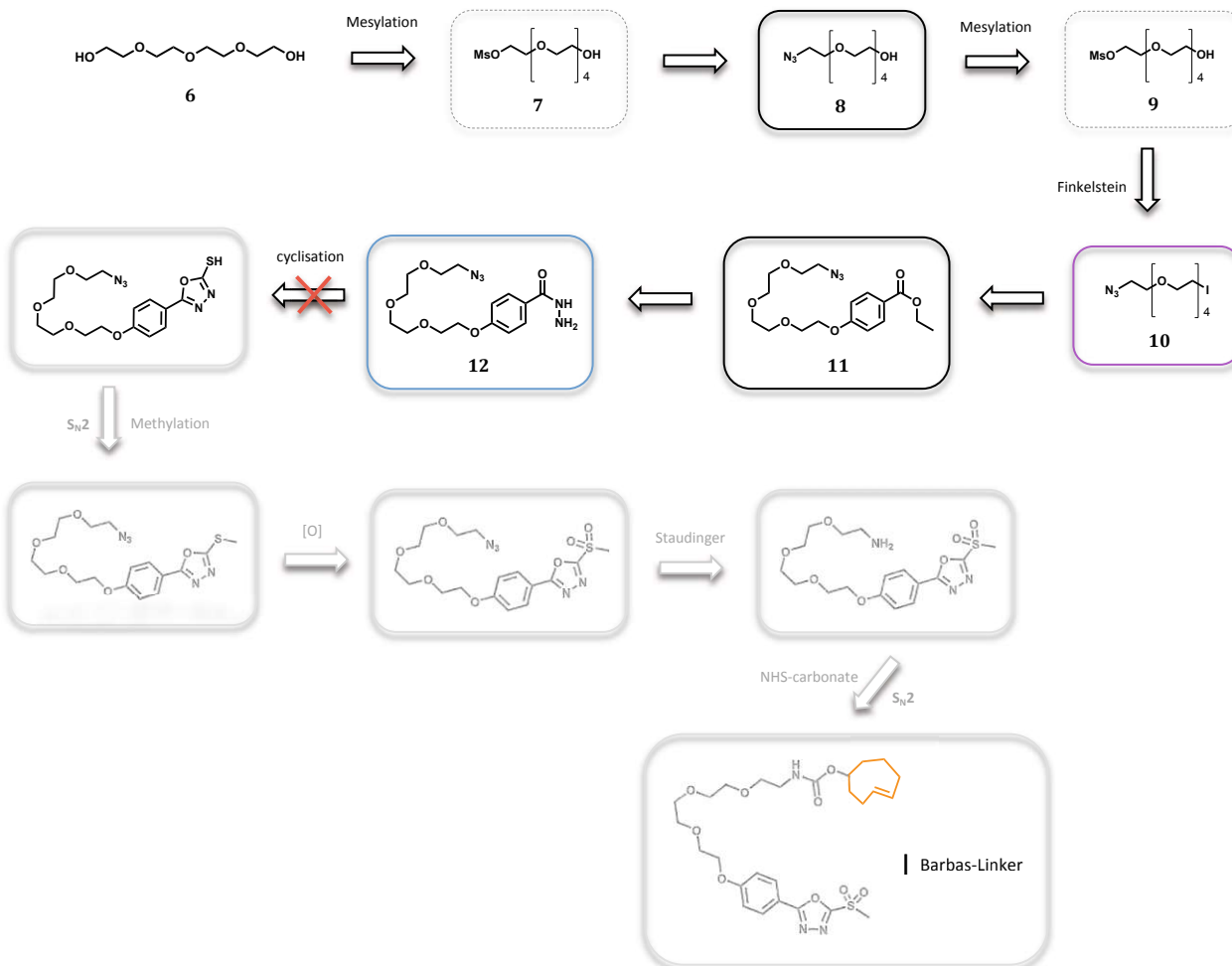
III. STRATEGY



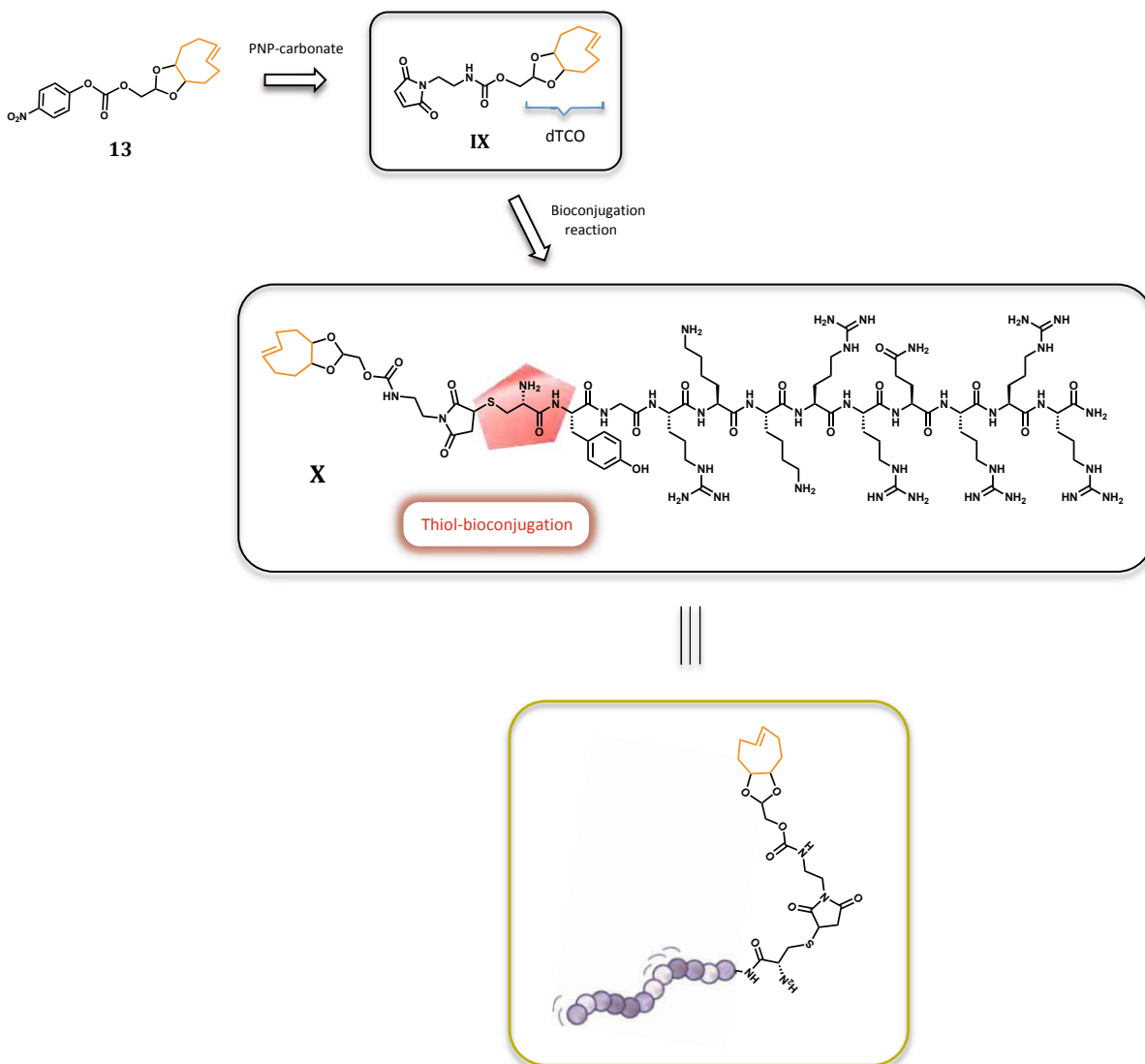
I. STRATEGY



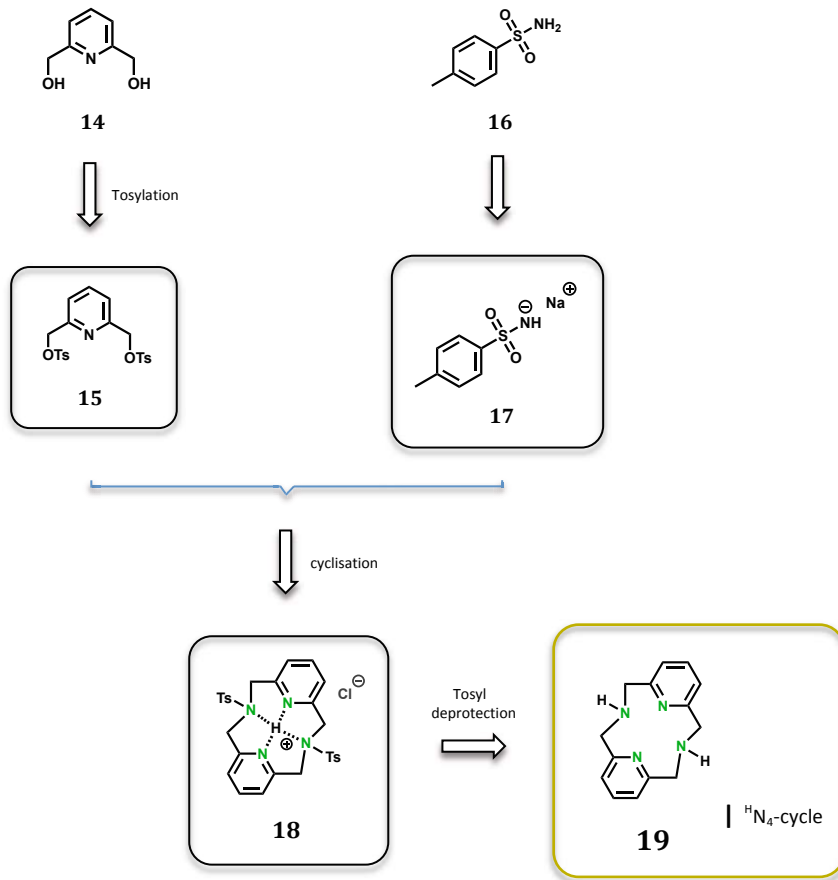
II. STRATEGY



III. STRATEGY



Upcoming complex formation of radionuclides



Building blocks for different further modifications

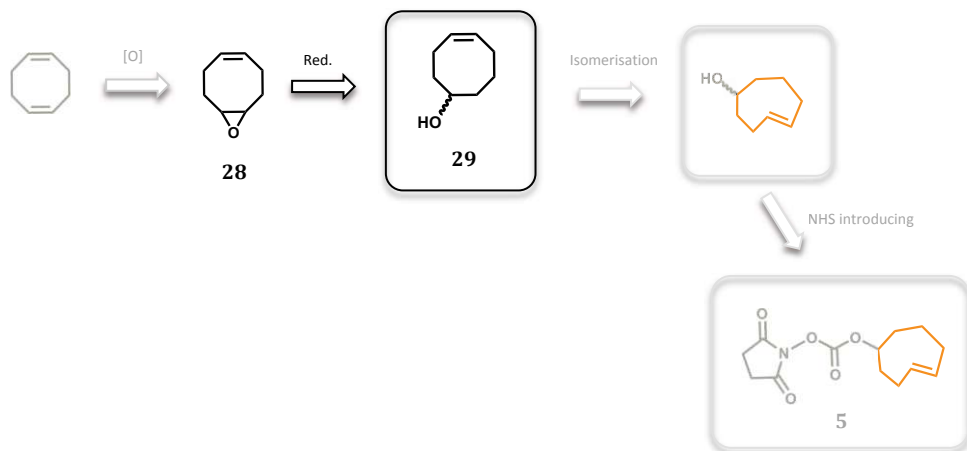
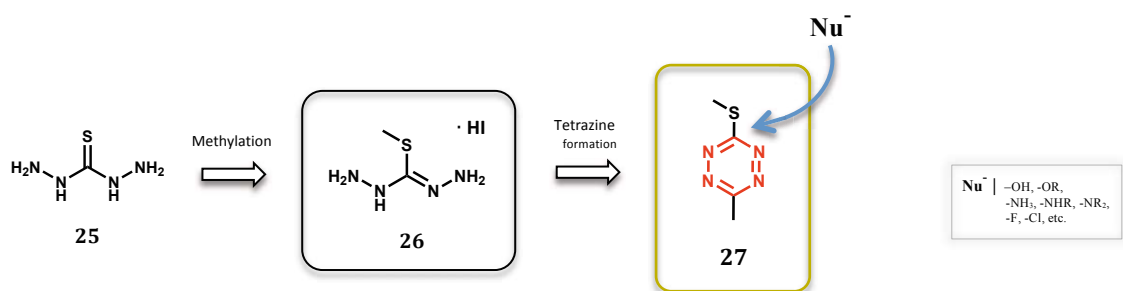
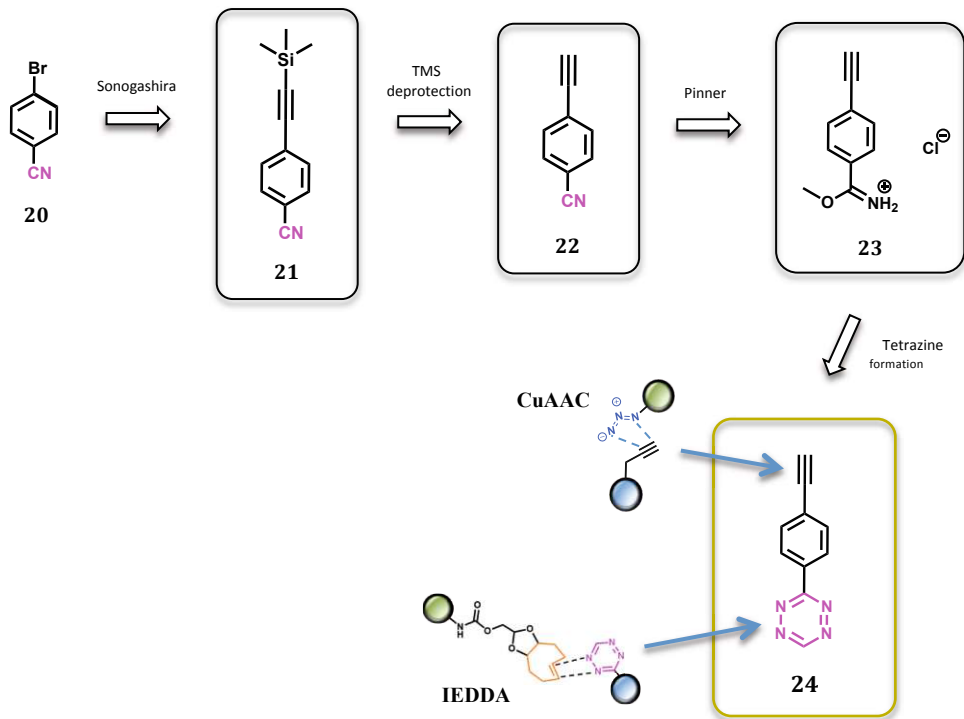


TABLE OF CONTENTS

I	Abstract	i
II	Thesis Illustration.....	iv
III	Chemical Comics.....	vii
IV	Acknowledgement.....	xv
V	Abbreviations.....	xvii
VI	Schemes.....	xxiii

1 | INTRODUCTION..... 5

1.1	Nuclear Medicine.....	5
1.1.1	Radionuclides used for Diagnosis and Therapy	8
1.1.2	Nuclear Medicine Imaging Instruments.....	10
1.1.3	Auger Electron Emitters.....	11
1.2	Overview of various Cancer Therapies	13
1.2.1	Targeted Radionuclide Therapy	13
1.2.2	Pre-targeting Strategies in Radionuclide Therapy	14
1.2.3	Hormone Therapy	15
1.2.4	Angiogenesis Inhibitors.....	15
1.2.5	Apoptosis Inducers	16
1.2.6	Immune Checkpoint Inhibitors	16
1.2.7	Viral Therapy.....	16
1.2.8	Signaltransduction Inhibitors.....	16
1.2.9	Small molecule PROTACs Degraders.....	17
1.3	Bioorthogonal Chemistry.....	18
1.3.1	IEDDA – Inverse electron demand Diels-Alder reaction	21
1.4	Triggered Cell Uptake of Auger emitters	23
1.4.1	Tumor targeting peptide.....	23
1.4.2	Cell-penetrating peptide [CPP]	24
1.4.3	Overall Concept	26

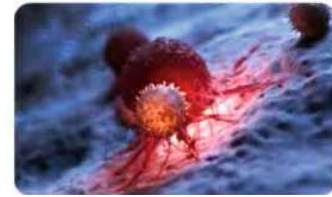
2 | RESULTS AND DISCUSSION.....28

2.1	Synthesis of Building Blocks.....	28
2.1.1	Synthesis of 1,2,4,5-Tetrazines	28
2.1.2	Synthesis of trans-Cyclooctenes [TCOs].....	30
2.2	Modification of Tumor Targeting Carrier Molecules	33
2.2.1	Modifying Bombesin peptide [RM26]-analogon.....	33
2.2.2	Modifying cys-TAT peptide [47-57].....	39
2.3	Synthesis of other Building Blocks for further modifications	41
2.3.1	Synthesis of Ligand $^{14}\text{N}_4$	41
2.3.2	Synthesis of “Dual-Click”-Tetrazine	43
2.3.3	Synthesis of 5-tetrazine	46
2.3.4	Synthesis route for NHS-TCO-carbonate	47
2.4	<i>In vitro</i> studies	48

3 CONCLUSION AND OUTLOOK	50
3.1 Findings.....	50
3.2 Outlook.....	50
VII Materials and Methods.....	xxx
4 EXPERIMENTAL PART	53
5 APPENDIX	97
VIII Reflexion.....	xxxiv
IX References.....	xxxvi
X Table of Figures.....	xxxviii

1 | INTRODUCTION

Human health is a key factor, when talking about everybody's life quality. Therefore medicine in collaboration with chemical, biological and biochemical divisions, all interconnected have a great interest in ensuring living standards to be as high as possible. There exist a broad variety of human diseases, with cancer protruding, that keeps scientists in conducting research with meticulous precision.



Exemplaric picture of a tumor cell¹

Nuclear medicine leads the path to a very promising fashion of diagnosing and treating several diseases, having the opportunity to more or less mark mechanisms occurring in the human body on molecular level. Hence, the diagnosis and therapy of cancer varieties have made a great move in terms of establishing capabilities to successfully fight against tumor cells, without or hardly any impact on healthy cells and tissue, as well.

In order to achieve these characteristics, more and more highly tuned instruments and biological effective radiopharmaceuticals have been developed on nuclear medicine scope. Consequently, the medicinal treatment of all different diseases, not entirely cancer, is more and more proceeding to one that is capable of meeting patients' individual requirements which is actually very powerful, noting that not every person tolerates therapy extent in the same or similar manner.^[1]

1.1 | Nuclear Medicine

Over the past 50 years nuclear medicine has developed and uses radionuclides to perform both non-invasive diagnosis and therapy of several diseases with multi-disciplinary speciality.^[1] Via combination either with other elements to form chemical compounds or combination with well-established pharmaceuticals to obtain so called radiopharmaceuticals, the localisation and accumulation to specific organs or cellular receptors is traceable, once drug doses are administered to the human body (Figure 1).^[2]

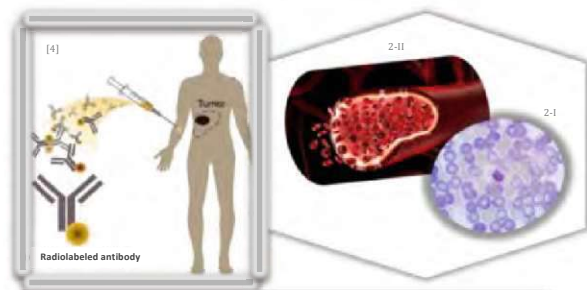


Figure 1 | Administered radiopharmaceuticals are passing through the bloodstream, before accumulating in specific organs (edited)^{[4],2-1,2-II}

As a result, nuclear medicine studies provide an opportunity to monitor the proliferation as well as the extent of diseases via imaging methodologies. Hence, cellular function and physiology are investigated and are very often leading to earlier identification of medical problems – diseases leave marks more likely when they are already far progressed.^[2] So nuclear medicine imaging gives very good diagnostic scope opportunities towards treatment of diseases, „in contrast to imaging techniques that mainly show anatomy (e.g., conventional ultrasound, computed tomography [CT], or magnetic resonance imaging [MRI]), ...“^[1]. Thus, it „can provide important quantitative functional information about normal tissues or disease conditions in living subjects.“^[1]

¹ <https://www.drugtargetreview.com/news/36948/stopping-cancer-cells-in-their-tumour-highways/>, last downloaded 04/2019

²⁻¹ <https://www.imperial.ac.uk/news/138687/malaria-drug-target-raises-hopes-treatments/>, last downloaded 04/2019

^{2-II} <https://www.drugtargetreview.com/news/30643/switch-converts-blood-stem-cells/>, last downloaded 04/2019

Compared to well-known radiotherapy where external radiation beam in form of γ -rays or X-rays is applied consequently from outside the body to fight against tumor cells, in nuclear medicine the generated radiation evolves from inside, speaking also about “endoradiology”.^[2] A significant drawback of traditional radiotherapy using external radiation sources is that very often not only cancer cells are affected, but also healthy ones, and tissue as well (also in terms of chemotherapy). On the contrary, nuclear medicine relies on radioactive emission from within the body. The radiation affects almost only disease relevant regions in the human organism, since the radioisotopes are first circulating in the whole body to finally accumulate only at specific sites.

However, the development path of radiopharmaceuticals to finally enter the drug market, takes between 10 and 15 years on average, which is very long-lasting. One of many similar pathways is depicted in **Figure 2** in form of a “nuclearmedicine cycle”, starting with synthesizing building blocks suitable for modifying tumor targeting “carrier molecules” in a so called radiolabeling step to form “radiotracers” that are supposed to show favoured biological effectiveness. These conjugated compounds are then evaluated and tested by means of *in vitro* investigations, to move on to *in vivo* tests that shall give the go-ahead for reaching preclinical studies and in further consequence the clinical trials.

Within these clinical studies that occupy the longest time scale of usually more than seven years, time will tell if the radiolabeled pharmaceuticals are uncritical concerning human safety and side-effects as well as if they show appropriate site-specific effectiveness, and thus if they are approved for launching onto the drug market.

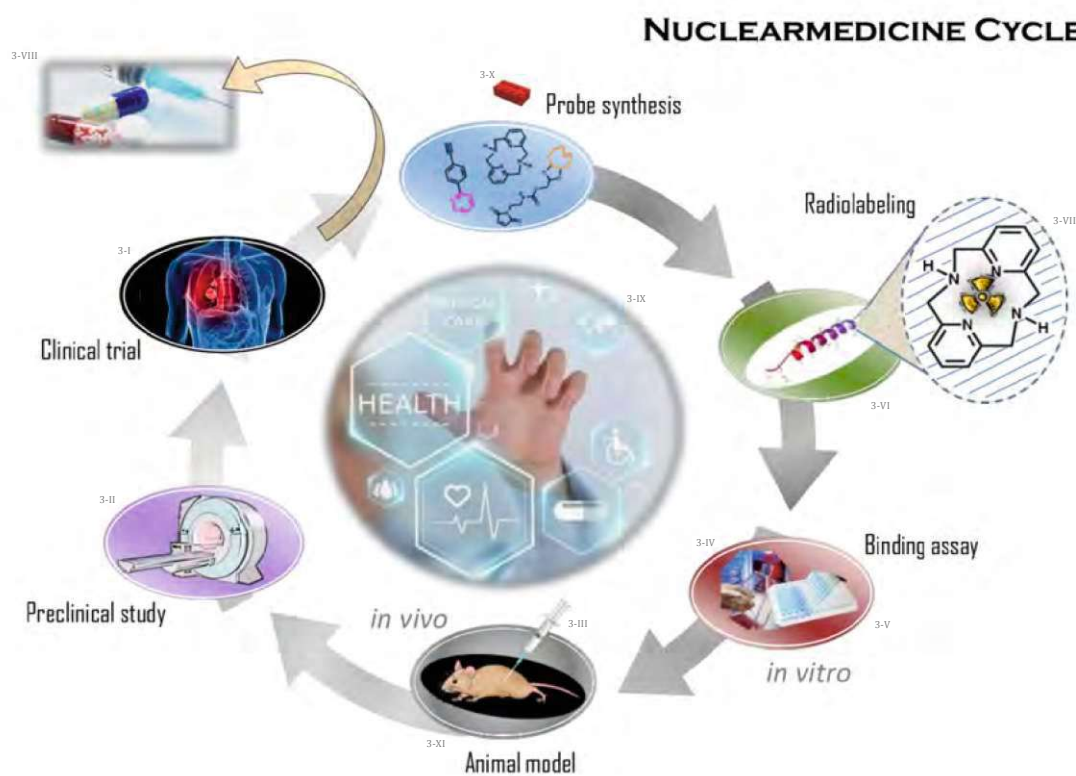


Figure 2 | Development path of a radiopharmaceutical – from radiolabeling step towards drug market (edited)^{3-I,3-II,3-III,3-IV,3-V,3-VI,3-VII,3-VIII,3-IX,3-X,3-XI}

^{3-I} <https://bowelcancer.org.nz/about-bowel-cancer/metastatic-bowel-cancer/>, last downloaded 04/2019, ^{3-II} <https://www.urologe-zigeuner.at/de/untersuchungen/magnetresonananz-mr/>, last downloaded 05/2019, ^{3-III} <https://de.clipartlogo.com/istock/syringe-1716082.html>, last downloaded 05/2019, ^{3-IV} <https://www.sigmaaldrich.com/catalog/product/sigma/clc3073?lang=de®ion=AT>, last downloaded 04/2019, ^{3-V} <https://www.dreamstime.com/stock-photo-multichannel-pipette-test-sample-wells-plate-blue-solution-image47881809>, last downloaded 05/2019, ^{3-VI} https://fr.123rf.com/photo_16083355_la-structure-chimique-d-une-mol%C3%A9cule-de-glucagon-le-glucagon-est-une-hormone-peptidique-produite-pa.html, last downloaded 05/2019, ^{3-VII} <https://www.pngkey.com/pngs/radiation-symbol/>, last downloaded 04/2019, ^{3-VIII} <https://www.infosperber.ch/Gesundheit/G%C3%B6tzsche-Todliche-Medizin-und-organisierte-Kriminalit%C3%A4t>, last downloaded 05/2019, ^{3-IX} <https://www.heinze-pruefungsanfechtung.de/pruefungsanfechtung-medizin/>, last downloaded 05/2019, ^{3-X} <https://www.amazon.de/legosteine-rot/s?k=legosteine+rot>, last downloaded 05/2019, ^{3-XI} <http://clipartandscrap.com/mouse-clip-art/>, last downloaded 05/2019

HISTORY OF NUCLEAR MEDICINE^[1]

1960s

Scientists at ORNL discover the affinity of radioisotope **gallium-67** for soft-tissue tumors. This radioisotope has been used to image lymphomas, lung cancer, and brain tumors.

At Brookhaven National Laboratory in 1957 the development of a **technetium-99m generator**, based on adsorption of carrier-free molybdenum-99 on alumina column, was attained.⁴



4-I

1970s

Fluorine-18-FDG, a positron-emitting compound, was synthesized first by Tatsuo Ido, Alfred P. Wolf and Joanna Fowler at BNL.

Scientists at the University of Pennsylvania and at the NIH use fluorine-18-FDG to image **glucose metabolism** in the human brain.

1980s

A new radiopharmaceutical, **iodine-131 m-iodine-benzyl-guanidine (I-131 MIBG)**, is developed by Donald Wieland for the diagnosis and treatment of rare childhood cancers.

Michael Welch of Washington University and John Katzenellenbogen of the University of Illinois develop the **first PET radiotracer** used to image tumors expressing the estrogen receptor.

Chemists developed methods to **synthesize high-specific-activity C-11- and F-18-labeled** compounds for imaging neurotransmitter and other physiological activities.

1990s

A **high-resolution PET scanner** designed to image small laboratory animals (i.e., microPET) is developed at UCLA by Simon Cherry.

21st century

The first commercially available **hybrid PET/CT scanner** was developed at University of Zurich⁴ by General Electric in 2001, followed by **PET/MRT hybrid devices**, firstly applied at research centre Jülich⁴ six years later in 2007.

In recent years, **Total Body Scans** have emerged and allow the diagnosis of the whole human body in drastic shortened acquisition time, using up to 100 moving coils simultaneously.



4-II

History of Nuclear Medicine [1960s – today]^[1,4,4-I,4-II]

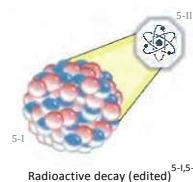
⁴ <http://www.med.harvard.edu/jpnm/physics/isotopes/Tc/Tc99m/hist.html>, last downloaded 05/2019,
https://web.archive.org/web/20131202233701/http://www.grstiftung.ch/de/portfolio/projekte/alle/y_1998/GRS-071-98.html, last downloaded 05/2019,
<https://www.dw.com/de/9komma4-ein-tomograf-der-extraklasse/a-4214283>, last downloaded 05/2019

^{4-I} <https://www.aecoc.es/articulos/reglamentos-udi-el-nuevo-reto-de-la-industria-de-producto-sanitario-y-de-diagnostico-in-vitro/>, last downloaded 04/2019

^{4-II} <https://us.medical.canon/products/computed-tomography/celesteion/experience/>, last downloaded 05/2019

1.1.1 | Radionuclides used for Diagnosis and Therapy

In general, the nucleus of a radionuclide turns into stable species by emitting energy in the form of particles, referring to α - and β -particles, respectively, but also in the form of electromagnetic radiation, with regard to the γ -rays. Despite the fact that radioactive chemical compounds occur in nature, radionuclides used in targeted tumor therapy are generated in linear accelerators, cyclotrons or nuclear reactors. The wide variety of radionuclides with different types of radiation and therefore unique properties per se, leads to plenty possible ways to be successful on diagnostic and therapeutic scope.^[1] **Figure 3** highlights the most commonly used radionuclides in diagnosis as well as in therapy.^[3]



	Radionuclide	$T_{1/2}$	type	gamma [keV]	positron [keV]
Diagnosis	Technetium-m99	6.0 h	IT, γ emitter	140	-
	Iodine-123	13.2 h	ϵ , γ emitter	159	-
	Thallium-201	3.0 d	ϵ , γ emitter	167	-
	Indium-111	2.8 d	ϵ , γ emitter	245	-
	Fluorine-18	110 min	β^+ emitter	(511)	249.8
	Rubidium-82	1.3 min	β^+ emitter	(511)	3.4
Therapy	Yttrium-90	2.7 d	β^- emitter	-	2.3
	Iodine-131	8.0 d	β^- emitter	364	0.8
	Actinium-225	10.0 d	α emitter	440	-

α

SPECT/PET imaging^{3-II}

Figure 3 | Most commonly used radionuclides in nuclear medicine diagnosis and therapy, respectively (edited)^{[3],3-II}

Metastable Technetium-m99 (^{99m}Tc) is marked in red as one of the most applied radionuclides on diagnostic scope, by using SPECT (= single photon emission computer tomography) imaging method for analysis. Regarding the alternative imaging method, PET (= positron emission tomography), Fluorine-18 (^{18}F) is highlighted in green. Located on the right hand side of **Figure 3**, γ -radiation or positron emission (β^+), as well as radiation based on electron capture (ϵ) or isomeric transition (IT), are implemented in diagnosis, in terms of both SPECT and PET methodologies.^{[1][4]}

For therapy issues, Yttrium-90 (^{90}Y) and Iodine-131 (^{131}I) are well-established radioactive isotopes, being β -emitters with higher energies (β^-).^[1] Moreover, also α -particles with even greater energy levels have been used for therapeutic approaches, like for example Actinium-225 (^{225}Ac) (ref., 1.2.1).

Having a look at the properties of the different types of radiation, **Figure 4** illustrates each penetration level that increases when going from alpha over beta to gamma radiation type. Concerning the energy that is transferred by these emissions, the so called Linear Energy Transfer (= LET) gives useful information on that.



Figure 4 | Penetration levels of alpha, beta and gamma radiation types⁶

⁵⁻¹ https://en.wikipedia.org/wiki/Radioactive_decay, last downloaded 05/2019

^{5-II} https://www.iconfinder.com/icons/354051/atom_chemistry_physics_science_icon, last downloaded 05/2019

⁶ <https://www.enec.gov.ae/discover/fueling-the-barakah-plant/what-is-radiation-/>, last downloaded 04/2019

As α -particles are helium-4 (${}^4\text{He}$) atoms (ref. **Figure 5**), formed within radioactive decay process, they have much higher LET energies (50-230 keV/ μm) than β -particles (0.1-1.0 keV/ μm), that are of clearly smaller size (ref., **Figure 8** | page 11). By contrast, γ -emission takes place in form of γ -rays as being constituted of electromagnetic nature instead of mentioned particles. Thus, LET energies are far less than the ones of particles originated from alpha and beta decay, which makes gamma emitters applicable almost entirely for diagnostic purposes.^[4]




Decay Type	Radiation Emitted	Generic Equation	Model
Alpha decay	${}^4_2\alpha$	${}^A_ZX \longrightarrow {}^{A-4}_{Z-2}X' + {}^4_2\alpha$	 Parent → Daughter + Alpha Particle
Beta decay	${}^0_{-1}\beta$	${}^A_ZX \longrightarrow {}^A_{Z+1}X' + {}^0_{-1}\beta$	 Parent → Daughter + Beta Particle
Gamma emission	${}^0_0\gamma$	${}^A_ZX^* \xrightarrow{\text{Relaxation}} {}^A_ZX' + {}^0_0\gamma$	 Parent (excited nuclear state) → Daughter + Gamma ray

Figure 5 | Decay characteristics of alpha, beta and gamma radiation types⁷

Moreover, the unit of the LET energies is declared in keV/ μm , which means properly the extent of energy related to range. So it describes the energy that is transferred to affected tissue and consequently, to affected cells, taking account of the track length and therefore indicates actually how many cells are radiated (ref. **Figure 8** | page 11). While α -particles in comparison have a rather short range which is accompanied by high LET energy levels, the deposition in tumor cells leads to high potency for annihilating them. Additionally, alpha radiation moderates the so called “cross-fire effect”, by preferably having an impact on targeted cells and lowering non-specific radiotoxicity while only 5-10 cells are radiated on average.^[4]

On the contrary, beta emitters are more feasible in terms of eradicating cancer growth that is of larger magnitude, due to their higher range and despite having a low energy transfer. Nevertheless, β -radiation involves more non-specific cell affecting, by greatly exceeding the diameter of a single cell and enhancing associated “cross-fire effect”, having an impact on 200 up to 1000 cells.^[4]

Since the administered radiopharmaceuticals, containing the required radionuclide, can be detected and monitored with nuclear medicine imaging instruments, their properties as well as their application scale are explained in the following chapter.

⁷ [https://chem.libretexts.org/Courses/Eastern_Wyoming_College/EWC%3A_Introductory_Chemistry_\(Budhi\)/17%3A_Radioactivity_and_Nuclear_Chemistry/17.03%3A_Types_of_Radioactivity%3A_Alpha%2C_Beta%2C_and_Gamma_Decay](https://chem.libretexts.org/Courses/Eastern_Wyoming_College/EWC%3A_Introductory_Chemistry_(Budhi)/17%3A_Radioactivity_and_Nuclear_Chemistry/17.03%3A_Types_of_Radioactivity%3A_Alpha%2C_Beta%2C_and_Gamma_Decay), last downloaded 05/2019

1.1.2 | Nuclear Medicine Imaging Instruments

Positron emission tomography (= PET) represents one nuclear medicine imaging technique (**Figure 6**) that relies on physical decay of positron-emitting (β^+) radionuclides. Once, subsequent to decay, emitted positrons interact with surrounding electrons inside the human body, two gamma ray photons are formed. These in opposite direction moving photons are detected simultaneously by PET instrument. That way, the medicinal device (almost entirely fused PET/CT or PET/MRT) is capable of realising 3D-images of radionuclide distribution in the human body, thus provides information on biochemical metabolic processes [functional imaging + anatomic imaging].^{[1][5]}



Figure 6 | PET instrument (edited)^{8,[11]}

A descriptive example is represented by the well-known radiopharmaceutical fluorine-18 (^{18}F) fluorodeoxyglucose (FDG), which is a modified, radiolabeled sugar molecule, usable for PET-imaging (FDG-PET). After administering the radiotracer, it is allowed to accumulate within the patient. During the scan, the application detects deviations between normal, healthy cells and tumor cells, due to the fact that cancer and metastases consume much more sugar and therefore tend to proliferate much faster. However, diagnostic specificity stays limited as other lesions may also gather sugar substance.^[1]

Single photon emission computed tomography (= SPECT) is an alternative imaging technique (**Figure 7**) to the just mentioned PET imaging. Thereby, the methodology relies on the principle of scintigraphy, as light flashes going off the scintillation crystal are detected. The light flashes derive from excitation of the crystal with gamma radiation, evolving from applied radionuclides.^{[1][6]}



Figure 7 | SPECT instrument (edited)^{9-I,9-II}

A SPECT instrument uses a gamma camera that rotates around the patient to make 3D images. So compared to conventional CT scan, where X-rays are the source of the information, SPECT traces gamma rays instead. SPECT medicinal devices are used extensively in terms of studying cardiac health and imaging human brain, accompanied by blood flow, for both.^[6]

Having the two well-applied imaging varieties compared, the main advantage of PET/CT is the very high resolution of the recorded scans by using CdTe detectors, providing more sensitive physiological facets. On the contrary, SPECT is a rather low cost application and relies on great availability of radionuclides with longer half-life and hence with large-scale applicability.^[1]

⁸ <https://us.medical.canon/products/computed-tomography/celesteion/experience/>, last downloaded 05/2019

^{9-I} <https://radiologykey.com/paediatric-neuroradiology-2/>, last downloaded 04/2019,

^{9-II} http://www3.gehealthcare.de/de-de/produkte/kategorien/nuklearmedizin/universal-gammakameras/brivo_nm615, last downloaded 05/2019

1.1.3 | Auger Electron Emitters

Beside the two previously mentioned radiation types that are commonly used in cancer therapy, another possibility for accomplishing successful treatment of tumor disease emerged, illustrated also in **Figure 8**. Auger electron emitters are meant, and are supposed to make the difference in targeted radionuclide therapy. In this case, these are radionuclides that emit high numbers of Auger electrons and are forced to decay by means of electron capture (ϵ) or isomeric transition (IT).^[4]

While “high energy beta emitters may not be efficient for micrometastases”^[2], annihilating “single cells, alpha emitting radionuclides or Auger nuclides, which have shorter ranged particles and higher LET may be more adequate.”^[2]

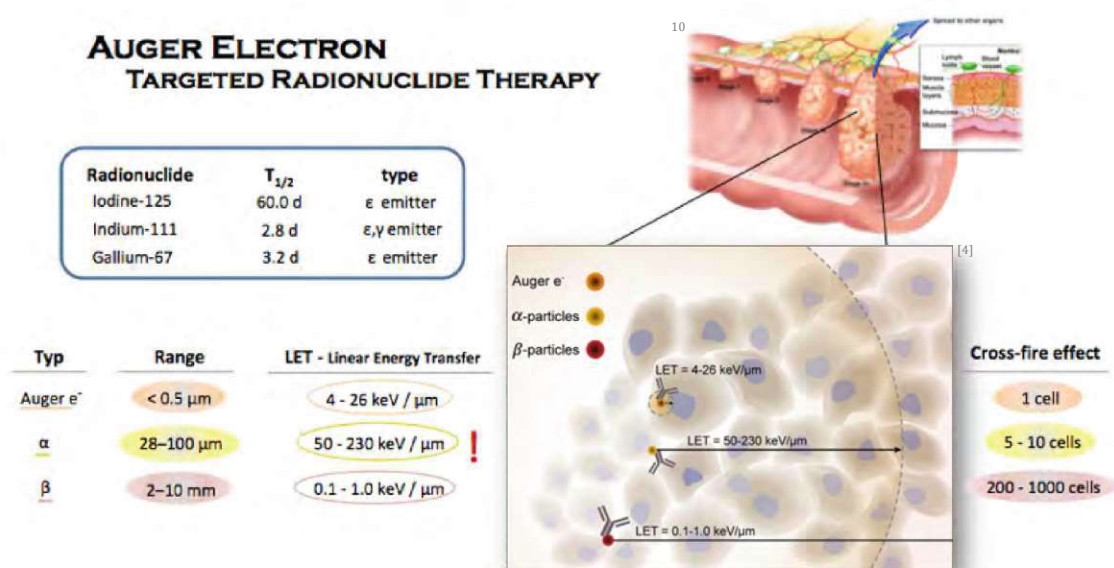


Figure 8 | LET-energy comparison of the three different therapeutic radiation types and examples for used Auger electron emitting radionuclides (edited)^{[4],10}

They have a track length in the range of a single cell only, which is why they show hardly any “cross-fire effect”, affecting more or less just targeted cells. With characteristic moderate LET energies of 4-26 $\text{keV}/\mu\text{m}$, which are high enough for being capable of achieving **tumor cell death by breaking and damaging the double-stranded DNA**, the only requirement for Auger electrons to be biological effective is, that they have to be channelled right into the cell or even cell nucleus of the targeted cancer cells.^[4]

Hence, Auger electron emitting radionuclides shall be capable of transforming diagnostics into therapeutics via mediated Cell Uptake strategy by triggering radiotoxicity within nucleus.

Conclusively, Auger electron emitters deserve the term of being distinctive radioisotopes, since they are expected to perform some sort of specific engineering skills on molecular level. “The highly localized cytotoxicity of Auger electrons is particularly attractive for targeted radionuclide therapy of microscopic or metastatic disease because it allows the irradiation of tumor cells while sparing healthy tissues.” (Paillas, Pouget *et al.*, 2016).^[7]

¹⁰ <https://www.bowelcancer australia.org/bowel-cancer-staging>, last downloaded 04/2019

Imstepf and coworkers^[8] could prove an up to 80 % dose-dependent reduction in terms of cell line viability by emission of low-energy Auger electrons, leading the path for very promising treatment strategies. “As demonstrated, Auger emitters may provoke inhibition of cell survival at concentrations which are much lower than the ones of their chemotoxic counterparts.”^[8]

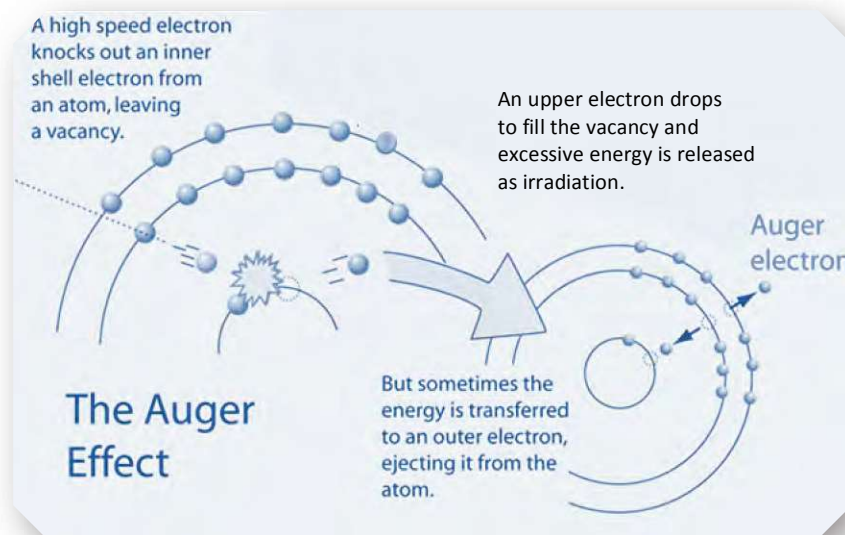


Figure 9 | The Auger Effect-mechanism – electron capture (ϵ) or isomeric transition (IT), both lead to vacancies at inner shell, providing the starting point for generating Auger electrons (edited)¹¹

The previous described Auger electrons are generated by means of the so called Auger Effect, as depicted in **Figure 9**. Usually, a high speed electron knocks out an inner shell electron, leading to a vacancy left behind. In case of Auger electron emitters the vacancies are formed within electron capture (ϵ) or isomeric transition (IT) processes, respectively. An upper electron drops to fill the vacancy and the excessive energy is released as irradiation. But sometimes this excessive energy is transferred to an outer electron, which leads to ejecting it from the atom – an Auger electron is generated.¹¹

¹¹ <http://hyperphysics.phy-astr.gsu.edu/hbase/Atomic/auger.html>, last downloaded 04/2019

1.2 | Overview of various Cancer Therapies

So being in the field of cancer, a patient receives radioactive drug doses in parenteral or gastro-intestinal way, in the form of so called “radiotracers” that participate in metabolic processes within the human body, thus at least diagnosis is achievable (Figure 10). For quite some time now, scientists have started to move on and turn this applied diagnostics even into therapeutics – preferentially talking about “theranostics”, having combined both scopes.

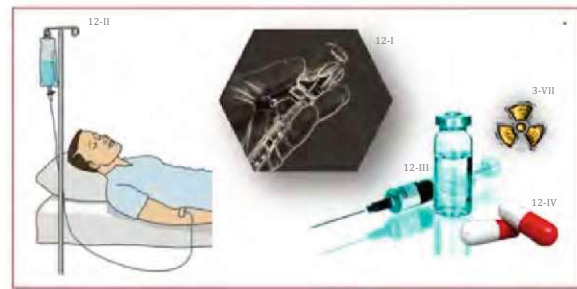


Figure 10 | In nuclear medicine a patient receives drug doses in the form of so called “radiotracers” (edited)^{12-I,12-II,12-III,12-IV}

The within the previous chapters broached issue concerning tumor targeted radionuclide therapy will be described herein, going into more detail. In addition, also some more tumor targeted therapies are introduced that don’t use any form of radioactive species.

1.2.1 | Targeted Radionuclide Therapy

Radionuclide therapy is in needs of radiopharmaceuticals that are administered to patient’s body, where they participate in the to be monitored metabolic processes. Thereby, the applied radiotracer consists of a “carrier molecule”, being for example a peptide or a monoclonal antibody, that is labeled with radionuclide species and seeks out unique, specific receptor or antigen on cells, respectively (Figure 11).¹³ Depending on treatment method, different radionuclides are attached on these carrier molecules to ensure satisfying results.

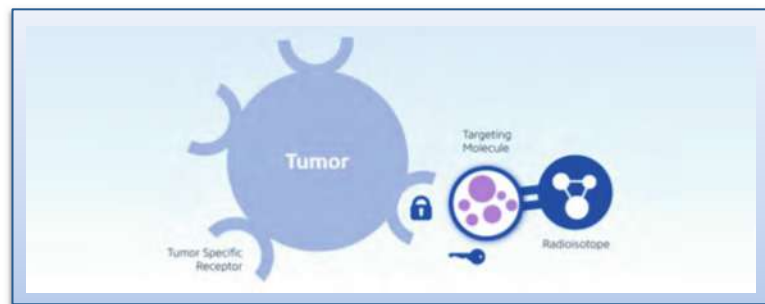


Figure 11 | Concept of targeted radionuclide therapy – achieving the attachment on tumor cells in a key-lock pair manner¹³

“It is this modular nature, where the two components can be varied like Lego® pieces to match characteristics specific to the tumor that makes targeted radionuclide therapy an attractive approach to cancer treatment.”^[9] (Zalutsky, 2003). This statement refers perfectly to the possibility to chemically synthesize numerous modified molecules, which is indeed very indispensable. Currently, a wide variety of new pathway targeting anticancer compounds are evaluated in phase II and phase III of clinical trials.^[1]

Mentioning one representative example, Bhusari and coworkers^[10] have described Lu-177-trastuzumab as an applied radiopharmaceutical on therapy scope to address overexpressed HER2-positive tumor receptors specifically (Figure 12 | page 14). Therefore the FDA approved humanized monoclonal antibody trastuzumab (better known under brand name Herceptin®) is conjugated with the bifunctional, macrocyclic chelator DOTA (= 1,4,7,10-tetraazacyclododecane tetra-acetic acid). Via complex formation of radioactive species ¹⁷⁷Lu, radio-labeling is accomplished and radionuclide-anti-

^{12-I} <http://www.africaprocessing.com/pharmaceutical-injection-manufacturing/attachment/pharmaceutical-injection-production-line-africa/>, last downloaded 04/2019

^{12-II} <https://clipground.com/portal-of-entry-clipart.html>, ^{12-III} <http://www.thirdpartymanufacturers.in/product/edaravone.injection-manufacturers/>, last downloaded 04/2019

^{12-IV} https://www.kncvtbc.org/en/2018/07/25/bedaquiline-price-reduction-could-benefit-the-world/pills_png16549/, last downloaded 04/2019

¹³ <https://ccr.cancer.gov/news/article/clinical-trial-will-investigate-targeted-radionuclide-therapy-for-inoperable-rare-tumors>, last downloaded 05/2019

body-conjugate for therapy use is ready.^[10]

“Lu-177-trastuzumab may prove to be a potential palliative agent for HER2 metastatic breast disease which may improve the quality of life of these patients especially when other conventional treatments fail to prove effective or when patients prove resistant to conventional therapies.”^[10] Besides, ¹⁷⁷Lu with a half-life of 6.7 days is a short-range β-emitter and ensures good localization and contrast in imaging processes, despite the slow metabolising antibodies at tumor site.^[10]

Another to be mentioned, very well-known and commonly used radiopharmaceutical is Zevalin®, consisting of a Yttrium-90 labeled Ibritumomab-Tiuxetan, approved in 2002 by FDA.^[1]

As cancer is not only proliferating in a very fast manner, and thus capable of local broadening, it spreads also daughter metastases all over the whole body. While therapy of original breast cancer very often leads to successful regression of tumor cells, the metastatic form emerges to be rather difficult-to-treat. But, by developing targeted radionuclide therapy over decades, breast cancer is not known for being associated with the worst prognosis anymore.^[10]

„For treatment, highly targeted radiopharmaceuticals may be used to deposit lethal radiation at tumor sites.“^[1] The PSMA targeted α-radiation therapy of metastatic prostate cancer has been very successful, concerning a patient who only had a life expectancy of two up to four weeks left before the treatment and showed immense tumor cell regression. This story depicts an extraordinary increase of the patient’s life quality, as well as the far reaching potential in this specific branch of cancer research, opening up lots of promising opportunities to come.^[11]

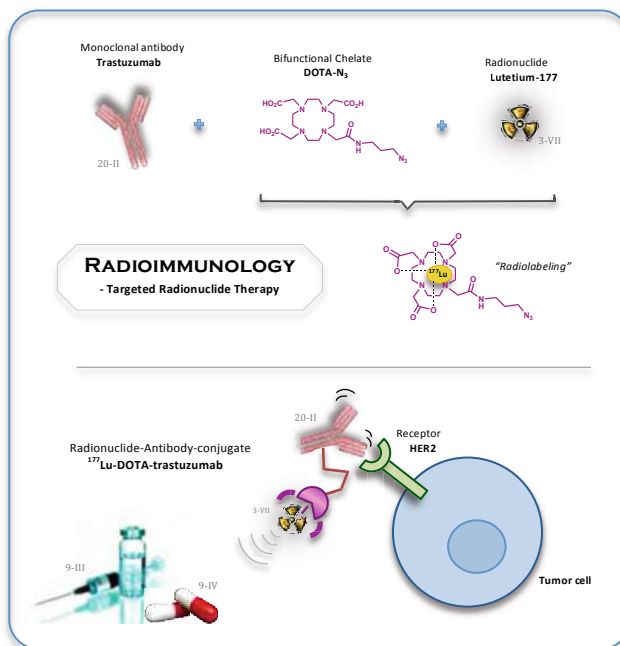


Figure 12 | Targeted radionuclide therapy – illustration of an example (edited)^{3-VII,9-III,9-IV,20-II}

1.2.2 | Pre-targeting Strategies in Radionuclide Therapy

Although radiolabeled monoclonal antibodies have been investigated with high priority to finally discover the breakthrough-making drug agent, smaller molecules as carrier moiety like for example peptides have been revealed more and more, providing advantages in several applications, such as attaining rapid accumulation in cancer and metastases, as well as clearance from healthy, normal cells and tissue. „A number of regulatory peptides and their corresponding receptors that are overexpressed on certain types of tumors are being evaluated for possible application of targeted radionuclide therapy.“^[1]

In **Figure 13** (page 15), each and every step of an example in pre-targeted radionuclide therapy is illustrated in systematic way, starting with administration of a tumor targeting carrier molecule (a peptide in this case), which is modified by clicking tool *trans*-cyclooctene (TCO). As soon as accumulation process is finished, the second compound, a radiolabeled tetrazine, is administered to the patient and upon a ligation reaction between both, the click product is formed very fast.

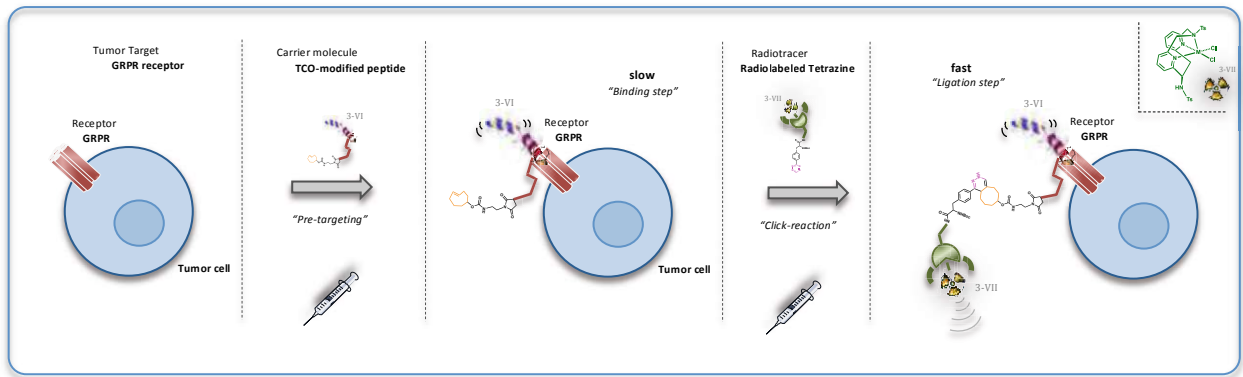


Figure 13 | Pre-targeted radionuclide therapy – slow accumulation of specific peptide on tumor cells, followed by fast “Click reaction” of radiotracer^{3-VI,3-VII}

So the main focus is on „achieving a balance between maximizing the absolute amount of radionuclide that can be delivered to the tumor and meeting the requirement that the tumor-to-normal organ dose ratios be as high as possible. The problem is that large molecules such as antibodies provide the highest tumor accumulation, while smaller molecules such as peptides provide the highest tumor-to-normal organ dose ratios.“^[1] Combination of both, hence boosts cancer treatment to become very specific as well as more efficient, which is reported in detail among others by Rossin and Robillard.^[12]

Summarizing, pre-targeted radionuclide therapy is not alone approachable via click chemistry reaction using smallish molecules, but also by taking advantage of the binding affinity between a tumor targeting monoclonal antibody (instead of peptide in **Figure 13**) and a radiolabeled peptide (instead of tetrazine species) that binds specifically to the already attached antibody.^[1]

1.2.3 | Hormone Therapy^[13]

The hormone therapy relies on the capability of certain medications to slow down and delay or even stop the tumor growth by having an impact on hormone-sensitive cancer types, which require individual hormones for proliferation. In other words, hormone therapy ensures that the patient’s body does not produce any hormones anymore, or that the natural pathways of hormones are interfered. Therapies for both breast and prostate cancer are acquainted.

1.2.4 | Angiogenesis Inhibitors^[13]

Tumor sites are diverting blood vessels (= angiogenesis) from healthy cells and tissue, to provide oxygen and nutrient supply that they need for continuing growth and spreading (**Figure 14**). There exist specific inhibitors to interfere and block angiogenesis action (e.g., VEGF, vascular endothelial growth factor; protein for stimulating new blood vessel formation).

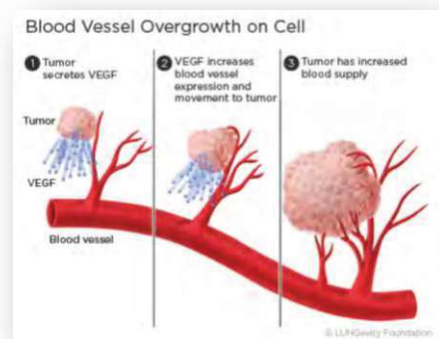


Figure 14 | Angiogenesis – blood vessel diversion from healthy cells to cancer excretion¹⁴

¹⁴ <https://lungevity.org/for-patients-caregivers/lung-cancer-101/treatment-options/angiogenesis-inhibitors>, last downloaded 05/2019

1.2.5 | Apoptosis Inducers^[13]

Apoptosis terms the process of controlled or programmed, natural cell death whereby essential mechanisms within the human body are taking place to do some sort of “repairing the whole system”, as unfavourable processes are occurring during lifetime. Since cancer and its metastases are able to circumvent this programmed cell death, apoptosis inducers are applied to force tumor cells getting mortal.

1.2.6 | Immune Checkpoint Inhibitors^[13]

Within this kind of cancer therapy tumor cells are eliminated by triggering the immune system. Therefore, monoclonal antibodies that address specific molecules on the cancerous surface are used (Figure 15). Via binding trial, tumor cells are annihilated by initializing immune actions. “Marking” the foreign bodies, which are subsequently traced back to cancer origin, alarms the immune cells. Targeted immunotherapy is similar to radioimmunology (1.2.1), but does not utilise any radionuclides.

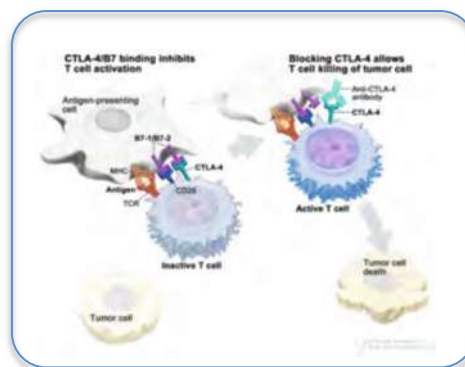
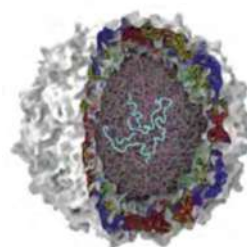


Figure 15 | Illustration of signal transduction pathway¹⁵

1.2.7 | Viral Therapy¹⁶

Viruses that tend to infect and erase tumor cells without harming any healthy sites are often referred to the term of oncolytic viruses. They are supposed to trigger „an immune response in the body against the cancer.“¹⁶ After infection a virus is capable of making copies of itself, thus leading to cell rapture. Since dead cancer cells are releasing cell substances, like for example antigens, the immune system notices the foreign objects.



Picture of structural virus¹⁶

„ ‘Oncolytic viruses are alerting the immune system that something’s wrong,’ said Jason Chesney, M.D., Ph.D., director oft he University of Louisville’s James Graham Brown Cancer Center.“¹⁶ Another interesting topic on viral therapy is hat some patients have reached good remission, however very often just for temporary timeframe, after they have suffered under viral infection.

1.2.8 | Signaltransduction Inhibitors^[13]

These inhibitors are able to block molecules and their intentions to respond to signals on cellular level, and as a consequence are interfering the signal transduction pathway (Figure 16). This pathway relies on „a series of biochemical reactions that ultimately

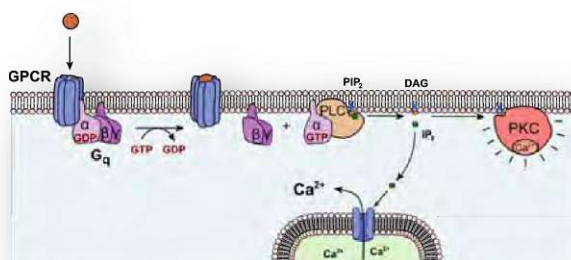


Figure 16 | Illustration of signal transduction pathway¹⁷

¹⁵ <https://www.cancer.gov/publications/dictionaries/cancer-terms/def/immune-checkpoint-inhibitor>, last downloaded 05/2019

¹⁶ <https://www.cancer.gov/news-events/cancer-currents-blog/2018/oncolytic-viruses-to-treat-cancer>, last downloaded 05/2019

¹⁷ https://de.wikipedia.org/wiki/Proteinkinase_C, last downloaded 05/2019

produce the appropriate response(s).^[13] to specific signals.

Recently, oncologists have recognized that subtypes of, for instance, breast cancer are of different biological nature and thus have diverse disease characteristics. Since there exist HER2 (= human epidermal growth factor receptor 2) receptors in both, negative and positive fashion, but in massive varying amount, as a consequent these kinds of types have to be treated biologically different.^[1]

Monoclonal antibody trastuzumab, more commonly known under trade name Herceptin®, is very well targeting breast cancer that overexpresses HER2 receptor. “By differentiating the tumors based on molecular differences and targeting these differences, more effective treatment can be delivered to the patient.”^[1]

1.2.9 | Small molecule PROTACs Degraders

Proteolysis-targeting Chimeras (= PROTACs) induce the intracellular proteasome to degrade targeted proteins selectively by transferring small ubiquitin proteins onto them. These heterobifunctional degraders consist of two ligands, one for addressing the target protein’s pocket and a second for being attached to E3 ubiquitin ligase, both connected via a linker (**Figure 17**).^[14]

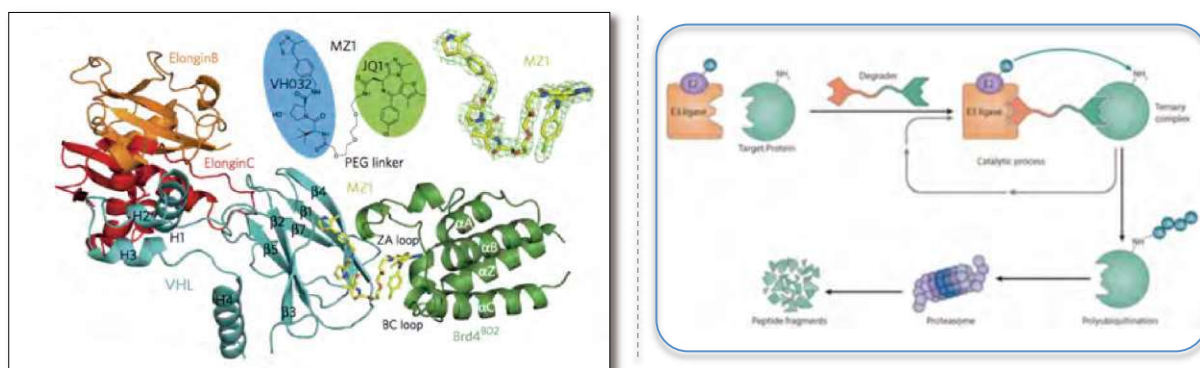


Figure 17 | left: PROTACs forming a ternary complex with target protein (green) and E3 ubiquitin ligase (blue)^[14], right: illustration in mechanistic manner¹⁸

Once the target protein, PROTAC and E3 ubiquitin ligase are forming a ternary complex, “E2 ubiquitin-conjugating enzymes transfer ubiquitin to lysine residues on the surface of the target protein.”^[15] (An, Fu, 2018). It is the protein complex proteasome’s turn now, recognizing the lysine-polyubiquitination signal and further on starting degradation of the target. “In recent years, small-molecule PROTACs with good pharmaceutical properties have been reported.”^[15]

While monoclonal antibodies are capable of blocking targets extracellularly, small molecules serving as inhibitors are getting through cell membranes, being highly cell permeable, having them both interrupting in various ways. They represent the two major types of targeted cancer therapy, but a definitely not irrelevant drawback concerning them, is the fact that “About 75% of the human proteome lack active sites (e.g., transcription, scaffolding proteins, and non-enzymatic proteins) and are thus undruggable in this strategy.”^[15]

¹⁸ <https://www.tocris.com/product-type/targeted-protein-degradation>, last downloaded 05/2019

1.3 | Bioorthogonal Chemistry

With knowledge of and insight into application range of nuclear medicine, particularly in targeted radionuclide therapy, we are coming at this point to the more chemical part, introducing the by now indispensable potency of bioorthogonal chemistry reactions for *in vivo* ligations, as being massive engineering tools on molecular level.



Alchemist painting by Arturas Slapsys – artworks (edited)¹⁹

In order to gain such potential chemical reaction partners without any limitation for *in vivo* applications, the characteristic ligation herein relies on high selectivity and reasonable reaction rates. In this regard “Click Chemistry” reactions are the most favoured one.

Starting with the click reaction between azides and alkynes, catalysed by copper(I), abbreviated CuAAC (= copper-assisted Azide-Alkyne cycloaddition), this ligation was firstly discovered in 2002 by Sharpless *et al.*^[16] and Meldal *et al.*^[17], both independently (ref., **Figure 19** | page 19). This kind of reaction displays the modified reaction pioneered by Huisgen^[18] (1963), which needed heat, though and additionally, very often poor selectivity was obtained by forming isomers. Despite being in no need of thermal energy anymore and pointing out appropriate labeling feasibility of, for instance, various proteins in living systems, copper implication in CuAAC reactions leads unfortunately to potential *in vivo*-toxicity.^[19]

This obstacle could be circumvented by emerging the so called Staudinger ligation^[20] (**Figure 18**) and SPAAC reaction (= strain promoted Azide-Alkyne cycloaddition), being the first described bioorthogonal reactions in this case, developed by Bertozzi and coworkers in 2000^[21] and 2004^[22], respectively (**Figure 19**, page 19). The Staudinger ligation is not list-

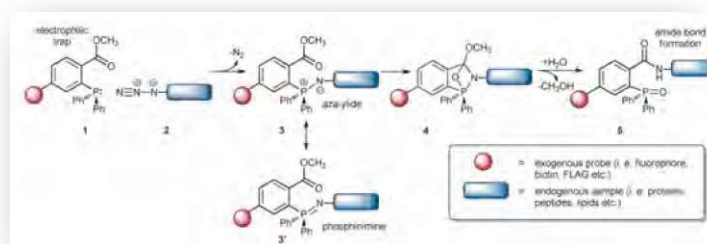


Figure 18 | Staudinger ligation – bioorthogonal reaction between azide and phosphine component to form a bioconjugate^[20]

¹⁹ <https://www.celesteprize.com/artwork/ido:199593/>, last downloaded 05/2019

ed because of having very slow reaction rates in comparison.

It has also been Bertozzi *et al.*^[23] in 2008 who did the first *in vivo* trials based on copper-free click chemistry reaction (SPAAC) for imaging of membrane-associated glycans in zebrafish embryos.

Bioorthogonality in general stands for selectivity in chemical reactions, feasibility for *in vivo* investigations, thus for biocompatibility with hardly any impact on metabolic processes, and is furthermore characterised by adding the touch to as fast reaction kinetics as possible (ref., **Figure 21** | page 20). Although, the Staudinger ligation and SPAAC ligation are both of bioorthogonal nature, they are limited in terms of reaction rates, having comparatively too low speed in living systems' environment.

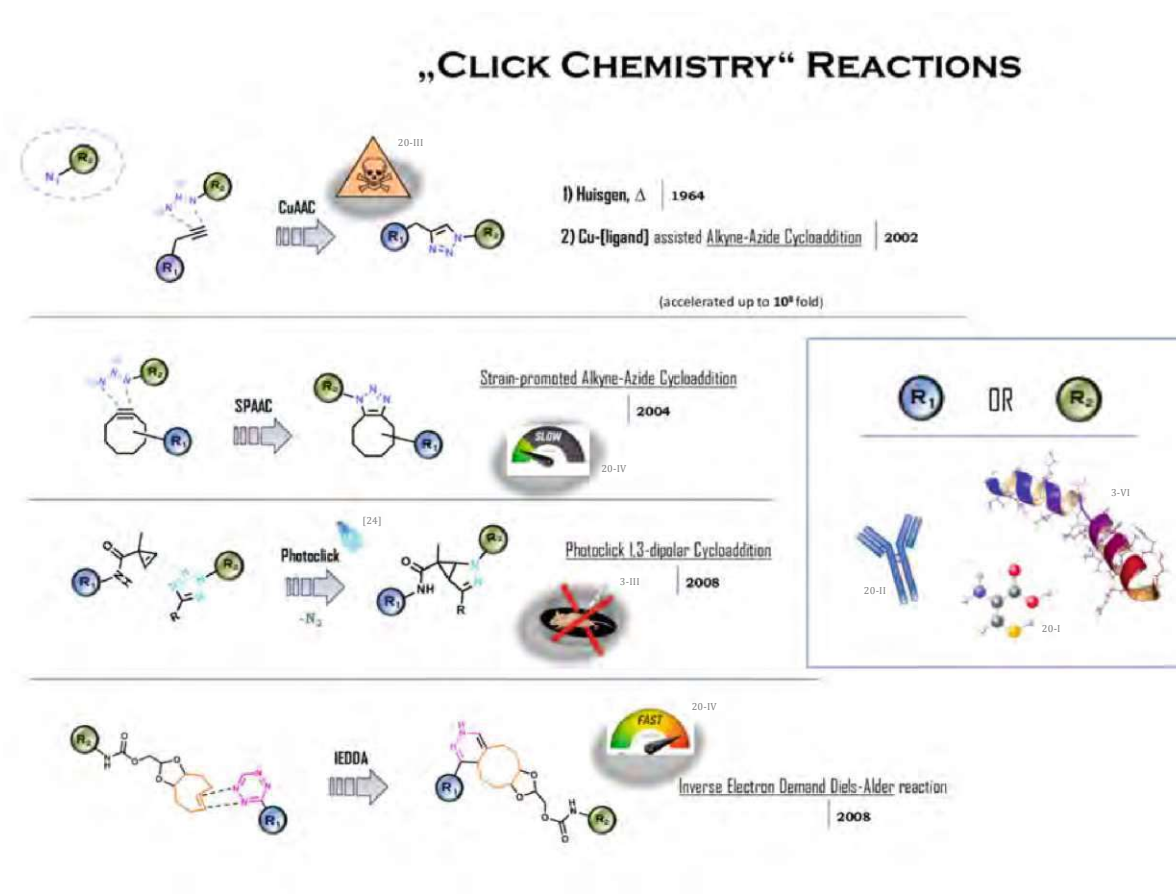


Figure 19 | Overview of various Click Chemistry reactions for labeling strategies in living systems; plus properties with regard to *in vivo* applicability (edited)^{3-III,3-VI,20-II,20-III,20-IV}

Besides, photoclick 1,3-dipolar cycloaddition^[24] is another variant for doing bioorthogonal reactions (**Figure 19**). Nevertheless, the key challenge here, is made up by providing the stimulating light source right next to the chemical compounds which is not the easiest way in technical respect and farther makes it some sort of a special field of application methodology. As a result, we have decided to not rely on this approach, since we want to reach *in vivo* investigations to come, which would be kind of possible herein, but rather challenging, as said before.

Referring to **Figure 19**, the so called Inverse Electron Demand Diels-Alder reaction (= IEDDA), first discovered by the groups of Fox^[25] and Weissleder^[26] in 2008, occurs to be the fastest bioorthogonal ligation reaction amongst all of them (more detailed in **1.3.1**).

^{20-I} <https://www.vectorstock.com/royalty-free-vector/cysteine-proteinogenic-amino-acid-vector-10742395>, last downloaded 04/2019

^{20-II} <https://www.krebsinformationsdienst.de/behandlung/monoklonale-antikoeper.php>, last downloaded 04/2019, ^{20-III} <http://clipart-library.com/toxic-cliparts.html>, last downloaded 04/2019, ^{20-IV} <http://www.canstockphoto.at/herunterladen-langsam-schnell-32280957.html>, last downloaded 04/2019

Figure 20, on the right hand side, describes the reaction between strained alkenes such as *trans*-cyclooctenes (TCO) as dienophiles and on the other hand 1,2,4,5-tetrazines as dienes. Within the inverse electron demand DA ligation, which is based on a [4+2]-

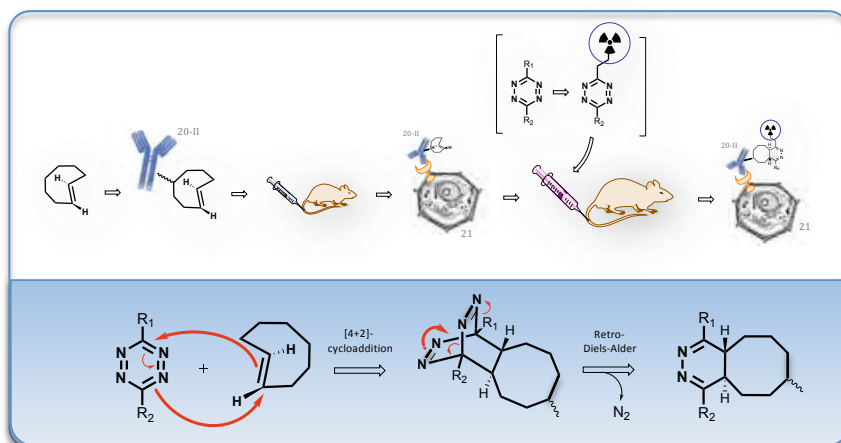


Figure 20 | Mechanism of the IEDDA ligation reaction between 1,2,4,5-tetrazines and *trans*-cyclooctenes (TCOs) for *in vivo* trial (edited)^{20-II,21}

cycloaddition, a tricyclic intermediate is formed and as soon as one equivalent of nitrogen gas is released, dihydropyridazine species as anellated, bicyclic product is obtained.^[27] **Figure 21** shows the comparison between the two variants, being in line for usage in living systems due to their kinetics behaviour, alongside being non-toxic. SPAAC and IEDDA ligations are meant thereby, whereas IEDDA has a characteristic reaction rate, which is 1 000 000 (10⁶) fold higher, bringing this kind of reaction in an outstanding position.

The IEDDA ligation reaction, using tetrazines and TCOs as clicking tools, relies on high selectivity, chemical and biological inertness, biocompatibility to not interfere with physiological processes, high reaction rates as well as accessible engineering for numerous modifications to analyse mechanisms and bioactive functions in living systems (ref., **Figure 21**). As a consequence it represents an impressive tool for emerging additional engineering opportunities on molecular level, including turn-on probes^[28], bioorthogonal PET imaging approaches^[29], protein labelling^[30], engineering extracellular matrices^[31], very currently investigated Click-to-Release strategies^{[32][33]}. Biological proceedings are operated and desired vital function for human beings are reachable.

KEY POINTS

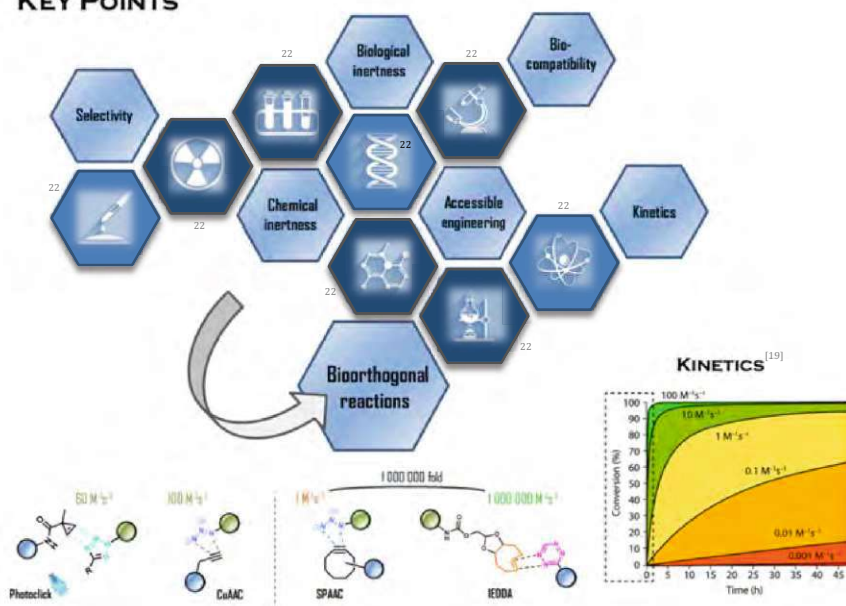
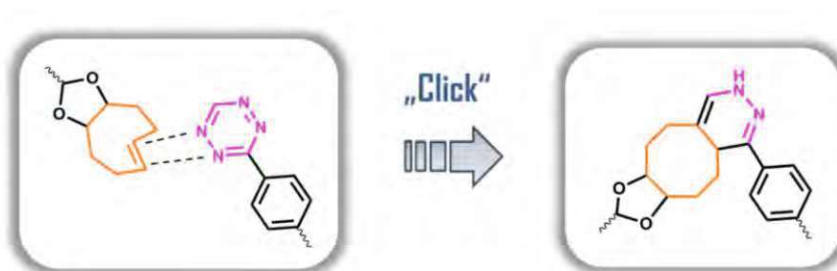


Figure 21 | Key points of bioorthogonality; plus kinetic characteristics of different click chemistry reactions (both references edited)^{[19],22}

²¹ https://pngtree.com/freepng/color-nuclear-structure_3526126.html, last downloaded 04/2019

²² <https://de.vecteezy.com/vektorkunst/435830-wissenschafts-laborikonen-eingestellt>, last downloaded 05/2019

1.3.1 | IEDDA – Inverse electron demand Diels-Alder reaction



In this chapter, the field of operation, the physical properties and the synthetic accessibility of IEDDA bioorthogonal reactions are highlighted distinctly, by going into more detail.

Since these rapid ligation reactions meet the requirements for *in vivo* efforts in superior manner like exemplary reported by van Duijnhoven, Rossin and coworkers^[34] concerning pretargeted radionuclide strategies, a wide variety of applications in biomedical research divisions is now approachable. These include, “but not limited to, (i) bioconjugation; (ii) molecular imaging of proteins, surface antigens, small molecules/modified drugs, lipids, or glycans; (iii) cell modification with nanomaterials for clinical diagnostics; (iv) the development of smart fluorogenic probes; (v) bioorthogonal approaches to the identification of drug targets in living cells; and (vi) healthcare materials.”^[27]

As the IEDDA ligation is based on a Diels-Alder reaction, but with inverse electron demand, the electron poor diene lowers the LUMO-orbital (= lowest unoccupied molecule orbital), whereas the electron rich dienophile raises the HOMO-orbital (= highest occupied molecule orbital) (Figure 22). Consequently, the energy gap between $HOMO_{dienophile}$ und $LUMO_{diene}$

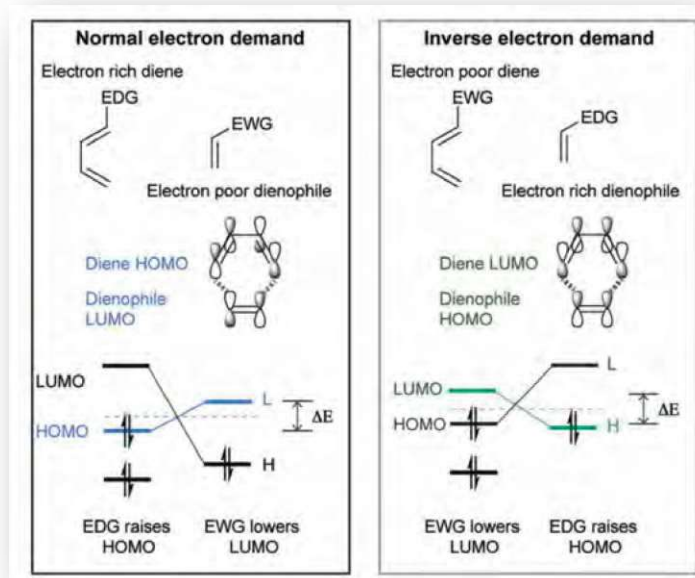


Figure 22 | Molecule orbital diagram – comparison of normal and inverse electron demand DA^[19]

is declining and in contrast this leads to enhancement of reaction rate.^[19]

“Therefore, by electronically tuning the cycloaddends it is possible to manipulate the $LUMO_{diene} - HOMO_{dienophile}$ energy gap and enhance their reactivity.”^[19] The diene is herein representing the 1,2,4,5-tetrazine, while the *trans*-cyclooctene (TCO) component is depicted by the dienophile.^[19]

So again, the reactivity of the clicking agents depends on their substituents. Figure 23 shows the trend of 1,2,4,5-tetrazines, from high reaction rates to rather low ones by introducing different electron withdrawing groups (EWG) and electron donating groups (EDG). Notably, ester groups as being EWG and thus lowering the LUMO energy,

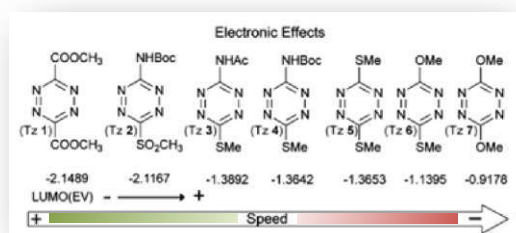


Figure 23 | Dependency of reactivity with regard to electronic effects induced by substituents of tetrazines as dienes (edited)^[19]

provide high accelerated reactivity in click reaction. On the contrary, methoxy groups have an opposite effect by donating electrons and farther raising the energy of LUMO orbital, which is why they are reducing ligation speed.^[19]

Several synthetic routes of 1,2,4,5-tetrazines as building blocks are described by Clavier and Audebert^[35] with corresponding reaction mechanisms included, as well as by Mayer and Lang^[36] with their use in biology.

In the case of dienophiles, olefinic dienophiles are described to outmatch acetylenic ones, because of the less electron withdrawing character of the double bond. Furthermore, of course EDG in dienophiles, raise HOMO energies and lead to high reaction kinetics (ref., **Figure 22**). “Independent from the electronic effect of the dienophile substituents, ring strain plays the most important role in the IEDDA reaction rate by raising the HOMO_{dienophile}.”^[19] As depicted in **Figure 24**, cyclopropene in comparison with related usual cyclic alkenes cyclobutene, cyclopentene, cyclohexene and *cis*-cyclooctene, has the highest ring strain and forces click reaction to be carried out most rapidly.^[19]

On the contrary, *trans*-cyclooctene (TCO) in the course of computational studies was predicted to have lower reaction rates by interacting with tetrazine reaction partners, due to lower conformation energy (crown formation, ref., **Figure 24**). Nevertheless, TCOs are 7 orders of magnitude faster reacting than *cis*-cyclooctenes (half-chair conformation).^[19]

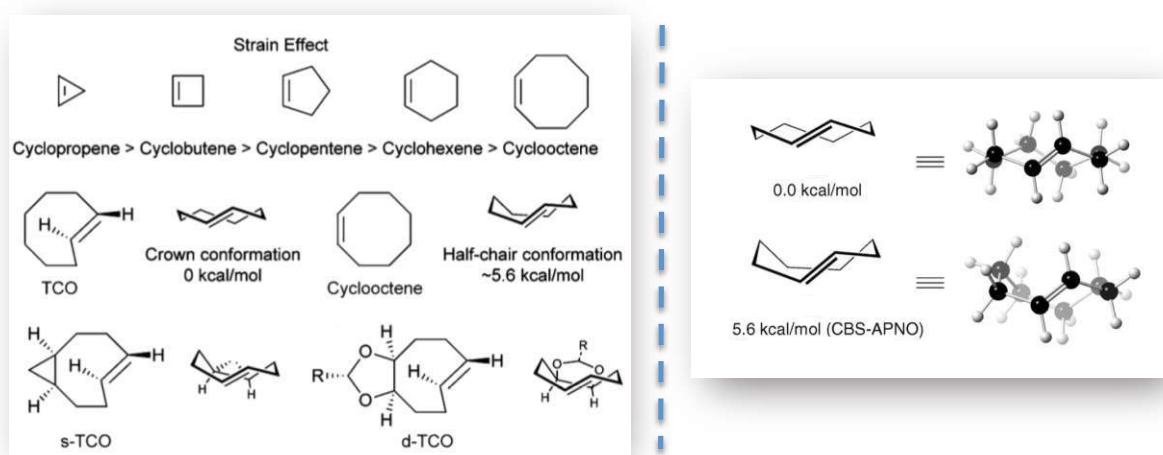


Figure 24 | Strain Effect of different dienophiles; crown conformation of *trans*-cyclooctene (TCO); plus *cis*-ring fusion locks ring strain for *s*-TCO, *d*-TCO (left) (edited)^[19]; TCO conformations – crown vs. half-chair (right) (edited)^[37]

“Based on *ab initio* calculations, the fusion of a cyclopropane ring with *trans*-cyclooctene to form *s*-TCO was proposed as a strategy to induce the formation of a non-crown conformer which was expected to increase the reactivity towards tetrazines.”^[19] The result for the highly strained *s*TCO was extraordinary, surpassing the original TCO with reaction kinetics that are 160 fold higher. Since *s*TCO is not quite manageable in terms of stability and hydrophilicity, a similar reactive ring strain compound was evolved. The *cis*-dioxolane-fused TCO, abbreviated *d*TCO, is also plenty applicable for doing rapid labelling in living cells, after all reacting still 27 times faster than the original TCO.^[19]

1.4 | Triggered Cell Uptake of Auger emitters

The idea of mediating Cell Uptake strategy for reaching triggered Auger therapy later on, was sophisticated by Prof. Mindt Thomas, Head of Molecular Imaging Biomarkers unit at the Ludwig Boltzmann Institute of Applied Diagnostics, situated at the General Hospital in Vienna. It was him together with my supervisor Univ. Ass. Denk Christoph who merged a cooperative partnership to work on this very enthralling and promising topic.

As broached in 1.1.3 and 1.2.1 our main aim within the scope of this work has been to deliver a large number of Auger electrons emitted by radionuclides, being channelled into the nucleus and exerting cancer cell death via DNA break. Therefore, we have been in needs of targeting only the tumor cells specifically, leaving out healthy ones uninvolved, and arranging a Cell Uptake in the next step (Figure 25).

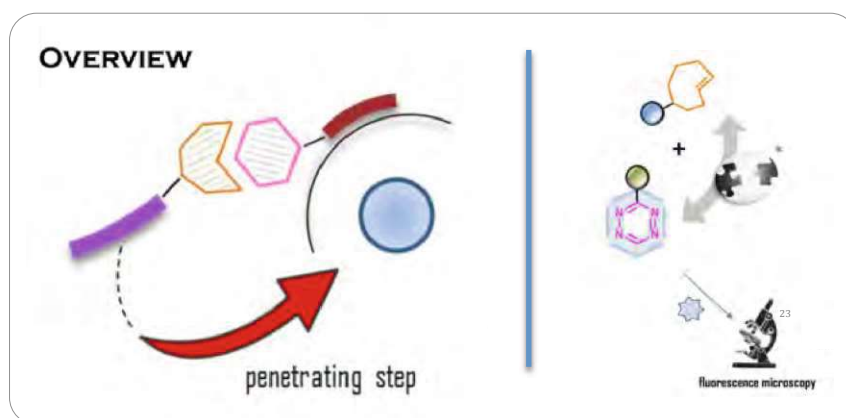


Figure 25 | Cell Uptake strategy in theory – combination of specific, extracellular binding and a cell-penetrating peptide; mediated by Click Chemistry reaction and visualized by fluorescence microscopy (edited)²³

Considering that, we have chosen bombesin peptide, more precisely a bombesin analogon with the shorthand symbol RM26, to realise a specific binding step at tumor cell receptors extracellularly. The cysteine tagged TAT-peptide variant [47-57] emerged to ensure the translocation through the cell membrane into the nucleus, and furthermore to be modified very easily within a bioconjugation reaction. Besides, both peptides can be easily linked together via labelling of two different and matching clicking tags on each compound, in particular these are a tetrazine and a *trans*-cyclooctene [TCO] moiety, respectively – bombesin species will also have a fluorescent agent incorporated.

1.4.1 | Tumor targeting peptide

Tumor cells have several different receptors over-expressed as potential binding regions, which allow diseased parts in the human body to be addressed specifically by receptor-ligand interactions. As reported by Valverde, Huxol and Mindt^[38], bombesin as the amphibian peptide analogon of the mammalian Gastrin-Releasing Peptide (= GRP) has a high affinity and specificity towards GRPR receptors that are over-expressed “in a variety of clinically relevant tumors including prostate, breast, colon, and small-cell lung

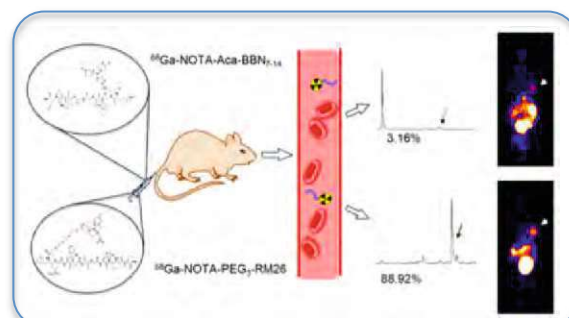


Figure 26 | Comparison of GRPR agonist (top) and GRPR antagonist (bottom, RM26)^[39]

²³ <https://www.kisspng.com/png-optical-microscope-clip-art-black-and-white-art-de-191880/>, last downloaded 05/2019

carcinoms.”^[38] The bombesin RM26 GRPR antagonist is already investigated and applied in nuclear medicine, being already reported by Cheng *et al.*^[39] Within their work they have compared a GRPR bombesin agonist BBN₇₋₁₄ and antagonist RM26 (**Figure 26**, page 23). In this context, the antagonist RM26 species demonstrated more favorable *in vivo*-pharmacokinetics as well as metabolic stability, being feasible for PET-imaging of prostate cancer.^[39]

This is why we have decided to choose bombesin antagonist peptide RM26 for our concept (**Figure 27**). This “carrier molecule” contains the unusual amino acid Statin^[40] and has been modified with 1,2,4,5-tetrazine as well as the fluorescent agent BODIPY, respectively. Further on, “Radio-labeled GRPR antagonists are not internalized into cells but exhibit a persistent attachment to tumors resulting in an overall increased accumulation of radioactivity at tumors and metastases *in vivo*.”^[38], which has been previously reported by Mansi *et al.*^[41] However, Mansi and coworkers also described that cell internalization might be induced by bombesin RM26, even though in small amount, and thus has to be minded during *in vitro* investigations.^[41]

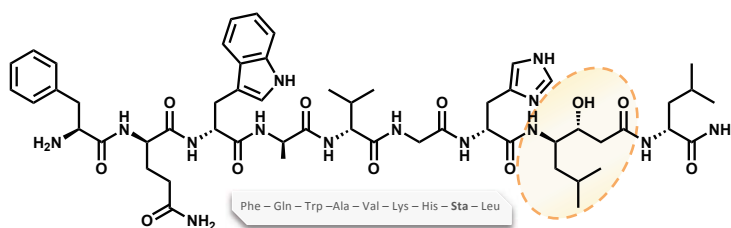


Figure 27 | Bombesin [RM26] analog as GRPR antagonist; contains unusual Statin^[40] amino acid; 9 amino acids

1.4.2 | Cell-penetrating peptide [CPP]

A wide variety of cargoes featured with therapeutic effectiveness are hydrophilic by nature. When it comes to transfer them into certain cells regarding specific approaches, the cell membrane very often turns out to only let pass compounds that rather imply sufficient hydrophobicity, regardless of whether size they are, ranging from small drug molecules, to peptides or even more complex proteins as well as DNA/RNA structures. In order to overwhelm this interaction issues, so called cell-penetrating peptides, abbreviated named CPPs, meet the requirements to cross cell membranes and are “considered one of the most promising tools to improve non-invasive cellular delivery of therapeutic molecules”^[42] (**Figure 28**).^[42]

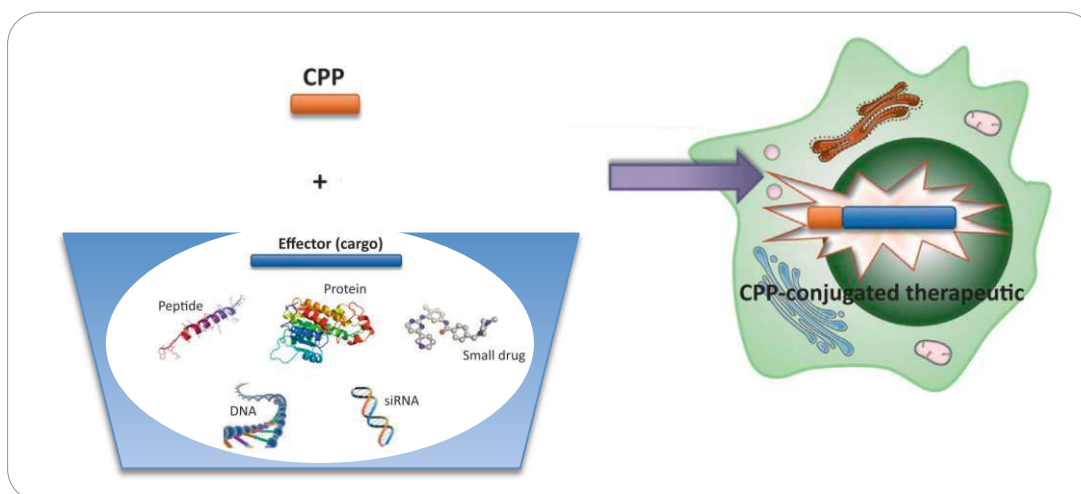


Figure 28 | Cell-penetrating peptides [CPP] enabling native hydrophilic drugs to get through the cell membrane as CPP-effector conjugates and reach intracellular areas – thus, achieving therapeutic effectiveness getting enhanced (edited)^[42]

Therefore, CPPs manage the intended access to intracellular areas, providing versatile cell uptake strategies to be coming up soon. They are capable of channelling cargoes such as peptides, proteins, small drugs or DNA strands into cells by either creating a pore formation, or an inverted cell formation, or by means of endocytosis (**Figure 29**).^[42]

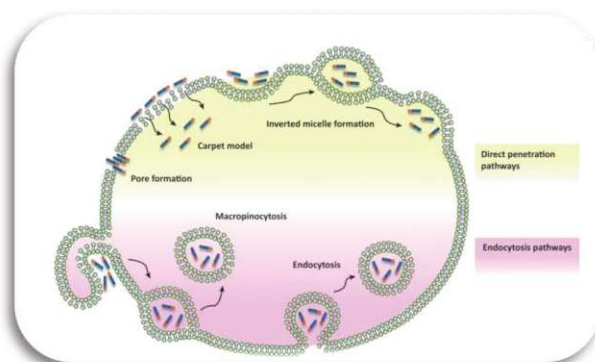


Figure 29 | Cell entering options of CPPs – endocytosis; inverse micelle formation or pore formation^[42]

The cationic TAT (= Transactivator of Transcription) protein derived from the HIV-1 (= Human Immune-deficiency Virus) is among the well-investigated CPPs described by Raucher and Ryu^[43], and has been firstly discovered in 1988 by two independent groups, headed by Frankel and Pabo^[44], as well as Green and Loewenstein^[45]. The arginine-rich peptide is translocated in intracellular area via macropinocytosis (ref., **Figure 28**, page 24) as one endocytotic pathway, leading to nucleus internalization of CPP (nuclear localisation signal - NLS), which has been reported by Trabulo *et al.*^[46]

Since the basic arginine groups are responsible for cell uptake action, researchers find out that the “key motif for transduction could be reduced even more”, reported by Guidotti *et al.*^[42] In this regard we used the amino acid sequence [47-57] of TAT protein, with a cysteine tag for modification (**Figure 30**). “This was ascribed to the capacity of the guanidine head group of arginine to form bidentate hydrogen bonds with the negatively charged carboxylic, sulfate, and phosphate groups of cell membrane constituents, leading to cellular internalization of CPPs under conditions of physiological pH.”^[42]

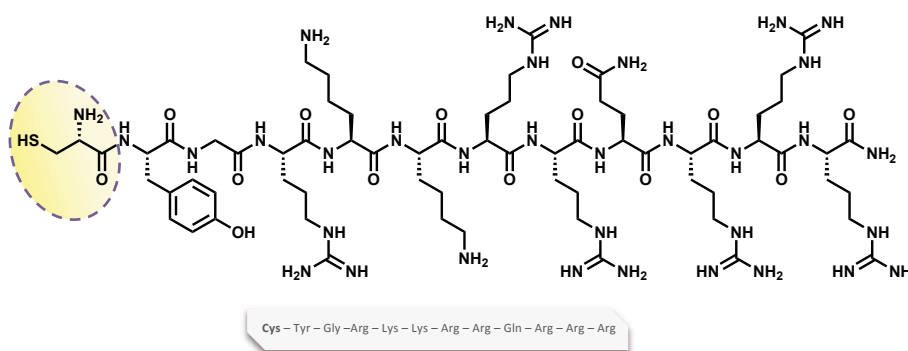
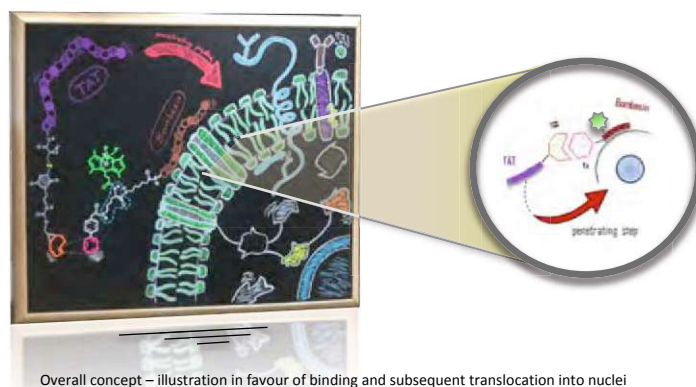


Figure 30 | TAT [47-57] analogon with a cysteine tag; 12 amino acids

1.4.3 | Overall Concept

The previously described IEDDA ligation reaction between tetrazines and *trans*-cyclooctenes was predestinated for linking together two tumor targeting carrier molecules. In order to get bound specifically to the targeted cancer cells, a peptide bombesin RM26-analogue modified with fluorescent agent and tetrazine, representing the clicking tool, was chosen. The second peptide, a cell penetrating peptide [CPP] named TAT, was renownedly supposed to enter various kinds of cells due to feasibility to get through cell membranes. As soon as they interact with each other, both undergo the Click Chemistry reaction to form the anellated product dihydropyridazine (ref., **Figure 20** | page 20).



The optimal case we have aimed for during this thesis, is to accomplish not only the cell entering step of TAT peptide after the click chemistry reaction, but farther realising some sort of pulling the bombesin species off the GRPR receptor and subsequently dragging it all along through the cell membrane, until both peptides including BODIPY fluorescent agent end up within the cell nucleus (**Figure 31**).

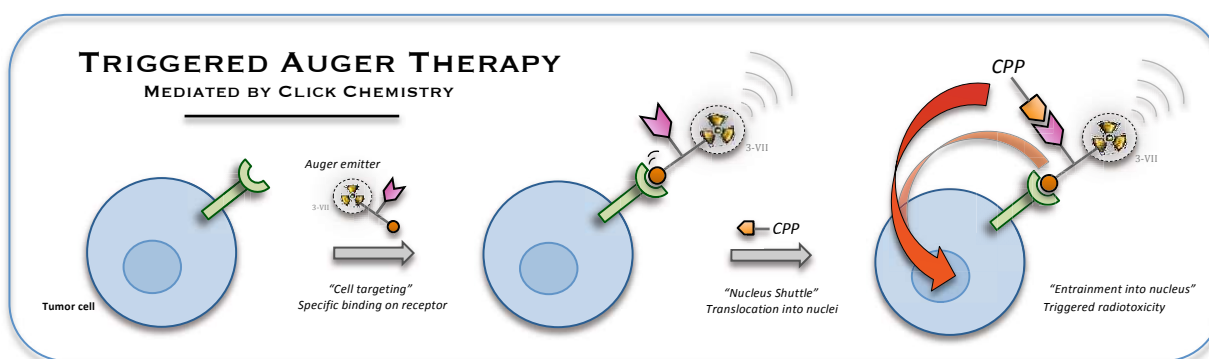


Figure 31 | Cell Uptake Strategy – cell targeting step allows diagnostics; bioorthogonal reaction mediates triggered Auger therapy via translocation step into nucleus and thus, transforms diagnostics into therapeutics optionally^{3-VII}

Therefore, this approach has to be evaluated particularly in terms of feasibility, but also compound stability, reaction kinetics and site specificity. In order to achieve the proof of concept, we are generally able to visualize “cell ongoings” via fluorescence microscopy, capturing fluorescent agent’s induced emission.

As soon as *in vitro* tests (ref. **2.4**) show positive results in the course of fluorescent microscopy, BODIPY dye will be substituted with upcoming radionuclides that are usually chemically bonded in complex formation, using appropriate ligands.

The radioisotopes that emit Auger electrons ensure non-cytotoxic diagnosis by specific binding on tumor cell receptors. As soon as TAT peptide, modified with corresponding clicking tag TCO, interacts with tumor targeted bombesin species, triggered Auger therapy is applicable via translocation into cell nucleus. Overall, a click chemistry reaction mediates the cell uptake to trigger radiotoxicity – thus, transforming diagnostics into therapeutics will be achievable.

KEY POINTS

- 1) Transforming diagnostic radionuclides into therapeutics
- 2) Strategy for triggered Auger emitters translocation into cell nucleus
- 3) Specific binding of radiolabeled carrier molecule onto tumor cells
- 4) Click chemistry mediated translocation of radioisotope into nucleus via using CPP to trigger radio-toxicity
- 5) *in vitro* assay - proof of concept

The cell-ongoings we shall observe via *in vitro* trials using fluorescence microscopy are illustrated in **Figure 32**. After specific binding step of bombesin species, the bioorthogonal ligation between 1,2,4,5-tetrazine and TCO moieties mediates the cell-penetrating step of TAT peptide. Having both peptides translocated into the cell nucleus in the end, by channelling through the cell membrane, this would accomplish the proof of concept and would lead to promising initial position for triggered Auger therapy.

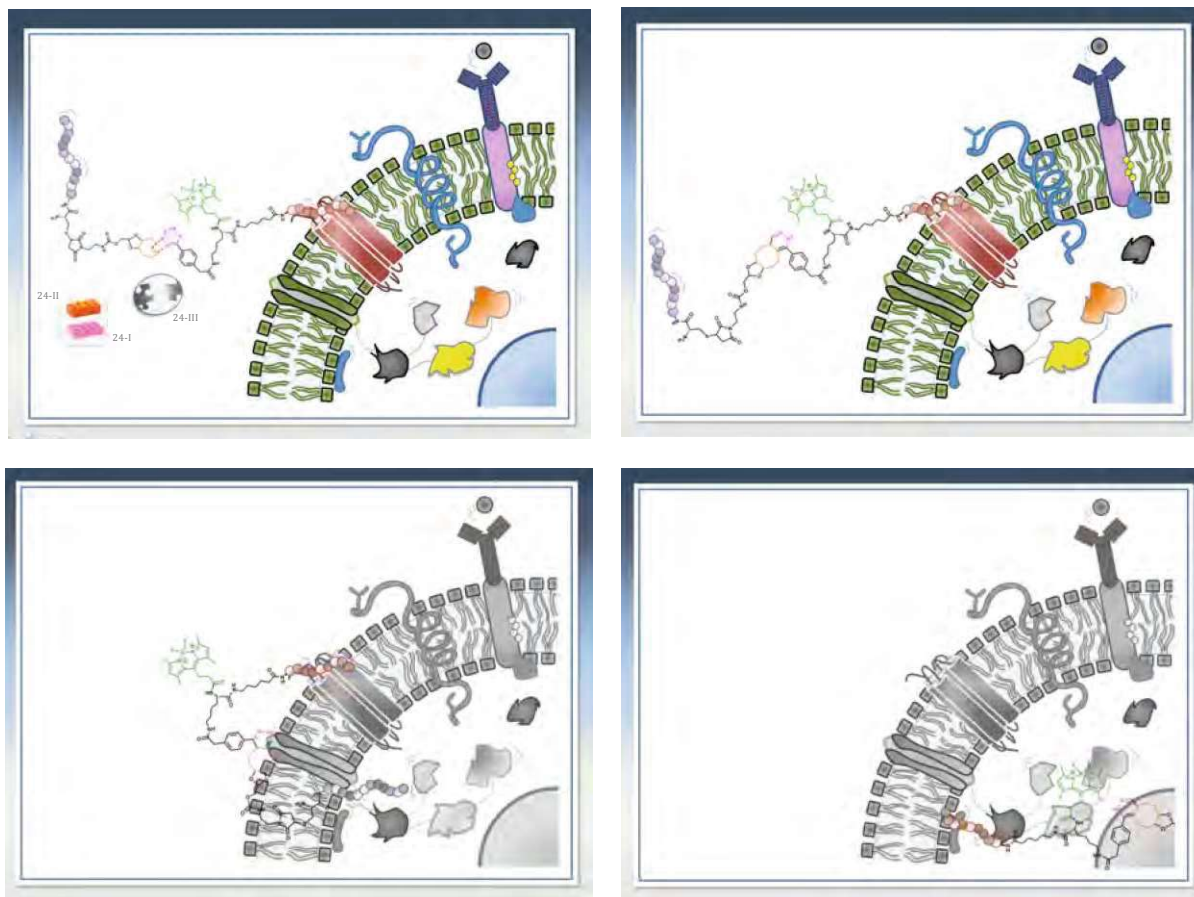


Figure 32 | Illustration of Cell Uptake strategy; specific binding step, bioorthogonal ligation, translocation into cell nucleus (edited)^{24-I,24-II,24-III}

^{24-I} http://www.brick-shop.de/product_info.php?info=p4461_lego-stein-2x4-pink--3001-.html, last downloaded 05/2019, ^{24-II} http://www.brick-shop.de/product_info.php?info=p223_lego-stein-2x4-orange--3001-.html, last downloaded 05/2019, ^{24-III} <https://www.scarymommy.com/puzzles/>, last downloaded 05/2019

2 | RESULTS AND DISCUSSION

2.1 | Synthesis of Building Blocks

In order to acquire the considered modified peptides for doing the Cell Uptake strategy, first of all, building blocks for being the start materials in terms of modification had to be synthesized. For that reason, different 1,2,4,5-tetrazines as well as *trans*-cyclooctenes (TCOs) were formed in the early stage of this thesis. Peptide modification strategies and the synthesis of a ligand for upcoming radionuclide complex formation were conducted next. Besides, also building blocks unrelated to our core strategy were synthesized and stocked, which allow further modifications in simple chemical reactions.

2.1.1 | Synthesis of 1,2,4,5-Tetrazines

As both peptides each need to have one of the two smart clicking tools installed, we started with the synthesis of two similar 1,2,4,5-tetrazines **2** and **3**. Even though the methyl containing one indicates more chemical stability, the electron donating methyl group entails decreased reactivity in IEDDA click reactions than the unsymmetrically substituted H-tetrazine, which has probably also higher reaction rates due to lower steric hindrance. Within this course we successfully prepared a total of four different unsymmetrically substituted tetrazines **2**, **3**, **24** and **27**, whereas all, with the exception of the red oil **27**, gave characteristic pink crystals.

H-Phenylalanine-D,L-(Boc)-1,2,4,5-tetrazine **2** was synthesized by using the corresponding phenylalanine-benzonitrile compound as starting material, based on previously described procedure by Sauer *et al.*^[47] and Ni with coworkers^[48]. **Figure 33** illustrates the proposed mechanism by Li and colleagues^[49] on this kind of tetrazine formation, implying sulphur.

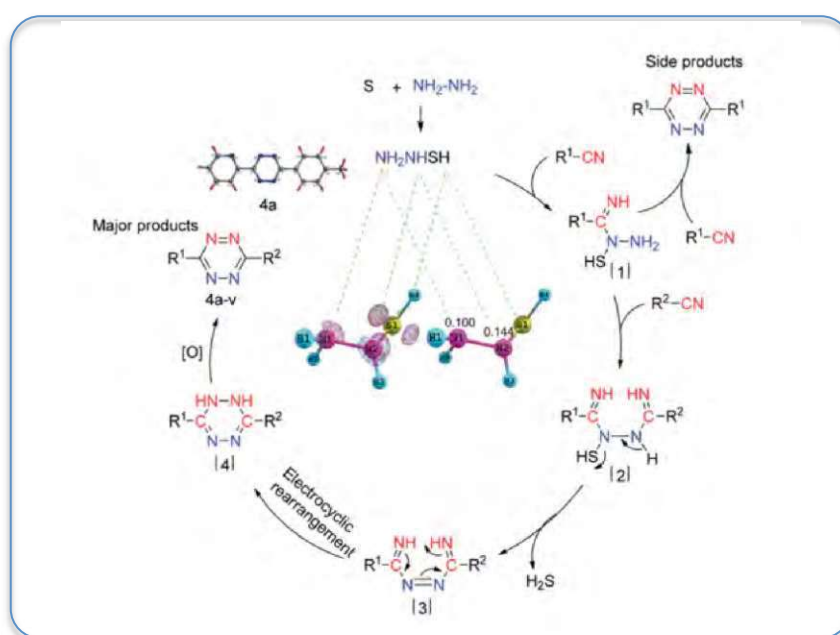
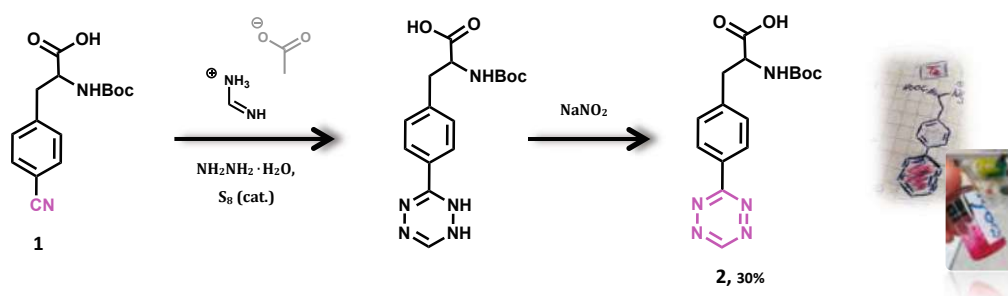


Figure 33 | Mechanism of tetrazine formation by using elementary sulphur as catalyst^[49]

Once adduct NH_2NHS of sulphur and hydrazine is generated, it attacks the carbon atom of nitrile starting material in nucleophilic fashion. A second nucleophilic addition follows, either on a second nitrile compound or like in our case an amidine derivative to do a so called Addition-Elimination-Rearrangement to end up with 1,2-dihydro-1,2,4,5-tetrazine, as volatile hydrogen sulphide is released one step prior. In the last sequence, aromatization is attainable *via* oxidation by adding sodium nitrite, for instance. All in all, either symmetrically or unsymmetrically substituted tetrazines are approachable.

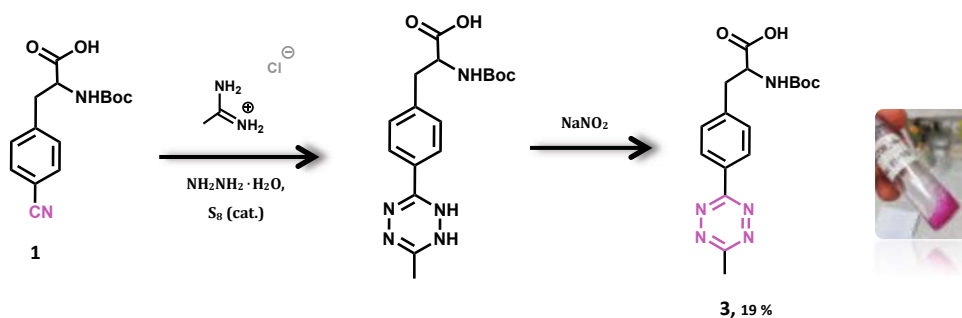
So in the presence of sulphur as catalyst, hydrazine monohydrate accompanied with formamidine acetate, led to desired ring closure towards the 1,2-dihydro-1,2,4,5-tetrazine species (**Scheme 1**). Extraction steps with dichloromethane were about to follow. As the yellow intermediate stayed dissolved in water layer, further reaction was carried out in aqueous phase and addition of sodium nitrite as well as 1 N HCl led to obtaining the oxidized, unsymmetrically substituted pink product, H-phenylalanine-D,L-(Boc)-1,2,4,5-tetrazine **2**. With yields of about 30 %, this synthesis was rather pleasurable.



Scheme 1 | Formation of H-Phenylalanine-D,L-(Boc)-1,2,4,5-tetrazine with sulphur (cat.)

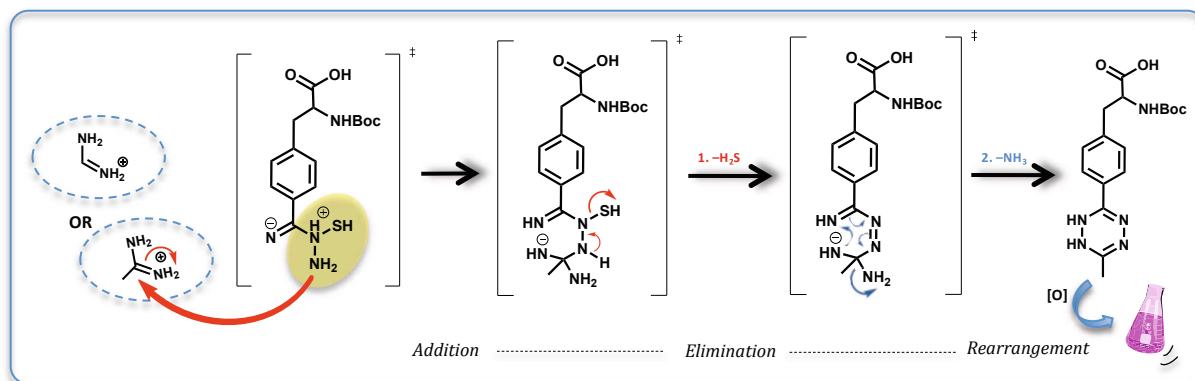
At the point where no excess of hydrazine monohydrate was left anymore because of neutralisation with hydrochloric acid, bubbling started due to generating NO gas out of HNO_2 , which had been formed from sodium nitrite-salt. Prior to any further addition of 1 N HCl, the flask was pivoted and allowed to stand until no more bubbles were visible. Volatile symmetrically substituted H-1,2,4,5-tetrazine as side-product was separated *via* evaporation, before purification *via* NP-LC chromatography followed.

The same procedure was conducted in case of Me-phenylalanine-D,L-(Boc)-1,2,4,5-tetrazine **3** formation, with the exception of using acetamidine hydrochloride instead of formamidine acetate (**Scheme 2**), and with moderate yields of 19 %.



Scheme 2 | Formation of Me-Phenylalanine-D,L-(Boc)-1,2,4,5-tetrazine with sulphur (cat.)

The particular mechanism for both, unsymmetrically substituted Me- and H-1,2,4,5-tetrazine formation is illustrated in **Scheme 3**, by reference to methyl containing phenylalanine-tetrazine.



Scheme 3 | Mechanism for both unsymmetrically substituted 1,2,4,5-tetrazine formations (H, Me) with sulphur (cat.)

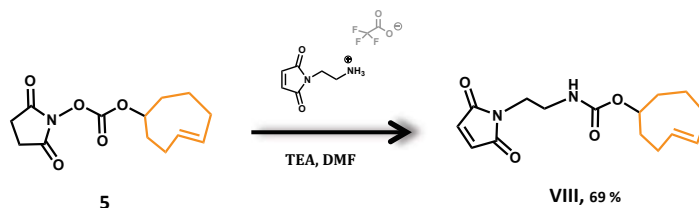
Mechanistic steps are equal to those described for **Figure 33** (page 28), with the exception of additional elimination of gaseous ammonia to enforce ring closure.

As the 1,2,4,5-tetrazines **24** and **27** were not used in the main part of this thesis, the according syntheses are described in **2.3.2** and **2.3.3**, respectively.

2.1.2 | Synthesis of *trans*-Cyclooctenes [TCOs]

The matching clicking tool for 1,2,4,5-tetrazines is represented by the *trans*-cyclooctene species, abbreviated TCO. In order to do a simple thiol-maleimide-bioconjugation reaction with the to be modified, cysteine tagged TAT peptide, we prepared the maleimidyl-TCO carbamate **VIII** compound.

Therefore, NHS-TCO carbonate (*N*-hydroxysuccinimidyl-TCO) **5** was dissolved in DMF, dry and subsequently after adjusting basic condition by using TEA, the starting material **5** reacted with *N*-(2-aminoethyl) maleimide trifluoroacetate to obtain product formation (**Scheme 4**). NHS group served as good leaving group in this nucleophilic S_N2-substitution reaction. The impure maleimidyl-TCO carbamate **VIII** was purified *via* RP-HPLC chromatography, ending up with good yields of 69 %.

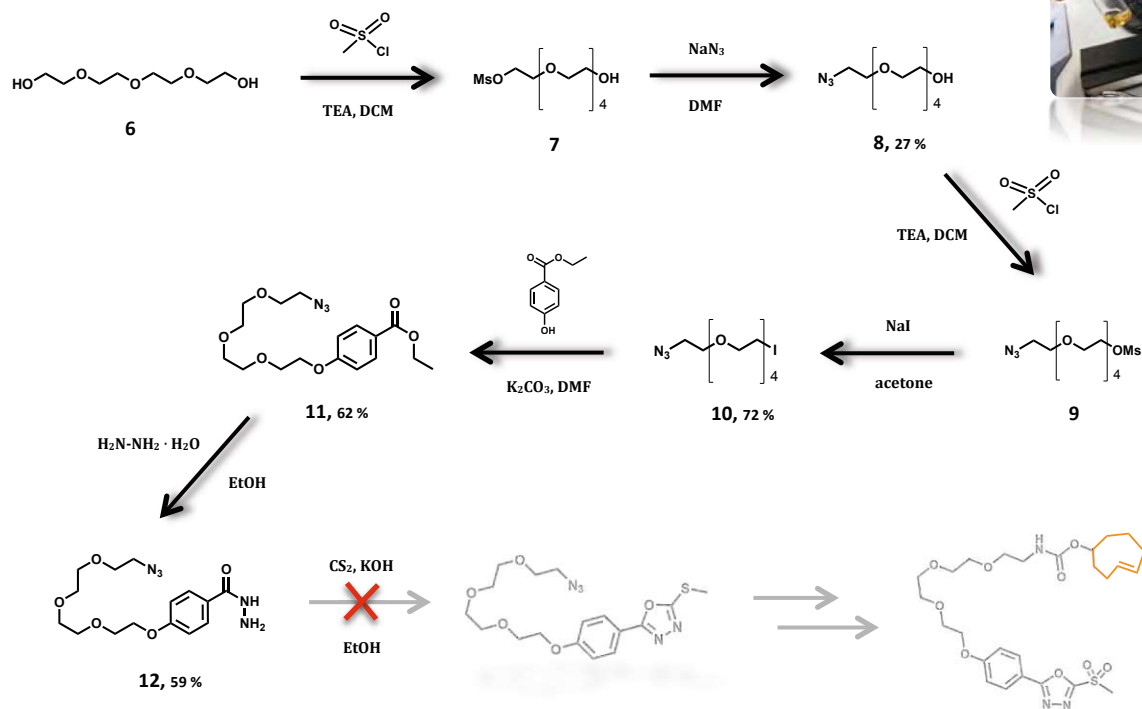


Scheme 4 | Formation of maleimidyl-TCO carbamate in a S_N2-reaction



Since the bioconjugation reaction of **VIII** with TAT peptide failed (see **2.2.2**), we aimed for site-specific conjugation with sulfone linkers, in particular with a so called Barbas linker, reported by Patterson *et al.*^[50] The phenyloxadiazole sulfone linker bioconjugation is supposed to have improved *in vivo* stability compared to more generally applied, above mentioned maleimide-thiol conjugation.

The synthetic route for Barbas linker preparation is depicted beneath in **Scheme 5**.



Scheme 5 | Synthetic route for preparation of the Barbas linker

Synthesis steps up to product **10** inclusively were conducted according to procedure of Goswami *et al.*^[51] Right at the start, tetraethylenglycol [TEG] was mono-mesylated by adding methylsulfonylchloride (MsCl) dropwise under basic conditions. As a side-product also the corresponding di-mesylated compound was formed, statistically. At this stage no yields are stated, since **7** was not isolated, previous to following azidation reaction step in acetone. The overall yields for obtaining mono-azide-tetraethylenglycol **8** were quite low with about 27 %, which was certainly owed to the statistical distribution of desired product and side-product.

In order to form the iodo-azide-TEG **10** via Finkelstein reaction using sodium iodide, once again a mesyl-group serves as a good leaving group. The mesylation was conducted equally to mentioned above one and the formed azide-mesylated intermediate product **9** was used in nucleophilic substitution S_N2 -reaction without further purification. In this case compound **10** was obtained in much accepting overall yields of 72 %.

Preparation of products **11** and also **12** were carried out based on research work of Toda and co-workers^[52]. Within the next synthetic step, the formation of azide-TEG-benzoic acid, ethyl ester **11** was achieved by using starting material **10**, potassium carbonate and 4-hydroxybenzoic acid, ethyl ester in DMF. Once more, suitable yields amounting to 62 % were observed.

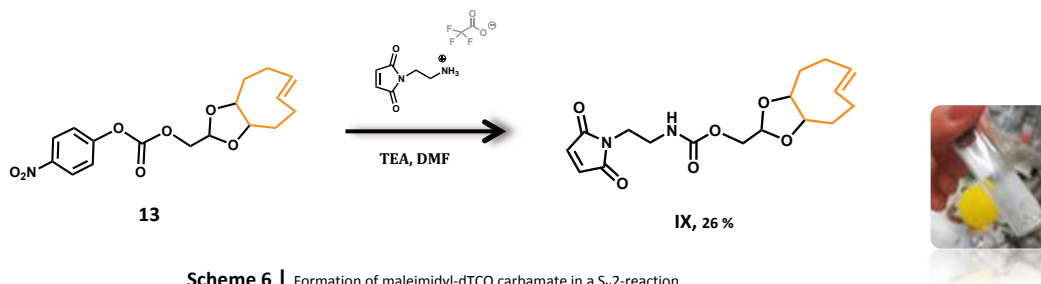
Since the addition of 1.5 eq hydrazine monohydrate to compound **11** in ethanol led to very low yields to afford azide-TEG-benzoic acid, hydrazide **12**, we modified the procedure by adding even 5 eq of hydrazine monohydrate. In doing so, highly increased yields of 59 % were obtained.

Despite that, the cyclisation to form the (methylthio)-1,3,4-oxadiazole by addition of carbon-disulfide and potassium hydroxide, failed in a total of three formulations. Since no starting material **12** was left anymore, the TCO-modified Barbas sulfone linker was not reached. Due to the fact, that we concurrently pursued another strategy, we considered to neglect the time-consuming preparation of Barbas linker component, even if synthesis was straight forward.



Regarding the products **8**, **11** and **12**, NP-chromatography was applied for purification steps, whereas in case of compound **10** simple filtration was sufficient.

Although the bioconjugation reaction between TAT peptide and maleimidyl-TCO carbamate was not achievable, we did not avert this kind of approach and successfully prepared a very similar compound **IX** (ref., **Scheme 6**).



Scheme 6 | Formation of maleimidyl-dTCO carbamate in a S_N2 -reaction

Therefore, the (para-nitrophenol)-dTCO carbonate [PNP-dTCO] **13** was used as starting material to react with (2-aminoethyl)maleimide trifluoroacetate (ref., **Scheme 4** | page 30) under basic conditions within 1 hour. The crude product was purified via RP-HPLC chromatography. With yields of 26 %, maleimidyl-dTCO carbamate **IX** was obtained in sobering manner, compared to **VIII**.

2.2 | Modification of Tumor Targeting Carrier Molecules

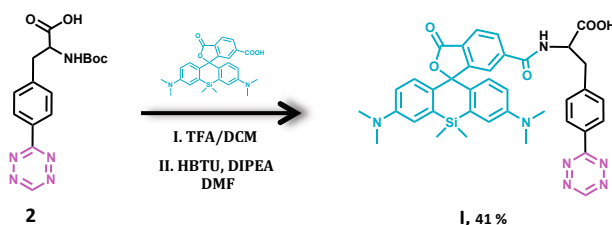
2.2.1 | Modifying Bombesin peptide [RM26]-analogon

The bombesin-RM26 analogon, which was synthesized at the Ludwig Boltzmann Institute of Applied Diagnostics by Marie Brandt, was meant for being modified twice to afford a carrier molecule that is linked to 1,2,4,5-tetrazine clicking tool and fluorescent agent SiR-Dye (= *Silicon-Rhodamine species*), respectively.

As reported by Kowada *et al.*^[53], BODIPY (= *Boron-dipyrromethene species*) dye shows so called FRET (= Förster resonance energy transfer, ref., **Figure 34**) especially when around thiol-containing compartments in living systems. Within this energy transfer BODIPY fluorescent agent is quenched and shows no longer characteristic emission. Hence, SiR-Dye, depicted in **Scheme 7**,

was used for labeling strategy prior to BODIPY. Additionally, fluorescence microscopy provides images with higher resolution by using SiR-Dye species, thanks to low background emission.

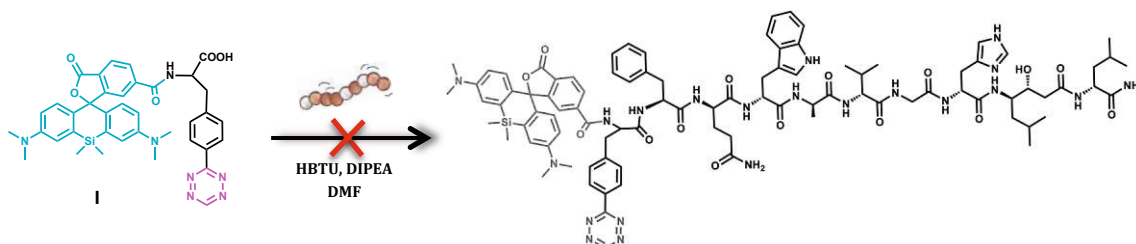
The first synthetic strategy involved the ligation of H-phenylalanine-1,2,4,5-tetrazine **2** with fluorescent agent SiR-Dye in a very common HBTU coupling reaction (**Scheme 7**).



Scheme 7 | Formation of SiR-Dye coupled tetrazin-3-yl-D,L-phenylalanine

At first instance, Boc protecting group of 1,2,4,5-tetrazine derivative **2** was cleaved off via addition of 16 % TFA/DCM mixture and volatiles removed in *high vacuo*. For the coupling reaction, SiR-Dye acid was activated with HBTU reagent and base DIPEA for at least 20 min, before deprotected H-phenyl-alanine-1,2,4,5-tetrazine was added. Purification via RP-HPLC chromatography led to coupled product Tz-SiR-Dye **I** with yields of 41 %.

Via another HBTU-coupling reaction, the SiR-Dye-Tz compound **I** should be linked to bombesin RM26 analogon to afford the looked-for modified tumor targeting peptide (**Scheme 8**).



Scheme 8 | Formation of SiR-Dye-Tz-bombesin RM26 failed

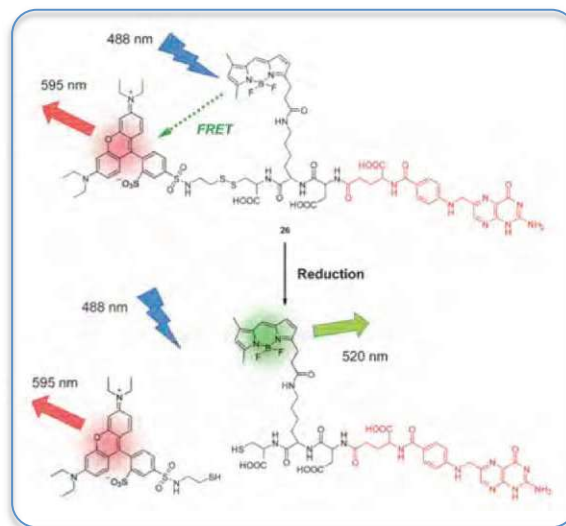


Figure 34 | FRET phenomena in living system, involving thiol groups^[53]

The same procedure as previously described was carried out for this labeling step. However, the synthesis failed, as we could not see any product formation in HPLC-MS measurements. More likely it seemed that the starting material **I** was reacting in an intramolecular fashion to form a cycle product ($m/z = 670$, HPLC-MS, ref. **Figure 35**), which would not undergo coupling reaction with bombesin anymore. Nevertheless, it is not clear until now and also $^1\text{H-NMR}$ could not confirm the cyclic side-product.

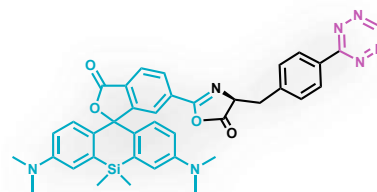
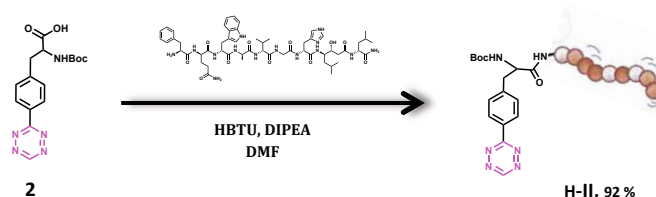


Figure 35 | Hypothetic presumption – intramolecular cyclisation

Since, common HBTU coupling conditions did not work, we left out activation of the carbonic acid. Once, coupling agent HBTU, SiR-Dye-Tz-acid **I** and bombesin were all mixed and dissolved in DMF, base DIPEA was added to start the coupling reaction. In this case we observed very small amount of product mass in HPLC-MS measurement. This indicates that intramolecular attack might be slightly pushed back by coupling reaction.

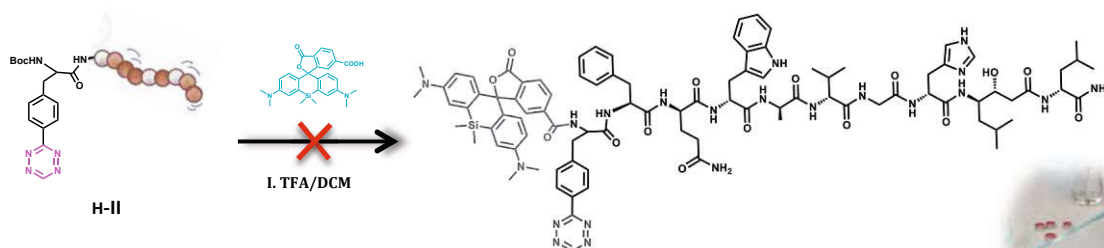
In addition, HBTU led to guanidine formation with amino group of bombesin RM26. This kind of side-reaction is described by Dubey and co-worker^[54].

So we started with a HBTU coupling reaction of peptide bombesin RM26 analogon (prepared by Ludwig Boltzmann Institute, GH) with H-phenyl-alanine-D,L-(Boc)-1,2,4,5-tetrazine, here again with usual reaction conditions implying carbonic acid activation step (**Scheme 9**).



Scheme 9 | Formation of bombesin RM26 coupled H-phenylalanine-(Boc)-1,2,4,5-tetrazine

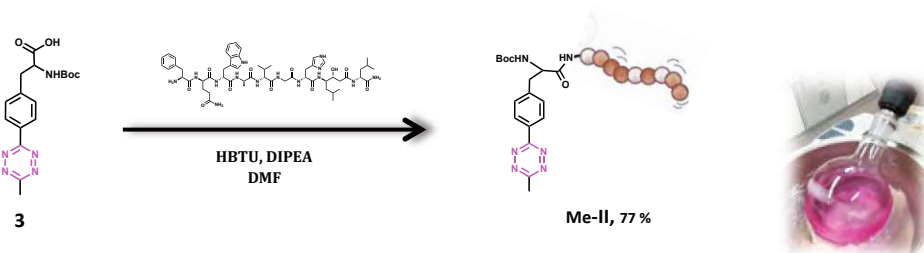
After purification via RP-HPLC chromatography, the tetrazine modified peptide **H-II** was isolated with very high yields of 92 %.



Scheme 10 | Formation of SiR-Dye-Tz-bombesin RM26 failed at deprotection step with TFA/DCM

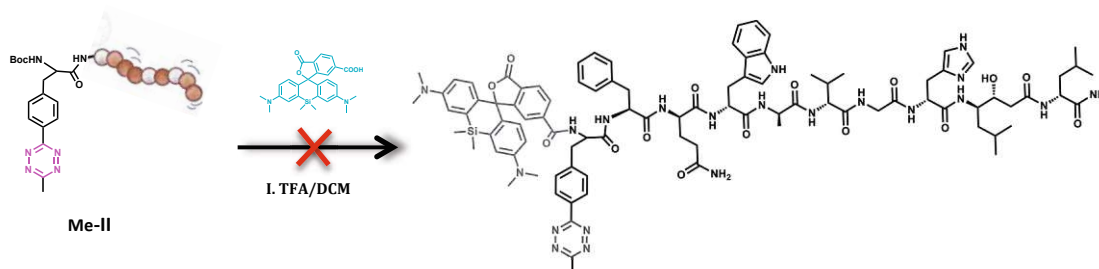
In terms of conducting a further coupling reaction, Boc protecting group of compound **H-II** was cleaved off with 16 % TFA/DCM mixture. We tried the deprotecting step twice, as we assumed that the water bath temperature of the rotary evaporator within the first attempt got too high and led to decomposition of our tetrazine species.

Peptide modification strategy using Me-phenylalanine-D,L-(Boc)-1,2,4,5-tetrazine component was based on exactly the same procedure (**Scheme 11**). As the CH₃-group is electron donating, the methyl containing tetrazine is supposed to be more stable, accompanied by decreased reaction kinetics in IEDDA ligations.



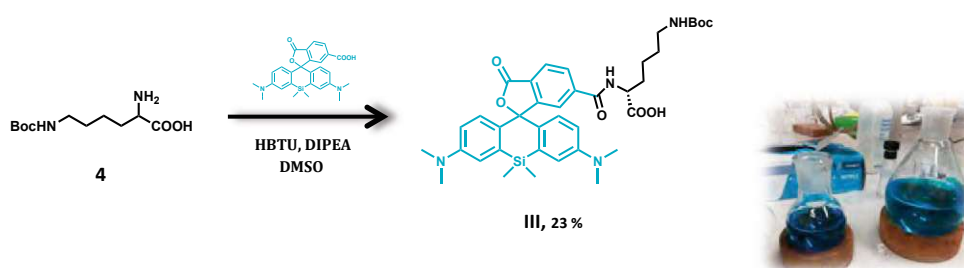
Scheme 11 | Formation of bombesin RM26 coupled Me-phenylalanine-(Boc)-1,2,4,5-tetrazine

Although Me-Tz-bombesin species **Me-II** was synthesized again with very good yields of 77 %, this approach in the end also did not work due to compound decomposition during TFA-acidic deprotection, as a result no SiR-Dye-Me-Tz-bombesin RM26 peptide was attainable (**Scheme 12**).



Scheme 12 | Formation of SiR-Dye-Me-Tz-bombesin RM26 failed at deprotection step with TFA/DCM

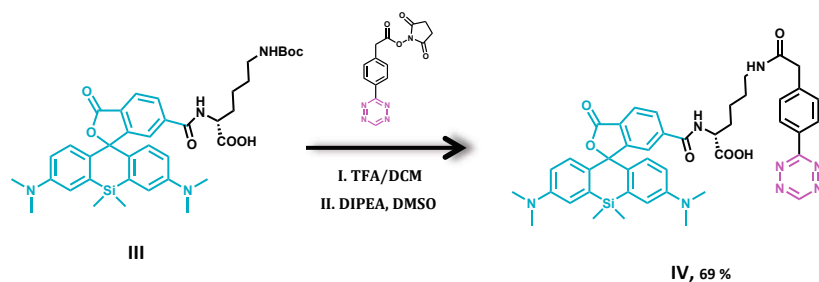
At this point, we considered to incorporate Boc-L-lysine as a “linker” and tried the coupling steps once again (**Scheme 13**).



Scheme 13 | Formation of SiR-Dye coupled Boc-L-lysine

Fluorescent agent SiR-Dye acid was activated with HBTU and DIPEA, respectively. As the linker Boc-L-lysine **4** was hardly soluble, the reaction vial was placed in an ultrasonic bath for 15 min. Addition of activated dye to amino acid **4** led to desired coupled product **III**, which was purified via RP-HPLC chromatography to observe yields of 23 %. Since, Boc-L-lysine can also form dimer and trimer species, the product yields were rather low.

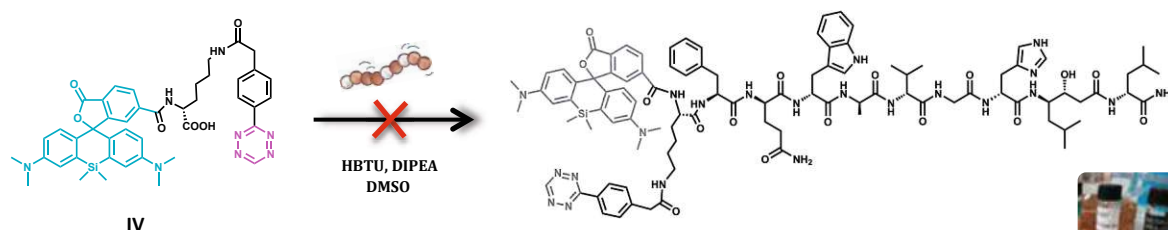
Next, a slightly different tetrazine was used for additionally modifying the previous coupled SiR-Dye-Boc-L-lysine (**Scheme 14**).



Scheme 14 | Formation of SiR-Dye-bz-Tz linked L-lysine

For that reason compound **III** was deprotected with 16 % TFA/DCM mixture, followed by nucleophilic substitution reaction with NHS-benzyl-1,2,4,5-tetrazine, using DIPEA in DMSO. The yields after RP-HPLC-purification were good, amounting about 69 % of product **IV**.

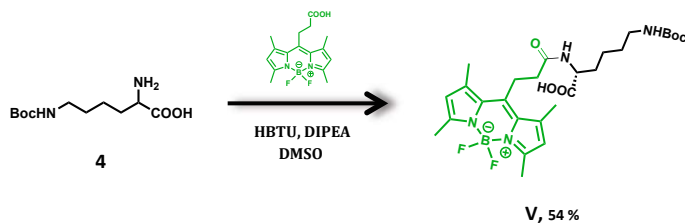
Nevertheless, the final coupling reaction with bombesin peptide failed again, no product arranged (**Scheme 15**).



Scheme 15 | Formation of (SiR-Dye-bz-Tz linked L-lysine) modified bombesin RM26 failed

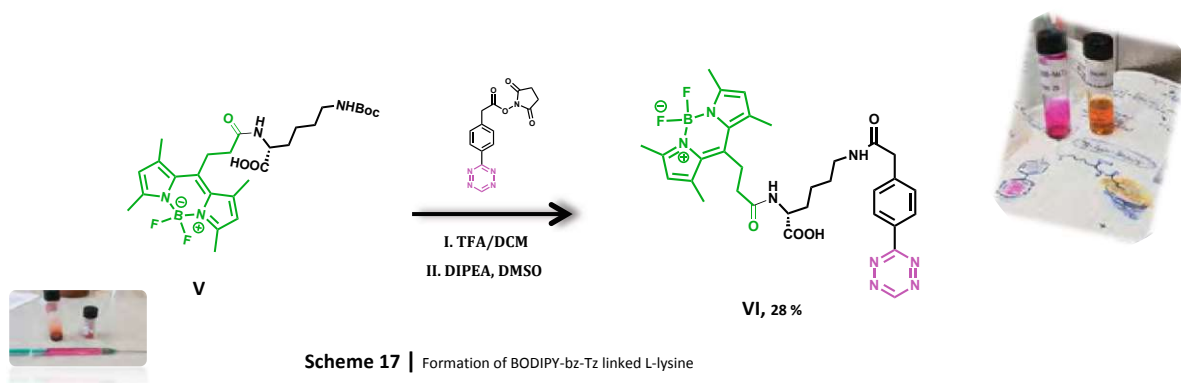
Furthermore, we recognized that the characteristic mass of starting compound **IV** got 30 g/mol lower than originally applied, which indicates that two methyl groups, one at each (dimethyl)amino-group of SiR-Dye moiety, were cleaved off under basic conditions.

Consequently, we tried another more stable fluorescent agent and moved on to using BODIPY. We pursued exact the same synthetic approach, as pointed out in **Scheme 16 - Scheme 18**.



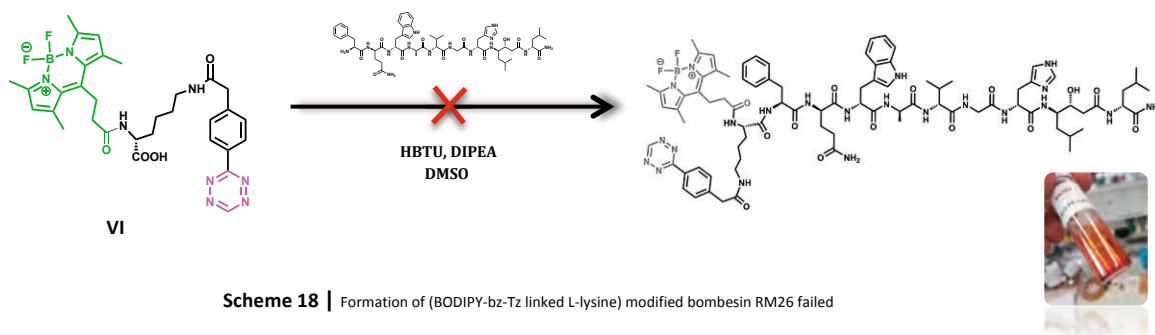
Scheme 16 | Formation of BODIPY coupled Boc-L-lysine

Since, Boc-L-lysine can also form dimer and trimer species within coupling reaction like already mentioned in case of SiR-Dye (page 32), it was used in little excess of only 1.1 eq. And that actually payed off, with increased yields of 54 % after RP-HPLC chromatography purification, for obtaining BODIPY coupled Boc-L-lysine **V**.

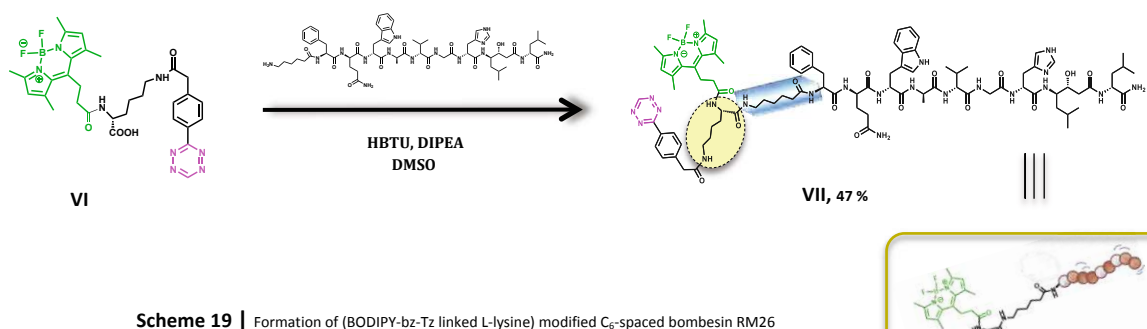


After deprotection of Boc-group with 16 % TFA/DCM, NHS-benzyl-1,2,4,5-tetrazine was added to basic solution of deprotected BODIPY coupled L-lysine **V**. With rather low yields of 28 %, pure BODIPY-bz-Tz linked L-lysine **VI** was gathered (**Scheme 17**). H,H-COSY 2D NMR was recorded for the product (**Figure 36**, page 38).

Herein again, the last step to finally modify the tumor targeting peptide bombesin (**Scheme 18**) did not work.



As applying Boc-L-lysine as linker did not provide the desired results, we considered to elongate bombesin species with ϵ -amino caproic acid (spacer), which was also synthesized by Marie Brandt (Ludwig Boltzmann Institute, GH Vienna). Another HBTU coupling reaction was carried out between already prepared BODIPY-bz-Tz linked L-lysine **VI** and the C_6 -spaced bombesin RM26 analogon (**Scheme 19**) without activation step as described on page 31.



Reaction was monitored with HPLC-MS and plenty of product formation was observed. We really appreciate to, in the end, have successfully synthesized the modified tumor targeting carrier molecule **VII**, with yields of approximately 47 %. So, implying a spacer actually helped to reduce steric hindrance in the course of coupling reaction.

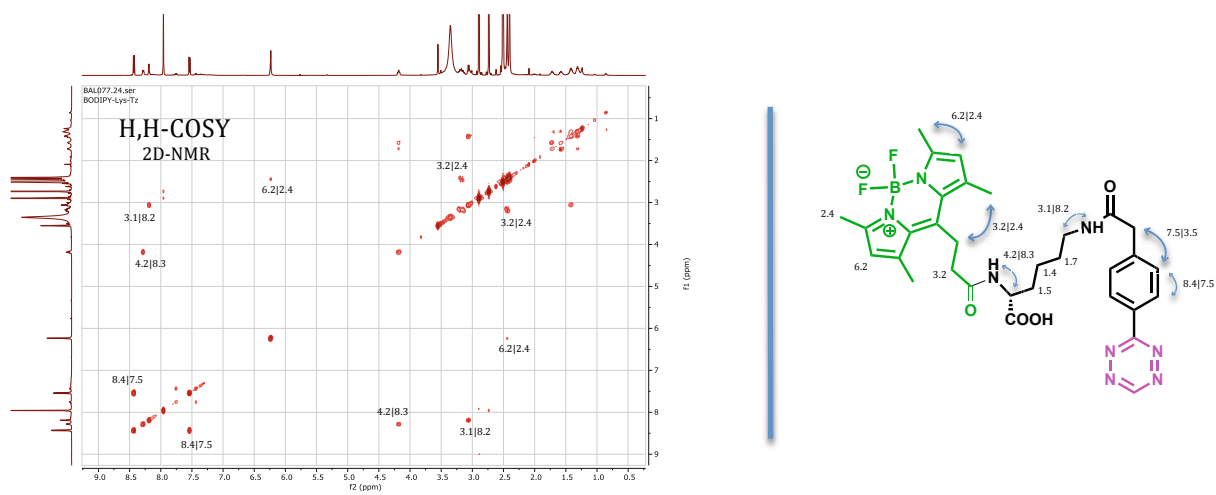


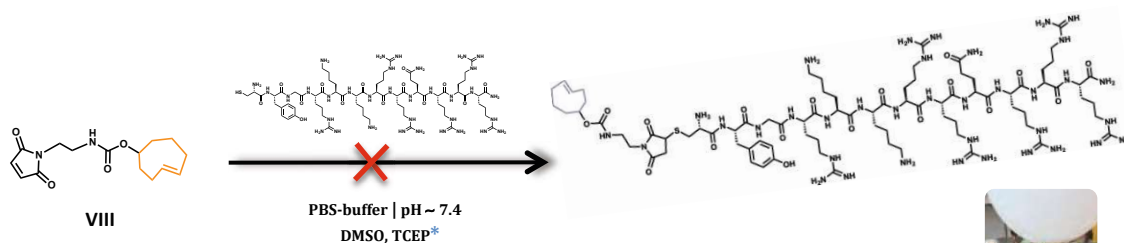
Figure 36 | H,H-COSY 2D NMR for BODIPY-benzyl-tetrazine linked L-lysine VI

2.2.2 | Modifying cys-TAT peptide [47-57]

The counterpart to specific tumor targeting bombesin compound is the modified cell penetrating peptide cystTAT [47-57] peptide, which involves a cysteine tag. The cysteinyl thiol group is well described by Radu and coworkers^[55] for undergoing bioconjugation reactions with corresponding maleimide derivatives in a Michael addition reaction type.

Farther, hydrolysis sensitivity of according maleimide species is reported by Kalia *et al.*^[56], which leads to unreactive ring-hydrolysed compound, especially under basic conditions. Once the bioconjugates are formed, though, they become resistant towards exchange with other thiol-containing compartments in living system, as soon as they are hydrolysed.

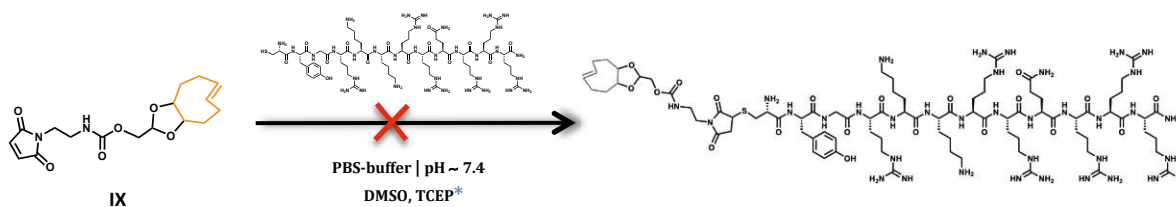
Thiol-maleimide bioconjugation was applied for modifying cystTAT [47-57] peptide with maleimidyl-TCO compound **VIII** in PBS-buffer (pH ~ 7.4), whereby at first instance TAT peptide was treated with 10 eq TCEP (**Scheme 20**). Tris(2-carboxyethyl)phosphine (= TCEP) is commonly used for reducing the disulfide bridges in thiol-containing peptides or proteins.



Scheme 20 | Formation of maleimidyl-TCO modified cystTAT [47-57] failed (under Ar atmosphere)

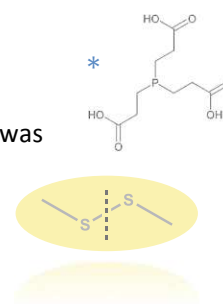
As the first trials to form the desired bioconjugate failed, PBS buffer concentrations were varied in numerous attempts, without having any effect. The reaction mixture was exposed to different temperatures as well, ranging from -18°C up to room temperature, including so called “freeze-defrost” cycles.

Since none of the adaptations led to product formation and additionally, starting material **VIII** got largely ring-hydrolysed, we synthesized a similar maleimidyl-TCO species. HSQC- and H,H-COSY 2D NMRs were recorded for this compound (**Figure 37**, page 40). The dTCO compound **IX** tended to be more stable in terms of hydrolysis, but bioconjugation step failed again (**Scheme 21**).

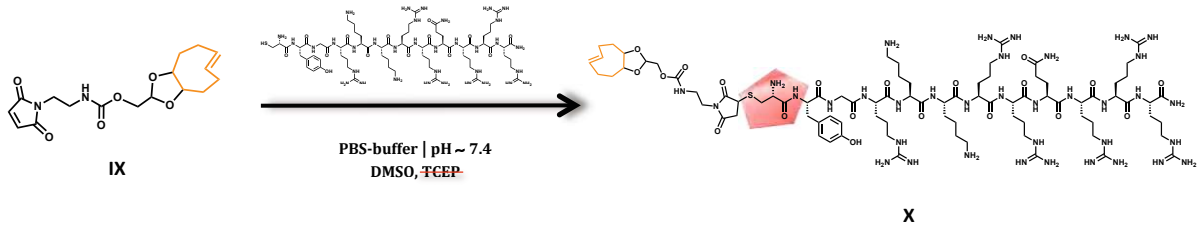


Scheme 21 | Formation of maleimidyl-dTCO modified cystTAT [47-57] failed, too

It was only when we decided to leave out TCEP that bioconjugate formation **X** was observed in HPLC-MS measurement even after only 2 min (!) (**Scheme 22**, page 40). Besides, the same principle of procedure was found later in a research paper of Pessi *et al.*^[57] However, having achieved the modification of the second required cell uptake peptide, we could not manage to isolate it after purification runs



via RP-HPLC chromatography despite trying different C-18 column types with various solvent gradients and also one Chromolith® column.



Since no product purification was achieved reaction led to very good product turnover, we decided to use 1.1 eq of dTCO-compound IX instead of 10 eq to obtain very little impurities. Consequently, no yields are stated.

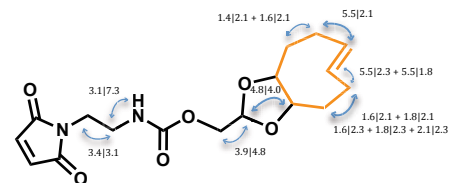
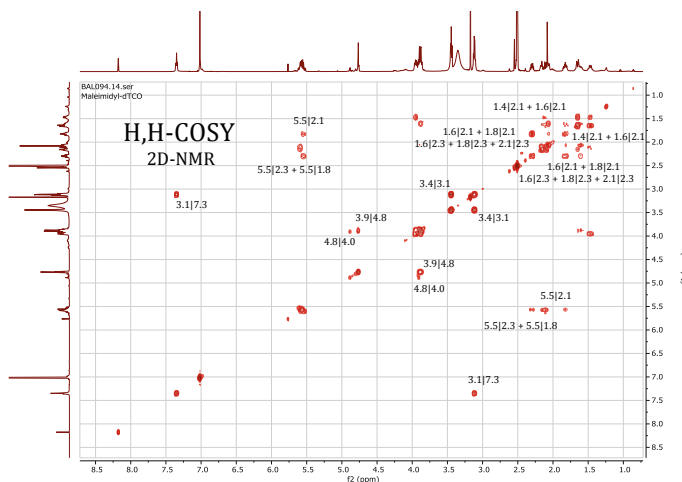
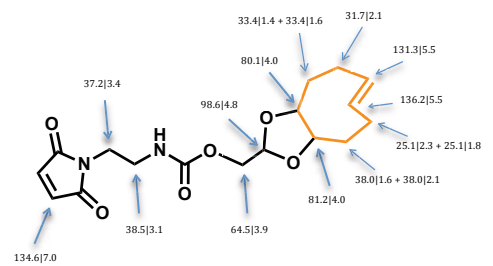
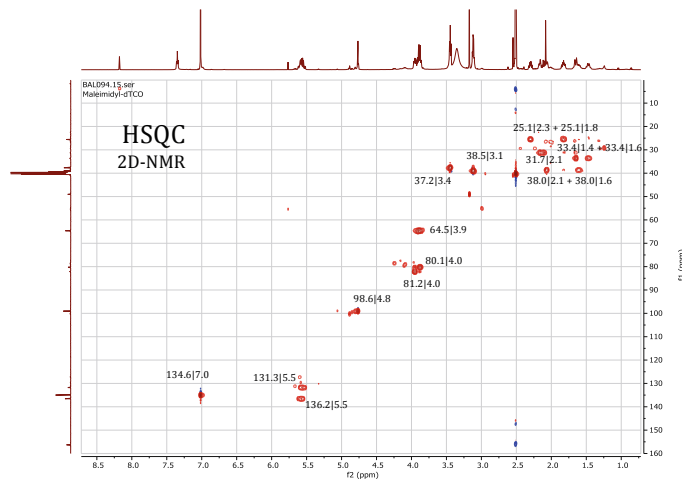
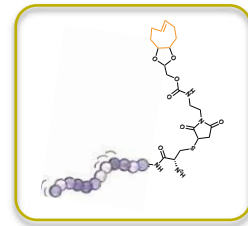


Figure 37 | HSQC- and H,H-COSY 2D NMRs for maleimidyl-dTCO compound IX

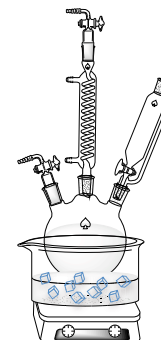
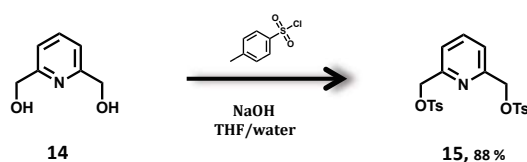
2.3 | Synthesis of other Building Blocks for further modifications

2.3.1 | Synthesis of Ligand ${}^{\text{H}}\text{N}_4$

Radiopharmaceuticals contain radioisotopes that are chemically bonded to molecule scaffold via radiolabeling (ref., **1.2.1**). Therefore, a ligand ensures the appropriate complex formation of the radioactive species on carrier molecules such as peptides.

Within this work we synthesized a pyridinophane chelator, abbreviated ${}^{\text{H}}\text{N}_4$ and already described by Wessel *et al.*^[58], for upcoming radionuclide complex formation. For that, two compounds had to be prepared independently and prior to their usage in later reaction.

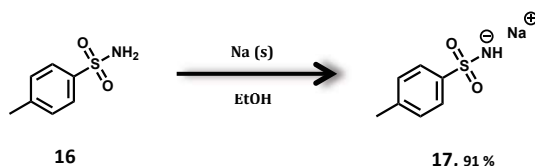
2,6-Bis(hydroxymethyl)pyridine **14** was tosylated under argon atmosphere by dropwise addition of tosylchloride [TsCl] under basic conditions in water/THF mixture at 0°C (**Scheme 23**).



Scheme 23 | Formation of 2,6-Bis(tosylmethyl)pyridine via tosylation in basic solution

After extraction steps and drying in high vacuo, the product 2,6-Bis(tosylmethyl)pyridine **15** was obtained with high yields of 88 %.

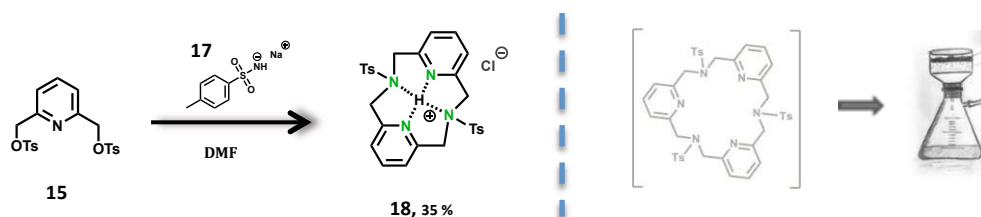
The second compound was synthesized via refluxing tosylamide **16** in sodium ethoxide solution at 80 °C (**Scheme 24**).



Scheme 24 | Formation of sodium tosylamide in sodium ethoxide solution

Formed product sodium tosylamide **17** was filtered and dried in high vacuo to afford white crystals, with high yields once again, amounting 91 %.

As denoted above, 2,6-Bis(tosylmethyl)pyridine **15** and sodium tosylamide **17** are the starting materials for the next synthesis (**Scheme 25**).



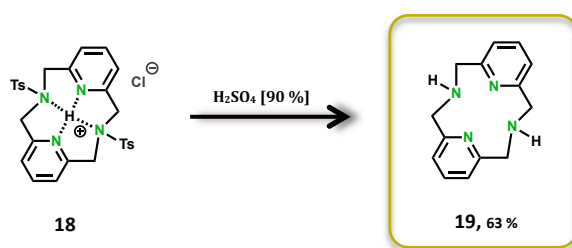
Scheme 25 | Formation of di-tosylated pyridinophane hydrochloride ligand (Dimer); the trimeric side product forms no hydrochloride and is filtered off as solid

A solution of compound **15** in DMF was herein added dropwise at 80 °C to tosylamide species **17** and stirring of the reaction mixture was continued at 80 °C over weekend. Within this reaction not only the desired di-tosylated pyridophane ligand $^{\text{Ts}}\text{N}_4$ is formed as cyclised Dimer, but also the trimeric side product.

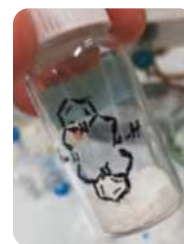
At this point, Wessel and coworkers^[58] have reported a very smart method for separation of both components. The mixture was suspended in 95 % ethanol, 1 M HCl was added and reaction mixture stirred overnight. While the Dimer is capable of stabilizing the hydrogen atom and thus forms the product di-tosylated $^{\text{Ts}}\text{N}_4$ hydrochloride **18**, the Trimer is not. As a consequence, product **18** stayed in water solution and the trimeric side product was filtered off as solid.

The white product was obtained after evaporation of solvents under reduced pressure with good yields in respect of side-product formation, ending up with 35 %.

Finally, the two tosyl-groups were cleaved via refluxing at 110 °C in H_2SO_4 [90 %] (**Scheme 26**). After neutralisation and extraction steps with chloroform, the product was dried in high vacuo. Pyridinophane ligand $^{\text{H}}\text{N}_4$ **19** was afforded with 63 % yields as white powder.



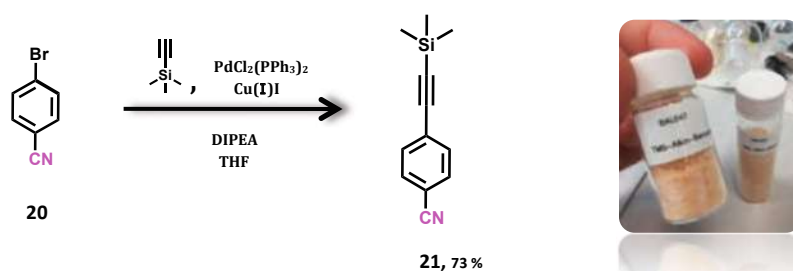
Scheme 26 | Formation of pyridinophane ligand $^{\text{H}}\text{N}_4$ in sulphuric acid [90 %]



2.3.2 | Synthesis of “Dual-Click”-Tetrazine

“Dual-Click” 1,2,4,5-tetrazines offer the possibility to be modified at two different sites of the molecule via two different reaction modalities. Therefore, each reaction occurs in specific fashion under unique reaction conditions, having no effect on the other moiety. As this building block is very useful for a wide variety of ligations, as reported by one of my group members M. Wilkovitsch^[59] in the course of pre-targeting approaches, it was synthesized and stocked accessibly for internal usage.

In the first step, as depicted in **Scheme 27**, a Sonogashira coupling reaction between 4-bromobenzonitrile **20** and trimethylsilylacetylene was carried out in THF under inert gas atmosphere, as reported by Dirk *et al.*^[60]



Scheme 27 | Formation of 4-(TMS-ethynyl)benzonitrile via Sonogashira coupling reaction

The reaction mixture contained Bis(triphenylphosphine)palladium dichloride and copper(I)iodide in catalytic amount and was stirred overnight at 45 °C under basic conditions. As the phase separation of the layers was poorly visible using DCM/water during the following extraction steps, the organic layer was diluted with diethyl ether.

Impure product 4-(TMS-ethynyl)benzonitrile **21** was purified via NP-LC chromatography (solid loading was required) to afford beige-colored crystals with gratifying yields of 73 %.

The reaction mechanism is illustrated on the right hand side in **Figure 38**. Chinchilla and colleagues^[61] published the following mechanistic proposal. Pd(II)-precatalyst interacts with base to form the activated Pd⁰-species of catalyst (A). This initiates the oxidative addition [OA] of Arylhalogenide R¹-X to palladium (B). Within transmetalation step [TM] between L_nPd(II)R¹X and copper acetylide (generated via “copper cycle”, steps D-F), L_nPd(II)R¹(C≡C-R²) species is formed (C). After reductive elimination [RE] as well as *trans/cis* isomerisation, palladium (II) is regenerated to active form Pd⁰ (A) and coupled alkyne product is obtained.

Although the copper cycle is poorly known, this proposal is looks reasonable. Copper halogenide CuX (D) interacts with alkyne species, leading to copper-acetylide formation (E). Then base abstracts acidic hydrogen and halogenide, leading to alkyne copper complex Cu(C≡C-R²) (F).

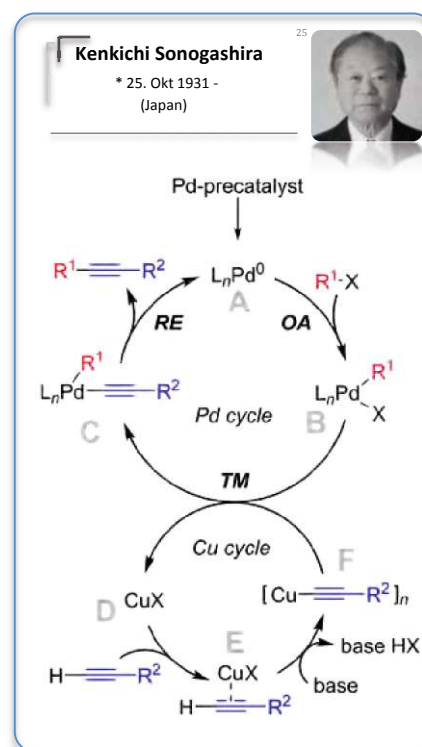
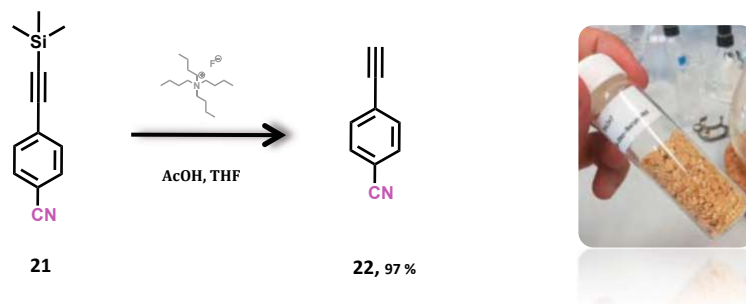


Figure 38 | Mechanism of Sonogashira coupling; discovered by K. Sonogashira^{[61],25}

²⁵ <https://www.together.tum.de/alumni-portraits/kenkichi-sonogashira/>, last downloaded 05/2019

TMS-group was cleaved off in the following synthetic step (**Scheme 28**), by using TBAF and acetic acid in THF, under Ar atmosphere and while cooling with an ice-bath [0 °C].



Scheme 28 | Formation of 4-ethynylbenzonitrile via deprotection using TBAF

The reaction was fully converted after two hours and the reaction mixture was washed with water, NaHCO₃ and brine, respectively, before organic layers were dried over MgSO₄. Deprotected product 4-ethynylbenzonitrile **22** was afforded as cereal-lookalike beige-brown powder with very high yields of 97 %.

In order to form a so called PINNER-salt (**Scheme 29**) according to procedure of Lang *et al.*^[62], the starting material **22** was dissolved in anhydrous MeOH/diethyl ether mixture. As illustrated in **Figure 39**, hydrogen chloride gas was generated via dropwise addition of H₂SO₄ [conc] to 100 g ammonium chloride in a 1000 ml three-necked round-bottom flask and passed into the reaction flask between 0°C and room temperature. To ensure having anhydrous (!) HCl-gas, a wash bottle (middle, **Figure 39**) with sulphuric acid, conc. as drying agent was installed right ahead the reaction flask.

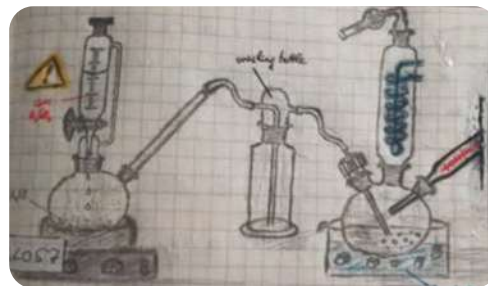
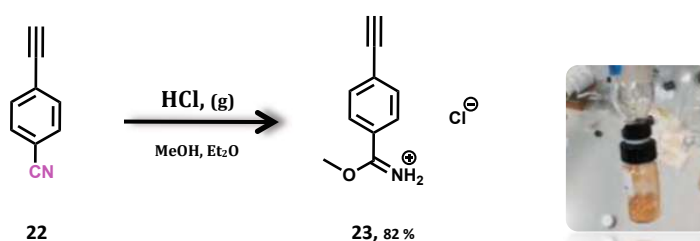


Figure 39 | Illustration of PINNER reaction; generating HCl gas

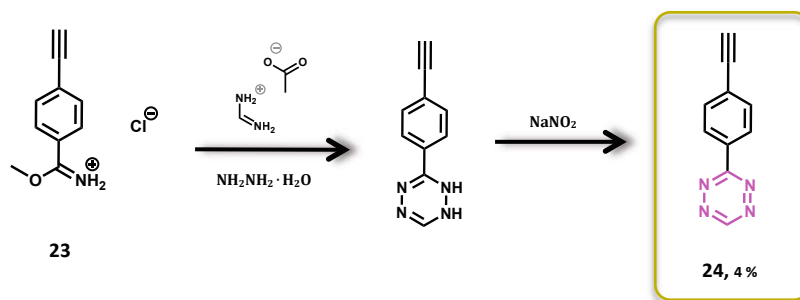


Scheme 29 | Formation of methyl-4-ethynyl benziminoester hydrochloride via PINNER reaction

As the product methyl-4-ethynyl benziminoester HCl **23** precipitated in refrigerator at 4 °C overnight, the solid was dried in high vacuo after filtration, affording pretty good yields 82 % (crude).

Within the last step of this synthetic approach, Pinner salt **23** led to 1,2,4,5-tetrazine formation without the use of sulphur as catalyst, in comparison with previously described tetrazine compounds (ref., **2.1.1**). Therefore hydrazine monohydrate was added dropwise to a mixture of formamidine

acetate and starting material **23** under Ar atmosphere and while cooling with an ice-bath [0 °C] (Scheme 30).



Scheme 30 | Formation of 4-ethynylphenyl-1,2,4,5-tetrazine without sulphur as catalyst

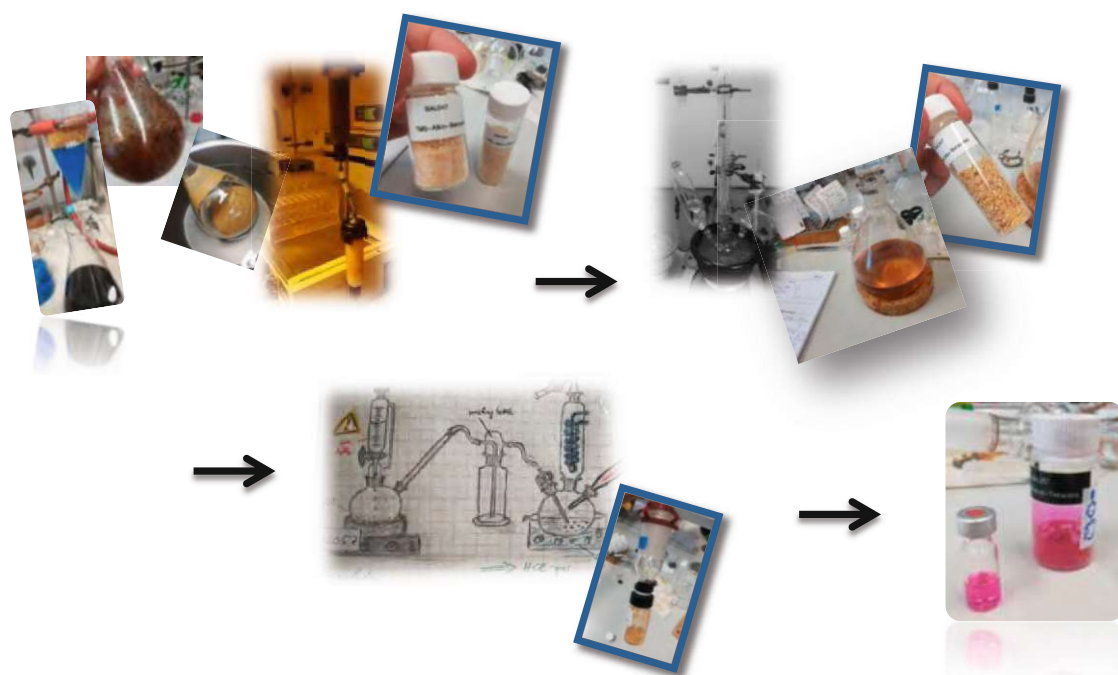
Since the methoxy group served as good leaving group and activated the carbon atom from the imine arrangement, the reaction was in no needs of any catalyst. Here again, at first 1,2-dihydro-1,2,4,5-tetrazine was formed in similar mechanistic manner as reported in 2.1.1, previous to oxidation steps.

Farther, two oxidation pathways were compared, although in both cases almost the same amount of product was obtained.

Starting with one, wherein half amount of the just obtained dihydro-tetrazine was dissolved in a mixture of MeOH/water. While keeping the temperature between 0 °C and 5 °C, sodium nitrite was added to reaction mixture within 10 min. Afterwards, 1 N HCl was added dropwise to form the desired tetrazine moiety. After evaporation of solvents and drying in high vacuo, the formed pink crude product methyl-4-ethynylphenyl-1,2,4,5-tetrazine **24** was purified via NP-LC chromatography.

The other half amount of dihydro-Tz-species was dissolved in glacial acetic acid. Again, solid sodium nitrite was added within 10 min at temperature levels between 0 °C and 5 °C. The impure product **24** precipitated by pouring on ice-cold water and was filtered. The pink compound was finally also purified via NP-LC chromatography.

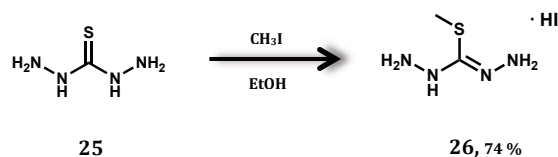
In both cases the product was obtained as quite admirable pink crystals with very low yields of 4 %.



2.3.3 | Synthesis of S-tetrazine

In the course of this diploma thesis another 1,2,4,5-tetrazine derivative was synthesized to be stocked for research group-intern usage, too. As thiomethyl substituents are replaced by nucleophiles via nucleophilic substitution reactions rather easily, as well-described by Zhou^[63], we prepared the unsymmetrically substituted 3-methyl-6-methylthio-1,2,4,5-tetrazine. In that way, alkoxy- (OR), hydroxy- (OH), amino- (NH₂), alkylamino- (NHR, NR₂) as well as halogenide- (F, Cl) substituted 1,2,4,5-tetrazines are accessible.

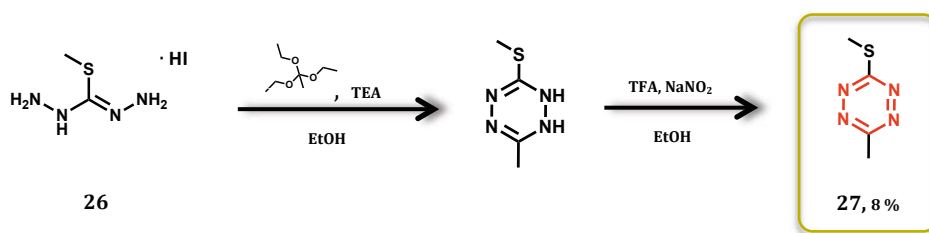
S-Methylisothio-carbohydrazide HI **26** was obtained via dropwise addition of methyl iodide to a refluxing suspension of thiocarbohydrazide **25** in EtOH at 80 °C (**Scheme 31**), as reported by Scott and coworkers.^[64] The product was filtered hot and crystallized on cooling – appropriate yields of 74 % were observed.



Scheme 31 | Formation of S-methylisothio-carbohydrazide, hydrogeniodide

The tetrazine formation is achieved by following synthesis, described by Heil *et al.*^[65] To a suspension of starting material **26** in ethanol under Ar atmosphere, triethyl orthoacetate and base TEA were added (**Scheme 32**). After refluxing for one hour at 80 °C and forming corresponding dihydrotetrazine, addition of sodium nitrite and TFA led to product observation, indicated by color change to a deep red.

Having a look at the reaction mechanism, this tetrazine formation relies on substitution and also elimination of ethoxy groups from the triethyl orthoacetate compound by some sort of “bidental” nucleophilic attack of carbohydrazide.



Scheme 32 | Formation of 3-methyl-6-methylthio-1,2,4,5-tetrazine

After addition of n-hexane and water, the red product 3-methyl-6-methylthio-1,2,4,5-tetrazine **27** was extracted with diethyl ether. After purification via NP-LC chromatography the product fractions were collected to obtain product as a red oil with low yields of 8 %.

2.3.4 | Synthesis route for NHS-TCO-carbonate

In our research group a smart method for an efficient low-cost preparation of *trans*-cyclooctenes [TCOs] has been elaborated and is reported by Svatunek, Denk (my supervisor) *et al.*^[66] It allows the photoisomerisation of *cis*-cyclooctenes to corresponding *trans*-cyclooctenes which are actually 7 orders of magnitude faster reacting with 1,2,4,5-tetrazines (ref., 1.3.1). For that, low pressure Hg lamps supply the required irradiation with the dominant wavelength of 254 nm (Figure 40).

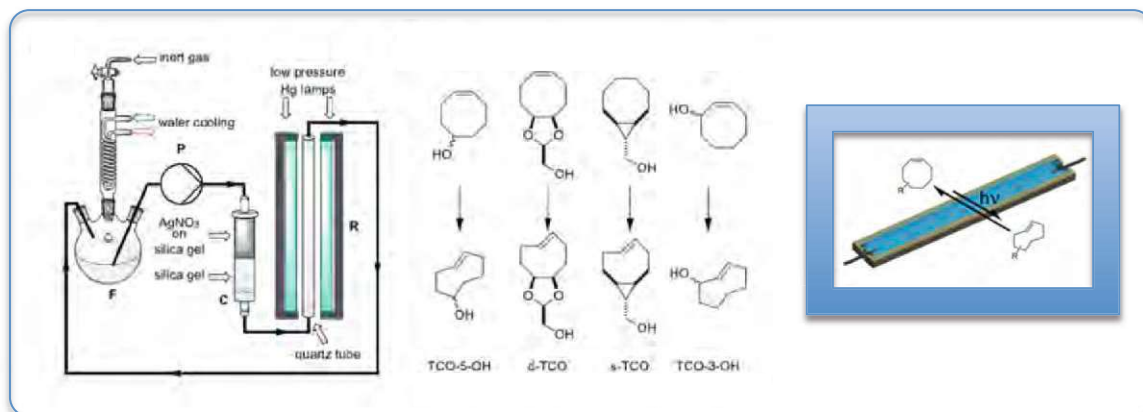


Figure 40 | Photoisomerisation setup for preparation of different *trans*-cyclooctenes [TCOs] by using Hg lamps (254 nm) (edited)^[66]

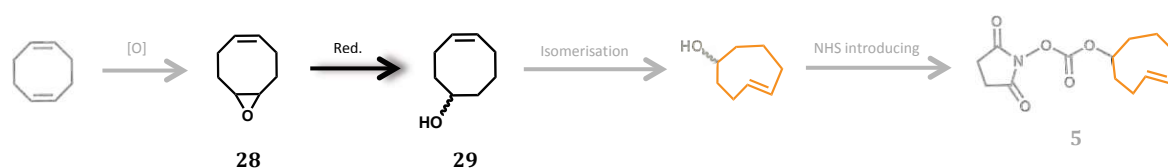
Analogous to that, we prepared (Z)-cyclooct-4-en-1-ol **29** via reduction, prior to photoisomerisation reaction (Scheme 33). By adding (Z)-9-oxabicyclo[6.1.0]non-4-ene **28** dropwise to a suspension of lithium aluminium hydride in THF at 0 °C and further stirring at room temperature overnight, product was formed. The following hydrolysis and extraction steps were conducted based on the so called Fieser workup procedure (ref., chapter 4 | experimental part) which helped to get rid of the mud in a very simple way and without any mess.



Scheme 33 | Formation of (Z)-cyclooct-4-en-1-ol via reduction



Scheme 34 shows the synthetic route for preparation of NHS-TCO carbonate **5**, which is also stored in the freezer for internal usage.



Scheme 34 | Synthetic route for preparation of NHS-TCO carbonate, starting with cycloocta-1,5-dien (COD)

2.4 | *In vitro* studies



The two modified peptides bombesin [RM26] and cystAT [47-57] described in synthetic part 2.2.1 and 2.2.2, respectively, were used in the course of *in vitro* assays for evaluating the proof of concept regarding the cell uptake strategy (ref., 1.4.3).

All following steps were carried out in sterile work area, based on cell culture book of Schmitz^[67]. Right at the start, the tumor cells of PC-3 cell line had been stored in liquid nitrogen [-179 °C] before usage. One week prior to the cell culture tests the cells were defrosted and cultivated by using T25 cell culture flasks with Dubbelco's Medium DMEM, which includes 10 % FBS (= fetal bovine serum; supports cell growth), indicator Phenol Red and 0.5 % antibiotics. Therefore, the applied incubator *New Brunswick Galaxy*® 48R (Figure 41) ensured conditions of high humidity, set temperature of 37 °C, and 4 % CO₂ as well as 3 % O₂.



Figure 41 | Incubator²⁶

After two days, adherent cells were split after dissociation step with the aid of enzyme trypsin containing Medium. The Medium DMEM was removed to add new one for further incubation. The day before starting the *in vitro* assays, the PC-3 cells were seeded into two 96-well plates (ref., Figure 42), 10 000 cells per well, for incubation times of 1 and 3 hours, respectively.

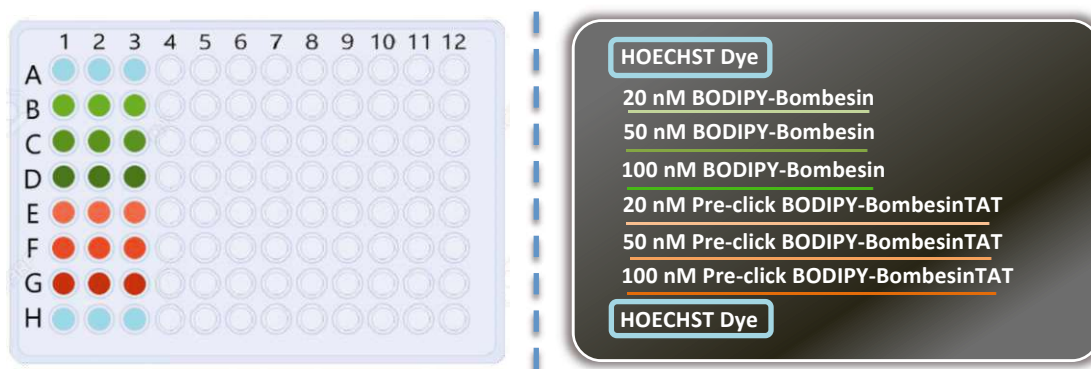


Figure 42 | Plotting for *in vitro* assay (edited)²⁷

So the next day, Medium was aspirated and BODIPY-Tz-bombesin as well as a Pre-click mixture of BODIPY-Tz-bombesin and TAT-dTCO, both were added in different concentrations [20, 50 and 100 nM, ref., Figure 42], followed by further incubation. We used DMSO stock solutions and MilliQ-water for according dilutions. After an incubation time of 1 hour, Medium of the first 96-well plate was removed and new one was added. This washing step was carried out twice before incubating for another 15 min. Further exchange of Medium and 15 min incubation ensured enough time for diffusion processes.

Then, 500 ppm HOECHST dye [33342] was added to cells in new Medium DMEM (without indicator; yellow) to be incubated for 15 min again. After washing steps with the Medium (yellow), addition of FluoroBrite DMEM provided significant lowering of background fluorescence, and thus enhancing the signal-to-noise ratio.

²⁶ <https://www.americanpharmaceuticalreview.com/25303-Pharmaceutical-Incubators/8452255-New-Brunswick-Galaxy-48-R/>, last downloaded 05/2019

²⁷ <https://www.sigmaldrich.com/technical-documents/articles/biology/96-well-plate-template.html>, last downloaded 05/2019

Additionally, wells A1-A3 (top, **Figure 42**, page 48) and also H1-H3 (bottom) contained only HOECHST dye for serving as blank samples. In this regard, HOECHST-dye is able to intercalate to double-stranded DNA or RNA and as a result stains the cells of bacteria or eukaryotes (**Figure 43**).

The same procedure was conducted for the second 96-well plate after 3 hours of incubation time.

Cell imaging was conducted at Live Imaging Microscope (OLYMPUS IX83, **Figure 44**) without removing FluoroBrite Medium. This microscope is equipped with incubation chambers for CO₂- and humidity supply, with fast and sensitive camera Hamamatsu Orca flash 4 sCMOS, as well as with a motorized stage for manual control of movable 96-well plate desk. In addition it offers various filtersets, including DAPI, FITC, Cy3, Cy5, CFP and YFP.

In the course of the *in vitro* investigations we could not visualize our fluorescent agent BODIPY-impinging compound. As a consequence we obtained no pictures, but rather saw filaments next to the cells, which apart from that showed strange morphologic shape.

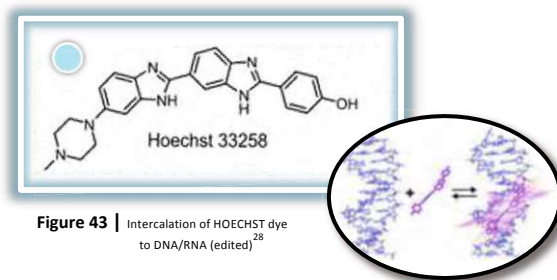


Figure 43 | Intercalation of HOECHST dye to DNA/RNA (edited)²⁸



Figure 44 | Live Imaging Microscope – OLYMPUS IX83²⁹

²⁸ https://www.researchgate.net/publication/324652762_The_Use_of_Hoechst_Dye_for_DNA_Staining_and_beyond/figures?lo=1, last downloaded 05/2019

²⁹ https://forschungsinfrastruktur.bmbwf.gv.at/en/fi/olympus-ix83-live-imaging-microscope_3703, last downloaded 05/2019

3 | CONCLUSION AND OUTLOOK

3.1 | Findings

Within this diploma thesis various building blocks at the very beginning were prepared that are applicable for further modifications. Since we met several problems in labeling the two peptides for cell uptake approach, we pursued one strategy after another to finally obtain the tumor targeting agents. Both, BODIPY-tetrazine labeled bombesin peptide and dTCO modified cystAT peptide were used to evaluate the proof of concept via *in vitro* investigations by using fluorescence microscopy. Nevertheless, we could not visualize the specific binding of bombesin species – with the aid of BODIPY as fluorescent agent – on tumor cell receptors extracellularly. Consequently, also the desired cell uptake mediated by click chemistry ligation was not feasible.

Besides, we successfully synthesized a ligand for upcoming radionuclide complex formation and some more building blocks, including “Dual-Click” tetrazine, methylthio-tetrazine and a precursor for NHS-TCO carbonate.

3.2 | Outlook

Even though we were not able to attain the proof of concept by visualizing the cell uptake strategy in the course of *in vitro* tests, the synthesized building blocks as well as precursors allow to modify a wide variety of carrier molecules for further tumor targeting strategies. In this regard, the building blocks and precursors were unscathed and remained stable in the freezer. This circumstance was observed in 2D-NMR and also HPLC-MS measurements that, in addition, confirmed the purity of our agents, before the following peptide modification steps were conducted.

Bombesin receptor-ligand interactions are indeed very specific, but cancerous cells possibly have limited numbers of this kind of receptors. Hence, other targets could be eligible to ensure the addressing of tumor cells, in large numbers.

In general, the specific binding action is farther influenced by cellular environment and cellular condition. In this context, the peculiar morphology and a slow cell growth of our applied immortalized PC-3 tumor cells certainly indicated cell culture contamination and infection with mycoplasmas. Therefore, cultivating of new PC-3 cell-line for additional *in vitro*-assays has to be performed.

REFERENCES

- [1] Committee on State of the Science of Nuclear Medicine (2007). Advancing Nuclear Medicine Through Innovation. In *United States of America: National Academy Press*.
- [2] <https://www.saintpetershcs.com/Services/Nuclear-Medicine>, last downloaded 05/2019
- [3] Unak, P., *Brazilian Archives of Biology and Technology* **2002**, 45(spe), 97–110.
- [4] Aghevlian, S., Boyle, A. J., & Reilly, R. M., *Advanced Drug Delivery Reviews* **2017**, 109, 102–118.
- [5] Phelps, M. E., Cherry, S. R., Dahlbom, M. (2006). Pp 1-10 in *PET: Molecular Imaging and Its Biology Applications*. Springer New York
- [6] Scuffham, J. W., Wilson, M. D., Seller, P., Veale, M. C., Sellin, P. J., Jacques, S. D. M., Cernik, R. J., *Journal of Instrumentation* **2012**, 7, P08027.
- [7] Paillass, S., Ladjounlou, R., Lozza, C., Pichard, A., Boudousq, V., Jarlier, M., ... Pouget, J.-P., *Antioxidants & Redox Signaling* **2016**, 25(8), 467–484.
- [8] Imstepf, S., Pierroz, V., Raposinho, P., Bauwens, M., Felber, M., Fox, T., ... Alberto, R., *Bioconjugate Chemistry* **2015**, 26(12), 2397–2407.
- [9] Zalutsky, M. R. (2003). Radionuclide therapy. Pp 315–348 in *Handbook of Nuclear Chemistry Volume 4: Radiochemistry and Radiopharmaceutical Chemistry in Life Sciences*. Roesch, F., ed. Dordrecht, Netherlands: Kluwer Academic
- [10] Bhusari, P., Vatsa, R., Singh, G., Parmar, M., Bal, A., Dhawan, D. K., ... Shukla, J., *International Journal of Cancer* **2017**, 140(4), 938–947.
- [11] Kratochwil, C., Bruchertseifer, F., Giesel, F. L., Weis, M., Verburg, F. A., Mottaghy, F., ... Morgenstern, A., *Journal of Nuclear Medicine* **2016**, 57(12), 1941–1944.
- [12] Rossin, R., & Robillard, M. S., *Current Opinion in Chemical Biology* **2014**, 21, 161–169.
- [13] <https://www.cancer.gov/about-cancer/treatment/types/targeted-therapies/targeted-therapies-fact-sheet>, last downloaded 05/2019
- [14] Gadd, M. S., Testa, A., Lucas, X., Chan, K., Chen, W., Lamont, D. J., Zengerle, M., Ciulli, A., *Nature Chemical Biology* **2017**, 13, 514–521.
- [15] An, S., Fu, L., *EBioMedicine* **2018**, 36, 553–562.
- [16] Kolb, H. C., Finn, M. G., & Sharpless, K. B., *Angewandte Chemie International Edition* **2001**, 40(11), 2004–2021.
- [17] Tornøe, C. W., Christensen, C., & Meldal, M., *The Journal of Organic Chemistry* **2002**, 67(9), 3057–3064.
- [18] Huisgen, R., *Angewandte Chemie International Edition in English* **1963**, 2(10), 565–598.
- [19] Oliveira, B. L., Guo, Z., & Bernardes, G. J. L., *Chemical Society Reviews* **2017**, 46(16), 4895–4950.
- [20] Schilling, C. I., Jung, N., Biskup, M., Schepers, U., & Bräse, S., *Chemical Society Reviews* **2011**, 40(9), 4840.
- [21] Saxon, E., Armstrong, J. I., & Bertozzi, C. R., *Organic Letters* **2000**, 2(14), 2141–2143.
- [22] Agard, N. J., Prescher, J. A., & Bertozzi, C. R., *Journal of the American Chemical Society* **2004**, 126(46), 15046–15047.
- [23] Laughlin, S. T., Baskin, J. M., Amacher, S. L., & Bertozzi, C. R., *Science* **2008**, 320(5876), 664–667.
- [24] Ramil, C. P., & Lin, Q., *Current Opinion in Chemical Biology* **2014**, 21, 89–95.
- [25] Blackman, M. L., Royzen, M., & Fox, J. M., *Journal of the American Chemical Society* **2008**, 130(41), 13518–13519.
- [26] Devaraj, N. K., Weissleder, R., & Hilderbrand, S. A., *Bioconjugate Chemistry* **2008**, 19(12), 2297–2299.
- [27] Kronister, S., Svatunek, D., Denk, C., & Mikula, H., *Synlett* **2018**, 29(10), 1297–1302.
- [28] Carlson, J. C. T., Meimetis, L. G., Hilderbrand, S. A., & Weissleder, R., *Angewandte Chemie International Edition* **2013**, 52(27), 6917–6920.
- [29] Denk, C., Svatunek, D., Filip, T., Wanek, T., Lumpi, D., Fröhlich, J., ... Mikula, H., *Angewandte Chemie International Edition* **2014**, 53(36), 9655–9659.
- [30] Lang, K., Davis, L., Torres-Kolbus, J., Chou, C., Deiters, A., & Chin, J. W., *Nature Chemistry* **2012**, 4(4), 298–304.
- [31] Madl, C. M., & Heilshorn, S. C., *Advanced Functional Materials* **2018**, 28(11), 1706046.
- [32] Carlson, J. C. T., Mikula, H., & Weissleder, R., *Journal of the American Chemical Society* **2018**, 140(10), 3603–3612.
- [33] Versteegen, R. M., Rossin, R., ten Hoeve, W., Janssen, H. M., & Robillard, M. S., *Angewandte Chemie International Edition* **2013**, 52(52), 14112–14116.
- [34] van Duijnhoven, S. M. J., Rossin, R., van den Bosch, S. M., Wheatcroft, M. P., Hudson, P. J., & Robillard, M. S., *Journal of Nuclear Medicine* **2015**, 56(9), 1422–1428.
- [35] Clavier, G., & Audebert, P., *Chemical Reviews* **2010**, 110(6), 3299–3314.

- [36] Mayer, S., & Lang, K., *Synthesis* **2016**, 49(04), 830–848.
- [37] Taylor, M. T., Blackman, M. L., Dmitrenko, O., & Fox, J. M., *Journal of the American Chemical Society* **2011**, 133(25), 9646–9649.
- [38] Valverde, I. E., Huxol, E., & Mindt, T. L., *Journal of Labelled Compounds and Radiopharmaceuticals* **2014**, 57(4), 275–278.
- [39] Cheng, S., Lang, L., Wang, Z., Jacobson, O., Yung, B., Zhu, G., ... Chen, X., *Bioconjugate Chemistry* **2018**, 29(2), 410–419.
- [40] Tossi, A., Bonin, I., Antcheva, N., Norbedo, S., Benedetti, F., Miertus, S., ... Romeo, D., *European Journal of Biochemistry* **2000**, 267(6), 1715–1722.
- [41] Abiraj, K., Mansi, R., Tamma, M.-L., Fani, M., Forrer, F., Nicolas, G., ... Maecke, H. R., *Journal of Nuclear Medicine* **2011**, 52(12), 1970–1978.
- [42] Guidotti, G., Brambilla, L., & Rossi, D., *Trends in Pharmacological Sciences* **2017**, 38(4), 406–424.
- [43] Raucher, D., & Ryu, J. S., *Trends in Molecular Medicine* **2015**, 21(9), 560–570.
- [44] Frankel, A. D. and Pabo, C. O., *Cell* **1988**, 55, 1189–1193
- [45] Green, M. and Loewenstein, P. M., *Cell* **1988**, 55, 1179–1188
- [46] Trabulo, S., Cardoso, A. L., Mano, M., & de Lima, M. C. P., *Pharmaceuticals* **2010**, 3(4), 961–993.
- [47] Sauer, J., Heldmann, D. K., Hetzenegger, J., Krauthan, J., Sichert, H., & Schuster, J., *European Journal of Organic Chemistry* **1998**, 1998(12), 2885–2896.
- [48] Ni, Z., Zhou, L., Li, X., Zhang, J., & Dong, S., *PLoS ONE* **2015**, 10(11), 2–10.
- [49] Li, C., Ge, H., Yin, B., She, M., Liu, P., Li, X., & Li, J., *RSC Advances* **2015**, 5(16), 12277–12286.
- [50] Patterson, J. T., Asano, S., Li, X., Rader, C., & Barbas, C. F., *Bioconjugate Chemistry* **2014**, 25(8), 1402–1407.
- [51] Goswami, L. N., Houston, Z. H., Sarma, S. J., Jalisatgi, S. S., & Hawthorne, M. F., *Organic and Biomolecular Chemistry* **2013**, 11(7), 1116–1126.
- [52] Toda, N., Asano, S., & Barbas, C. F., *Angewandte Chemie - International Edition* **2013**, 52(48), 12592–12596.
- [53] Kowada, T., Maeda, H., & Kikuchi, K., *Chemical Society Reviews* **2015**, 44(14), 4953–4972.
- [54] Dubey, L., *Ukrainica Bioorganica Acta* **2005**, 1, 13–19.
- [55] Radu, L. C., Yang, J., & Kopeček, J., *Macromolecular Bioscience* **2009**, 9(1), 36–44.
- [56] Kalia, D., Pawar, S. P., & Thopate, J. S., *Angewandte Chemie International Edition* **2017**, 56(7), 1885–1889.
- [57] Pessi, A., Langella, A., Capitò, E., Ghezzi, S., Vicenzi, E., Poli, G., ... Porotto, M., *PLoS ONE* **2012**, 7(5), 1–9.
- [58] Wessel, A. J., Schultz, J. W., Tang, F., Duan, H., & Mirica, L. M., *Organic & Biomolecular Chemistry* **2017**, 15(46), 9923–9931.
- [59] Wilkovitsch, M. (2017). Iodo-Tetrazines as Bioorthogonal Radiotheranostic Agents. *Diploma thesis* (Vienna University of Technology).
- [60] Dirk, S. M., & Tour, J. M., *Tetrahedron* **2003**, 59(3), 287–293.
- [61] Chinchilla, R., & Nájera, C., *Chemical Society Reviews* **2011**, 40(10), 5084.
- [62] Lang, S. A., Johnson, B. D., Cohen, E., *J. Heterocycl. Chem.* **1975**, 12, 1143–1153.
- [63] Zhou, Q. (2013). Synthesis of new tetrazines functionalized with photoactive and electroactive groups. *Dissertation* (Cachan Cedex, FR)
- [64] Scott, E. S., Audrieth, L. F., *The Journal of Organic Chemistry* **1954**, 19(8), 1231–1237.
- [65] Heil, C. S., Rittner, A., Goebel, B., Beyer, D., & Grininger, M., *Scientific Reports* **2018**, 8(1), 1–15
- [66] Svatunek, D., Denk, C., Rosecker, V., Sohr, B., Hametner, C., Allmaier, G., ... Mikula, H., *Monatshefte Fur Chemie* **2016**, 147(3), 579–585.
- [67] Schmitz, S. (2011). *Der Experimentator: Zellkultur*.

TABLE OF FIGURES

- I <https://cognigen-cellular.com/explore/education-clipart-board/#>, last downloaded **05/2019**
- II <https://www.buchi.com/de-de/products/preparative-chromatography/sepacore-flash-systems-x10-x50>, last downloaded **04/2019**
- III <https://www.golik.co.il/preparative-chromatography-1>, last downloaded **04/2019**
- IV <https://www.shimadzu.eu.com/nexera-sr>, last downloaded **04/2019**
- V <https://www.chromtech.com/12-x-32-mm-wide-mouth-crimp-55104>, last downloaded **04/2019**
- VI <https://www.news-medical.net/whitepaper/20151110/The-bedbug-aggregation-pheromone-and-NMR-spectroscopy-an-overview.aspx>, last downloaded **04/2019**
-
- 1 <https://www.drugtargetreview.com/news/36948/stopping-cancer-cells-in-their-tumour-highways/>, last downloaded **04/2019**
- 2-I <https://www.imperial.ac.uk/news/138687/malaria-drug-target-raises-hopes-treatments/>, last downloaded **04/2019**
- 2-II <https://www.drugtargetreview.com/news/30643/switch-converts-blood-stem-cells/>, last downloaded **04/2019**
- 3-I <https://bowelcancerz.org.nz/about-bowel-cancer/metastatic-bowel-cancer/>, last downloaded **04/2019**
- 3-II <https://www.urologe-zigeuner.at/de/untersuchungen/magnetresonanz-mr/>, last downloaded **05/2019**
- 3-III <https://de.clipartlogo.com/istock/syringe-1716082.html>, last downloaded **05/2019**
- 3-IV <https://www.sigmaldrich.com/catalog/product/sigma/cls3073?lang=de®ion=AT>, last downloaded **04/2019**
- 3-V <https://www.dreamstime.com/stock-photo-multichannel-pipette-test-sample-wells-plate-blue-solution-image47881809>, last downloaded **05/2019**
- 3-VI https://fr.123rf.com/photo_16083355_la-structure-chimique-d-une-mol%C3%A9cule-de-glucagon-le-glucagon-est-une-hormone-peptidique-produite-pa.html, last downloaded **05/2019**
- 3-VII <https://www.pngkey.com/pngs/radiation-symbol/>, last downloaded **04/2019**
- 3-VIII <https://www.infosperber.ch/Gesundheit/G0tzsche-Todliche-Medizin-und-organisierte-Kriminalitat>, last downloaded **05/2019**
- 3-IX <https://www.heinze-pruefungsanfechtung.de/pruefungsanfechtung-medizin/>, last downloaded **05/2019**
- 3-X <https://www.amazon.de/legosteine-rot/s?k=legosteine+rot>, last downloaded **05/2019**
- 3-XI <http://clipartandscrap.com/mouse-clip-art/>, last downloaded **05/2019**
- 4 <http://www.med.harvard.edu/jipnm/physics/isotopes/Tc/Tc99m/hist.html>, last downloaded **05/2019**,
https://web.archive.org/web/20131202233701/http://www.grstiftung.ch/de/portfolio/projekte/alle/y_1998/GRS-071-98.html,
last downloaded **05/2019**,
<https://www.dw.com/de/9komma4-ein-tomograf-der-extraklasse/a-4214283>, last downloaded **05/2019**
- 4-I <https://www.aecoc.es/articulos/reglamentos-udi-el-nuevo-reto-de-la-industria-de-producto-sanitario-y-de-agnostico-in-vitro/>,
last downloaded **04/2019**
- 4-II <https://us.medical.canon/products/computed-tomography/celesteion/experience/>, last downloaded **05/2019**
- 5-I https://en.wikipedia.org/wiki/Radioactive_decay, last downloaded **05/2019**
- 5-II https://www.iconfinder.com/icons/354051/atom_chemistry_physics_science_icon, last downloaded **05/2019**
- 6 <https://www.enec.gov.ae/discover/fueling-the-barakah-plant/what-is-radiation-/>, last downloaded **04/2019**
- 7 [https://chem.libretexts.org/Courses/Eastern_Wyoming_College/EWC%3A_Introductory_Chemistry_\(Budhi\)/17%3A_Radioactivity_and_Nuclear_Chemistry/17.03%3A_Types_of_Radioactivity%3A_Alpha%2C_Beta%2C_and_Gamma_Decay](https://chem.libretexts.org/Courses/Eastern_Wyoming_College/EWC%3A_Introductory_Chemistry_(Budhi)/17%3A_Radioactivity_and_Nuclear_Chemistry/17.03%3A_Types_of_Radioactivity%3A_Alpha%2C_Beta%2C_and_Gamma_Decay), last downloaded **05/2019**
- 8 <https://us.medical.canon/products/computed-tomography/celesteion/experience/>, last downloaded **05/2019**
- 9-I <https://radiologykey.com/paediatric-neuroradiology-2/>, last downloaded **04/2019**
- 9-II http://www3.gehealthcare.de/de-de/produkte/kategorien/nuklearmedizin/universal-gammakameras/brivo_nm615, last
downloaded **05/2019**
- 10 <https://www.bowelcancer australia.org/bowel-cancer-staging>, last downloaded **04/2019**
- 11 <http://hyperphysics.phy-astr.gsu.edu/hbase/Atomic/auger.html>, last downloaded **04/2019**

- 12-I <http://www.africaprocessing.com/pharmaceutical-injection-manufacturing/attachment/pharmaceutical-injection-production-line-africa/>, last downloaded **04/2019**
- 12-II <https://clipground.com/portal-of-entry-clipart.html>, last downloaded **04/2019**
- 12-III <http://www.thirdpartymanufacturers.in/product/edaravone.injection-manufacturers/>, last downloaded **04/2019**
- 12-IV https://www.kncvtbc.org/en/2018/07/25/bedaquiline-price-reduction-could-benefit-the-world/pills_png16549/, last downloaded **04/2019**
- 13 <https://ccr.cancer.gov/news/article/clinical-trial-will-investigate-targeted-radionuclide-therapy-for-inoperable-rare-tumors>, last downloaded **05/2019**
- 14 <https://lungevity.org/for-patients-caregivers/lung-cancer-101/treatment-options/angiogenesis-inhibitors>, last downloaded **05/2019**
- 15 <https://www.cancer.gov/publications/dictionaries/cancer-terms/def/immune-checkpoint-inhibitor>, last downloaded **05/2019**
- 16 <https://www.cancer.gov/news-events/cancer-currents-blog/2018/oncolytic-viruses-to-treat-cancer>, last downloaded **05/2019**
- 17 https://de.wikipedia.org/wiki/Proteinkinase_C, last downloaded **05/2019**
- 18 <https://www.tocris.com/product-type/targeted-protein-degradation>, last downloaded **05/2019**
- 19 <https://www.celesteprize.com/artwork/ido:199593/>, last downloaded **04/2019**
- 20-I <https://www.vectorstock.com/royalty-free-vector/cysteine-proteinogenic-amino-acid-vector-10742395>, last downloaded **04/2019**
- 20-II <https://www.krebsinformationsdienst.de/behandlung/monoklonale-antikoerper.php>, last downloaded **04/2019**
- 20-III <http://clipart-library.com/toxic-cliparts.html>, last downloaded **04/2019**
- 20-IV <http://www.canstockphoto.at/herunterladen-langsam-schnell-32280957.html>, last downloaded **04/2019**
- 21 https://pngtree.com/freepng/color-nuclear-structure_3526126.html, last downloaded **04/2019**
- 22 <https://de.vecteezy.com/vektorkunst/435830-wissenschafts-laborikonen-eingestellt>, last downloaded **05/2019**
- 23 <https://www.kisspng.com/png-optical-microscope-clip-art-black-and-white-art-de-191880/>, last downloaded **05/2019**
- 24-I http://www.brick-shop.de/product_info.php?info=p4461_lego-stein-2x4-pink--3001-.html, last downloaded **05/2019**
- 24-II http://www.brick-shop.de/product_info.php?info=p223_lego-stein-2x4-orange--3001-.html, last downloaded **05/2019**
- 24-III <https://www.scarymommy.com/puzzles/>, last downloaded **05/2019**
- 25 <https://www.together.tum.de/alumni-portraits/kenkichi-sonogashira/>, last downloaded **05/2019**
- 26 <https://www.americanpharmaceuticalreview.com/25303-Pharmaceutical-Incubators/8452255-New-Brunswick-Galaxy-48-R/>, last downloaded **05/2019**
- 27 <https://www.sigmaaldrich.com/technical-documents/articles/biology/96-well-plate-template.html>, last downloaded **05/2019**
- 28 https://www.researchgate.net/publication/324652762_The_Use_of_Hoechst_Dye_for_DNA_Staining_and_beyond/figures?lo=1, last downloaded **05/2019**
- 29 https://forschungsinfrastruktur.bmbwf.gv.at/en/fi/olympus-ix83-live-imaging-microscope_3703, last downloaded **05/2019**

MATERIALS AND METHODS

Reagents and Solvents

DCM, THF, MeOH and Et₂O were dried *via* PURESOLV-columns (Innovative Technology Inc.). Anhydrous DMF, anhydrous DMSO (both Sigma Aldrich) and anhydrous EtOH (Merck Millipore) were commercially acquired and stored *under argon*. HPLC-grade solvents MeCN and water were purchased from Sigma Aldrich and Merck Millipore, respectively. Drying organic solvents after extraction steps was carried out with MgSO₄ (Sigma Aldrich). Sensitive liquids, in terms of air and hygroscopy, were transferred *via* syringe. Starting materials were either commercially acquired or obtained from research group pool.

Chromatographic Methods

TLC (= thin layer chromatography) was conducted by using TLC alumina plates (Merck Millipore, silica gel 60, fluorescence indicator F254). Visualisation of chemical compounds was obtained by irradiating with UV-lamp [254 nm], or with aid of coloring agent Anisaldehyde-Sulphuric acid or Potassium permanganate, Cer-Molybdatophosphoric acid and also Tetrazine (for TCO-species).

Preparative column chromatography was performed with Büchi Sepacore® Flash System (2x Büchi Pump Module C-605, Büchi Pump Manager C-615, Büchi UV-Photometer C-635, Büchi Fraction Collector C-660) or alternatively a Reveleris® Grace system (flash mode) using silica gel 60 (40-63 µm, Merck Millipore) or already packed Büchi (NP) cartridges and distilled or redistilled solvents. Preparative HPLC was conducted on a Reveleris® Grace System (preparative mode) equipped with RP phenomenex® columns or NP ones as well and HPLC-grade solvents. Analytical UHPLC-MS measurements were carried out on Shimadzu Nexera® X2 (LC-30AD pump, SIL-30AC autosampler and CTO-30A column oven). Therefore samples were injected by applying small vials for UHPLC.



Büchi Sepacore® Flash System^{II}



Büchi Reveleris® Grace^{III}



Shimadzu Nexera® X2^{IV}

^{II} <https://www.buchi.com/de-de/products/preparative-chromatography/sepacore-flash-systems-x10-x50>, last downloaded 04/2019

^{III} <https://www.golik.co.il/preparative-chromatography-1>, last downloaded 04/2019

^{IV} <https://www.shimadzu.eu.com/nexera-sr>, last downloaded 04/2019

^V <https://www.chromtech.com/12-x-32-mm-wide-mouth-crimp-55104>, last downloaded 04/2019

NMR Spectroscopy

^1H -NMR, ^{13}C -NMR, H,H-COSY [2D-NMR] and HSQC [2D-NMR] spectra were recorded on a Bruker Avance III HD Ascend™ 600 MHz spectrometer equipped with a CryoProbe Prodigy™ BBO [-196 °C] or on a Bruker Avance III UltraShield™ 400 MHz spectrometer, respectively. The chemical shifts are depicted in ppm (δ) in reference to TMS (tetramethylsilane) and calibrated using solvent residual peaks. All used deuterated NMR-solvents were purchased from VWR (CDCl_3 , d_6 -DMSO, CDOD_3).

NMR analysis data is shown in the following manner:

- chemical shift, multiplicity (s=singlet, d=doublet, t=triplet, q=quartet, quin=quintet, m=multiplet), [coupling constant J] and integration



Bruker Ascend™ 600 MHz Avance III HD^{VI}

^{VI} <https://www.news-medical.net/whitepaper/20151110/The-bedbug-aggregation-pheromone-and-NMR-spectroscopy-an-overview.aspx>, last downloaded 04/2019

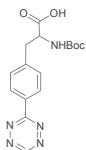
4 | EXPERIMENTAL PART



23-1



Building blocks | **Tetrazines**



4.1 | Synthesis of *N*-[(*tert*-butoxy)carbonyl]-4-(1,2,4,5-tetrazin-3-yl)-*D,L*-phenylalanine (**2**)

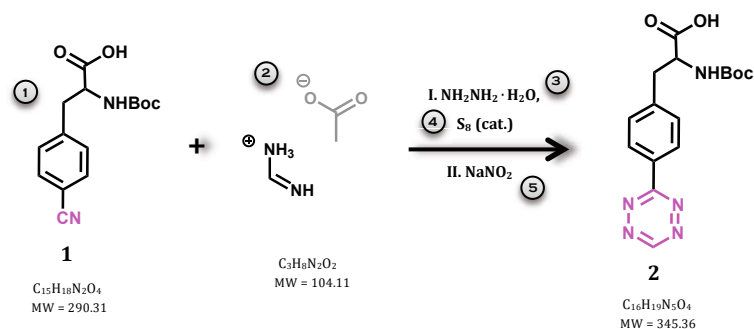


TABLE 1 | Synthesis of *N*-Boc-Phenylalanine-tetrazine (abbreviation)

	Name	Equivalents [-]	Amount of substance [mmol]	Mass [mg]	Volume [ml]	Molecular weight [g/mol]
①	Boc- <i>D,L</i> -4-cyanophenylalanine	1 eq	1.31	381.6	-	290.31
②	Formamidine acetate	4 eq	5.27	548.3	-	104.11
③	Sulphur	1 eq	1.33	42.7	-	32.00
④	Hydrazine monohydrate $\rho = 1.03 \text{ g/cm}^3$	40 eq	52.60	-	2.55	50.06
⑤	Sodium nitrite	7.7 eq	10.10	700.0	-	69.07

This procedure was conducted according to the work of Sauer *et al.*^[47]

The solids Boc-*D,L*-4-cyanophenylalanine **1** ($m = 381.6 \text{ mg}$, 1.31 mmol, 1 eq), formamidine acetate ($m = 548.3 \text{ mg}$, 5.26 mmol, 4 eq) and sulphur ($m = 42.7 \text{ mg}$, 1.31 mmol, 1 eq) were mixed in a round-bottom flask and stirred at room temperature, before hydrazine monohydrate ($V = 2.55 \text{ ml}$, 52.60 mmol, 40 eq) was added under *Ar-atmosphere*. The reaction mixture was stirred furthermore for 19 h overnight. The mixture turned orangey and TLC indicated full consumption of starting material **1**.

The reaction was quenched by addition of 30 ml water. Solid NaNO_2 ($m = 0.7 \text{ g}$, 10.1 mmol, 7.7 eq) was added to the solution. While cooling with an ice-bath [0 °C], 1 N HCl was added dropwise. The color of the solution turned more and more from orange over dark red to characteristic pink as tetrazine was formed.

After extraction with dichloromethane, the organic layer was dried over MgSO_4 , filtered and the solvent evaporated under reduced pressure.

²⁶ <https://www.kisspng.com/png-beaker-laboratory-flask-clip-art-science-png-image-104532/preview.html>

The impure product **2** crystallized after drying *in high vacuo*.

342 mg of impure product was purified *via* LC chromatography – normal phase (**NP**).

- column: silica, 90 g
- injection solvent: dichloromethane | 6 ml
- gradient: DCM / EtOAc + 0.2 % HAc [0 – 50 %]

As the product fractions [75-102] were collected and the solvents evaporated under reduced pressure, acetic acid remained due to lower vapour pressure. To get rid of HAc, an azeotropic mixture by adding toluene was formed, which was then evaporated *in high vacuo* and pink product **2** in form of crystals was obtained.

* | **TLC** – check for full conversion

- DCM/ethylacetate [1:1] + 0.5 % HAc
- r_f -value = 0.55

* | **NMR-DATA**

- $^1\text{H-NMR}$ (600 MHz, CDCl_3): δ = 1.44 (s, 9 H) 3.23 (m, 1 H) 3.37 (m, 1 H) 4.70 (m, 1 H) 5.03 (d, $J=7.6$ Hz, 1 H) 7.47 (d, $J=7.9$ Hz, 2 H) 8.59 (d, $J=7.9$ Hz, 2 H) 10.22 (s, 1 H) ppm

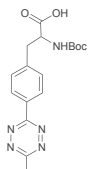
ID-number: BAL001-130

- $^{13}\text{C-NMR}$ (150 MHz, CDCl_3): δ = 28.04 (q) 37.65 (t) 53.85 (d) 80.43 (s) 128.30 (d) 130.24 (s) 132.09 (d) 141.45 (s) 155.12 (s) 157.55 (d) 166.07 (s) 174.65 (s) ppm

ID-number: BAL001-131

* | **YIELD**

- m = 137 mg \Rightarrow 30.3 % (10.01.2018)



4.2 | Synthesis of *N*-[(*tert*-butoxy)carbonyl]-4-(6-methyl-1,2,4,5-tetrazin-3-yl)-D,L-phenylalanine (**3**)

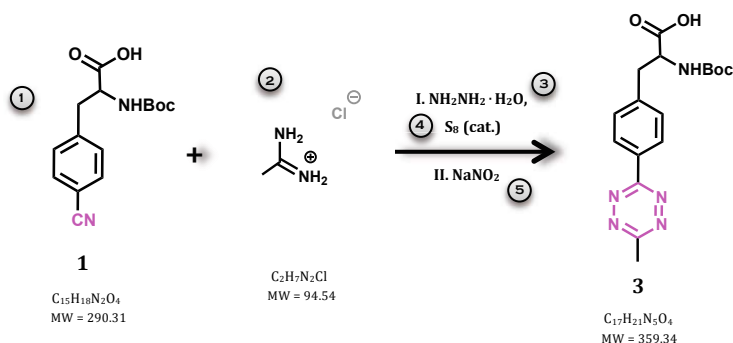


TABLE 2 | Synthesis of *N*-Boc-Phenylalanine-Me-tetrazine (abbreviation)

Name	Equivalents [-]	Amount of substance [mmol]	Mass [mg]	Volume [ml]	Molecular weight [g/mol]
① Boc-D,L-4-cyanophenylalanine	1 eq	1.31	381.6	-	290.31
② Acetamidine hydrochloride	4 eq	5.26	497.3	-	94.54
③ Sulfur	1 eq	1.31	41.9	-	32.00
④ Hydrazine monohydrate $\rho = 1.03 \text{ g/cm}^3$	41 eq	53.63	-	2.60	50.06
⑤ Sodium nitrite	7.7 eq	10.10	700.0	-	69.07

This procedure was carried out based on publication of Sauer and coworkers.^[47]

Boc-D,L-4-cyanophenylalanine **1** ($m = 381.6 \text{ mg}$, 1.31 mmol, 1 eq), acetamidine hydrochloride ($m = 497.3 \text{ mg}$, 5.26 mmol, 4 eq) and sulphur ($m = 41.9 \text{ mg}$, 1.31 mmol, 1 eq) were mixed in a round-bottom flask and stirred at room temperature, before hydrazine monohydrate ($V = 2.60 \text{ ml}$, 53.63 mmol, 41 eq) was added under *Ar-atmosphere*. The reaction mixture was stirred furthermore for 19.5 h overnight. The mixture turned orangey and TLC indicated full conversion to dihydro-tetrazine.

The reaction was quenched by addition of 30 ml water. Solid NaNO_2 ($m = 0.7 \text{ g}$, 10.1 mmol, 7.7 eq) was added to the solution. While cooling with an ice-bath [0 °C], 1 N HCl was added dropwise. The color of the solution turned more and more from orange over dark red to characteristic pink as methyl tetrazine was formed.

After extraction with dichloromethane, the organic layer was dried over MgSO_4 , filtered and the solvent evaporated under reduced pressure.

The dried, yet impure product **3** underwent further purification.

355 mg of impure product was purified *via* LC chromatography – normal phase (**NP**).

- column: silica, 90 g
- injection solvent: dichloromethane | 6 ml
- gradient: DCM / EtOAc + 0.2 % HAc [0 – 50 %]

As the product fractions [91-100] were collected and the solvents evaporated under reduced pressure, acetic acid remained due to lower vapour pressure. To get rid of HAc, an azeotropic mixture by adding toluene was formed, which was then evaporated *in high vacuo* and pink product **3** in form of crystals was obtained.

* | **TLC** – check for full conversion

- DCM/ethylacetate [1:1] + 0.5 % HAc
- r_f -value = 0.46

* | **NMR-DATA**

- $^1\text{H-NMR}$ (600 MHz, CDCl_3): δ = 1.44 (s, 9 H) 3.11 (s, 3 H) 3.22 (m, 1 H) 3.35 (m, 1 H) 4.68 (m, 1 H) 5.02 (d, $J=7.6$ Hz, 1 H) 7.44 (d, $J=7.9$ Hz, 2 H) 8.54 (d, $J=8.2$ Hz, 2 H) ppm

ID-number: BAL008-150

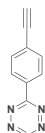
- $^{13}\text{C-NMR}$ (150 MHz, CDCl_3): δ = 20.95 (q) 28.04 (q) 37.57 (t) 53.87 (d) 80.41 (s) 127.94 (d) 130.12 (s) 132.10 (d) 140.70 (s) 155.15 (s) 163.70 (d) 167.01 (s) 174.65 (s) ppm

ID-number: BAL008-151

* | **YIELD**

- m = 91.0 mg \Rightarrow 19.3 %

(31.01.2018)



4.3 | Synthesis of 1-(4-Ethynylphenyl)-1,2,4,5-tetrazine (24)

Part I

4.3.1 | Synthesis of 4-[(Trimethylsilyl)ethynyl]benzonitrile (21)

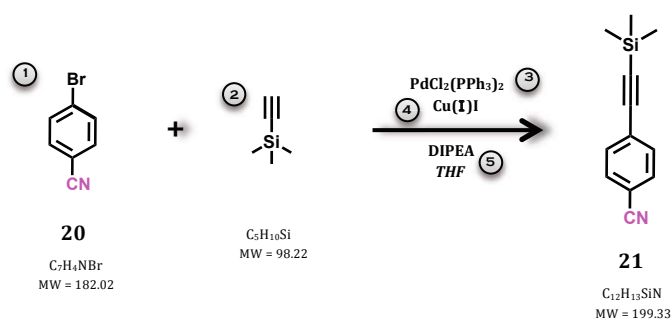


TABLE 3 | Synthesis of 4-(TMS-ethynyl)benzonitrile (abbreviation)

Name	Equivalents [-]	Amount of substance [mmol]	Mass [g]	Volume [ml]	Molecular weight [g/mol]
① 4-Bromobenzonitrile	1 eq	50.2	9.13	-	182.02
② Trimethylsilylacetylene $\rho = 0.71 \text{ g/cm}^3$	1.2 eq	60.2	-	8.57	98.22
③ Bis(triphenylphosphine) palladium dichloride	0.03 eq	1.5	1.06	-	701.90
④ Copper(I)iodide	0.03 eq	1.5	0.29	-	190.45
⑤ Diisopropylethylamine [DIPEA] $\rho = 0.74 \text{ g/cm}^3$	2.5 eq	129.5	-	21.3	69.07

This synthesis was made according to procedure described by Dirk *et al.*¹⁶⁰¹

4-Bromobenzonitrile **20** ($m = 9.13 \text{ g}$, 50.2 mmol, 1 eq), $\text{PdCl}_2(\text{PPh}_3)_2$ ($m = 1.06 \text{ g}$, 1.5 mmol, 0.03 eq) and copper(I)iodide ($m = 0.29 \text{ g}$, 1.5 mmol, 0.03 eq) were weighed out in an oven-dried round-bottom flask. Then liquid TMS-acetylene ($V = 8.57 \text{ ml}$, 60.2 mmol, 1.2 eq) was added to the solids. The reactants were homogenized by addition of 50 ml anhydrous THF, and the reaction mixture was degassed using *argon* on the ultrasonic bath. DIPEA ($V = 21.3 \text{ ml}$, 129.5 mmol, 2.5 eq) was added and the reaction mixture stirred overnight at 45 °C.

After cooling to room temp., the black reaction mixture was filtered and diluted with dichloromethane. The organic layers were washed with ammonium chloride solution, sat. The organic layer had to be diluted with diethyl ether, since the phase separation of the layers was poorly visible using DCM/water. The combined organic layers were dried over MgSO_4 , filtered and the solvents evaporated under reduced pressure.

The dark brown/black residue was purified *via* NP-LC chromatography.

- column: silica, 90 g
- **dry** loading
- gradient: PE / Et₂O [0 – 15 %]

Normal phase liquid chromatography in the manner of dry loading was carried out, as there was no proper solvent for liquid injection.

Product fractions [12-36] were collected and the solvents evaporated under reduced pressure to obtain beige-colored crystals of **21**.

* | **TLC** – check for full conversion

- PE / Et₂O [7:1]
- *r_f*-value = 0.63

* | **NMR-DATA**

- ¹H-NMR (400 MHz, CDCl₃): δ = 0.27 (s, 9 H) 7.53 – 7.61 (q, *J*=8.2 Hz, *J*=15.2 Hz, 4 H) ppm

ID-number: BAL047-10

- ¹³C-NMR (100 MHz, CDCl₃): δ = 0.29 (q) 99.55 (s) 102.96 (s) 111.77 (s) 118.40 (s) 128.00 (s) 131.91 (d)
132.43 (d) ppm

ID-number: BAL047-11

* | **YIELD**

- *m* = 7.27 g ⇒ 73.0 %

(25.05.2018)

Part II

4.3.2 | Synthesis of 4-Ethynylbenzonitrile (**22**)

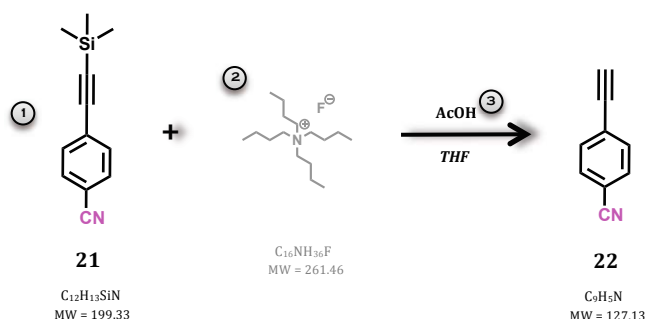


TABLE 4 | Synthesis of 4-Ethynylbenzonitrile

Name	Equivalents [-]	Amount of substance [mmol]	Mass [g]	Volume [ml]	Molecular weight [g/mol]
① 4-(TMS-ethynyl)-benzonitrile	1 eq	35.1	7.0	-	199.33
② Tetrabutylammonium fluoride [1 M] $\rho = 0.90 \text{ g/cm}^3$	1.1 eq	38.6	-	38.6	261.46
③ Acetic acid $\rho = 1.05 \text{ g/cm}^3$	1.5 eq	52.7	-	3.0	60.05

4-(TMS-ethynyl)benzonitrile **21** ($m = 7.0 \text{ g}$, 35.1 mmol, 1 eq) was dissolved in 100 ml anhydrous dichloromethane in a three-necked round-bottom flask. Under *Ar atmosphere* acetic acid ($V = 3.0 \text{ ml}$, 52.7 mmol, 1.5 eq) was added and the reaction mixture cooled to 0 °C with an ice-bath. A anhydrous THF-solution of TBAF [1 M] ($V = 38.6 \text{ ml}$, 38.6 mmol, 1.1 eq) was added dropwise to the mixture and the clear bright-yellow solution was stirred at 0 °C for 2 h until TLC confirmed full conversion – solution color turned to orange-brown.

* | TLC – check for full conversion

- PE / Et₂O [7:1]
- r_f -value = 0.40

The reaction mixture was allowed to warm to room temperature. It was washed with water [4x 50 ml] and NaHCO₃, sat. [4x 40 ml], respectively. The combined organic layers were furthermore washed with brine [2x 50 ml], dried over MgSO₄, filtered and the solvents evaporated under reduced pressure to obtain the cereal-lookalike beige-brown powdery product **22**.

* | NMR-DATA

- ¹H-NMR (400 MHz, CD₃OD): δ = 3.86 (s, 1 H) 7.63 (d, *J*=8.6 Hz, 2 H) 7.71 (d, *J*=7.8 Hz, 2 H) ppm

ID-number: BAL049-10

- ¹³C-NMR (100 MHz, CD₃OD): δ = 80.65 (d) 81.62 (s) 113.89 (s) 119.74 (s) 129.26 (s) 133.94 (d) 134.39 (d) ppm

ID-number: BAL049-11

* | YIELD

- m = 4.34 g → 97.0 %

(08.06.2018)

Part III

4.3.3 | Synthesis of Methyl-4-ethynyl benziminoester hydrochloride (23)

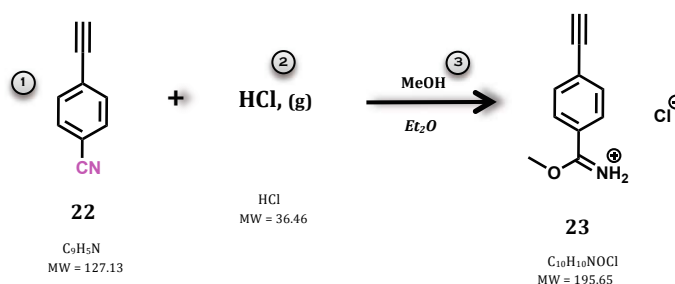


TABLE 5 | Synthesis of Me-4-ethynyl benziminoester HCl (abbreviation)

Name	Equivalents [-]	Amount of substance [mmol]	Mass [g]	Volume [ml]	Molecular weight [g/mol]
① Ethynyl benzonitrile	1 eq	10.2	1,30	-	127.13
② Hydrogen chloride gas	~ 60 eq	-	-	-	36.52
③ Methanol ρ = 0.79 g/cm ³	6.1 eq	61.9	-	2.7	32.04

This formulation was conducted based on the procedure of Lang and coworkers.^[62]

Ethynylbenzonitrile **22** (m = 1.3 g, 10.2 mmol, 1 eq) was dissolved in anhydrous MeOH (V = 2.7 ml, 61.9 mmol, 6.1 eq) and 50 ml anhydrous diethyl ether, in a three-necked round-bottom flask – equipped with reflux condenser – to give a red suspension. Via dropwise addition of H₂SO₄, conc. to 100 g NH₄Cl salt, HCl-gas was generated and passed into the reaction flask between 0°C and r.t. within 1.5 h. To ensure having anhydrous hydrogen chloride gas, a wash bottle with H₂SO₄, conc. as drying agent was installed right ahead the reaction flask.

The crude product solution was allowed to stand for the next day in refrigerator at 4°C to gain product precipitation.

The solvents were evaporated under reduced pressure to obtain **23** as a bright brown powdery *Pinner-salt* product.

* | **TLC** – check for full conversion

- PE / Et₂O [7:1]
- *r_F*-value = 0.06

* | **NMR-DATA**

- ¹H-NMR (400 MHz, CD₃OD): δ = 3.86 (s, 1 H) 4.33 (s, 3 H) 7.63 (d, *J*=9.0 Hz, 2 H) 7.71 (m, 2 H) 7.99 (d, *J*=9.0 Hz, 2 H) ppm

ID-number: BAL050-10

- ¹³C-NMR (100 MHz, CD₃OD): δ = 83.13 (d) 83.58 (q) 84.45 (s) 113.68 (s) 119.53 (s) 130.39 (s) 133.72 (d) 134.17 (d) ppm

ID-number: BAL050-11

* | **YIELD**

- *m* = 1.63 g ⇒ 81.5 % (12.06.2018)

Part IV

4.3.4 | **Synthesis of 4-Ethynylphenyl-1,2,4,5-tetrazine (24)**

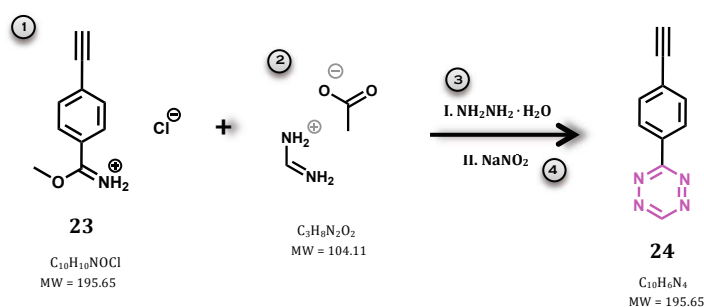


TABLE 6 | Synthesis of Ethynylphenyl tetrazine (abbreviation)

	Name	Equivalents [-]	Amount of substance [mmol]	Mass [g]	Volume [ml]	Molecular weight [g/mol]
①	Me-4-ethynyl benz-Iminoester HCl	1 eq	8.33	1,63	-	195.65
②	Formamidinium acetate	4 eq	33.33	3.47	-	104.11
③	Hydrazine monohydrate $\rho = 1.03 \text{ g/cm}^3$	40 eq	333.0	-	16.2	50.06
④	Sodium nitrite	7.7 eq	18.91	4.41	-	69.07

This synthesis had the same experimental approach as reported by Wilkovitsch.^[59]

A mixture of methyl-4-ethynyl benziminoester HCl **23** ($m = 1.63 \text{ g}$, 8.33 mmol, 1 eq) and formamidine acetate ($m = 3.47 \text{ g}$, 33.3 mmol, 4 eq) was weighed out in a three-necked round-bottom flask with stopcock and dropping funnel. Under *Ar atmosphere* hydrazine monohydrate ($V = 16.2 \text{ ml}$, 333 mmol, 40 eq) was added dropwise while cooling with an icebath [0 °C]. After allowing to warm to room temp., the red-brown reaction mixture was stirred for approx. 20 h overnight.

Pouring onto ice-water led to precipitation of the dihydro-tetrazine-derivative, which was collected by filtration as a bright brown solid. The remaining oxidation step was conducted upon two different strategies that were compared.

Starting with the one, wherein half amount of the just obtained dihydro-tetrazine ($m = 0.43 \text{ g}$) was dissolved in 70 ml MeOH and 20 ml water, respectively. While keeping the temperature between 0 °C and 5 °C using an ice bath, NaNO_2 ($m = 2.20 \text{ g}$, 9.95 mmol, 3.85 eq) was added to reaction mixture within 10 min. Afterwards, 1 N HCl was added dropwise to form the desired tetrazine moiety. Solvents were evaporated *in high vacuo* and the residue dissolved in small amounts of dichloromethane, as well as drops of MeOH, for purifying *via* NP-liquid chromatography.

The other half amount of dihydro-species was dissolved in 18 ml glacial acetic acid. Again, solid NaNO_2 ($m = 2.20 \text{ g}$, 9.95 mmol, 3.85 eq) was added within 10 min at temperature levels between 0 °C and 5 °C. The impure product **24** precipitated by pouring on ice-cold water and was filtered. The pink compound was finally purified *via* NP-liquid chromatography.

Both differently synthesized solids were purified *via* LC chromatography – normal phase (**NP**).

- column: silica, 90 g
- injection solvent: dichloromethane + drops of MeOH | 6 ml
- gradient: PE / EtOAc [0 – 30 %]

Product fractions were collected in almost same amounts concerning both strategies and the solvents evaporated under reduced pressure to obtain **24** as pink crystals.

* | **TLC** – check for full conversion

- PE / EE [2:1]
- r_f -value = 0.74

* | **NMR-DATA**

- $^1\text{H-NMR}$ (400 MHz, CD_3OD): $\delta = 3.79$ (s, 1 H) 7.72 (d, $J=8.6 \text{ Hz}$, 2 H) 8.58 (d, $J=8.6 \text{ Hz}$, 2 H) 10.35 (s, 1 H) ppm

ID-number: BAL057-80

- $^{13}\text{C-NMR}$ (100 MHz, CD_3OD): $\delta = 82.20$ (d) 82.22 (s) 117.63 (s) 128.53 (s) 129.23 (d) 134.04 (d) 159.44 (d) 167.49 (s) ppm

ID-number: BAL057-81

* | YIELD

- m = 74.3 mg → 4.0 %

(28.06.2018)



4.4 | Synthesis of 3-Methyl-6-methylthio-1,2,4,5-tetrazine (27)

Part I

4.4.1 | Synthesis of S-Methylisothio-carbohydrazide hydrogeniodide (26)

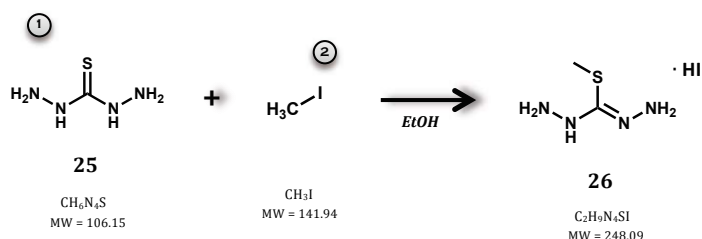


TABLE 7 | Synthesis of Methylisothio-carbohydrazide-HI (abbreviation)

Name	Equivalents [-]	Amount of substance [mmol]	Mass [g]	Volume [ml]	Molecular weight [g/mol]
① Thiocarbohydrazide	1 eq	145.6	15.45	-	106.15
② Methyl iodide $\rho = 2.28 \text{ g/cm}^3$	1.12 eq	163.0	-	10.2	141.94

This synthesis was conducted based on the work of Scott *et al.*^[64]

A suspension of thiocarbohydrazide **25** ($m = 15.45 \text{ g}$, 145.6 mmol, 1 eq) in 400 ml anhydrous EtOH was heated under reflux. Methyl iodide ($V = 10.2 \text{ ml}$, 163.0 mmol, 1.12 eq) was added dropwise, within 15 min. Heating continued for 2 h until solution became clear and TLC indicated full conversion.

The mixture was filtered hot and product **26** crystallized on cooling. After another filtration, the product was collected and dried *in vacuo*.

* | TLC – check for full conversion

- EE + drops of MeOH
- r_f -value = 0.87

* | NMR-DATA

- $^1\text{H-NMR}$ (400 MHz, d_6 -DMSO): $\delta = 2.38$ (s, 3 H) 5.28 (s, 4 H) 9.65 (s, 1 H) ppm

ID-number: BAL058-20

- $^{13}\text{C-NMR}$ (100 MHz, d_6 -DMSO): $\delta = 12.85$ (q) 171.07 (s) ppm

ID-number: BAL058-21

* | YIELD

- $m = 26.51 \text{ g} \Rightarrow 73.6 \%$ (10.07.2018)

Part II

4.4.2 | Synthesis of 3-Methyl-6-methylthio-1,2,4,5-tetrazine (27)

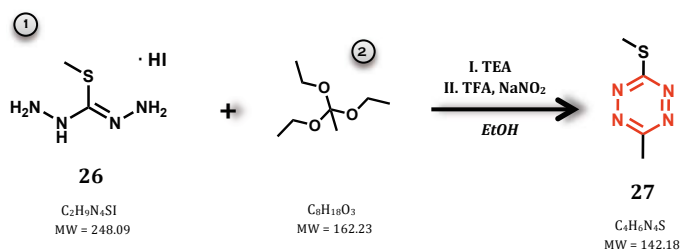


TABLE 8 | Synthesis of Methyl-methylthio-Tetrazine (abbreviation)

Name	Equivalents [-]	Amount of substance [mmol]	Mass [g]	Volume [ml]	Molecular weight [g/mol]
① S-Methylisothio-carbohydrazide HI	1 eq	20.2	5.0	-	248.09
② Triethyl-orthoacetate $\rho = 0.89 \text{ g/cm}^3$	1.4 eq	28.3	-	5.2	162.23
③ Triethylamine [TEA] $\rho = 0.73 \text{ g/cm}^3$	1 eq	20.2	-	2.8	101.19
④ Sodium nitrite	2.1 eq	42.4	2.9	-	68.99
⑤ Trifluoroacetic acid [TFA] $\rho = 1.48 \text{ g/cm}^3$	1 eq	20.2	-	1.6	114.02

This synthesis was carried out by following the procedure of Heil and coworkers.^[65]

S-Methylisothio-carbohydrazide HI **26** (m = 5.0 g, 20.2 mmol, 1 eq) was weighed out in a three-necked round-bottom flask and suspended in 150 ml anhydrous EtOH. The suspension was stirred for 30 min at room temperature. Then triethyl orthoacetate (V = 5.2 ml, 28.3 mmol, 1.4 eq) was added into the flask. Under atmosphere of *argon*, addition of base TEA (V = 2.8 ml, 20.2 mmol, 1 eq) followed and the reaction mixture was heated to reflux for 1 h.

Thereafter sodium nitrite (m = 2.9 g, 42.4 mmol, 2.1 eq) and TFA acid (V = 1.6 ml, 20.2 mmol, 1 eq) were added to the reaction mixture and the mixture was heated for another 30 min. The color of the solution turned from red to deep red.

After addition of n-hexane [150 ml], the solution was allowed to cool down to room temperature. Degassing with *argon* was applied and the mixture was stirred for further 30 min at rt. To the solution water [300 ml] was added and the red product was extracted with Et₂O [150 ml] three times, dried over MgSO₄ and the solvents evaporated under reduced pressure.

* | **TLC** – check for full conversion

- DCM / n-hexane [40 %]

- r_f -value = 0.19

Purification was carried out *via* LC chromatography - normal phase (**NP**).

- column: silica, 90 g
- injection solvent: dichloromethane + drops of MeOH | 6 ml
- gradient: n-hexane / DCM [30 – 100 %]

The product fractions [40-80] were combined and the solvents evaporated under reduced pressure to receive the desired product **27** as a deep red oil.

* | NMR-DATA

- ¹H-NMR (400 MHz, CDCl₃): δ = 2.74 (s, 3 H) 2.99 (s, 3 H) ppm

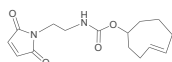
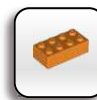
ID-number: *BAL093-40*

- ¹³C-NMR (100 MHz, CDCl₃): δ = 13.31 (q) 20.63 (q) 53.41 (s) ppm

ID-number: *BAL093-41*

* | YIELD

- m = 228 mg ⇒ 7.9 % (13.12.2018)



4.5 | Synthesis of (E)-cyclooct-4-en-1-yl N-[2-(1-maleimidyl)ethyl] carbamate (VIII)

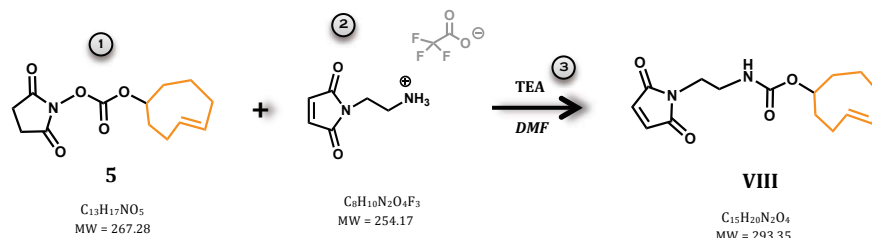


TABLE 9 | Synthesis of Maleimide-TCO carbamate (abbreviation)

Name	Equivalents [-]	Amount of substance [μmol]	Mass [mg]	Volume [μl]	Molecular weight [g/mol]
① (E)-cyclooct-4-enyl succinimidyl carbonate [TCO-NHS]	1 eq	34.0	9.1	-	267.28
② N-(2-aminoethyl) maleimide trifluoroacetate	1.1 eq	37.5	9.6	-	254.17
③ Triethylamine [TEA] $\rho = 0.73 \text{ g/cm}^3$	3 eq	102.0	-	14.8	101.19

N-(2-aminoethyl)maleimide trifluoroacetate ($m = 9.6 \text{ mg}$, $37.5 \mu\text{mol}$, 1.1 eq) was weighed out in a small vial and dissolved in 0.5 ml DMF, dry. Then base TEA ($V = 14.8 \mu\text{l}$, $102.0 \mu\text{mol}$, 3 eq) was added to the solution, followed by TCO-NHS carbonate [transcyclooctenyl N-hydroxy-succinimidyl carbonate] **5** ($m = 9.1 \text{ mg}$, $34.0 \mu\text{mol}$, 1 eq). The reaction mixture was stirred for 45 min at room temperature, after which LC-MS indicated full conversion.

* | HPLC-MS

- m/q: product | 294 & 315

* | TLC – check for full conversion

- DCM / n-hexane [40 %]

- r_f -value = 0.19

Impure product was purified *via* HPLC chromatography – reversed phase (RP).

- column: C-18, phenomenex

- injection solvent: DMSO / water [10%] | 4 ml

- gradient: water + 0.1 % FA / acetonitrile + 0.1 % FA [15 – 75 %]

Product fractions [29 & 30] were collected and the solvents evaporated *in high vacuo* to obtain **VIII** as bright orange oil.

* | NMR-DATA

- ¹H-NMR (400 MHz, d₆-DMSO): δ = 1.52 – 2.26 (m, 10 H) 3.08 (m, 2 H) 3.42 (t, *J*=5.9 Hz, 2 H) 4.17 (m, 1 H) 4.53 (s, 1 H) 5.42 (m, 1 H) 5.55 (m, 1 H) 6.99 (s, 2 H) ppm

ID-number: BAL015-60

- ¹³C-NMR (100 MHz, d₆-DMSO): δ = 30.60 (t) 32.14 (t) 33.75 (t) 37.44 (t) 38.36 (t) 40.58 (t) 79.12 (d) 132.52 (d) 134.48 (d) 134.91 (d) 155.89 (s) 171.05 (s) ppm

ID-number: BAL015-61

* | YIELD

- m = 6.9 mg ⇒ 69.0 %

(16.01.2018)

Barbas linker

4.6 | Synthesis of

2-[4-[2-[2-[2-(2-Azidoethoxy)ethoxy]ethoxy]ethoxy]phenyl]-5-(methylsulfonyl)-1,3,4-oxadiazole (12)

Part I

4.6.1 | Synthesis of

2-[2-[2-(2-Azidoethoxy)ethoxy]ethoxy]ethanol (8)

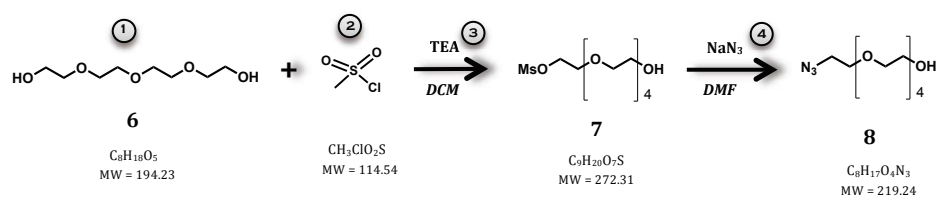


TABLE 10 | Synthesis of TEG-monoazid (abbreviation)

	Name	Equivalents [-]	Amount of substance [mmol]	Mass [g]	Volume [ml]	Molecular weight [g/mol]
①	Tetraethylglycol $\rho = 1.12 \text{ g/cm}^3$	1 eq	257	50.0	44.6	194.23
②	Methylsulfonylchloride [Mesyl-Cl] $\rho = 1.48 \text{ g/cm}^3$	0.9 eq	232	-	17.9	114.54
③	Triethylamine [TEA] $\rho = 0.73 \text{ g/cm}^3$	1.5 eq	395	-	54.8	101.19
④	Sodium azide	1.8 eq	460	29.9	-	65.01

This synthesis was carried out based on procedure already reported by Goswami *et al.*^[51]

Mesylchloride (V = 17.9 ml, 232 mmol, 0.9 eq) was added with the aid of a syringe pump dropwise to a solution of TEG **6** (m = 50.0 g, 257 mmol, 1 eq) and TEA (V = 54.8 ml, 395 mmol, 1.5 eq) in 300 ml anhydrous DCM, in a three-necked round bottom flask, under *nitrogen* at 0 °C. After finished addition, the mixture was stirred at 0 °C for 30 min. The mixture was allowed to warm to room temperature and stirred overnight.

¹H-NMR measurement of crude intermediate showed good conversion.

After filtering and thereupon evaporating the solvent, volatiles were removed *in vacuo*. The residue was washed with 3 % HCl and brine [100 ml each, 3x]. The product was extracted with DCM, the organic layers were combined and dried over MgSO₄. After filtration, the solvent was evaporated under reduced pressure.

The obtained TEG-OMs **7** was dissolved in 150 ml DMF, dry and sodium azide (m = 29.9 g, 460 mmol, 1.8 eq) was added. The reaction mixture was stirred for 72 h over weekend at 60 °C.

The crude mixture was filtered before evaporating DMF *in high vacuo*. The yellow oily crude product was filtered over a short plug of celite, followed by additional washing with ether twice. The solvent was evaporated and 5 g of crude product were purified *via* LC chromatography – normal phase (**NP**).

- column: silica, 90 g
- injection solvent: dichloromethane | 6 ml
- gradient: methanol / DCM [0 – 4 %]

Product fractions were collected and the solvents evaporated under reduced pressure to obtain the monoazide-product **8** as yellow-orange oil.

*** | TLC – check for full conversion**

- MeOH / dichloromethane [2 %]
- *r_f*-value = 0.22 (for mesylated intermediate) & 0.33 (for azide-product)

*** | NMR-DATA**

- ¹H-NMR (400 MHz, CD₃OD): δ = 3.37 (t, *J*=5.1 Hz, 2 H) 3.56 (t, *J*=5.1 Hz, 2 H) 3.66 (m, 12 H) 4.82 (s, 1 H) ppm

ID-number: BAL021-60

- ¹³C-NMR (100 MHz, CD₃OD): δ = 51.90 (t) 62.37 (t) 71.27 (t) 71.55 (t) 71.65(t) 71.77 (t) 71.81 (t) 73.82 (t) ppm

ID-number: BAL021-61

*** | YIELD**

- m = 1.36 g → 27.2 % (23.02.2018)

Part II

4.6.2 | Synthesis of 2-[2-[2-(2-Azidoethoxy)ethoxy]ethoxy]ethyl iodide (10)

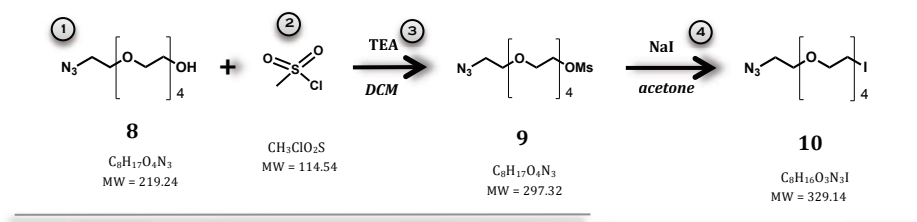


TABLE 11 | Synthesis of TEG-azide-iodide (abbreviation)

	Name	Equivalents [-]	Amount of substance [mmol]	Mass [g]	Volume [ml]	Molecular weight [g/mol]
①	TEG-monoazide	1 eq	5.79	1.27	-	219.24
②	Methylsulfonylchloride [Ms-Cl] $\rho = 1.48 \text{ g/cm}^3$	1.5 eq	8.69	-	0.7	114.54
③	Triethylamine [TEA] $\rho = 0.73 \text{ g/cm}^3$	2 eq	11.59	-	1.6	101.19
④	Sodium iodide	4 eq	16.68	2.50	-	149.89

This conduct has the same experimental approach as the previous synthetic step.^[51]

TEA (m = 1.17 g, 11.59 mmol, 2 eq) and TEG-monoazide **8** (m = 1.27 g, 5.79 mmol, 1 eq) were dissolved in 35 ml anhydrous DCM in a two-necked round-bottom flask, before adding MsCl (V = 0.7 ml, 8.69 mmol, 1.5 eq) in 20 ml anhydrous DCM, slowly over 30 min *via* perfusor, while stirring at 0 °C. After 1.5 h at 0 °C and further 2 h at room temperature, TLC was made to check turnover.

Extraction was conducted with DCM [150 ml, 3x]. The organic layer was washed with 3 % HCl and brine [100 ml each, 3x], dried over MgSO_4 , filtered and the solvent evaporated under reduced pressure.

TEG-azide-OMs **9** (m = 1.24 g, 4.17 mmol, 0.7 eq) was dissolved in 150 ml acetone, dry before sodium iodide (m = 2.5 g, 16.68 mmol, 4 eq) was added in one portion. The reaction mixture was stirred at 65 °C overnight for 15 h.

After filtration, the mixture was concentrated to dryness. The residue was filtered over celite, followed by additional washing with DCM. The product **10** was obtained after evaporating the solvent under reduced pressure.

* | **TLC** – check for full conversion

- MeOH / DCM [4 %]

- r_f -value = 0.44 (for mesylated intermediate) & 0.24 (for iodinated product)

* | NMR-DATA

- $^1\text{H-NMR}$ (400 MHz, CD_3OD): $\delta = 3.31$ (t, $J=8.3$ Hz, 2 H) 3.38 (t, $J=5.9$ Hz, 2 H) 3.66 (m, 10 H) 3.75 (t, $J=6.8$ Hz, 2 H) ppm

ID-number: BAL022-20

* | YIELD

- m = 1.37 g \Rightarrow 72.1 % (27.02.2018)

Part III

4.6.3 | Synthesis of 2-[2-[2-(2-Azidoethoxy)ethoxy]ethoxy]ethoxybenzoic acid, ethyl ester (11)

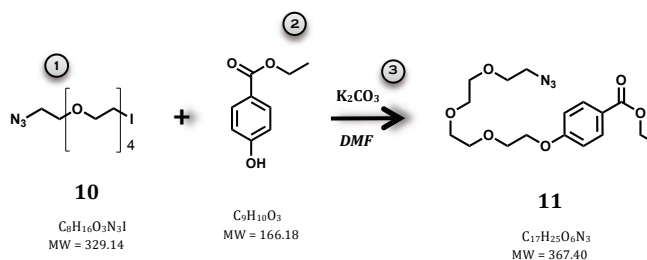


TABLE 12 | Synthesis of TEG-azide-benzoic acid, ethylester (abbreviation)

	Name	Equivalents [-]	Amount of substance [mmol]	Mass [g]	Volume [ml]	Molecular weight [g/mol]
①	TEG-azide-iodide	1.2 eq	4.15	1.37	-	329.14
②	4-Hydroxybenzoic acid, ethyl ester	1 eq	3.46	0.58	-	166.18
③	Potassium carbonate	3.3 eq	11.4	1.58	-	367.40

This procedure was carried out according to the publication of Toda and coworkers.^[52]

TEG-azide-iodide **10** (m = 1.37 g, 4.15 mmol, 1.2 eq) was weighed out in a three-necked round-bottom flask and dissolved in 60 ml DMF, dry. K_2CO_3 salt (m = 1.58 g, 11.4 mmol, 3.3 eq) was added to the solution. Thereafter, 4-Hydroxybenzoic acid, ethyl ester (m = 0.58 g, 3.46 mmol, 1 eq) was added to the flask mixture which was stirred at 65 °C overnight.

After removing solid material *per* filtration, organic solvents were evaporated *in high vacuo*.

Purification was applied *via* LC chromatography – normal phase (**NP**), after checking conversion with TLC.

- column: silica, 90 g
- injection solvent: dichloromethane + drops MeOH | 6 ml

- gradient: PE / EE [5 – 95 %]

The solvents were evaporated under reduced pressure after collecting the product **11** fractions [90-122].

* | **TLC** – check for full conversion

- EE + drops MeOH

- r_f -value = 0.19

* | **NMR-DATA**

- $^1\text{H-NMR}$ (400 MHz, CDCl_3): δ = 1.38 (t, $J=7.8$ Hz, 3 H) 3.38 (t, $J=5.9$ Hz, 2 H) 3.67 (m, 10 H) 3.88 (t, $J=5.1$ Hz, 2 H) 4.18 (t, $J=4.3$ Hz, 2 H) 4.35 (q, $J=8.2$ Hz, 2 H) 6.94 (d, $J=9.8$ Hz, 2 H) 7.98 (d, $J=9.0$ Hz, 2 H) ppm

ID-number: BAL023-60

- $^{13}\text{C-NMR}$ (100 MHz, CDCl_3): δ = 14.34 (q) 50.64 (t) 60.59 (t) 67.52 (t) 69.52 (t) 70.01 (t) 70.67 (t) 70.86 (t) 114.09 (d) 123.05 (s) 131.46 (d) 162.44 (s) 166.32 (s) ppm

ID-number: BAL023-61

* | **YIELD**

- $m = 0.95$ g \Rightarrow 62.1 %

(06.03.2018)

Part IV

4.6.4 | **Synthesis of**

2-[2-[2-(2-Azidoethoxy)ethoxy]ethoxy]ethoxybenzoic acid, hydrazide (12)

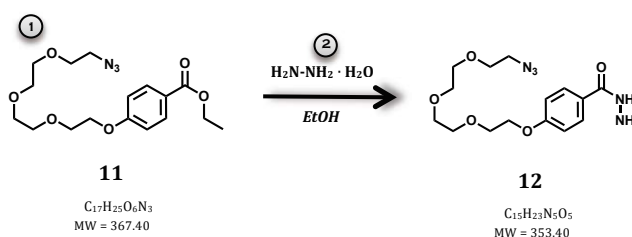


TABLE 13 | Synthesis of TEG-azide-benzoic acid, hydrazide (abbreviation)

	Name	Equivalents [-]	Amount of substance [mmol]	Mass [g]	Volume [μl]	Molecular weight [g/mol]
①	TEG-azide-benzoic acid, ethyl ester	1 eq	1.31	0.48	-	367.40
②	Hydrazine monohydrate $\rho = 1.03$ g/cm ³	5 eq	6.53	-	317	353.40

This synthesis was conducted according to the procedure of Toda and coworkers, as well.^[52]

To a solution of TEG-azide-benzoic acid, ethyl ester **11** (m = 0.48 g, 1.31 mmol, 1 eq) in 0.2 ml EtOH was added hydrazine monohydrate (V = 317 μ l, 6.53 mmol, 5 eq) at room temperature. The reaction mixture was stirred at 70 °C overnight.

The next day the solvent was removed *in vacuo*.

Purification was conducted *via* LC chromatography – normal phase (**NP**), after checking conversion with TLC.

- column: silica, 90 g
- injection solvent: dichloromethane + drops MeOH | 6 ml
- gradient: EE / MeOH [0 – 60 %]

The solvents were evaporated under reduced pressure after collecting the product **12** fractions [19-46].

*** | TLC – check for full conversion & HPLC-MS**

- EE / MeOH [3:1]
- r_f -value = 0.67

- m/q: product | 354 & 376

*** | NMR-DATA**

- $^1\text{H-NMR}$ (600 MHz, CD_3OD): δ = 3.35 (t, $J=4.4$ Hz, 2 H) 3.64 – 3.71 (m, 10 H) 3.86 (t, $J=4.1$ Hz, 2 H) 4.18 (t, $J=4.1$ Hz, 2 H) 7.01 (d, $J=8.8$ Hz, 2 H), 7.75 (d, $J=8.2$ Hz, 2 H) ppm

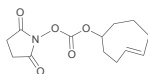
ID-number: *BAL029-10*

*** | YIELD**

- m = 0.27 g \Rightarrow 58.9 %

(29.03.2018)

TCO – synthesis from the start



4.7 | Synthesis of (Z)-cyclooct-4-en-1-ol (29)

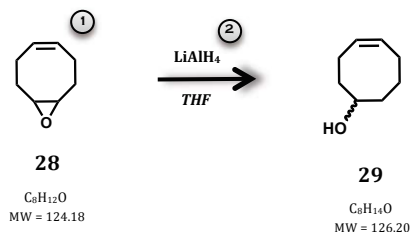


TABLE 14 | Synthesis of (Z)-cyclooct-4-en-1-ol

	Name	Equivalents [-]	Amount of substance [mmol]	Mass [g]	Volume [ml]	Molecular weight [g/mol]
①	(Z)-9-oxabicyclo[6.1.0]non-4-ene	1 eq	49.4	6.14	-	124.18
②	Lithium aluminium hydride	~ 4 eq	47.7	1.84	-	37.95

This synthesis was made by following the procedure that is commonly used within our research group.

To a suspension of LiAlH_4 ($m = 1.84 \text{ g}$, 47.7 mmol , 4 eq) in 100 ml anhydrous THF was added a solution of (Z)-9-oxabicyclo[6.1.0]non-4-ene **28** ($m = 6.14 \text{ g}$, 49.4 mmol , 1 eq) in 100 ml anhydrous THF dropwise in an ice-bath [$0 \text{ }^\circ\text{C}$]. After allowing the mixture to warm to room temperature, it was stirred overnight at $35\text{-}40 \text{ }^\circ\text{C}$.

The next day TLC confirmed the turnover. Hydrolysis followed, based upon the so called **Fieser workup procedure**². Therefore the reaction mixture was diluted with 50 ml diethyl ether and cooled to $0 \text{ }^\circ\text{C}$, followed by gently addition of $2 \text{ ml H}_2\text{O}$. Then $2 \text{ ml } 15 \text{ \% NaOH (w/w)}$ were added as well as $6 \text{ ml H}_2\text{O}$. The suspension was stirred rigorously for 15 min . Thereafter, the mixture was allowed to warm to room temperature and MgSO_4 was added. After another 15 min with stirring, the formed solid was filtered over a short plug of celite, additionally washed with THF. The organic layer was dried over MgSO_4 , filtered and the solvents evaporated under reduced pressure.

* | TLC – check for full conversion

- PE / EE [4:1]
- r_f -value = 0.36

No further purification steps were carried out concerning product **29**.

² http://chem.chem.rochester.edu/~nvd/pages/magic_formulas.php?page=aluminum_hydride_reduction

* | NMR-DATA

- ¹H-NMR (400 MHz, CDCl₃): δ = 1.60 – 1.86 (m, 6 H) 2.04 – 2.29 (m, 4 H) 3.77 (m, 1 H) 5.57 (m, 1 H)
5.65 (m, 1 H) ppm

ID-number: BAL020-20

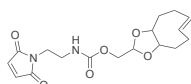
- ¹³C-NMR (100 MHz, CDCl₃): δ = 22.69 (t) 24.79 (t) 25.54 (t) 36.19 (t) 37.51 (t) 72.56 (d) 129.39 (d) 130.02 (d) ppm

ID-number: BAL020-21

* | YIELD

- m = 5.86 g ⇒ 94.0 %

(21.02.2018)



4.8 | Synthesis of (E)-cyclooct-7-en-1,3-dioxolyl-2-methyl N-[2-(1-maleimidyl)ethyl] carbamate (IX)

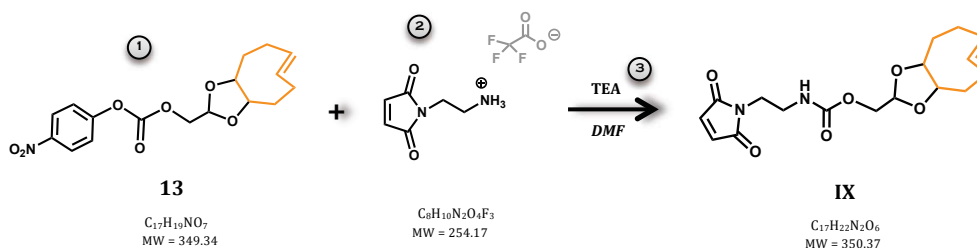


TABLE 15 | Synthesis of Maleimide-dTCO carbamate (abbreviation)

Name	Equivalents [-]	Amount of substance [mmol]	Mass [mg]	Volume [μ l]	Molecular weight [g/mol]
① (E)-cyclooct-7-en-1,3-dioxolyl-2-methyl 4-nitrophenyl carbonate [PNP-dTCO]	1 eq	0.16	56.2	-	349.34
② N-(2-aminoethyl)maleimide trifluoroacetate	1.1 eq	0.17	45.0	-	254.17
③ Triethylamine [TEA] $\rho = 0.73 \text{ g/cm}^3$	3 eq	0.48	-	66.6	101.19

N-(2-aminoethyl)maleimide trifluoroacetate (m = 45.0 mg, 0.17 mmol, 1.1 eq) was weighed out in a small vial before 0.5 ml DMF, dry was added to dissolve the salt. Base TEA (V = 66.6 μ l, 0.48 mmol, 3 eq) was added to the solution and immediately afterwards also compound *PNP-dTCO carbonate* [para-nitrophenyl-dioxolyl-transcyclooctenyl carbonate] **13** (m = 56.2 mg, 0.16 mmol, 1 eq). The reaction mixture was stirred for 1 h at room temperature. Conversion was confirmed *per* both, TLC and HPLC-MS measurement.

* | HPLC-MS

- m/q: product | 351 & 373

* | TLC – check for full conversion

- MeOH / DCM [5 %]

- r_f -value = 0.57

Impure product was purified *via* HPLC chromatography – normal phase (**NP**).

- column: silica, phenomenex

- injection solvent: dichloromethane | 3.5 ml

- gradient: DCM / MeOH [0 – 10 %]

Further purification step was carried out *via* HPLC chromatography – reversed phase (**RP**).

- column: C-18, phenomenex

- injection solvent: DMSO / water [1:1] | 3.5 ml

- gradient: water + 0.1 % FA / acetonitrile + 0.1 % FA [0 – 65 %]

Product fractions [44 & 45] were collected and the solvents evaporated *in high vacuo* to obtain **IX** as white product.

* | NMR-DATA

- $^1\text{H-NMR}$ (600 MHz, d_6 -DMSO): δ = 1.45 (m, 1 H) 1.63 (m, 2 H) 1.82 (m, 1 H) 2.01 (m, 1 H) 2.10 (m, 1 H) 2.15 (m, 1 H) 2.28 (m, 1 H) 3.11 (q, $J=5.3$ Hz, 2 H) 3.44 (t, $J=6.5$ Hz, 2 H) 3.89 (m, 2 H) 3.95 (m, 2 H) 4.76 (t, $J=4.4$ Hz, 1 H) 5.55 (m, 2 H) 7.01 (s, 2 H) 7.34 (t, $J=6.2$ Hz, 1 H) ppm

ID-number: BAL094-10

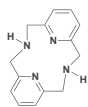
- $^{13}\text{C-NMR}$ (150 MHz, d_6 -DMSO): δ = 25.11 (t) 30.60 (t) 33.23 (t) 37.23 (t) 38.22 (t) 38.53 (t) 64.21 (t) 79.80 (d) 81.66 (d) 98.60 (d) 131.32 (d) 134.53 (d) 136.10 (d) 155.83 (s) 171.04 (s) ppm

ID-number: BAL094-11

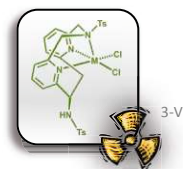
* | YIELD

- m = 14.5 mg \Rightarrow 25.7 %

(11.12.2018)



Building blocks | Ligand ($^H\text{N}_4$ -cycle)



4.9 | Synthesis of

3,11,17,18-Tetraazatricyclo[11.3.1.1^{5,9}]octadeca-1(17),5,7,9(18), 13,15-hexaene (19)

Part I

4.9.1 | Synthesis of

2,6-Bis(tosylmethyl)pyridine (15)

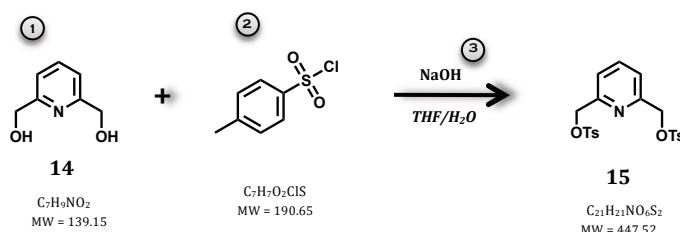


TABLE 16 | Synthesis of Bis(tosylmethyl)pyridine

	Name	Equivalents [-]	Amount of substance [mmol]	Mass [mg]	Volume [μl]	Molecular weight [g/mol]
①	2,6-Bis(hydroxymethyl)-pyridine	1 eq	36.0	5.0	-	139.15
②	4-Toluenesulfonylchloride [TsCl]	2 eq	72.9	13.7	-	190.65
③	Sodium hydroxide	3 eq	107.8	4.3	-	40.00

This synthesis was carried out based on the procedure already reported by Wessel *et al.*^[58]

To a three-necked round-bottom flask 2,6-bis(hydroxymethyl)pyridine **14** ($m = \underline{5.0\text{ g}}$, 36.0 mmol, 1 eq), NaOH ($m = \underline{4.3\text{ g}}$, 107.8 mmol, 3 eq), 30 ml THF and 25 ml water were added. The reaction mixture was stirred at 0 °C for 30 min under *argon* atmosphere. A solution of tosylchloride ($m = \underline{13.7\text{ g}}$, 72.9 mmol, 2 eq) in 25 ml THF was added dropwise to the reaction mixture at 0 °C. The mixture was allowed to warm to room temperature and stirred overnight.

The next day, TLC indicated product turnover, so then 60 ml water were added and product was extracted with chloroform, three times. After washing steps with water [100 ml, 3x], the organic layer was dried over MgSO_4 , filtered and the solvent evaporated under reduced pressure.

The formed bright lilac di-tosylated product **15** was dried *in high vacuo*.

* | TLC – check for full conversion

- MeOH / DCM [10 %]
- r_f -value = 0.51

* | NMR-DATA

- ¹H-NMR (400 MHz, CDCl₃): δ = 2.45 (s, 6 H) 5.06 (s, 4 H) 7.33 (d, *J*=8.2 Hz, 6 H) 7.70 (t, *J*=7.8 Hz, 1 H)
7.81 (d, *J*=7.8 Hz, 4 H) ppm

ID-number: BAL096-20

- ¹³C-NMR (100 MHz, CDCl₃): δ = 21.63 (q) 71.27 (t) 121.36 (d) 128.03 (d) 129.90 (d) 132.71 (d) 137.85 (s)
145.13 (s) 153.51 (s) ppm

ID-number: BAL096-21

* | YIELD

- m = 14.25 g ⇒ 87.7 %

(30.01.2019)

Part II

4.9.2 | Synthesis of Sodium tosylamide salt (17)

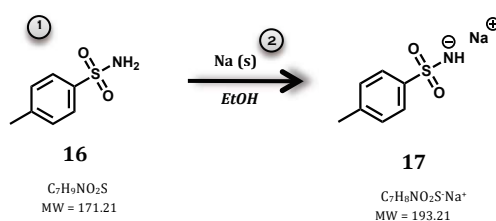


TABLE 17 | Synthesis of Sodium tosylamide

	Name	Equivalents [-]	Amount of substance [mol]	Mass [g]	Volume [μl]	Molecular weight [g/mol]
①	Tosylamide	1 eq	0.20	35.0	-	171.21
②	Sodium (s)	1.15 eq	0.24	5.4	-	23.00

This procedure was also based on the work of Wessel and coworkers.^[58]

Metallic sodium (*m* = 5.4 g, 0.24 mol, 1.15 eq) was cut in dry hexane into small pieces and then added under atmosphere of *argon* in portions into stirring anhydrous EtOH [200 ml] in a three-necked round-bottom flask. Heating up to 60-70 °C followed as soon as sodium was dissolved. Then solid tosylamide **16** (*m* = 35.0 g, 0.20 mol, 1 eq) was added portion wise with rigorous stirring. The mixture was thereafter refluxed for 2 h.

After cooling down to room temperature, the precipitate was filtered, washed with anhydrous EtOH and dried *in high vacuo*. The product **17** was obtained as white crystals.

* | NMR-DATA

- $^1\text{H-NMR}$ (400 MHz, d_6 -DMSO): δ = 2.27 (s, 3 H) 7.07 (d, $J=7.8$ Hz, 2 H) 7.53 (d, $J=8.2$ Hz, 2 H) ppm

ID-number: BAL097-10

- $^{13}\text{C-NMR}$ (100 MHz, d_6 -DMSO): δ = 20.56 (q) 124.94 (d) 127.97 (d) 137.71 (s) 147.86 (s) ppm

ID-number: BAL097-11

* | YIELD

- m = 35.85 g \Rightarrow 90.8 %

(01.02.2019)

Part III

4.9.3 | Synthesis of

3,11-Bis-tosyl-3,11,17,18-tetraazatricyclo[11.3.1.1^{5,9}]octadeca-1(17),5,7,9(18),13,15-hexaene (18)

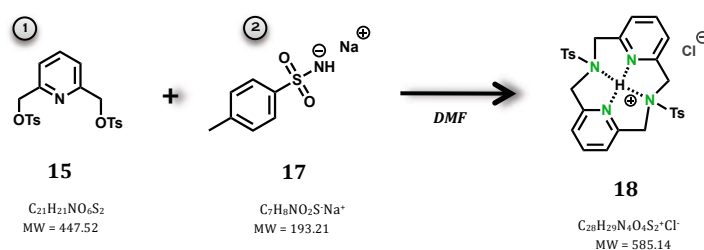


TABLE 18 | Synthesis of $^{\text{Ts}}\text{N}_4$ hydrochloride

	Name	Equivalents [-]	Amount of substance [mmol]	Mass [g]	Volume [μl]	Molecular weight [g/mol]
①	2,6-Bis(tosylmethyl)-pyridine	1 eq	11.2	5.0	-	447.52
②	Sodium tosylamide	2 eq	22.4	4.3	-	193.21

This synthesis was conducted by following up the procedure of Wessel *et al.*^[58]

Sodium tosylamide **17** (m = 4.3 g, 22.4 mmol, 2 eq) was dissolved in 208 ml DMF, dry under *argon* atmosphere in a three-necked round-bottom flask and heated up to 80 °C. 2,6-bis(tosylmethyl)pyridine **15** (m = 5.0 g, 11.2 mmol, 1 eq) solution in 52 ml DMF, dry was added dropwise. After addition, stirring at 80 °C continued for 70 h over weekend.

TLC and LC-MS measurement were carried out to verify converted product.

The mixture was allowed to cool down to room temperature and DMF evaporated under *high vacuo*. The solid residue was stirred in 52 ml MeOH for about 30 min. The formed suspension was filtered, washed with water and small amounts of MeOH, to obtain a mixture of Dimer product and Trimer side-product as white solid, which was dried in *high vacuo*.

To isolate the desired Dimer from Trimer, the residue was suspended in 95 % EtOH [130 ml] and 1 M HCl ($V = 3.7 \text{ ml}$, 1 eq) was added. The reaction mixture was stirred overnight.

Filtration on the next day led to their separation, having Dimer hydrochloride dissolved in the filtrate and Trimer filtered off as solid.

The solvent was evaporated under reduced pressure to obtain the product **18** as white solid.

* | **TLC** – check for full conversion

- MeOH / DCM [5 %]
- r_f -value = 0.69

* | **HPLC-MS**

- m/q: product | 548 & 549 + side-product 823

* | **NMR-DATA**

- $^1\text{H-NMR}$ (400 MHz, d_6 -DMSO): $\delta = 2.44$ (s, 6 H) 4.94 (s, 8 H) 7.49 (d, $J=8.2$ Hz, 4 H) 7.78 (d, $J=8.2$ Hz, 4 H) 7.87 (d, $J=7.8$ Hz, 4 H) 8.29 (t, $J=7.8$ Hz, 2 H) ppm

ID-number: *BAL098-20*

- $^{13}\text{C-NMR}$ (100 MHz, d_6 -DMSO): $\delta = 21.25$ (q) 53.12 (t) 122.95 (d) 127.75 (d) 130.36 (d) 134.07 (s) 137.72 (s) 143.14 (d) 144.71 (s) 156.00 (s) ppm

ID-number: *BAL098-21*

* | **YIELD**

- $m = 1.15 \text{ g} \Rightarrow 35.2 \%$

(05.02.2019)

Part IV

4.9.4 | Synthesis of

3,11,17,18-tetraazatricyclo[11.3.1.1^{5,9}]octadeca-1(17),5,7,9(18),13,15-hexaene (19)

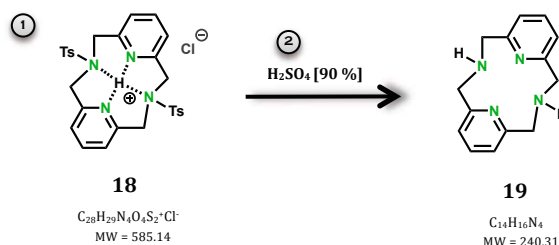


TABLE 19 | Synthesis of $^H N_4$ -cycle

	Name	Equivalents [-]	Amount of substance [mmol]	Mass [g]	Volume [ml]	Molecular weight [g/mol]
①	$Ts_2 N_4$ hydrochloride	1 eq	3.87	2.27	-	585.14
②	Sulphuric acid [90 %]	~ 95 eq	368	-	19.67	98.08

This synthesis is based on the publication of Wessel *et al.*^[58]

$Ts_2 N_4$ hydrochloride **18** ($m = 2.27$ g, 3.87 mmol, 1 eq) was weighed out in a round-bottom flask and H_2SO_4 , 90 % ($V = 19.67$ ml, 368 mmol, 95 eq) was added. The reaction mixture was stirred while heating up and refluxing at 110 °C for 2.5 h – black precipitate was formed after 30 min.

After allowing to cool down to room temperature, the mixture was poured gently on 40 ml water in an ice-bath [0 °C]. The acidic solution was neutralised with 5 M NaOH and the product extracted with chloroform [150 ml, 4x]. The combined organic layer was dried over K_2CO_3 , filtered and the solvent evaporated *in vacuo*.

Product **19** – the ligand for upcoming complex formation of suitable radionuclides – was finally dried *in high vacuo* to afford a white powder.

* | HPLC-MS

- m/q: product | 241

* | NMR-DATA

- 1H -NMR (400 MHz, d_6 -DMSO): $\delta = 3.95$ (s, 8 H) 6.49 (d, $J=8.2$ Hz, 4 H) 7.08 (t, $J=7.8$ Hz, 2 H) ppm

ID-number: BAL105-10

- ^{13}C -NMR (100 MHz, d_6 -DMSO): $\delta = 56.32$ (t) 120.08 (d) 136.03 (d) 159.73 (s) ppm

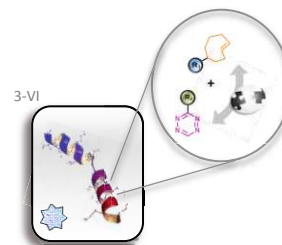
ID-number: BAL105-11

* | YIELD

- $m = 570$ mg \Rightarrow 62.6 %

(13.02.2019)

Synthesis of Radiotracer precursors by modifying tumor targeting carrier molecules



4.10 | Synthesis of SiR-Dye coupled tetrazin-3-yl-D,L-phenylalanine (I)

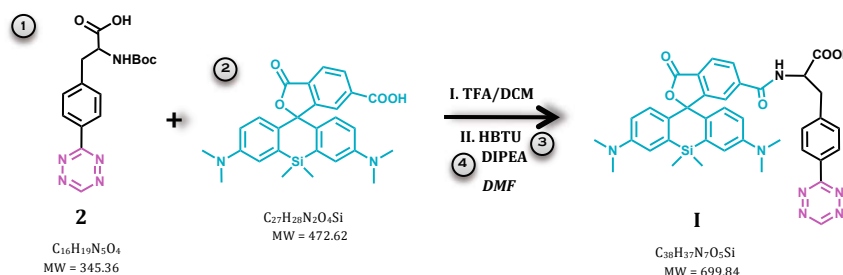


TABLE 20 | Synthesis of SiR-Dye coupled tetrazin-3-yl-D,L-phenylalanine (abbreviation)

	Name	Equivalents [-]	Amount of substance [μ mol]	Mass [mg]	Volume [μ l]	Molecular weight [g/mol]
①	Tetrazin-3-yl-D,L-Boc-phenylalanine	1 eq	11.4	4.0	-	345.36
②	SiR-Dye acid, <u>dye</u>	1 eq	11.4	5.5	-	472.62
③	[HBTU], <u>coupling reagent</u>	1.1 eq	12.7	4.8	-	379.24
④	Diisopropylethylamine [DIPEA] $\rho = 0.74 \text{ g/cm}^3$	5 eq	57.0	-	10.1	129.25

In a small vial Tetrazin-3-yl-D,L-Boc-phenylalanine **2** ($m = 4.0 \text{ mg}$, $11.4 \mu\text{mol}$, 1 eq) was dissolved in 0.5 ml TFA/DCM [16 %] for cleaving off Boc protecting group. After 20 min reaction time, TLC confirmed deprotected product formation $\{m/z = 245.36\}$. The volatiles were evaporated under reduced pressure. To get rid of TFA acid, a small amount of toluene was added and azeotropic mixture was evaporated *in high vacuo*.

SiR-Dye acid [*Silicon-Rhodamine derivative*] ($m = 5.5 \text{ mg}$, $11.4 \mu\text{mol}$, 1 eq) was dissolved in 1.5 ml DMF, dry and activated by adding coupling reagent HBTU [*H-Benzotriazol-tetramethyl-uronium*] ($m = 4.8 \text{ mg}$, $12.7 \mu\text{mol}$, 1.1 eq) and DIPEA ($V = 10.1 \mu\text{l}$, $57.0 \mu\text{mol}$, 5 eq). The reaction mixture turned from blue to yellow, was added to deprotected tetrazine compound and stirred for 50 min. Reaction was monitored *via* HPLC-MS, which indicated full conversion.

Purification of crude product was conducted *via* HPLC chromatography.

* | HPLC-MS

- m/q: product | 700

The impure product was purified *via* HPLC chromatography – reversed phase (RP).

- column: C-18, phenomenex
- injection solvent: DMSO / water [50%] | 4 ml
- gradient: water + 0.1 % FA / acetonitrile + 0.1 % FA [5 – 75 %]

Product fractions [36 - 39] were collected and the solvents evaporated *in high vacuo* to obtain **I** as blue solid.

* | YIELD

- m = 3.3 mg → 40.8 % (30.01.2018)

4.11 | Synthesis of

Tetrazin-3-yl-D,L-Boc-phenylalanine modified peptide bombesin [RM26-analogue] (H-II)

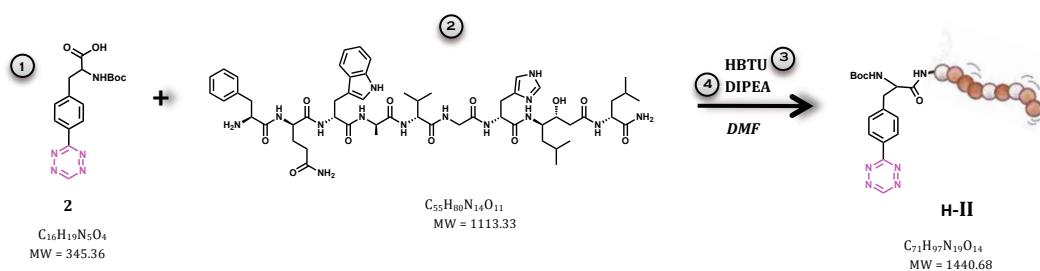


TABLE 21 | Synthesis of Tetrazin-3-yl-D,L-Boc-phenylalanine modified bombesin RM26-analogue (abbreviation)

Name	Equivalents [-]	Amount of substance [μ mol]	Mass [mg]	Volume [μ l]	Molecular weight [g/mol]
① Tetrazin-3-yl-D,L-Boc-phenylalanine	2 eq	0.90	0.31	62.0	345.36
② Bombesin [RM26]	1 eq	0.45	0.50	45.0	1113.33
③ [HBTU], coupling reagent	1.2 eq	0.54	0.20	20.0	379.24
④ Diisopropylethylamine [DIPEA] $\rho = 0.74 \text{ g/cm}^3$	5 eq	2.25	0.29	30.0	129.25

As the educt amounts for this coupling reaction were very small, **stock solutions** in DMF, dry were made in advance.

Tetrazin-3-yl-D,L-Boc-phenylalanine **2** ($V = 62.0 \mu\text{l}$, $0.90 \mu\text{mol}$, 2 eq, **5 mg/ml**) was added *via* pipet into small eppi and was activated with HBTU ($V = 20.0 \mu\text{l}$, $0.54 \mu\text{mol}$, 1.2 eq, **10 mg/ml**) and base DIPEA ($V = 30.0 \mu\text{l}$, $2.25 \mu\text{mol}$, 5 eq, **10 mg/ml**) for about 30 min. Then bombesin peptide ($V = 45.0 \mu\text{l}$, $0.45 \mu\text{mol}$, 1 eq, **11 mg/ml**) was added to reaction mixture and after 1 h, HPLC-MS measurement indicated product turnover.

* | HPLC-MS

- m/q: product | 721 & 1441

The impure product was purified *via* HPLC chromatography – reversed phase (RP).

- column: C-18, phenomenex

- injection solvent: DMSO / water [30%] | 3.5 ml

- gradient: water + 0.1 % FA / acetonitrile + 0.1 % FA [10 – 65 %]

Product fractions [34 - 35] were collected and the solvents evaporated *in high vacuo* to obtain **H-II** as bright pink solid.

* | YIELD

- m = 0.6 mg \Rightarrow 92 %

(23.03.2018)

4.12 | Synthesis of

6-Methyl-tetrazin-3-yl-D,L-Boc-phenylalanine modified peptide bombesin [RM26-analagon] (Me-II)

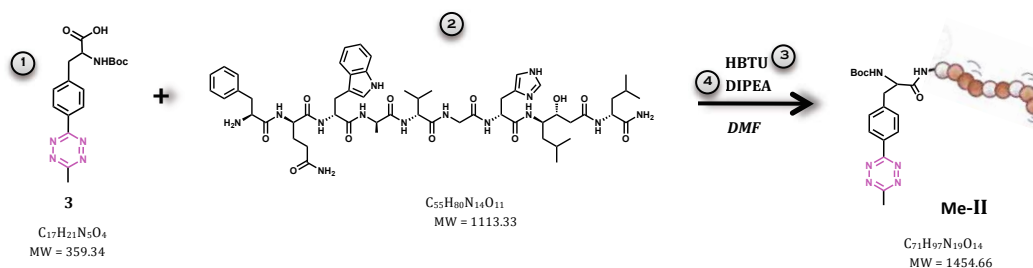


TABLE 22 | Synthesis of 6-Me-tetrazin-3-yl-D,L-Boc-phenylalanine modified bombesin RM26-analagon (abbreviation)

Name	Equivalents [-]	Amount of substance [μ mol]	Mass [mg]	Volume [μ l]	Molecular weight [g/mol]
① 6-Me-tetrazin-3-yl-D,L-Boc-phenylalanine	2 eq	0.90	0.32	64.0	359.34
② Bombesin [RM26]	1 eq	0.45	0.50	45.0	1113.33
③ [HBTU], coupling reagent	1.2 eq	0.54	0.20	20.0	379.24
④ Diisopropylethylamine [DIPEA] $\rho = 0.74 \text{ g/cm}^3$	5 eq	2.25	0.29	30.0	129.25

As the educt amounts for this coupling reaction were very small, **stock solutions** in DMF, dry were made in advance.

6-Methyl-tetrazin-3-yl-D,L-Boc-phenylalanine **2** ($V = 64.0 \mu\text{l}$, $0.90 \mu\text{mol}$, 2 eq, **5 mg/ml**) was added *via* pipet into small eppi and was activated with HBTU ($V = 20.0 \mu\text{l}$, $0.54 \mu\text{mol}$, 1.2 eq, **10 mg/ml**) and base DIPEA ($V = 30.0 \mu\text{l}$, $2.25 \mu\text{mol}$, 5 eq, **10 mg/ml**) for about 30 min. Then bombesin peptide ($V = 45.0 \mu\text{l}$, $0.45 \mu\text{mol}$, 1 eq, **11 mg/ml**) was added to reaction mixture and after 1 h, HPLC-MS measurement indicated product turnover.

* | HPLC-MS

- m/q: product | 728 & 1455

The impure product was purified *via* HPLC chromatography – reversed phase (**RP**).

- column: C-18, phenomenex

- injection solvent: DMSO / water [30%] | 3.5 ml

- gradient: water + 0.1% FA / acetonitrile + 0.1% FA [10 – 65 %]

Product fractions [38 - 40] were collected and the solvents evaporated *in high vacuo* to obtain **H-II** as bright pink solid.

* | YIELD

- m = 0.5 mg → 77 %

(09.04.2018)

4.13 | Synthesis of (SiR-Dye, benzyl-tetrazine) linked L-lysine (IV)

Part I

4.13.1 | Synthesis of SiR-Dye coupled Boc-L-lysine (III)

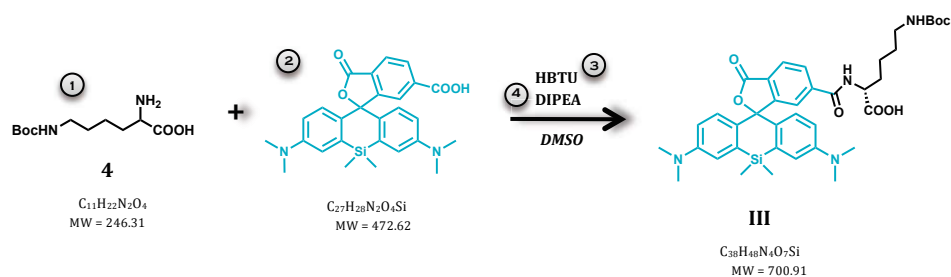


TABLE 23 | Synthesis of SiR-Dye coupled Boc-L-lysine (abbreviation)

Name	Equivalents [-]	Amount of substance [μ mol]	Mass [mg]	Volume [μ l]	Molecular weight [g/mol]
① Boc-N ϵ -L-lysine	1 eq	63.4	15.6	-	246.31
② SiR-Dye acid, <u>dye</u>	1 eq	63.4	30.0	-	472.62
③ [HBTU], <u>coupling reagent</u>	1.1 eq	70.0	26.5	-	379.24
④ Diisopropylethylamine [DIPEA] $\rho = 0.74 \text{ g/cm}^3$	5 eq	317	-	55.3	129.25

In a small vial fluorescent agent SiR-Dye acid [*Silicon-Rhodamine species*] ($m = 30.0 \text{ mg}$, $63.4 \mu\text{mol}$, 1 eq) was dissolved in 5 ml DMSO, dry and activated by adding coupling reagent HBTU [*H-Benzotriazol-tetramethyl-uronium*] ($m = 26.5 \text{ mg}$, $70.0 \mu\text{mol}$, 1.1 eq) and DIPEA ($V = 55.3 \mu\text{l}$, $317 \mu\text{mol}$, 5 eq) for about 30 min. Then Boc-lysine 4 ($m = 15.6 \text{ mg}$, $63.4 \mu\text{mol}$, 1 eq) dissolved in 4 ml DMSO, dry was added to the solution to start the coupling reaction.

As monitoring *via* HPLC-MS measurement confirmed full conversion after 1 h, purification *via* HPLC chromatography was conducted.

* | HPLC-MS

- m/q: product | 701

The impure product was purified *via* HPLC chromatography – reversed phase (RP).

- column: C-18, phenomenex

- injection solvent: DMSO / water [30%] | 4 ml

- gradient: water + 0.1 % FA / acetonitrile + 0.1 % FA [10 – 65 %]

Product fractions [20 - 25] were collected and the solvents evaporated *in high vacuo* to obtain **III** as blue solid.

* | YIELD

- m = 10.2 mg → 23.1 %

(23.04.2018)

Part II

4.13.2 | Synthesis of
(SiR-Dye, benzyl-tetrazine) linked L-lysine (**IV**)

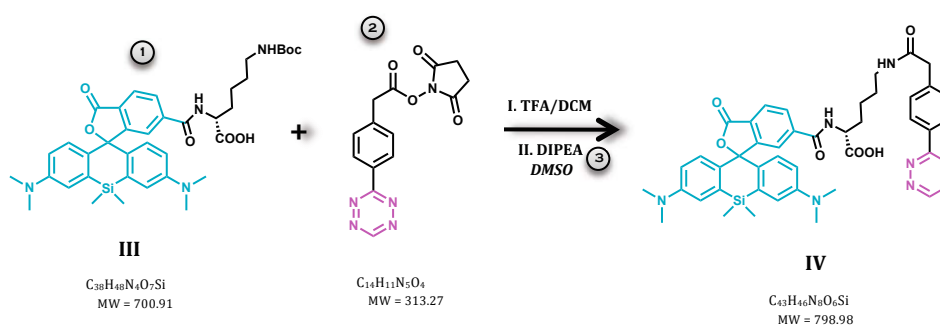


TABLE 24 | Synthesis of (SiR-Dye, benzyl-tetrazine) linked L-lysine (abbreviation)

Name	Equivalents [-]	Amount of substance [μmol]	Mass [mg]	Volume [μl]	Molecular weight [g/mol]
① SiR-Dye coupled Boc-L-lysine	1 eq	3.3	2.3	-	700.91
② NHS-[4-(tetrazin-3-yl)-phenylacetic acid], ester	1.2 eq	4.0	1.3	-	313.27
③ Diisopropylethylamine [DIPEA] $\rho = 0.74 \text{ g/cm}^3$	5 eq	16.5	-	2.9	129.25

SiR-Dye coupled Boc-L-lysine **III** (m = 2.3 mg, 3.3 μmol , 1 eq) was deprotected at first with 100 μl TFA/DCM [16 %]. HPLC-MS measurement indicated deprotected compound {m/z = 601} after 30 min reaction time, and the volatiles were evaporated under reduced pressure. To remove TFA acid, small amounts of toluene were added and the formed azeotropic mixture was evaporated *in high vacuo*.

NHS-tetrazine species (m = 1.3 mg, 4.0 μmol , 1.2 eq) was dissolved in 0.5 ml DMSO, dry and added to the reaction vial containing deprotected SiR-Dye-lysine compound. Thereafter also base DIPEA (V = 2.9 μl , 16.5 μmol , 5 eq) was added. The product turnover was monitored *via* HPLC-MS and full consumption of starting material was observed after 25 min reaction time.

* | HPLC-MS

- m/q: product | 799.5

The impure product was purified *via* HPLC chromatography – reversed phase (**RP**).

- column: C-18, phenomenex

- injection solvent: DMSO / water [1:1] | 3.5 ml

- gradient: water + 0.1 % FA / acetonitrile + 0.1 % FA [15 – 65 %]

Product fractions [31 - 32] were collected and the solvents evaporated *in high vacuo* to obtain **IV** as blue solid.

* | YIELD

- m = 1.8 mg → 69.2 %

(26.04.2018)

4.14 | Synthesis of

[(BODIPY, benzyl-tetrazine) linked L-lysine] modified C₆-alkyl spaced peptide bombesin [RM26-analogue] (VII)

Part I

4.14.1 | Synthesis of BODIPY coupled Boc-L-lysine (V)

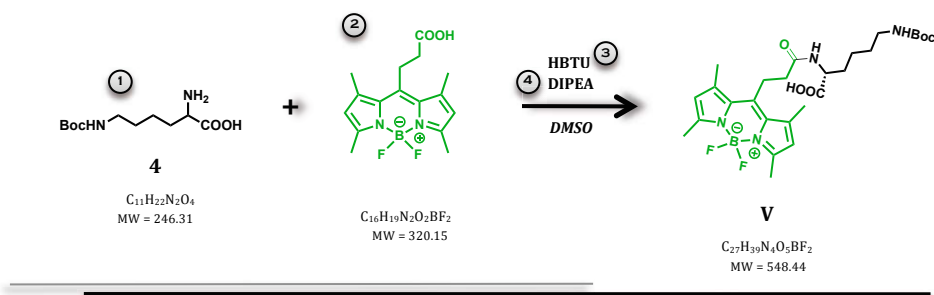


TABLE 25 | Synthesis of BODIPY coupled Boc-L-lysine (abbreviation)

Name	Equivalents [-]	Amount of substance [μ mol]	Mass [mg]	Volume [μ l]	Molecular weight [g/mol]
① Boc-N ϵ -L-lysine	1.1 eq	68.8	16.9	-	246.31
② BODIPY-propionic acid, dye	1 eq	62.5	20.0	-	320.15
③ [HBTU], coupling reagent	1.2 eq	75.0	28.4	-	379.24
④ Diisopropylethylamine [DIPEA] $\rho = 0.74 \text{ g/cm}^3$	5 eq	312.5	-	54.4	129.25

In a small vial fluorescent agent BODIPY-acid [*Boron-dipyrromethene species*] ($m = 20.0 \text{ mg}$, $62.5 \mu\text{mol}$, 1 eq) was dissolved in 1 ml DMSO, dry and activated by adding coupling reagent HBTU [*H-Benzotriazol-tetramethyl-uronium*] ($m = 28.4 \text{ mg}$, $75.0 \mu\text{mol}$, 1.2 eq) and DIPEA ($V = 54.4 \mu\text{l}$, $312.5 \mu\text{mol}$, 5 eq). After 30 min of reaction time, Boc-lysine 4 ($m = 16.9 \text{ mg}$, $68.8 \mu\text{mol}$, 1.1 eq) dissolved in 1 ml DMSO, dry was added to the solution to form the coupling product.

As HPLC-MS measurement showed full conversion after 1 h, purification *via* HPLC chromatography was conducted.

* | HPLC-MS

- m/q: product | 571 & 529

The impure product was purified *via* HPLC chromatography – reversed phase (RP).

- column: C-18, phenomenex

⁴ https://fr.123rf.com/photo_16083355_la-structure-chimique-d-une-molecule-de-glucagon-le-glucagon-est-une-hormone-peptidique-produite-pa.html

- injection solvent: DMSO / water [10%] | 4 ml
- gradient: water + 0.1 % FA / acetonitrile + 0.1 % FA [10 – 65 %]

Product fractions [61 - 67] were collected and the solvents evaporated *in high vacuo* to obtain **V** as red-orange solid.

* | YIELD

- m = 18.4 mg → 53.8 % (04.10.2018)

Part II

4.14.2 | Synthesis of (BODIPY, benzyl-tetrazine) linked L-lysine (**VI**)

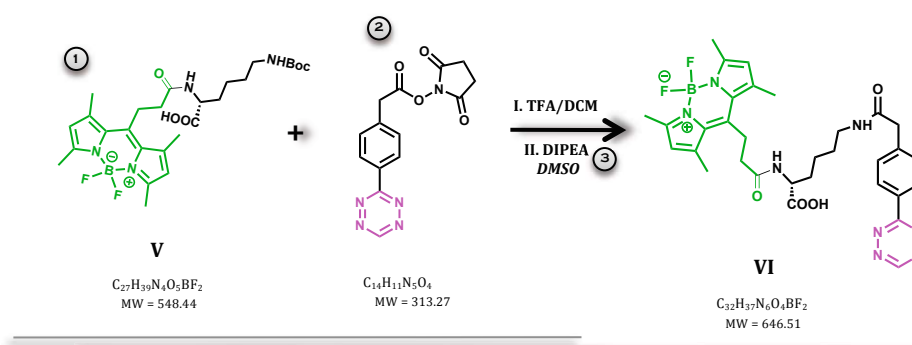


TABLE 26 | Synthesis of (BODIPY, benzyl-tetrazine) linked L-lysine (abbreviation)

Name	Equivalents [-]	Amount of substance [μ mol]	Mass [mg]	Volume [μ l]	Molecular weight [g/mol]
① BODIPY coupled Boc-L-lysine	1 eq	33.5	18.4	-	548.44
② <i>NHS</i> -[4-(tetrazin-3-yl)-phenylacetic acid], ester	1.2 eq	40.3	12.6	-	313.27
③ Diisopropylethylamine [DIPEA] $\rho = 0.74 \text{ g/cm}^3$	5 eq	167.7	-	29.2	129.25

BODIPY coupled Boc-L-lysine **V** (m = 18.4 mg, 33.5 μ mol, 1 eq) was deprotected at first with 480 μ l TFA/DCM [16 %]. HPLC-MS measurement confirmed deprotected compound {m/z = 448} after 20 min reaction time, and the volatiles were evaporated under reduced pressure. By forming an azeotrope with the aid of small amounts of toluene, TFA was evaporated *in high vacuo*.

⁴ https://fr.123rf.com/photo_16083355_la-structure-chimique-d-une-mol%C3%A9cule-de-glucagon-le-glucagon-est-une-hormone-peptidique-produite-pa.html

NHS-tetrazine species ($m = 12.6 \text{ mg}$, $40.3 \text{ } \mu\text{mol}$, 1.2 eq) dissolved in 1.5 ml DMSO, dry was added to the reaction vial, and thereafter also base DIPEA ($V = 29.2 \text{ } \mu\text{l}$, $167.7 \text{ } \mu\text{mol}$, 5 eq). The product turnover was confirmed by HPLC-MS after 80 min reaction time.

* | HPLC-MS

- m/q: product | 627 & 669

The impure product was purified *via* HPLC chromatography – reversed phase (RP).

- column: C-18, phenomenex

- injection solvent: DMSO / THF [40%] | 3.5 ml

- gradient: water + $0.1 \text{ } \%$ FA / acetonitrile + $0.1 \text{ } \%$ FA [15 – 65 %]

Product fractions [59 - 69] were collected and the solvents evaporated *in high vacuo* to obtain VI as red solid.

* | NMR-DATA

- $^1\text{H-NMR}$ (600 MHz, d_6 -DMSO): $\delta = 1.41$ (m, 2 H) 1.57 (m, 2 H) 1.72 (m, 2 H) 2.40 (s, 12 H) 3.05 (m, 2 H) 3.17 (m, 4 H) 3.54 (s, 2 H) 4.18 (m, 1 H) 6.23 (s, 2 H) 7.52 (d, $J=8.5 \text{ Hz}$, 2 H) 8.18 (t, $J=5.9 \text{ Hz}$, 1 H) 8.27 (d, $J=7.6 \text{ Hz}$, 1 H) 8.43 (d, $J=8.2 \text{ Hz}$, 2 H) 10.57 (s, 1 H) ppm

ID-number: BAL077-20

* | YIELD

- $m = 6.1 \text{ mg}$ \Rightarrow $28.2 \text{ } \%$

(08.10.2018)

Part III

4.14.3 | Synthesis of [(BODIPY, benzyl-tetrazine) linked L-lysine] modified C₆-alkyl spaced peptide bombesin [RM26-analagon] (VII)

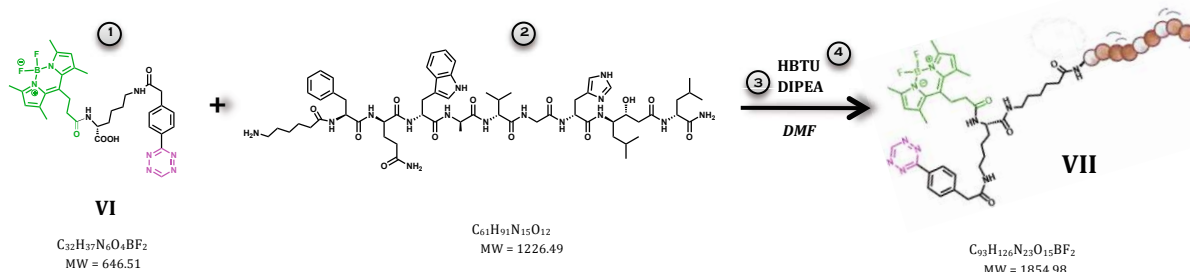


TABLE 27 | Synthesis of [(BODIPY, benzyl-tetrazine) linked L-lysine] modified C₆-bombesin RM26-analagon

Name	Equivalents [-]	Amount of substance [μmol]	Mass [mg]	Volume [μl]	Molecular weight [g/mol]
① (BODIPY, benzyl-Tz) linked L-lysine	2 eq	1.12	0.74	73.5	646.51
② C ₆ -alkyl spaced bombesin [RM26]	1 eq	0.56	0.70	70.0	1226.49
③ Diisopropylethylamine [DIPEA] ρ = 0.74 g/cm ³	10 eq	5.6	0.74	49.0	129.25
④ [HBTU], coupling reagent	2.2 eq	1.27	0.48	32.2	379.24

As the educt amounts for this coupling reaction were very small, **stock solutions** in DMF, dry were made in advance.

(BODIPY, benzyl-Tz) linked L-lysine **VI** (V = 73.5 μl, 1.12 μmol, 2 eq, **10 mg/ml**), peptide bombesin analogon RM26 (V = 70.0 μl, 0.56 μmol, 1 eq, **10 mg/ml**) and HBTU (V = 32.2 μl, 1.27 μmol, 2.2 eq, **15 mg/ml**) were added into eppi tube and seconds later base DIPEA (V = 49.0 μl, 5.6 μmol, 10 eq, **15 mg/ml**) was added to initiate the coupling reaction.

The reaction was monitored by HPLC-MS measurements. After 1 h no more consumption of starting material was detected and plenty of product **VII** was formed.

* | HPLC-MS

- m/q: product | 918

The impure product was purified *via* HPLC chromatography – reversed phase (**RP**).

- column: C-18, phenomenex

- injection solvent: DMSO / water [20%] | 3.5 ml

- gradient: water + 0.1% FA / acetonitrile + 0.1% FA [10 – 65 %]

Product fractions [18 - 22] were collected and the solvents evaporated *in high vacuo* to obtain the modified tumor targeting carrier molecule, the bombesin species **VII**.

* | YIELD

- m = 0.5 mg → 47 %

(11.10.2018)

4.15 | Synthesis of

Maleimidyl-dTCO bioconjugated cys-TAT [47-57] peptide (**X**)

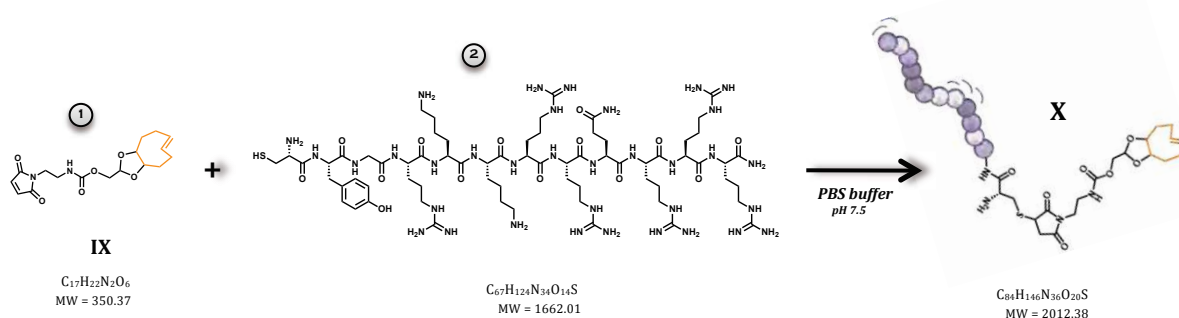


TABLE 28 | Synthesis of Maleimidyl-dTCO bioconjugated cystAT (abbreviation)

Name	Equivalents [-]	Amount of substance [μmol]	Mass [mg]	Volume [μl]	Molecular weight [g/mol]
① Cysteine-TAT peptide	1 eq	0.30	0.50	50.0	1662.01
② Maleimidyl-dTCO carbamate	1.1 eq	0.33	0.11	9.4	350.37

As the educt amounts for this coupling reaction were very small, **stock solutions** in DMSO, dry were made in advance.

30 μl PBS-buffer [85 mM] were added into eppi tube and degassed with *argon*. Then TAT-cys peptide (V = 50.0 μl, 0.30 μmol, 1 eq, 10 mg/ml) was added and dissolved in buffer solution, followed by further degassing with *argon*. After 5-10 min, dTCO-compound **IX** (V = 9.4 μl, 0.33 μmol, 1.1 eq, 12.1 mg/ml) was added to the reaction mixture to start the bioconjugation reaction. To reach a total reaction volume of 100 μl, additional 11.6 μl DMSO, dry were added.

HPLC-MS measurement indicated full conversion to the desired bioconjugate **X** after 3 h.

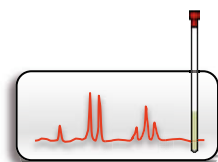
* | HPLC-MS

- m/q: product | 504, 672 & 473

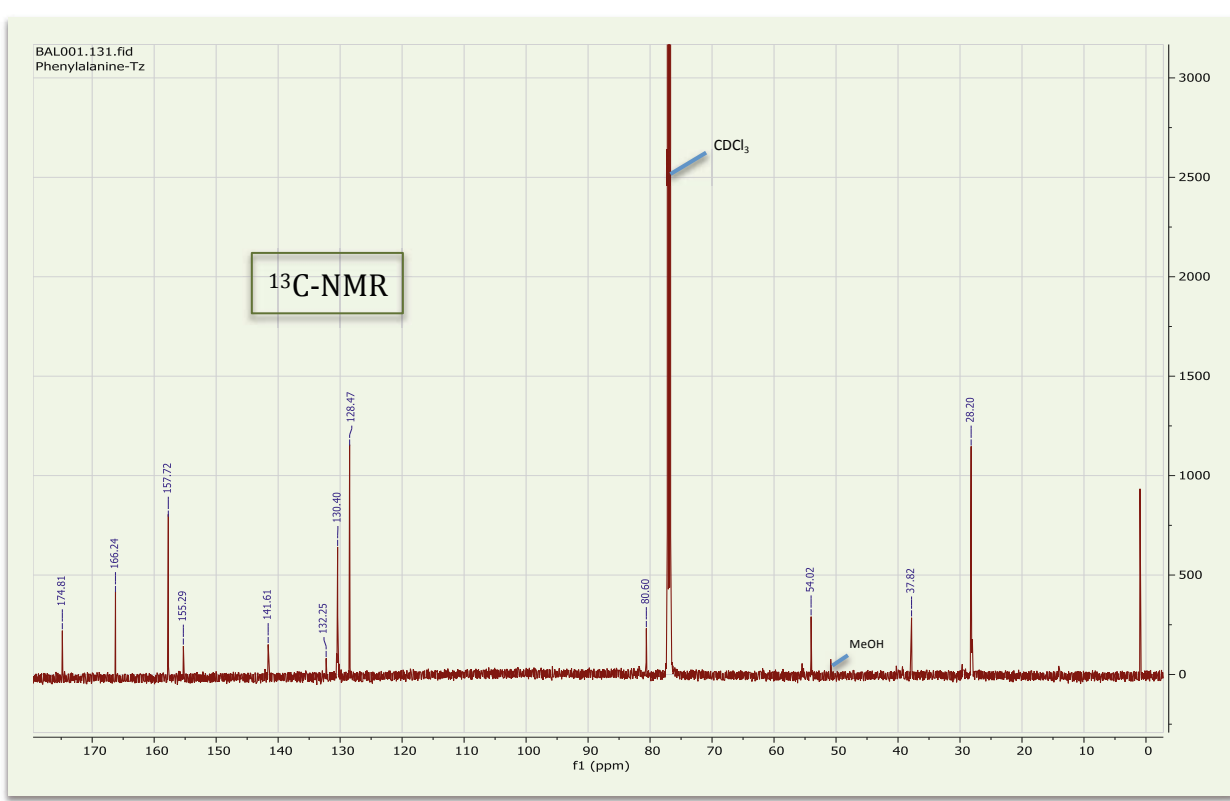
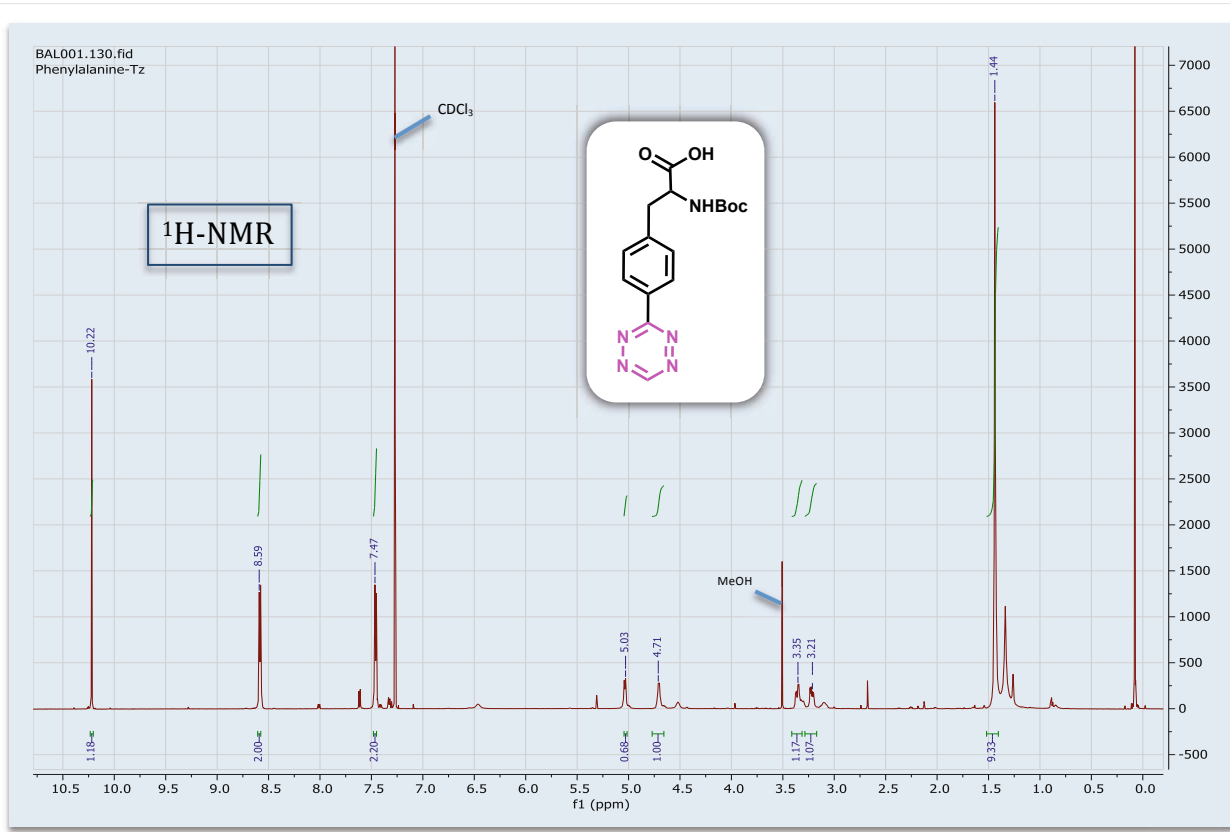
The dTCO modified TAT compound **X** was used as cell penetrating peptide without further purification.

(04.02.2019)

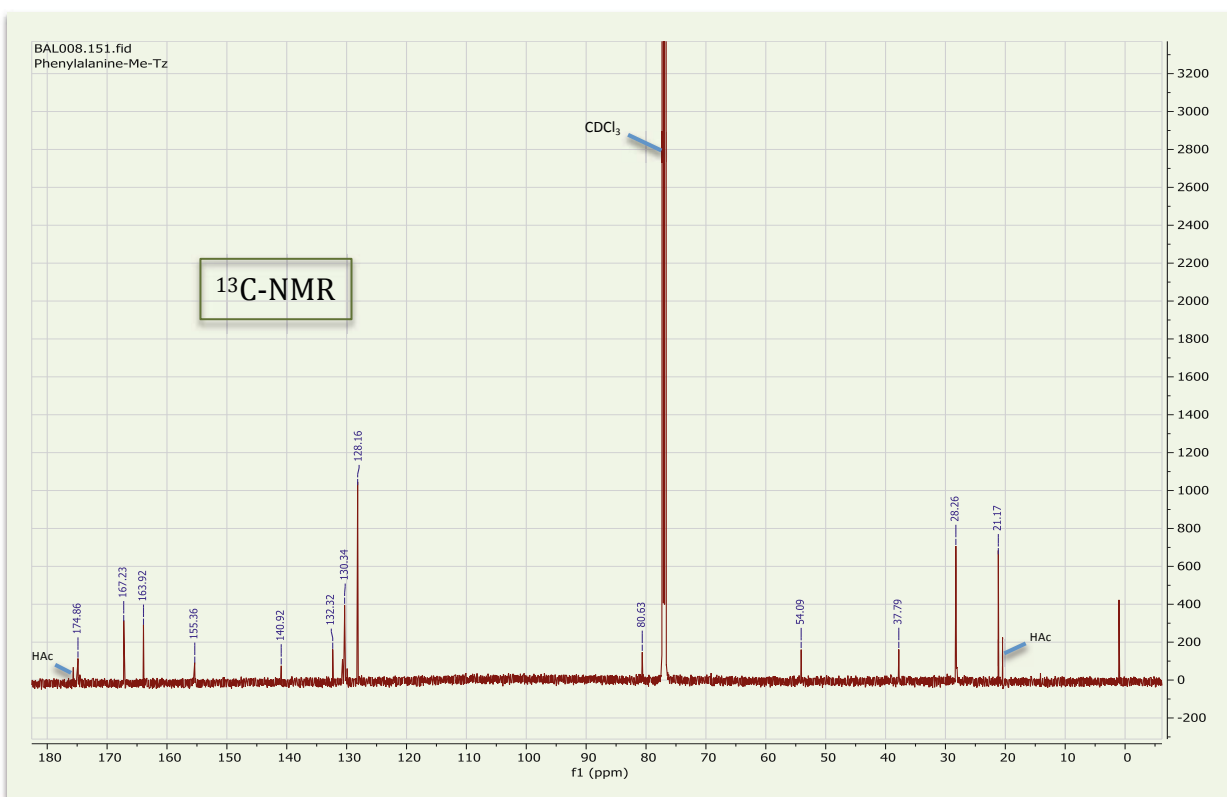
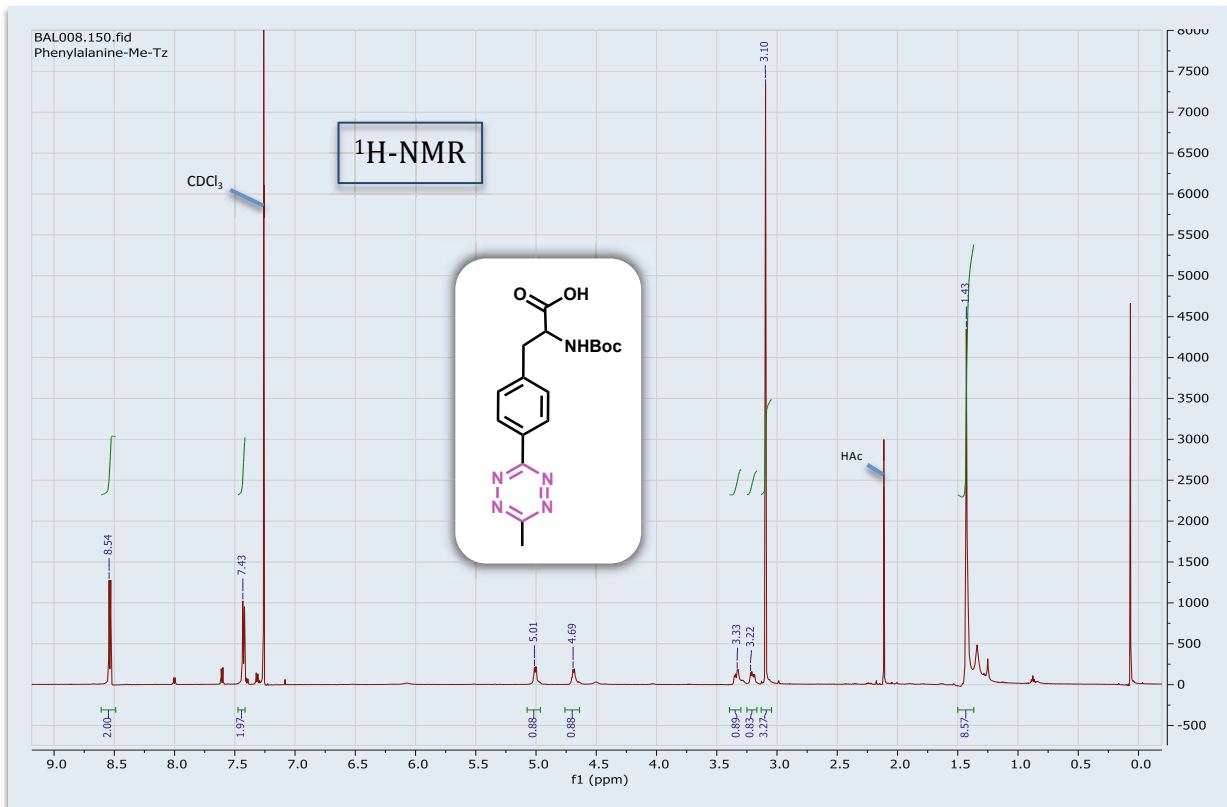
5 | APPENDIX [SPECTRA]

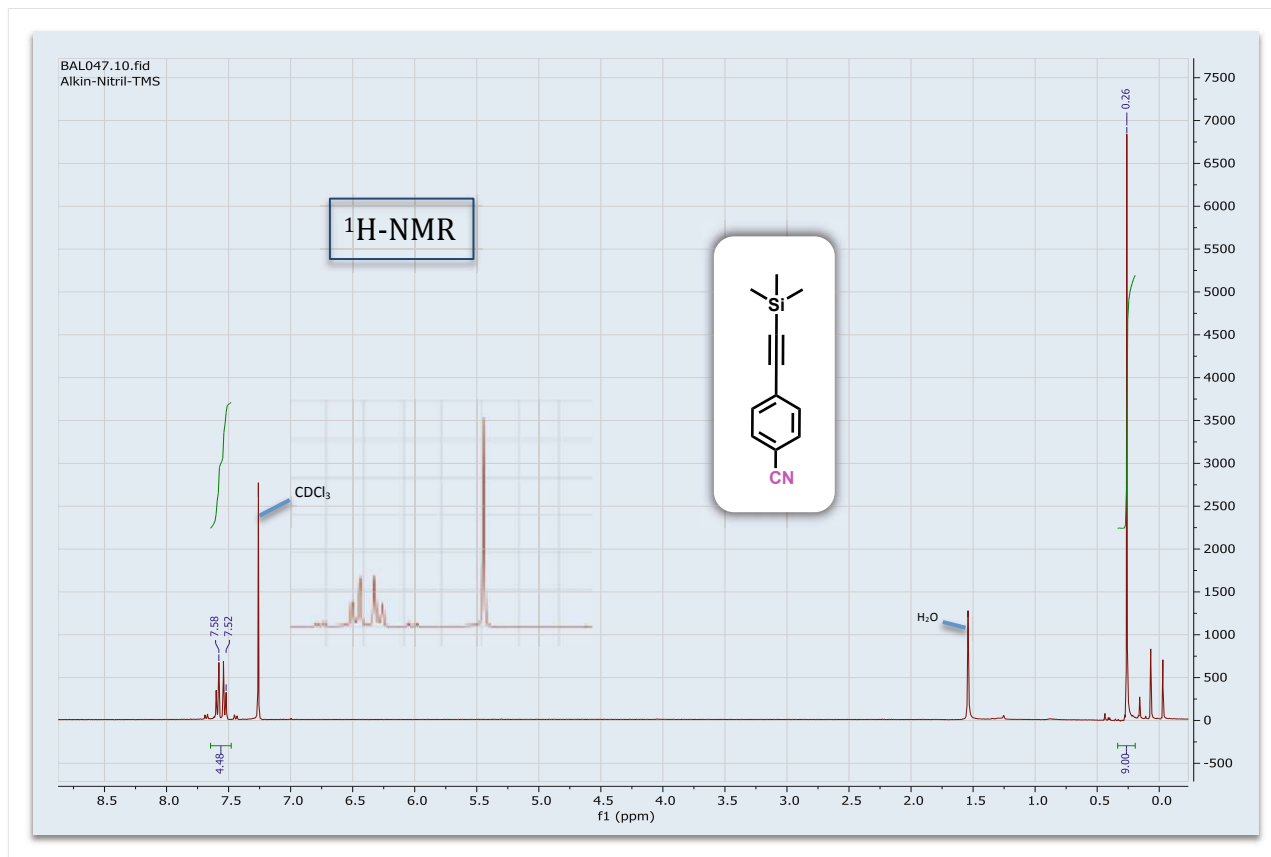


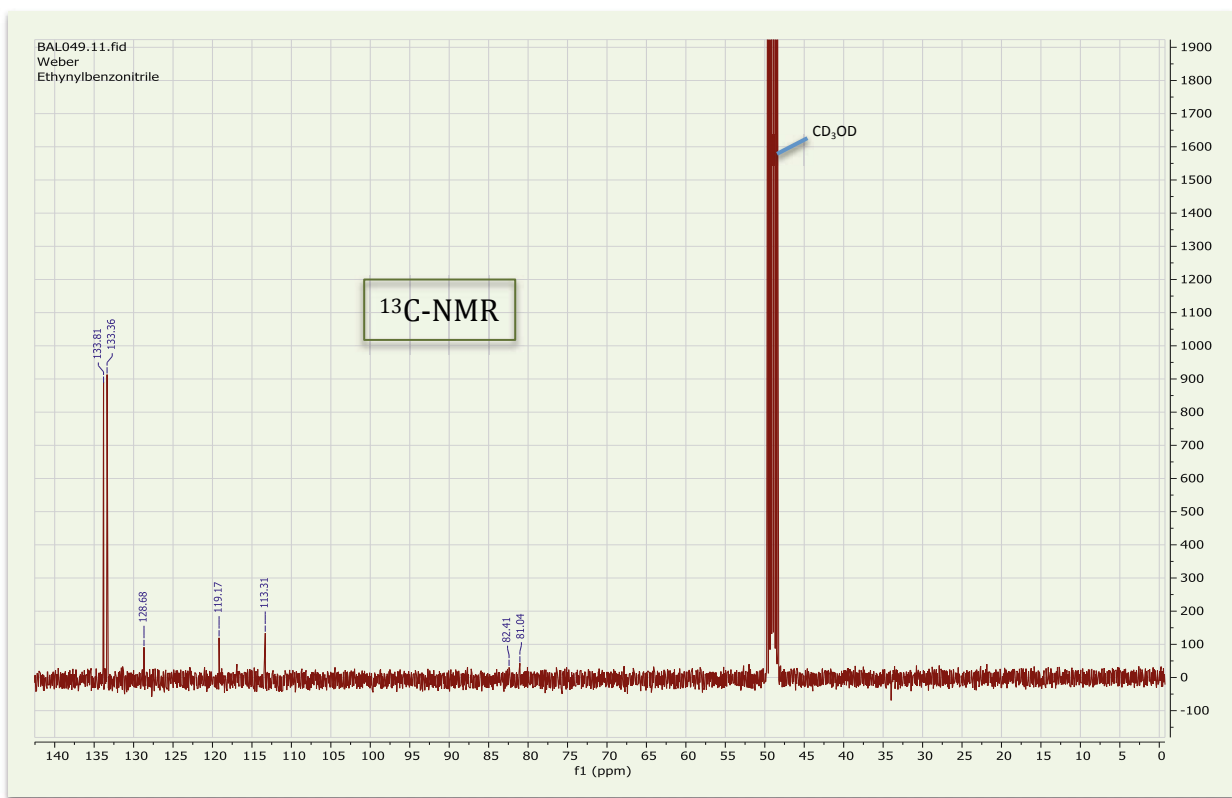
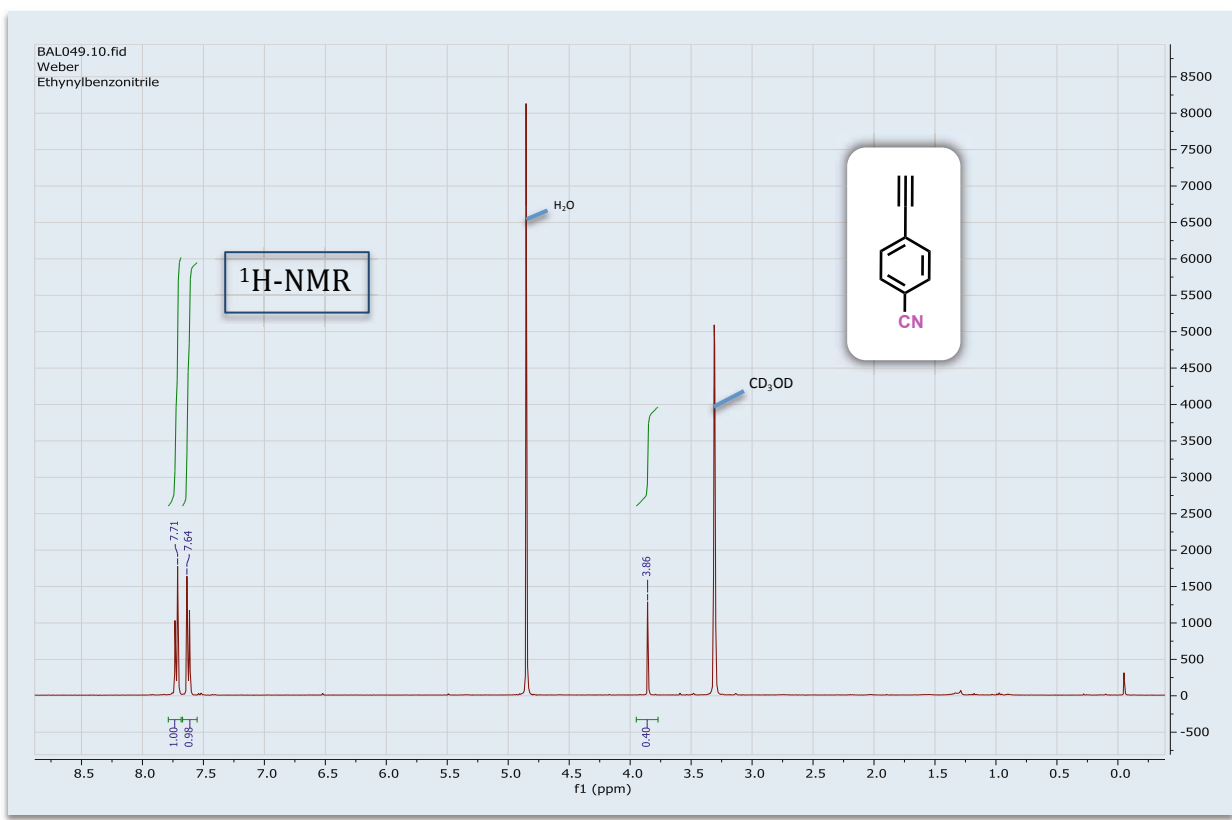
27

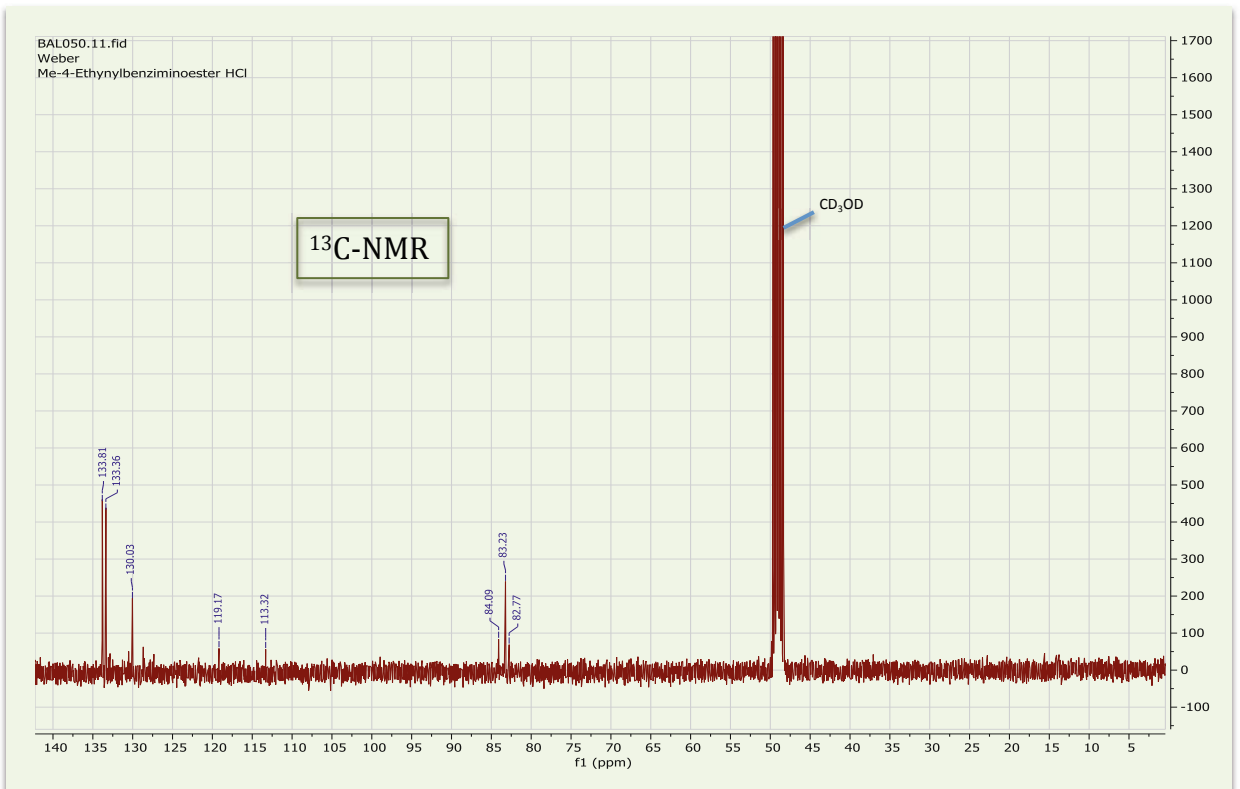
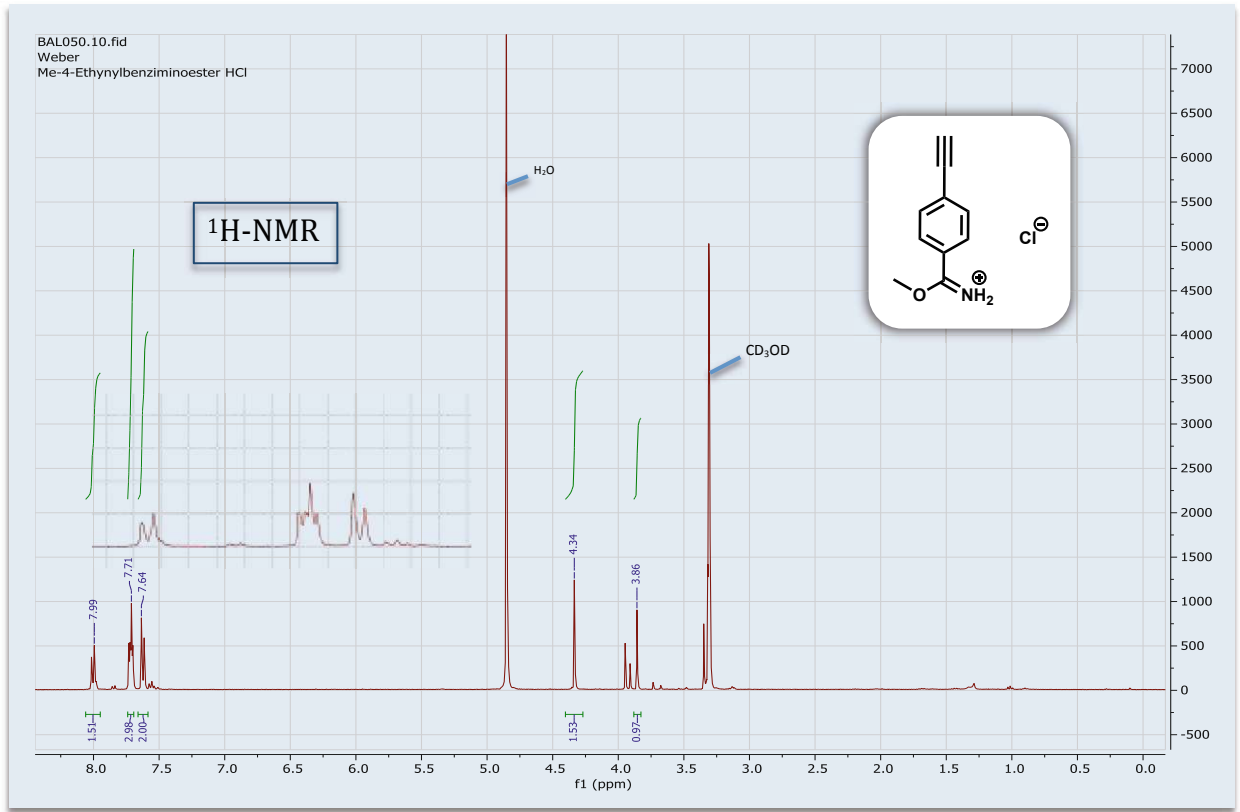


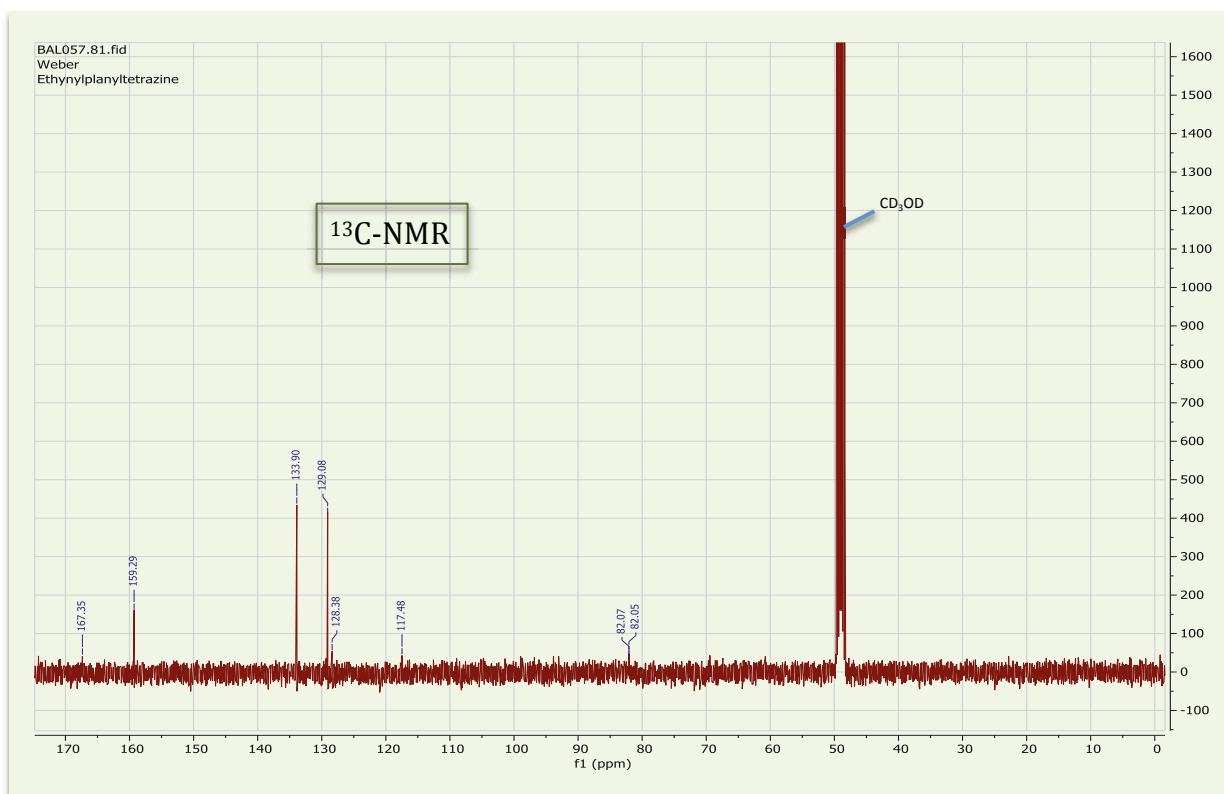
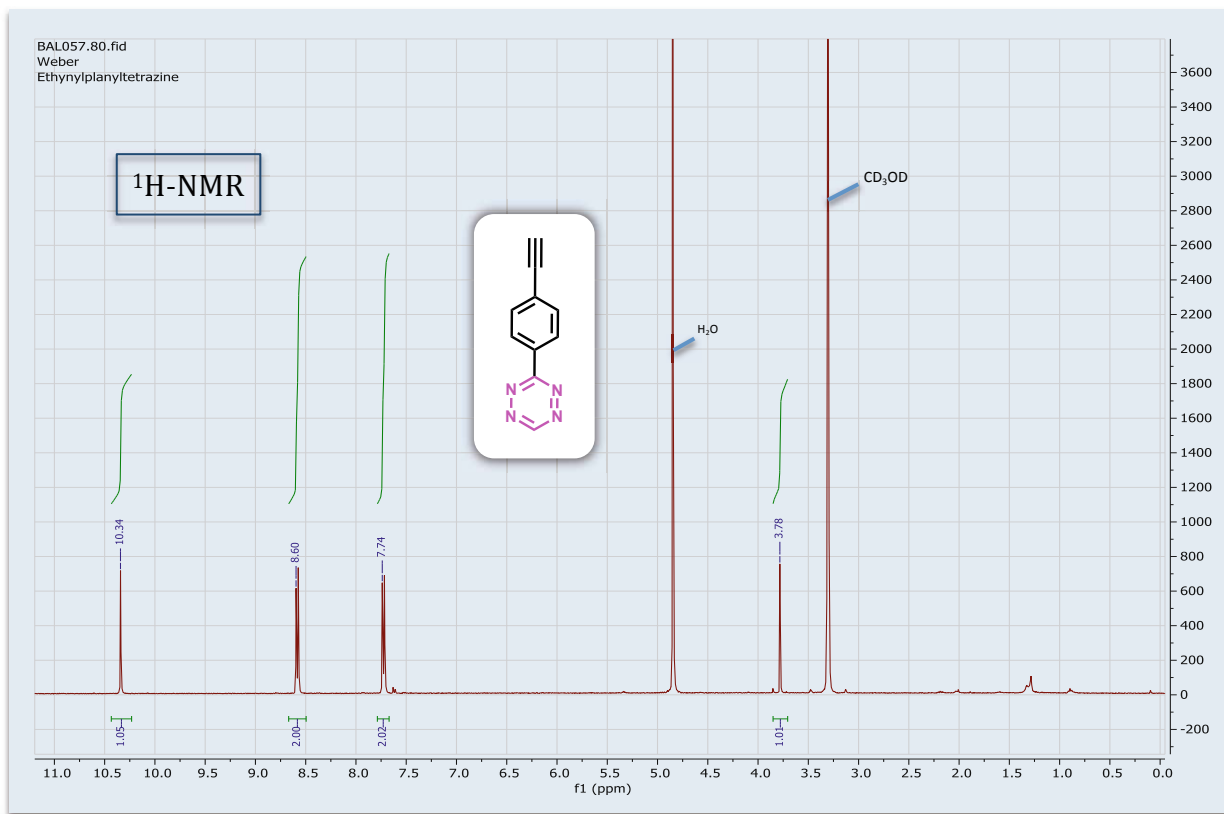
²⁷ http://www.publicdomainfiles.com/show_file.php?id=13534274413126, last downloaded 05/2019

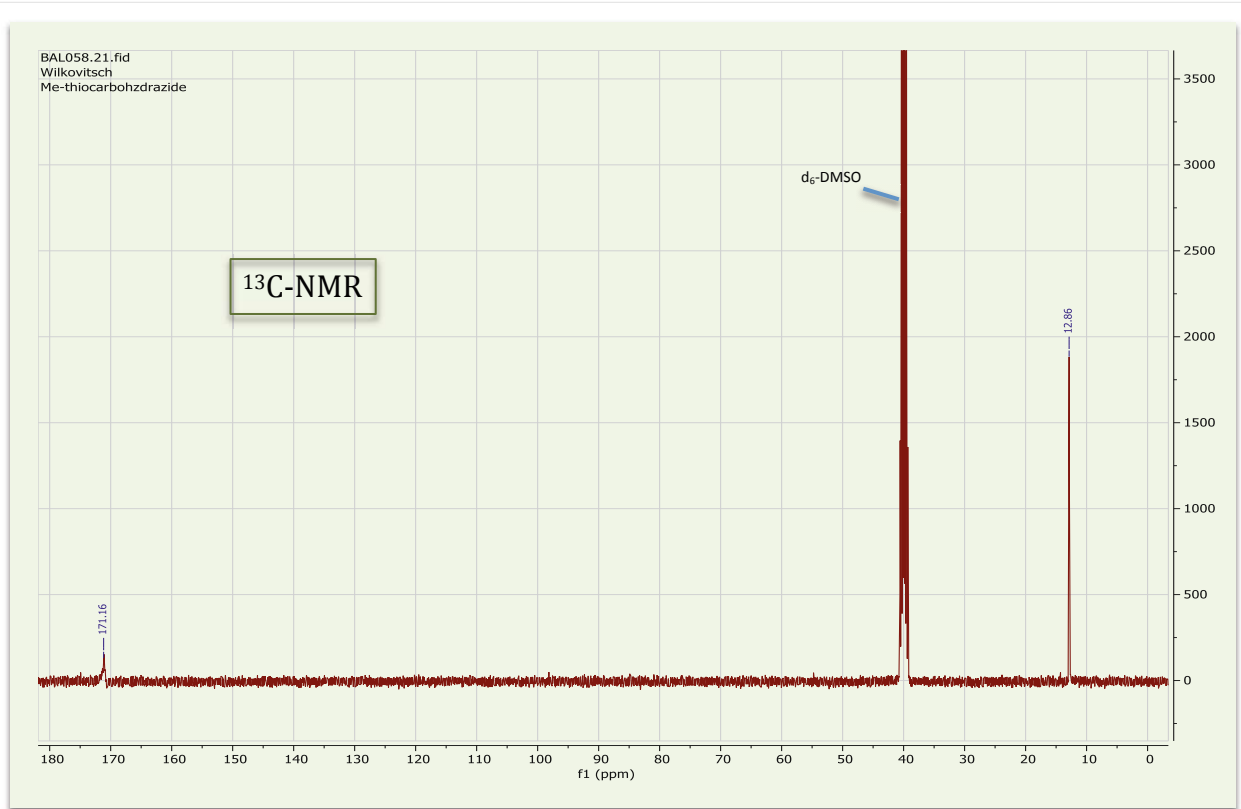
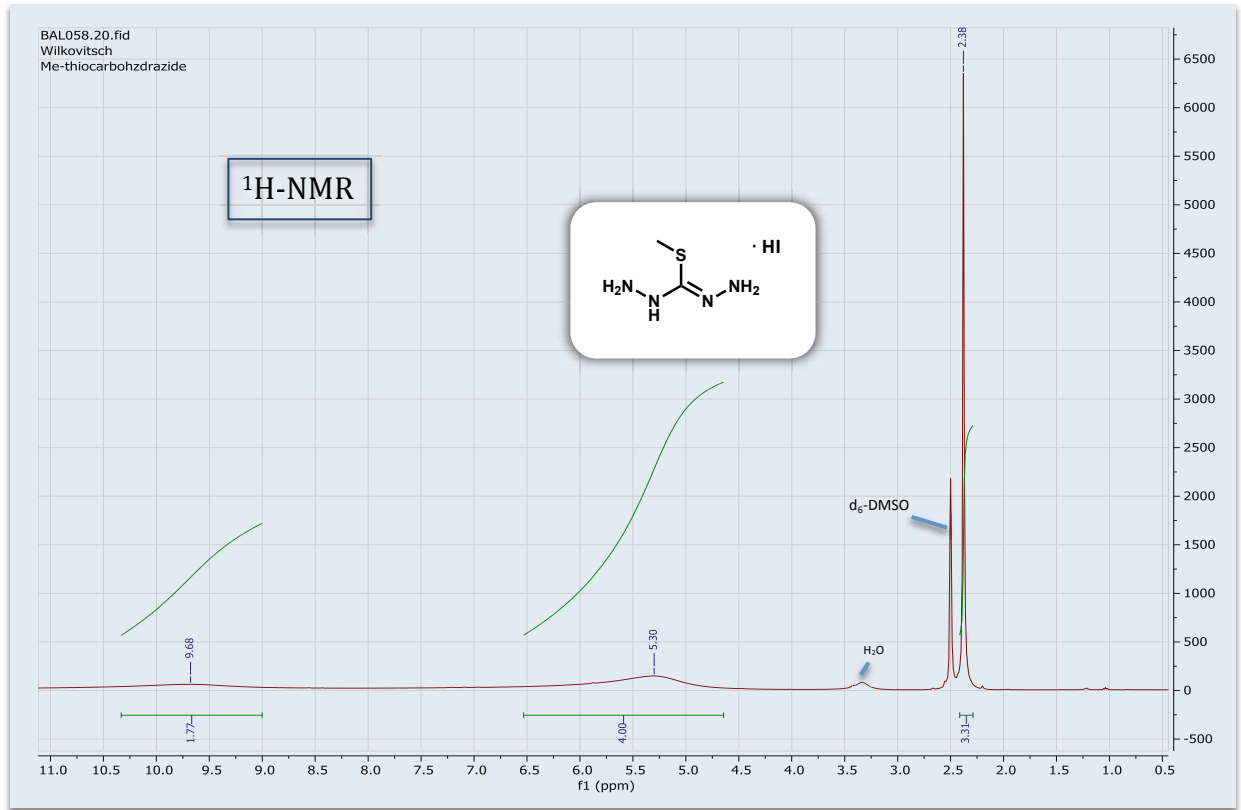


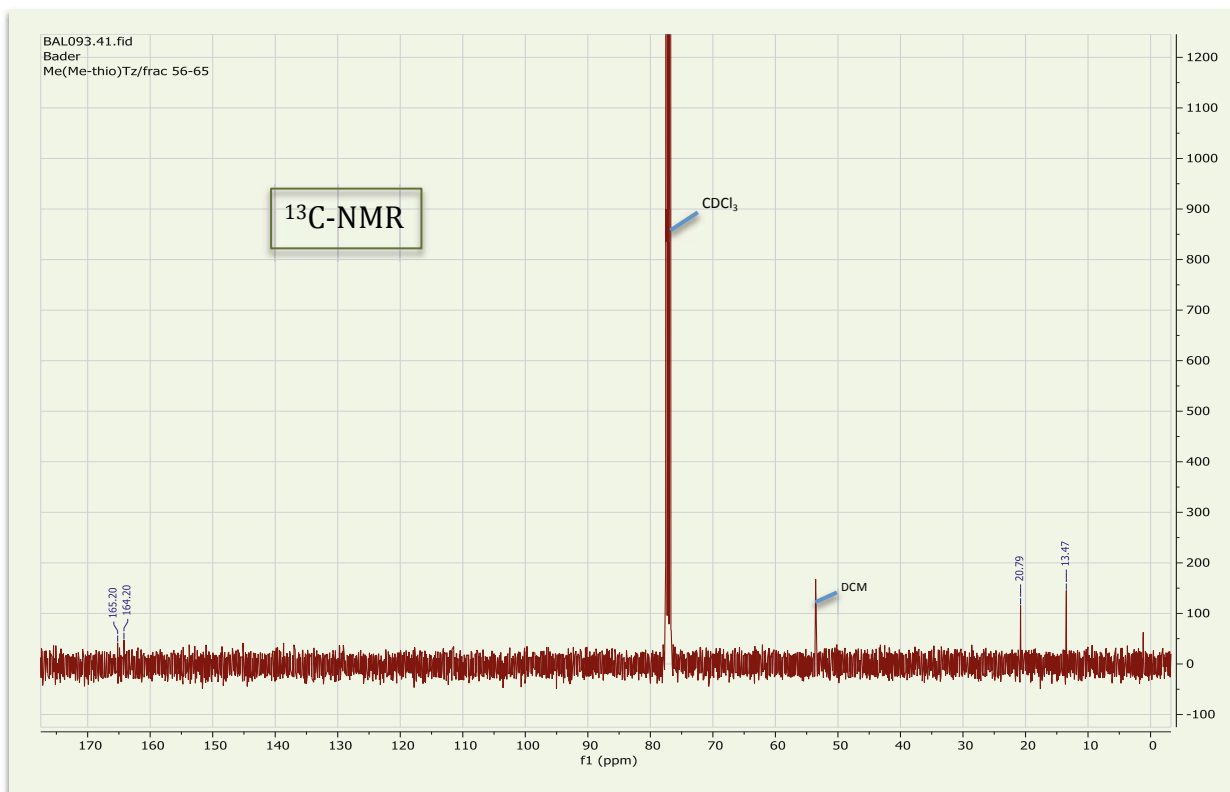
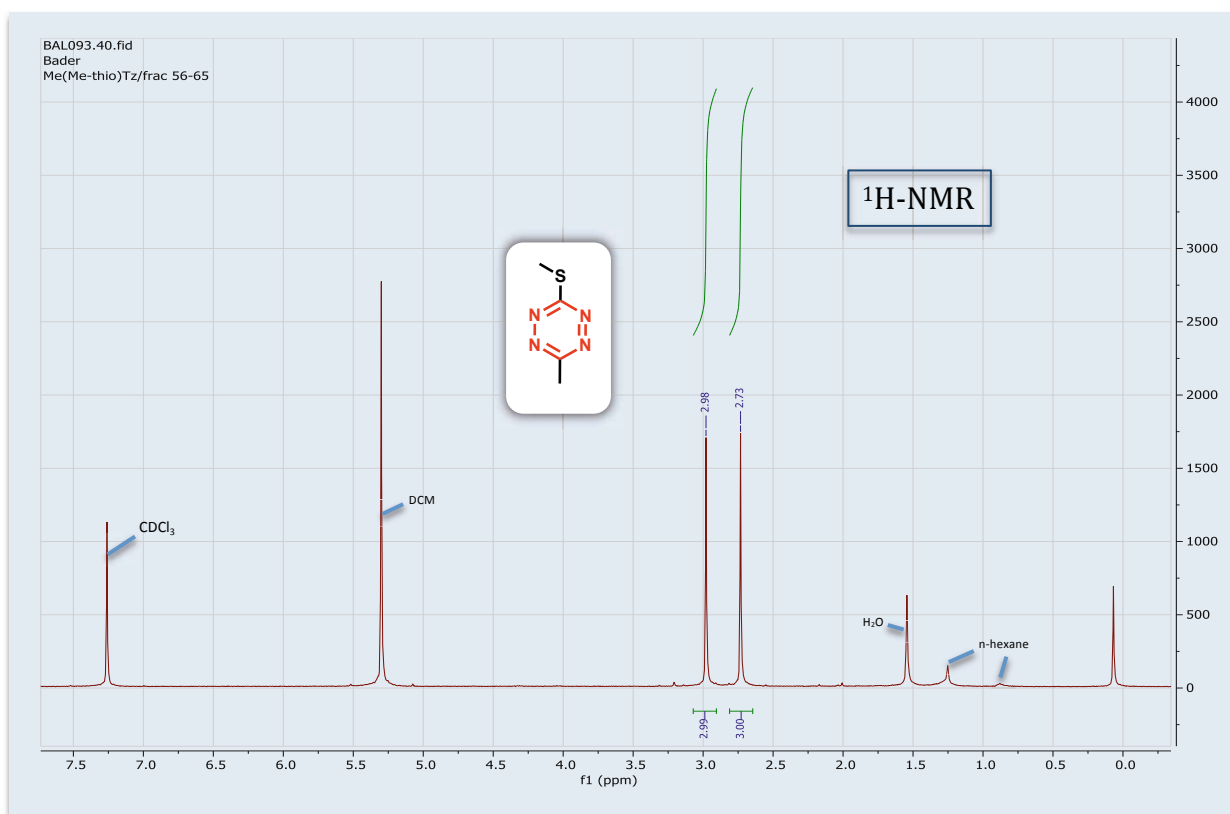


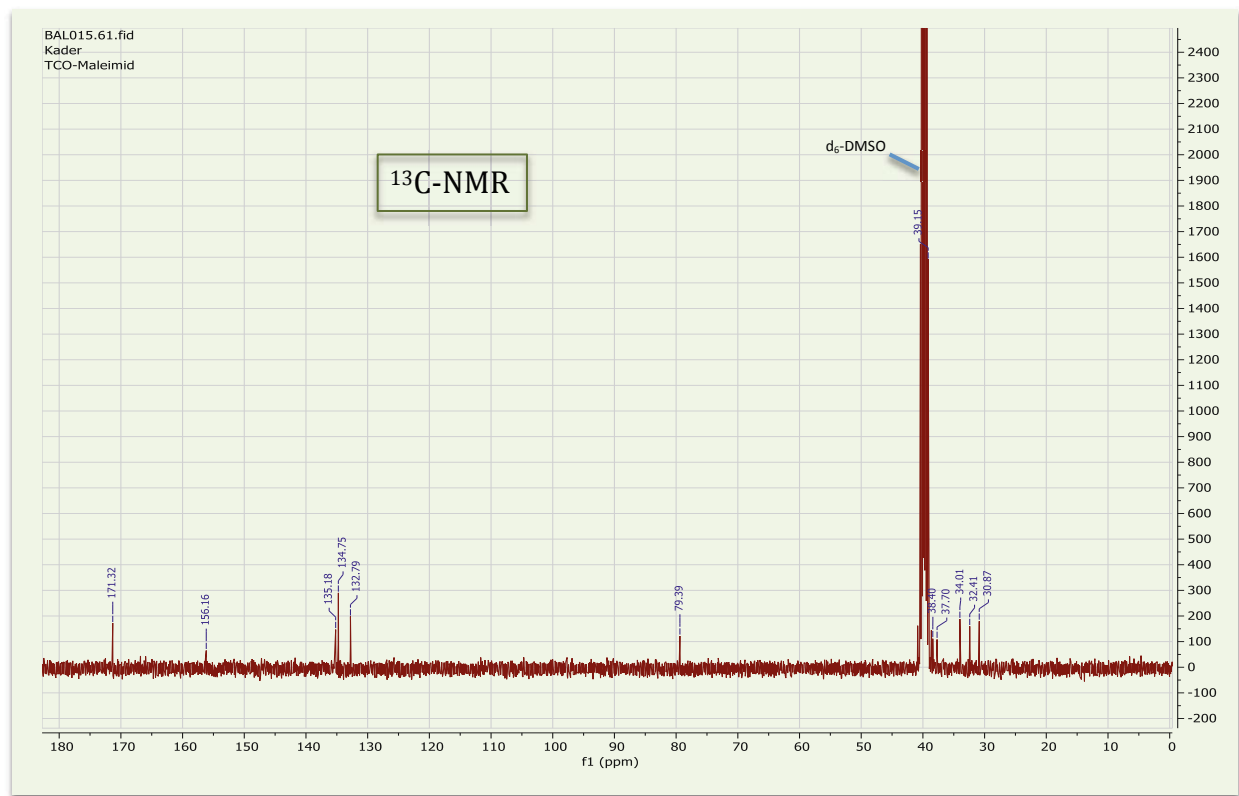
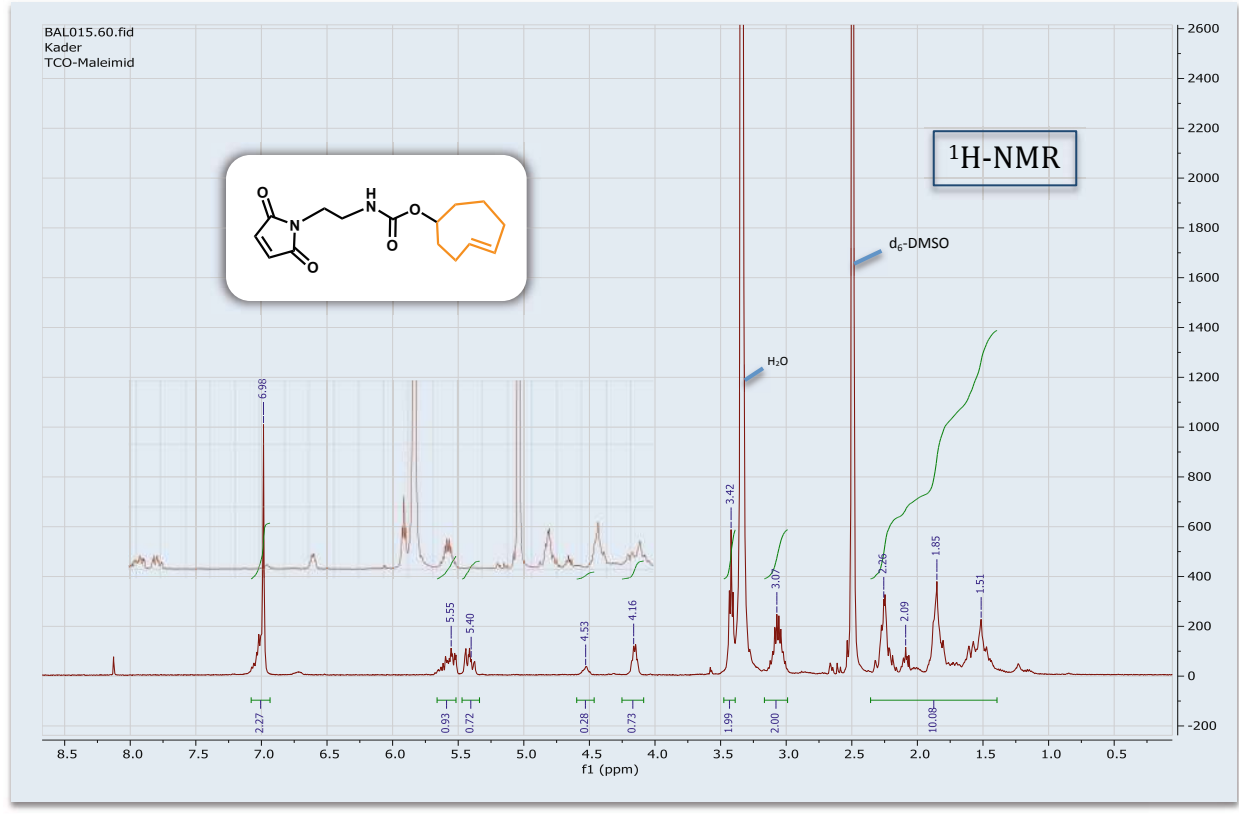


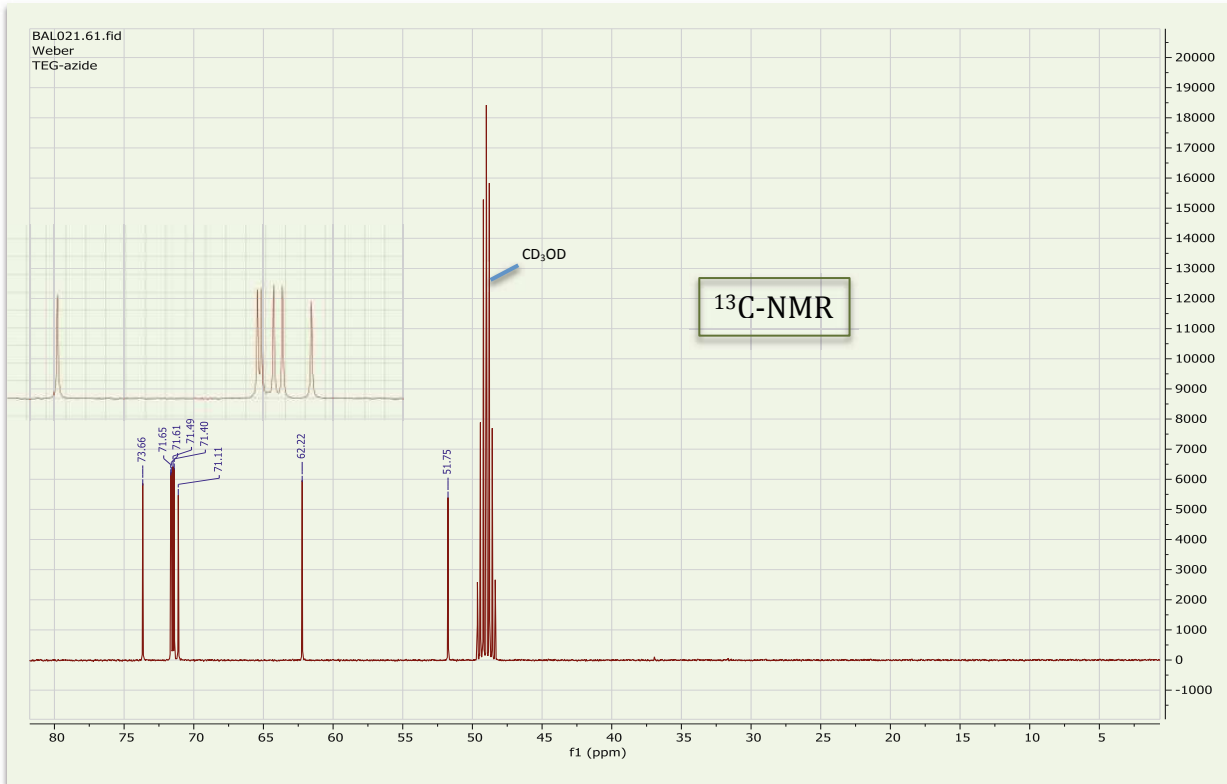
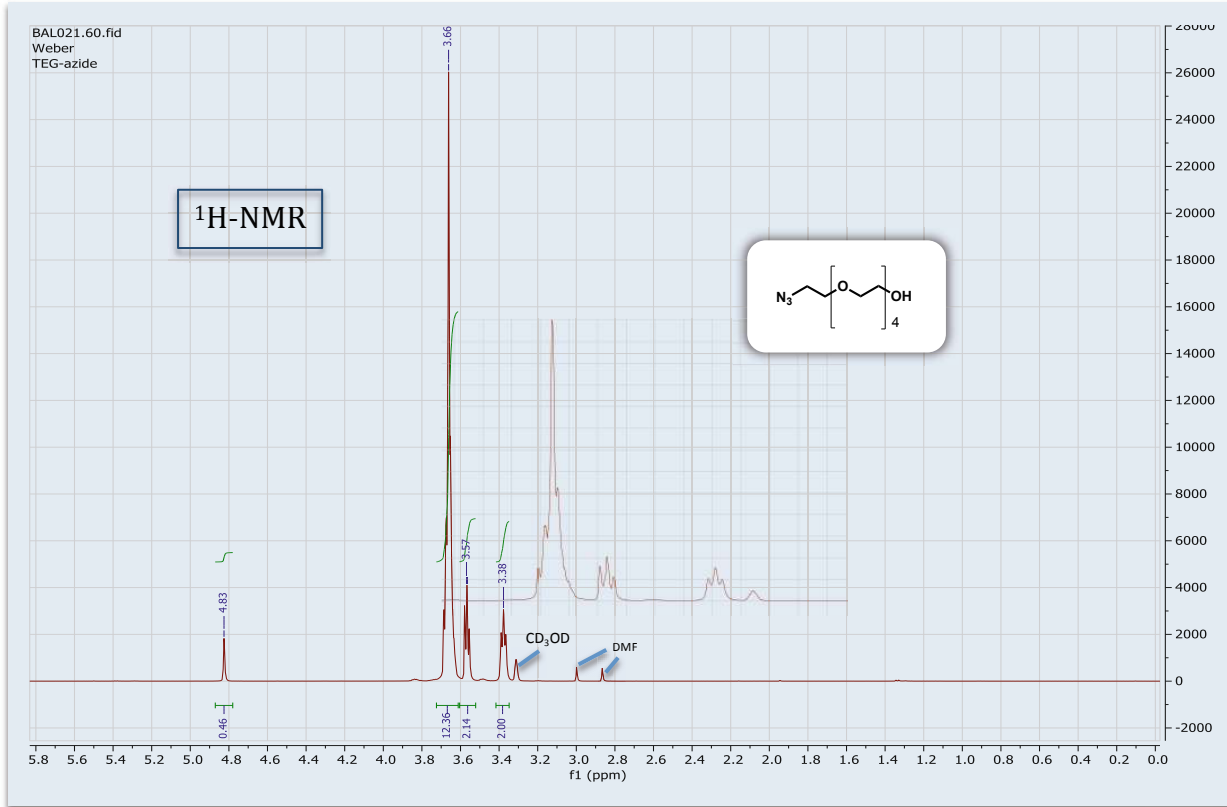


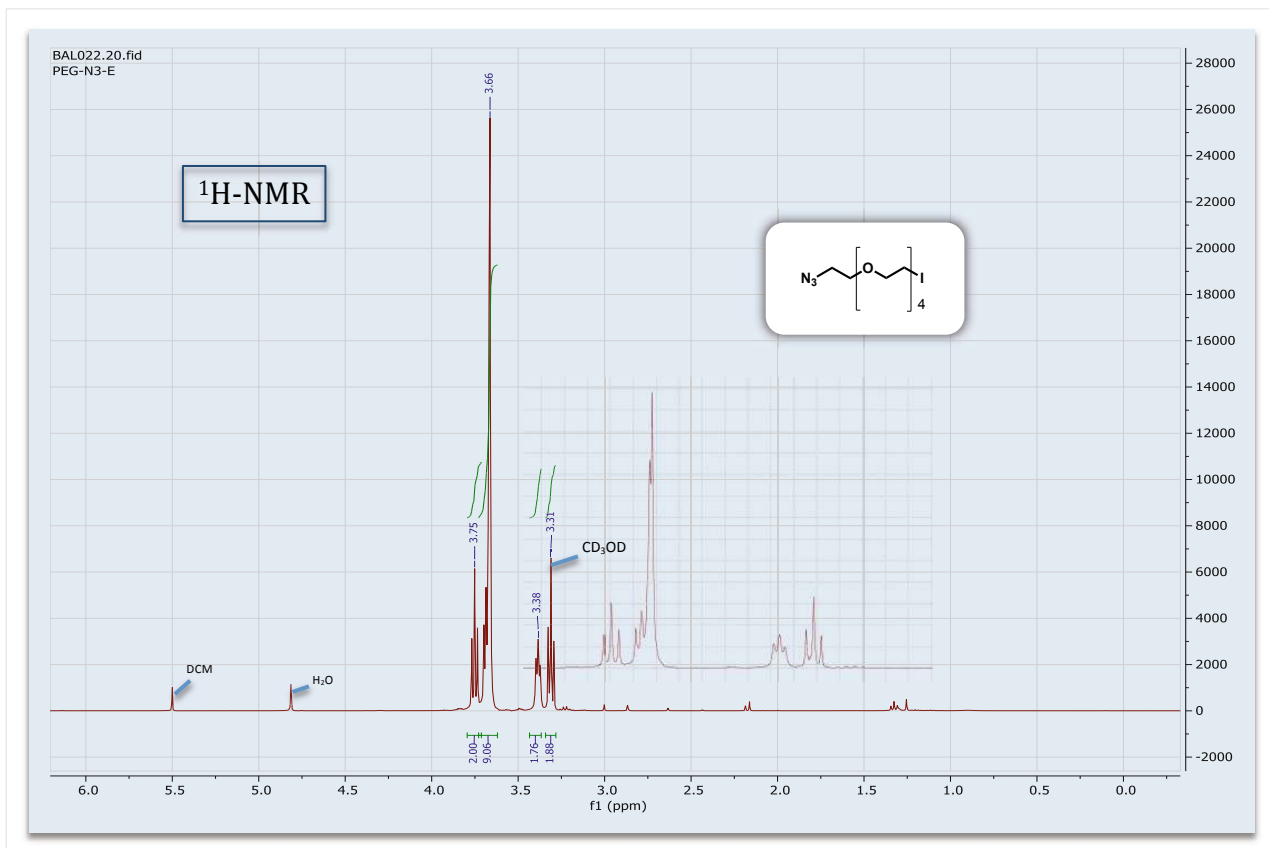
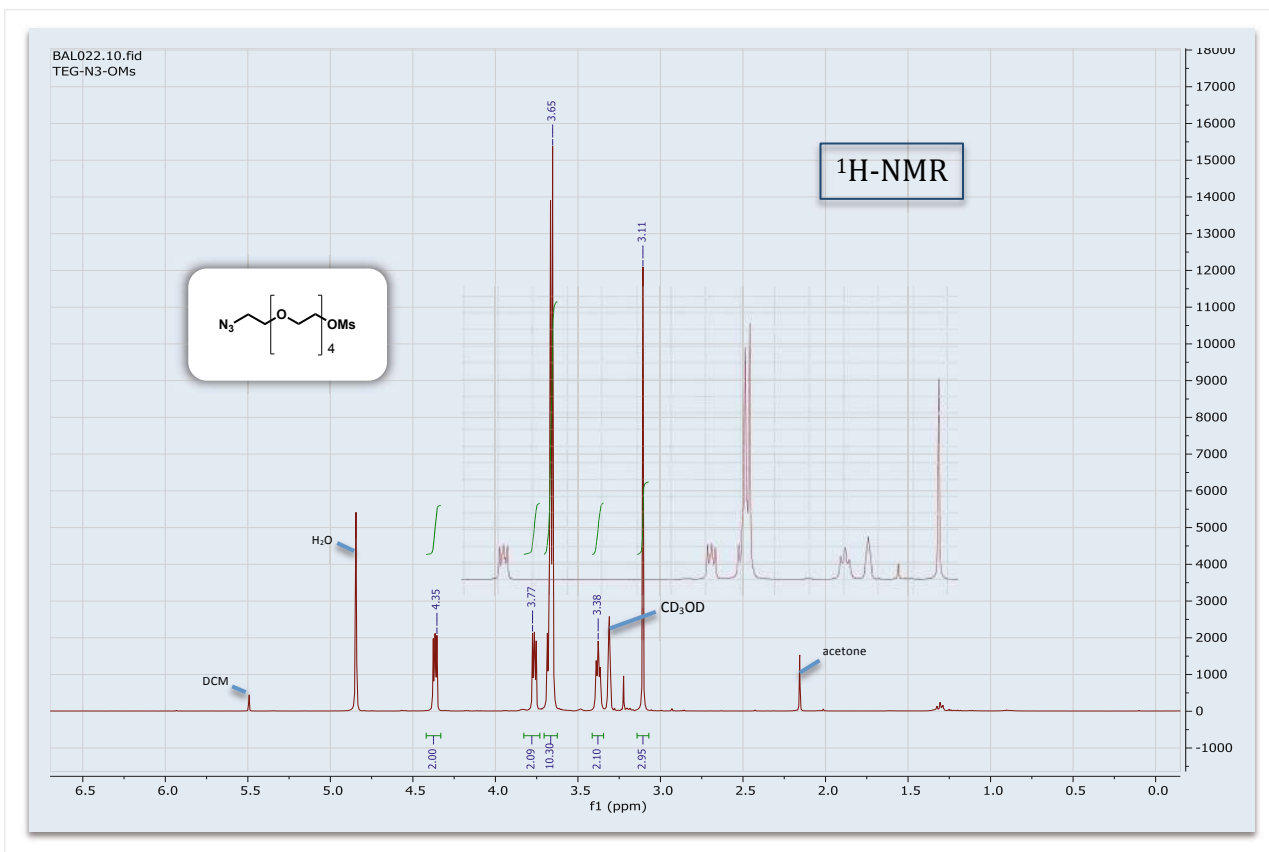


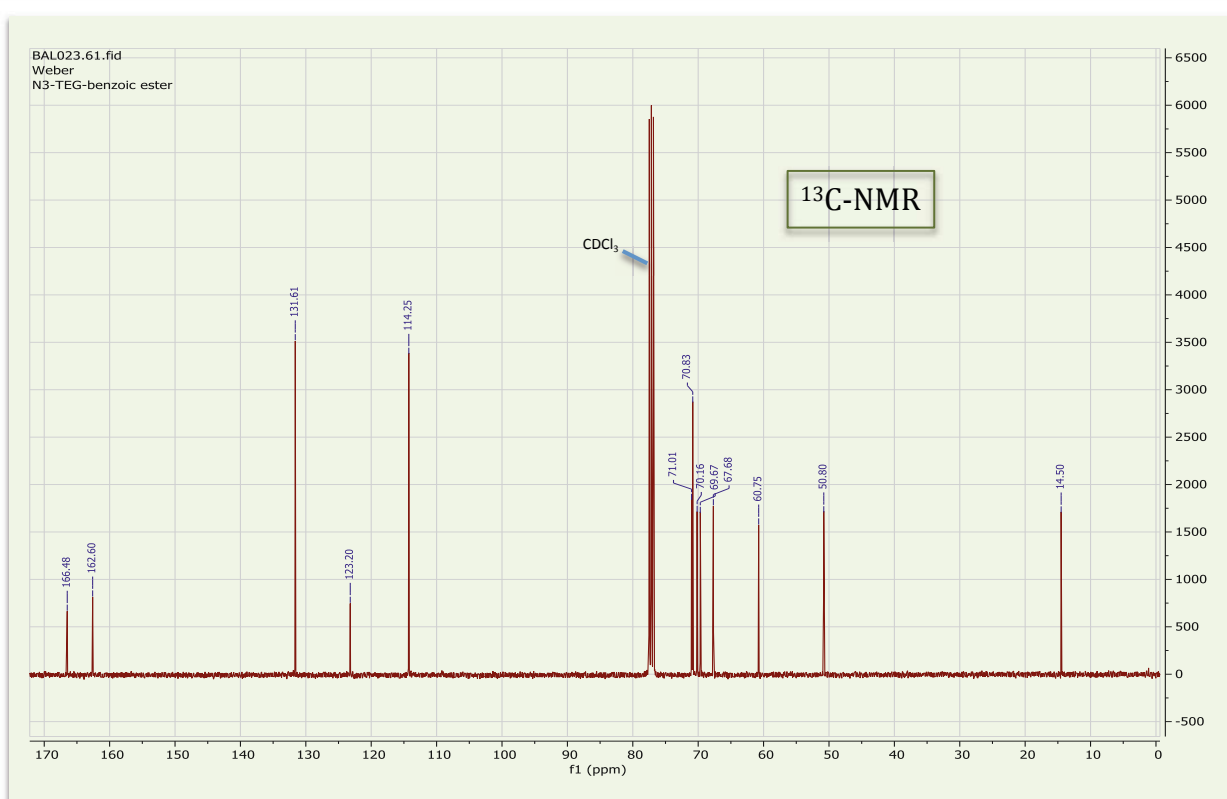
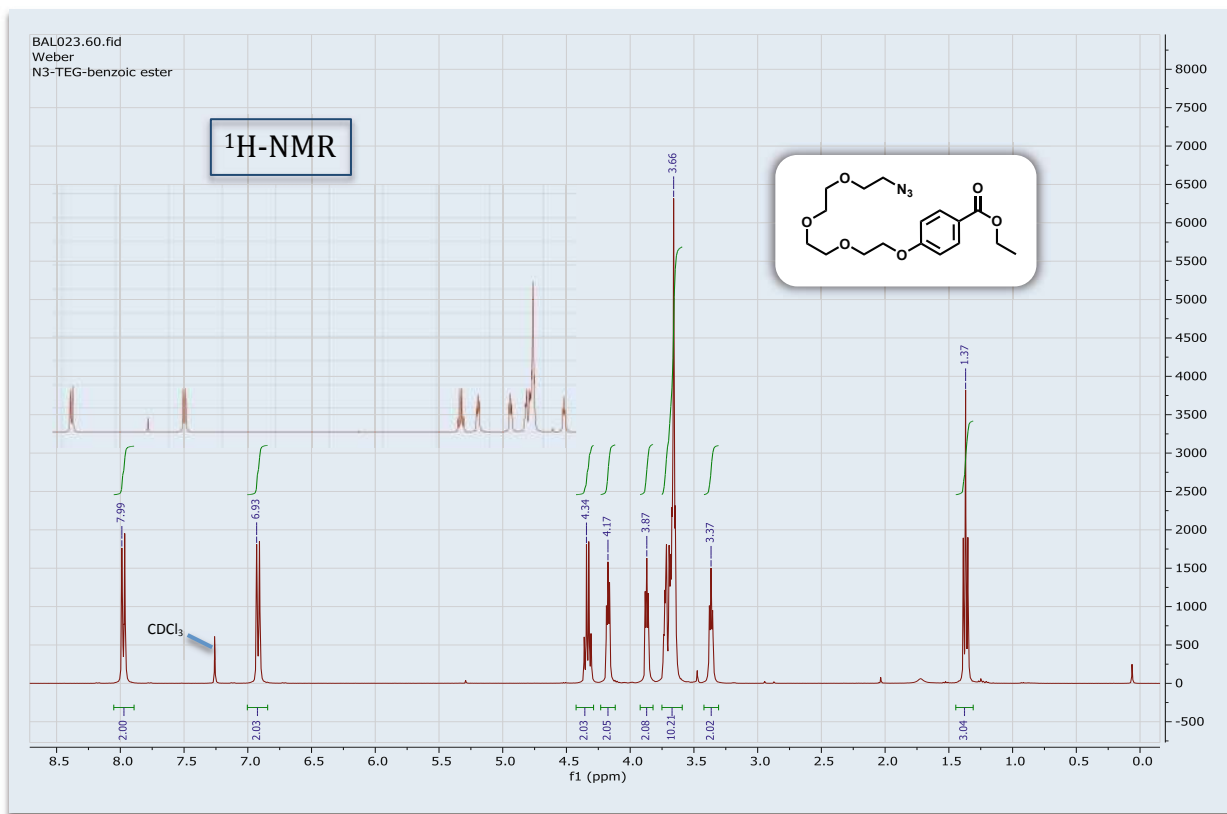


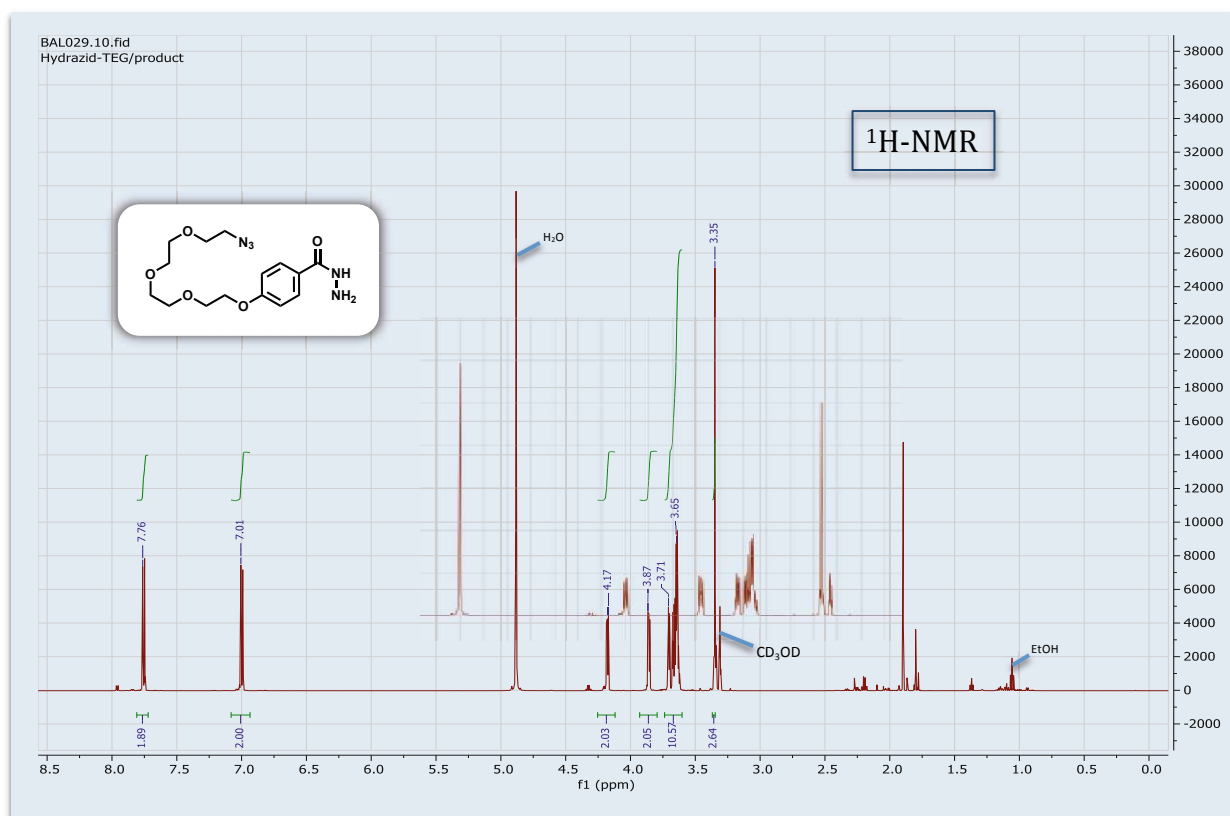


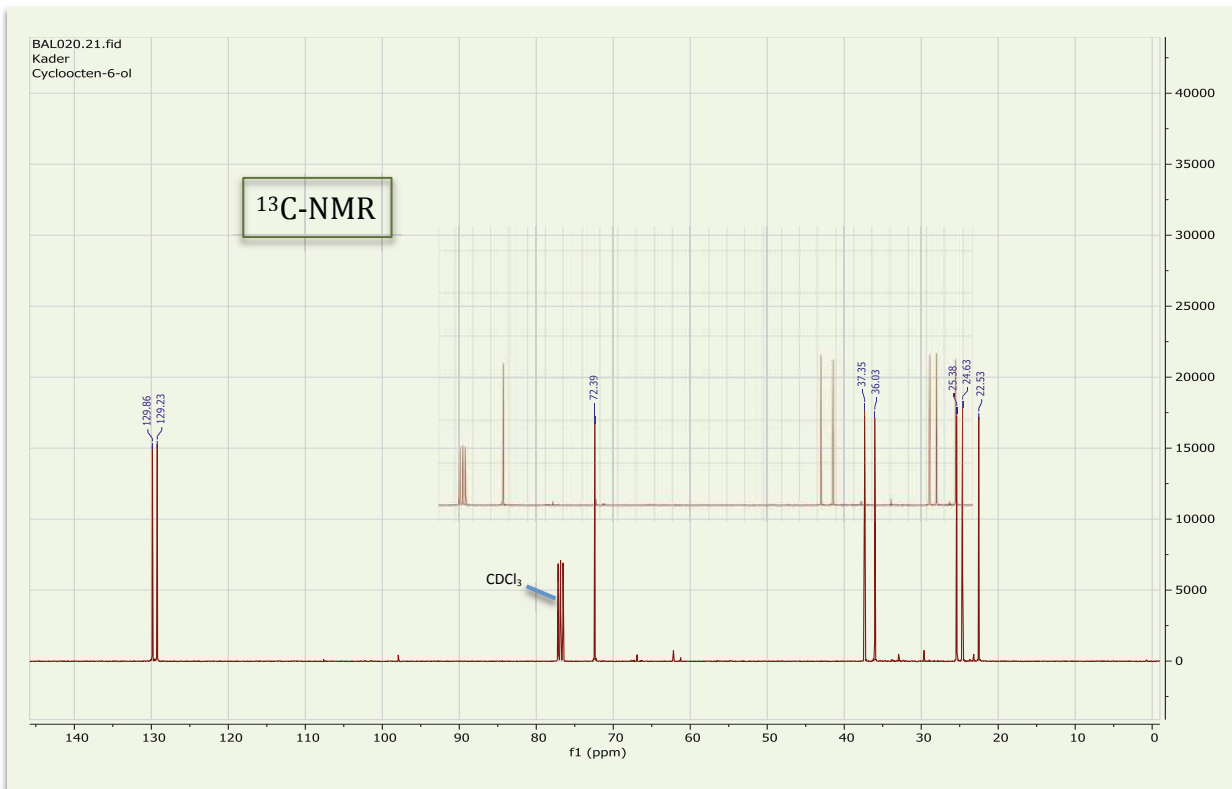
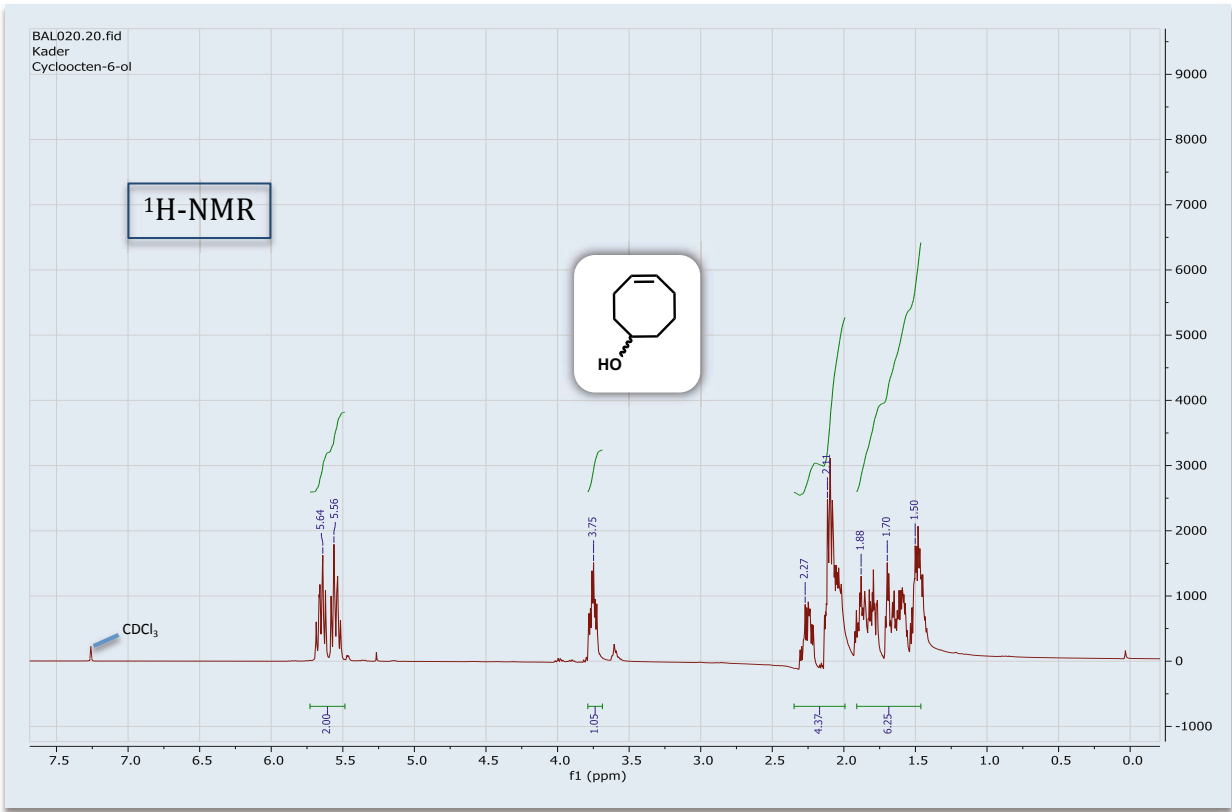


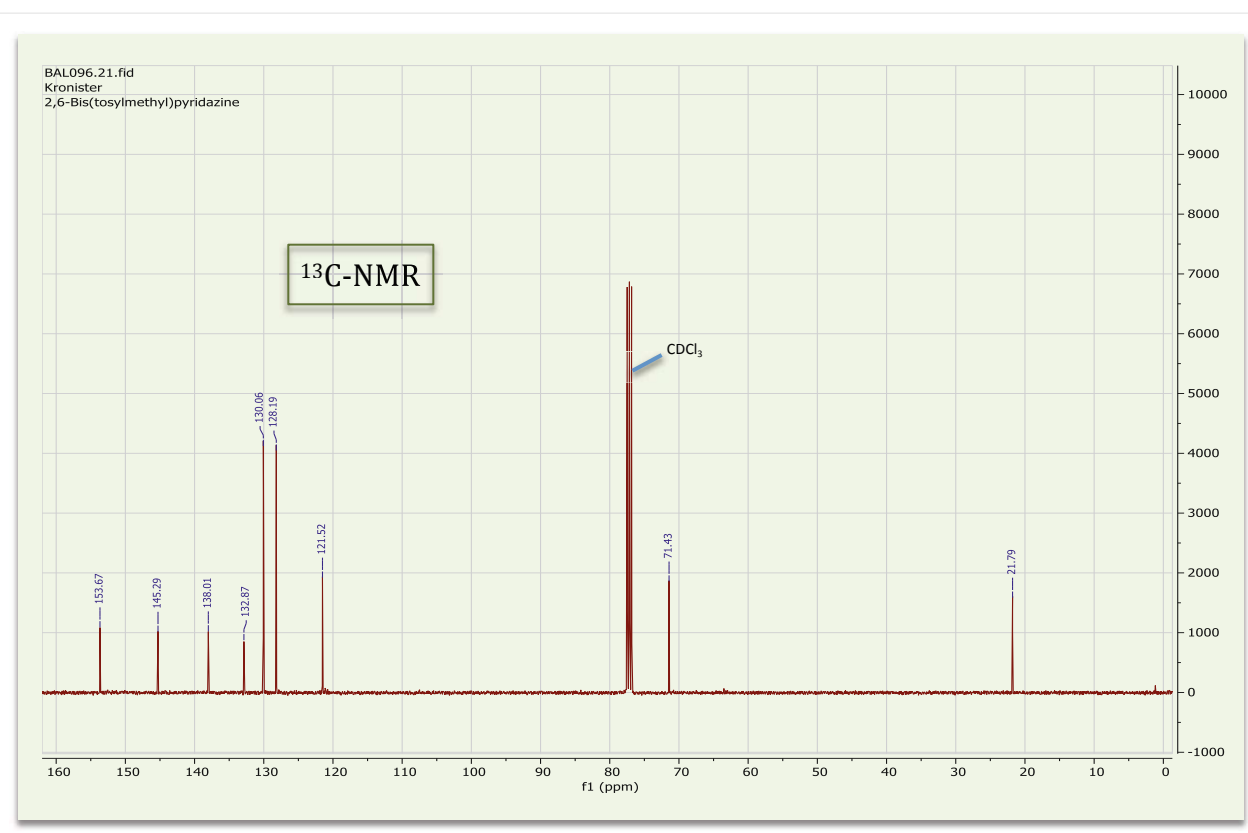
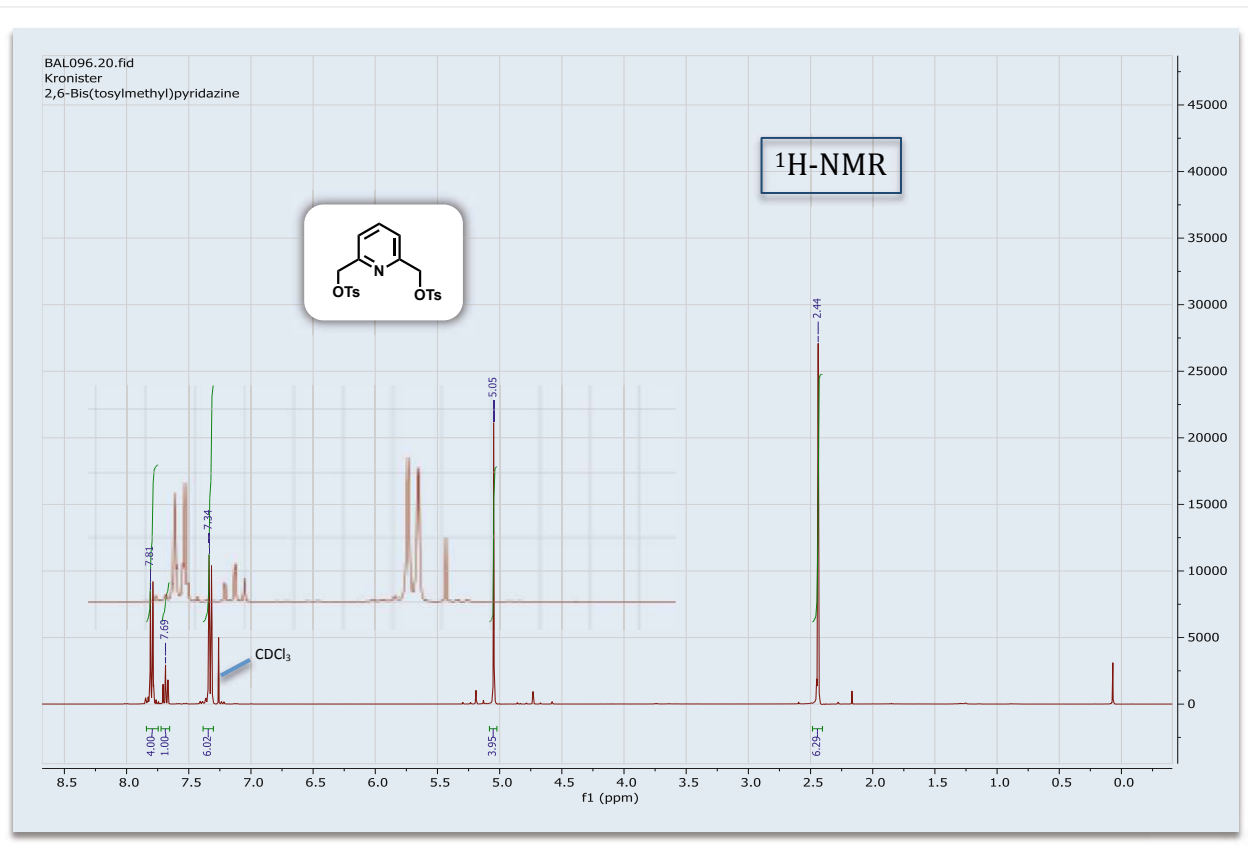


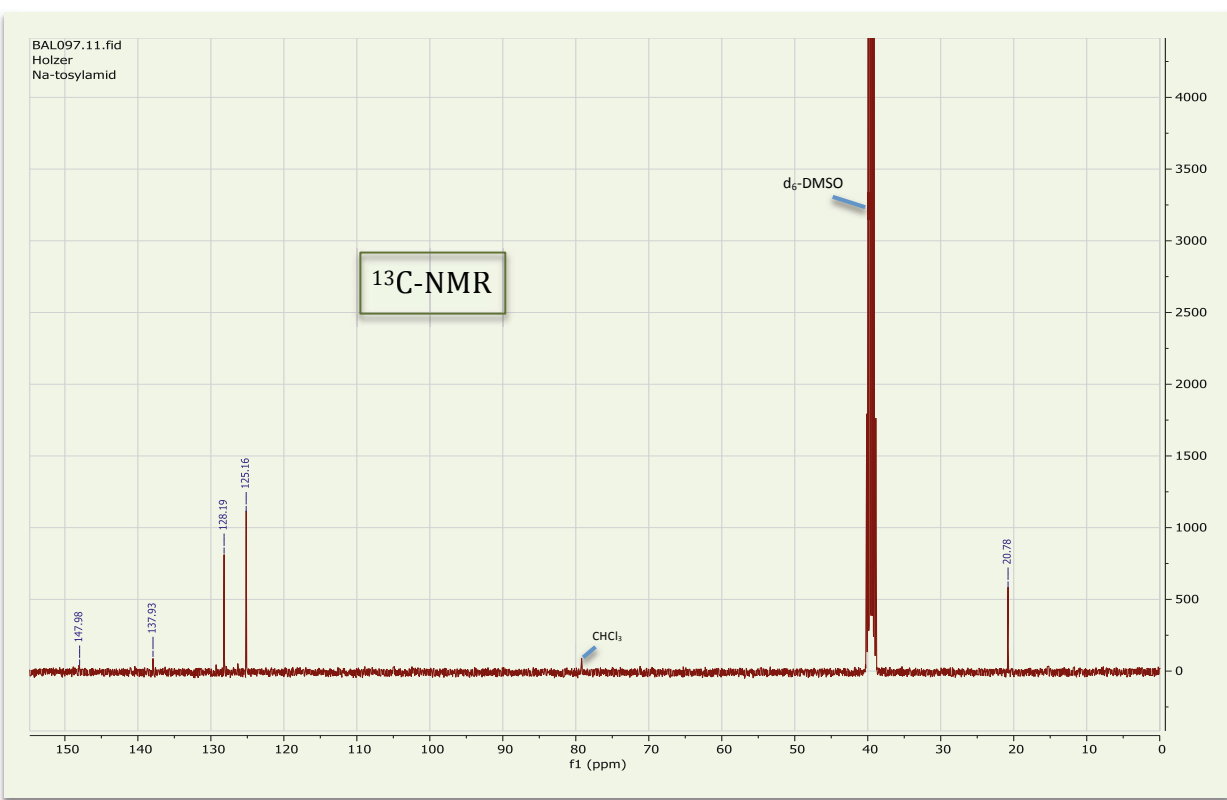
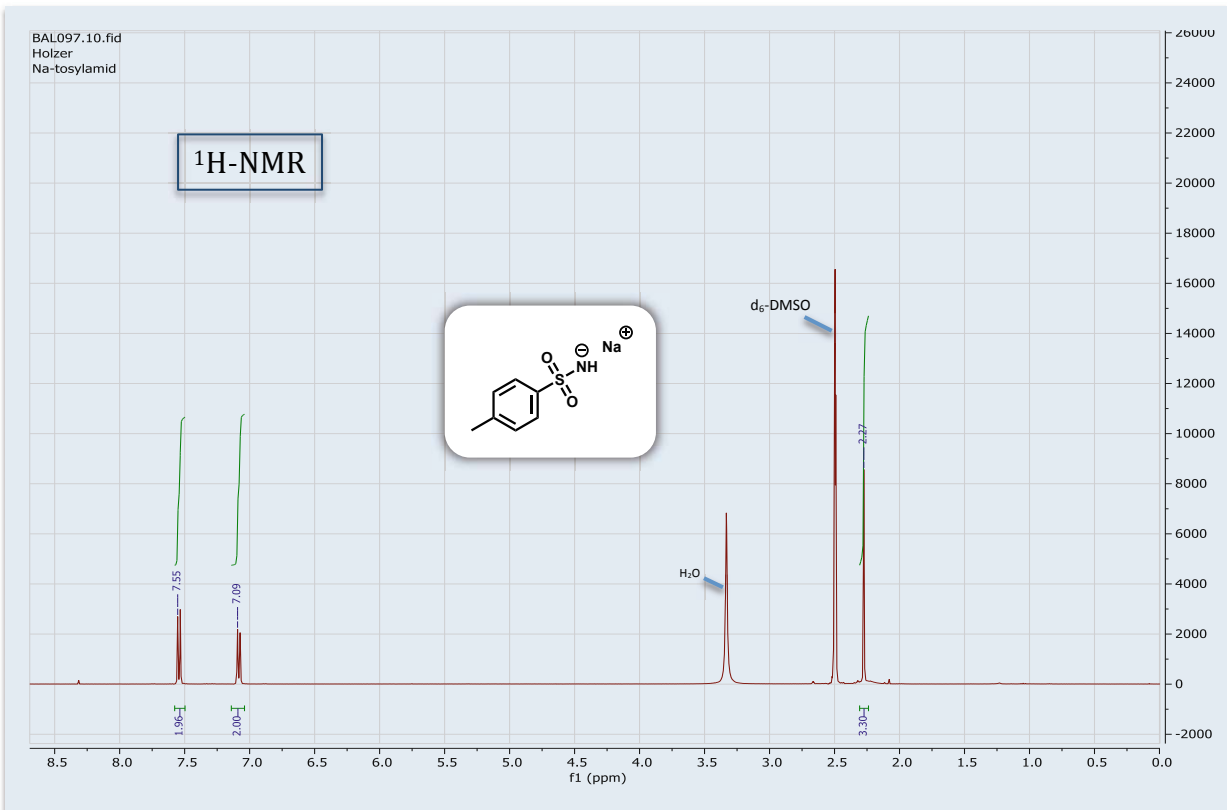


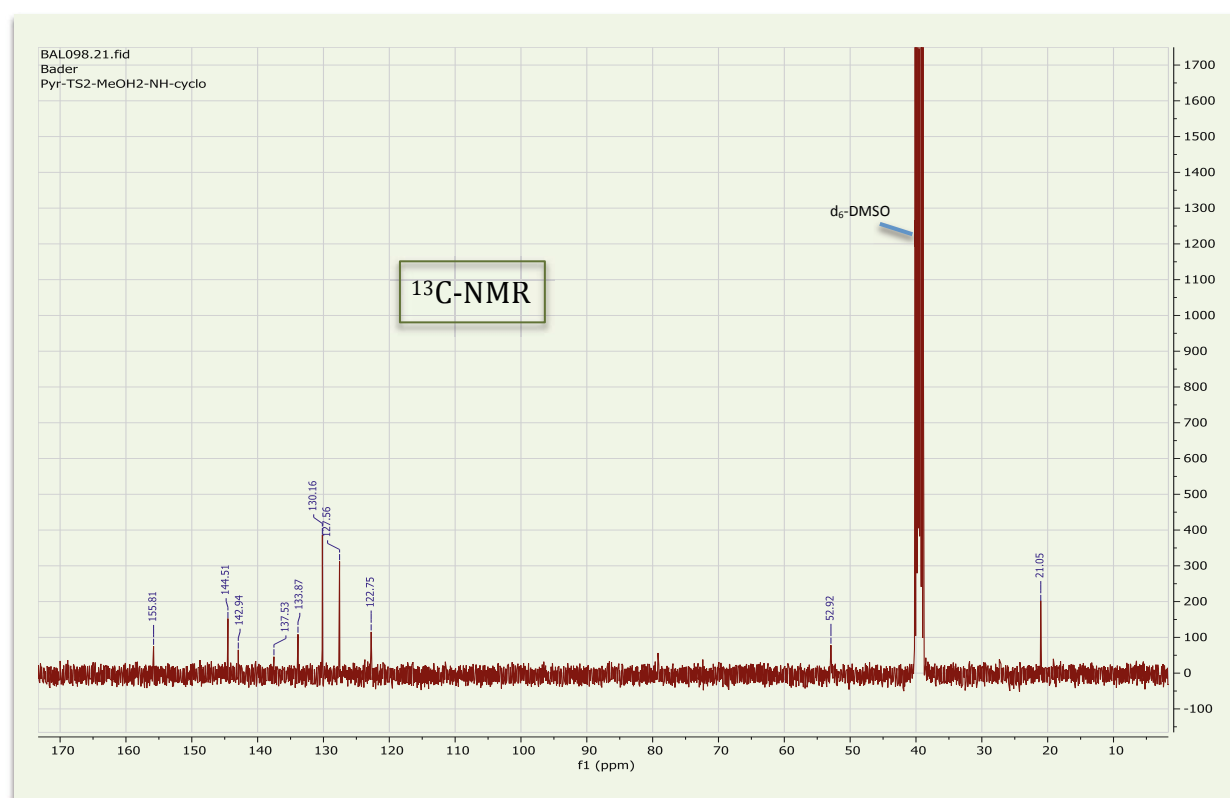
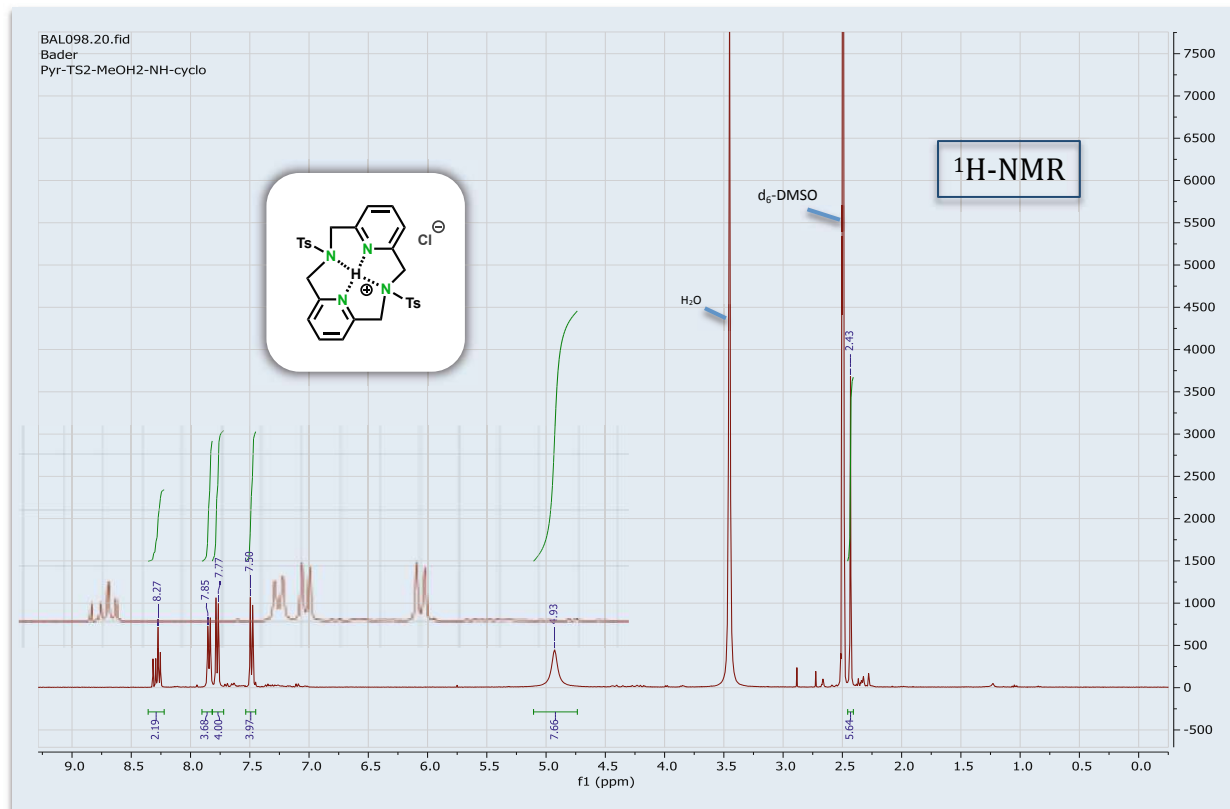


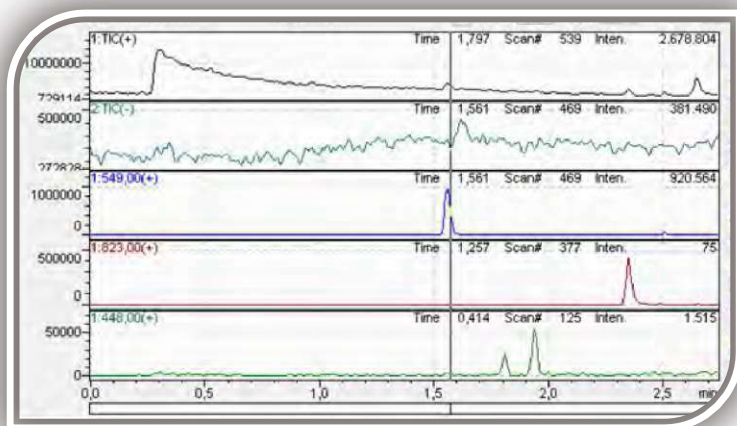




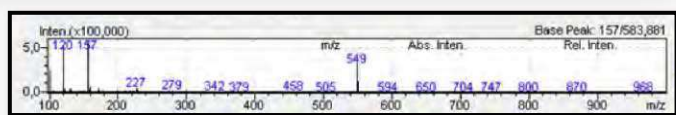
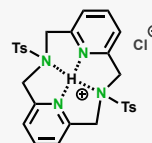






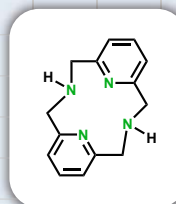
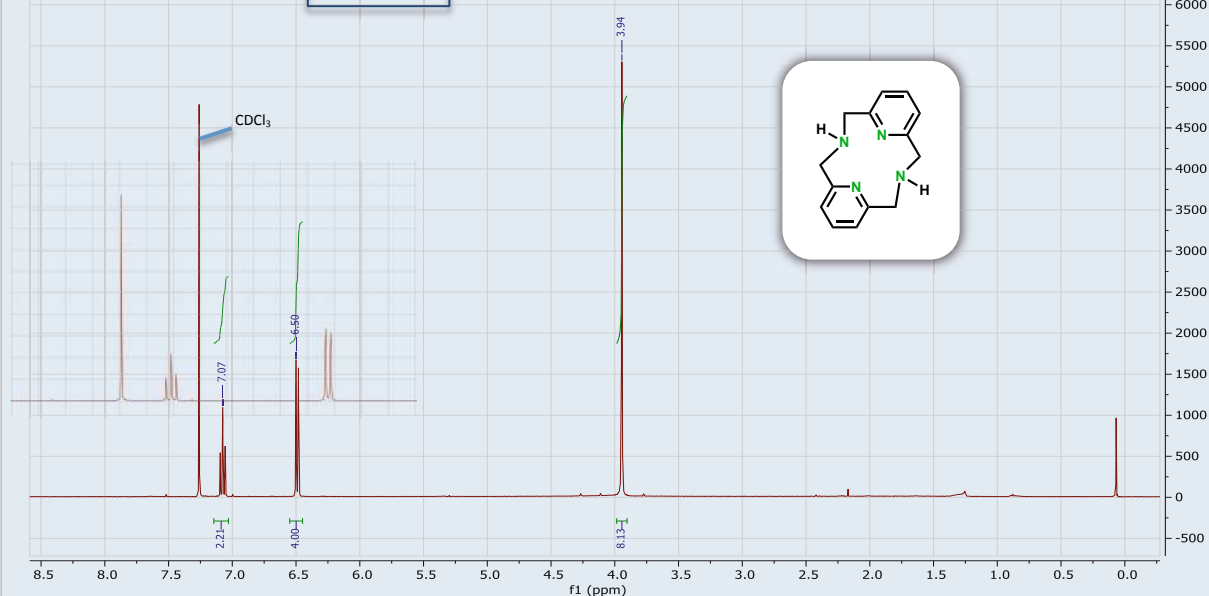


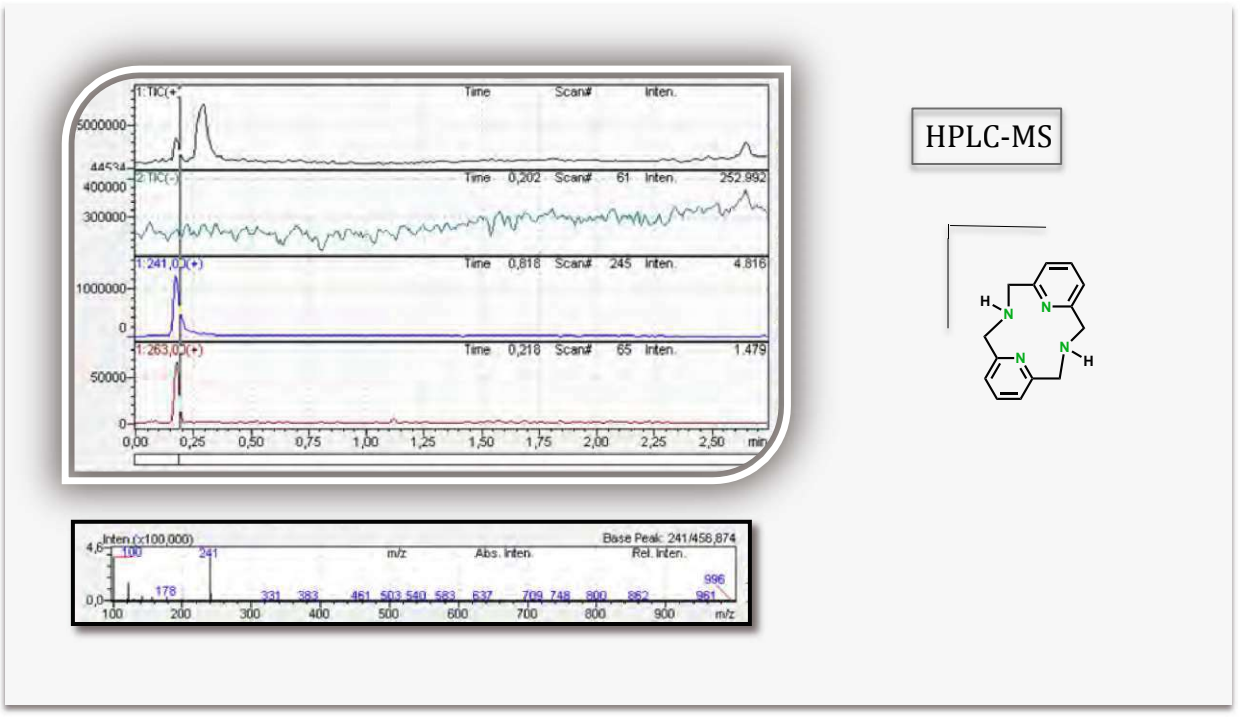
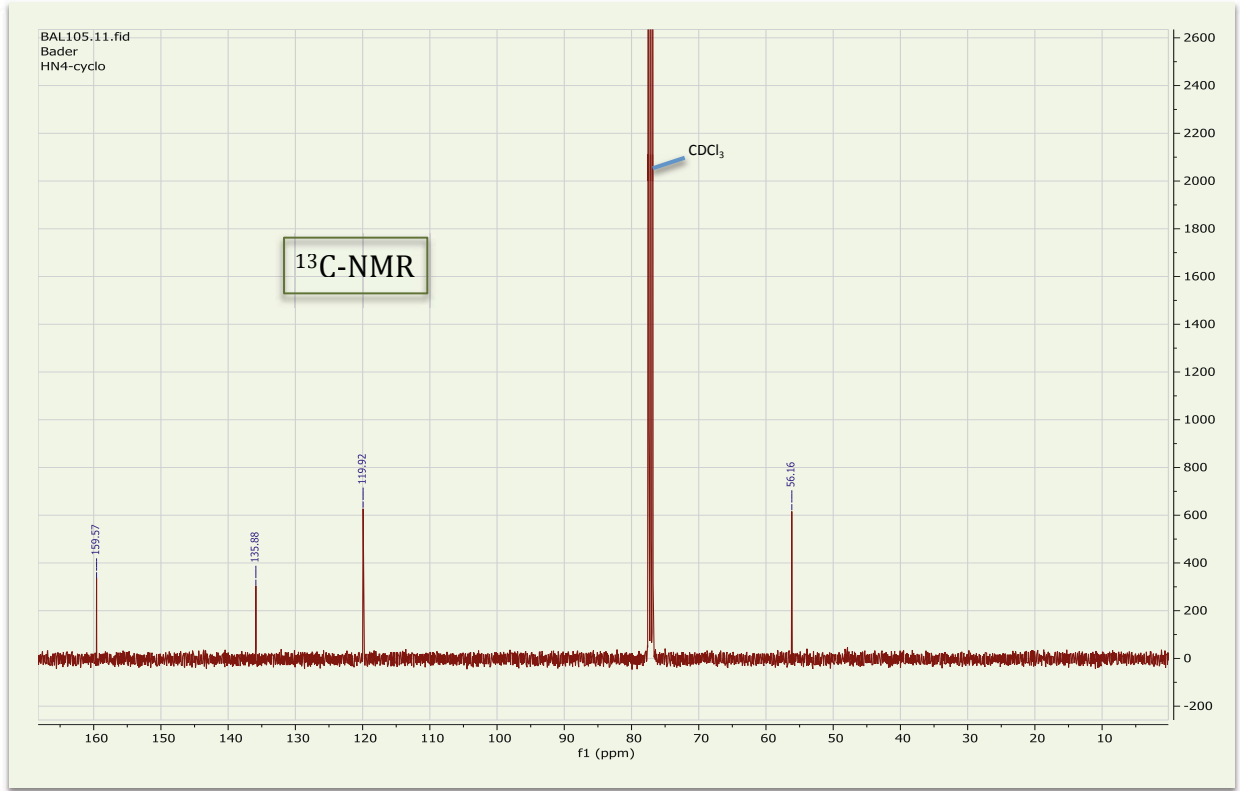
HPLC-MS

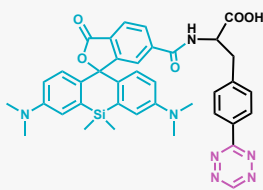
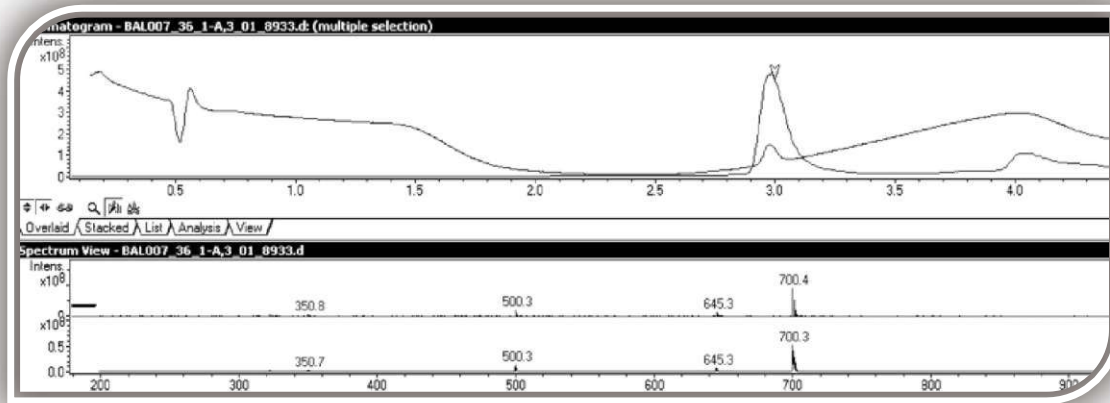


BAL105.10.fid
Bader
HN4-cyclo

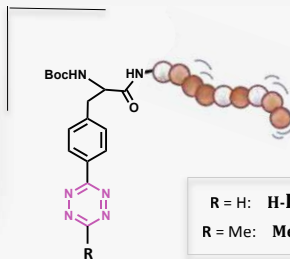
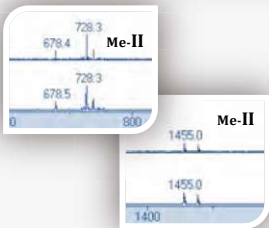
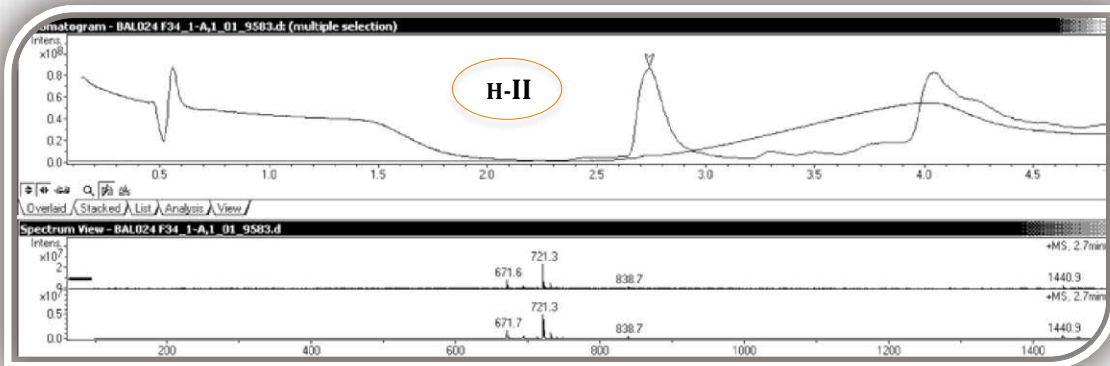
¹H-NMR





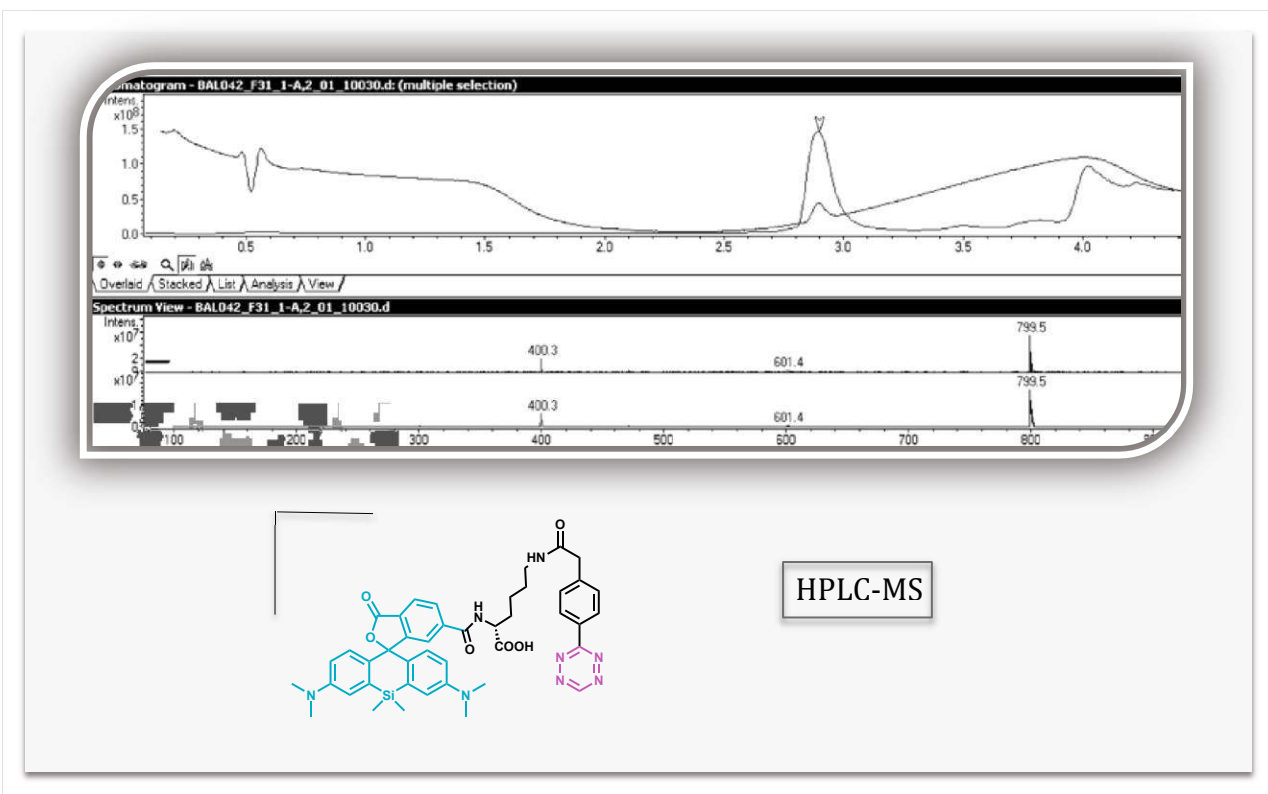
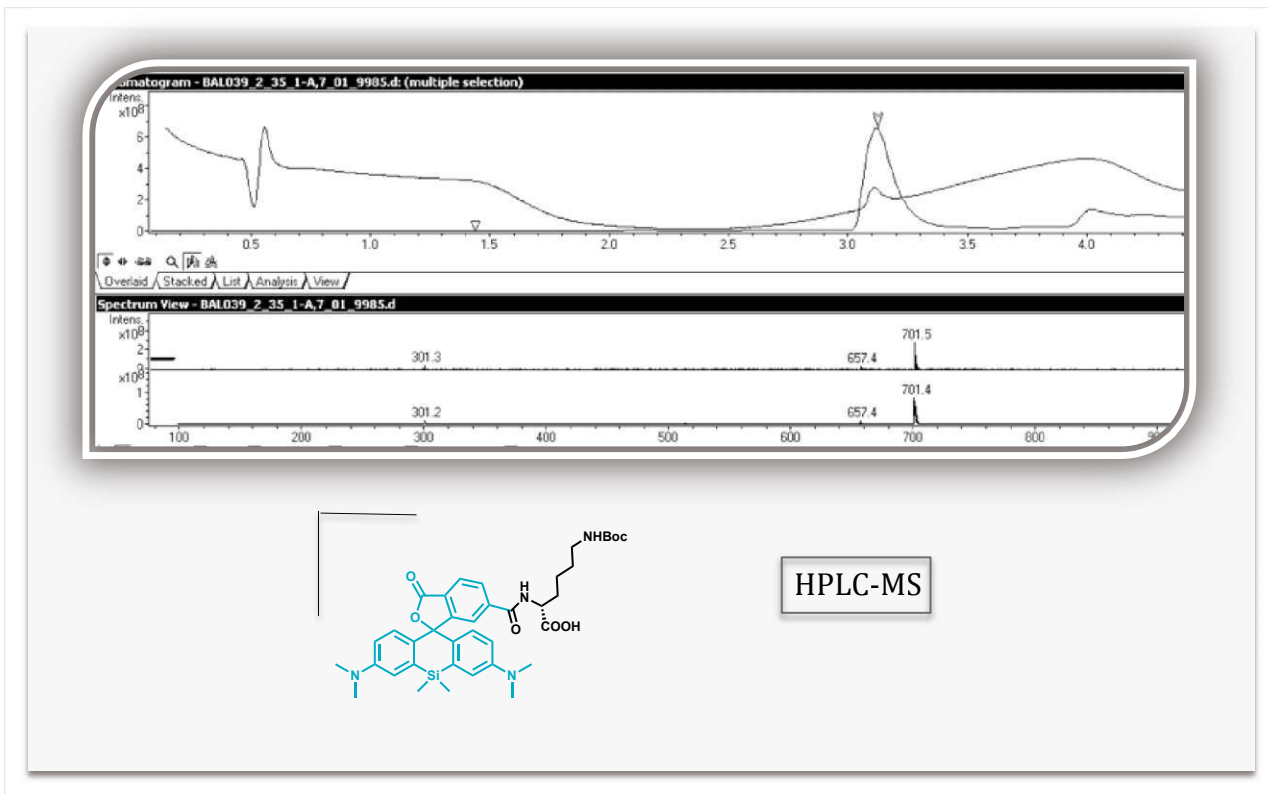


HPLC-MS



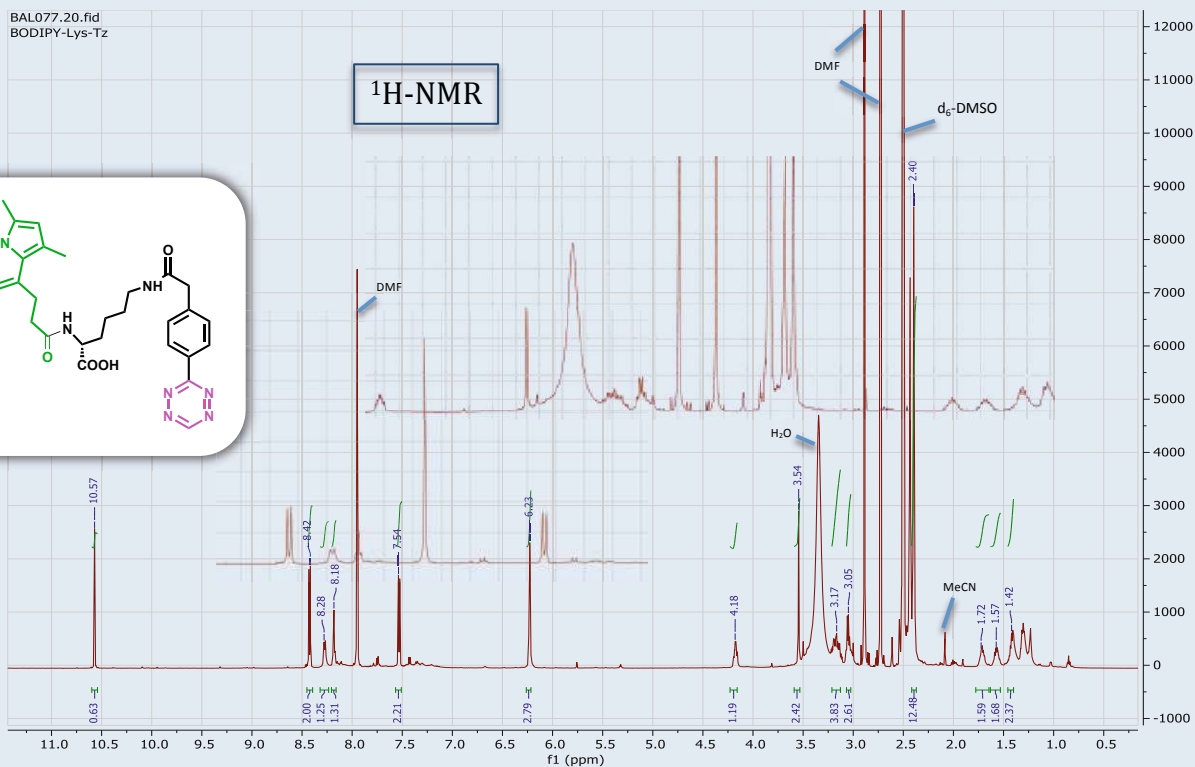
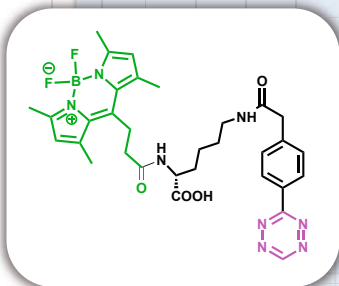
HPLC-MS





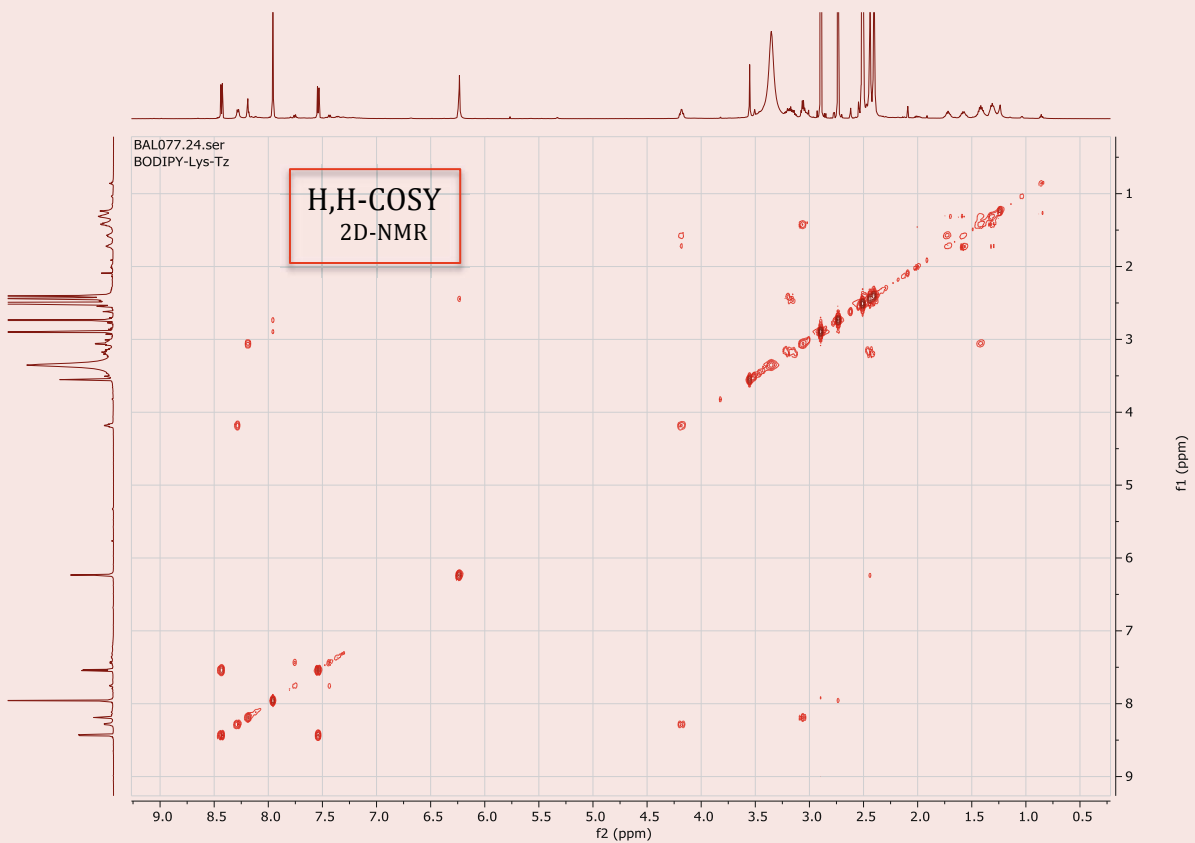
BAL077.20.fid
BODIPY-Lys-Tz

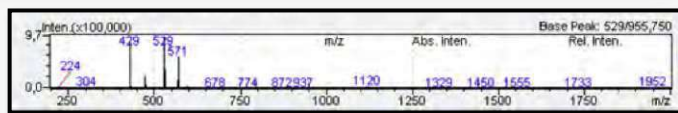
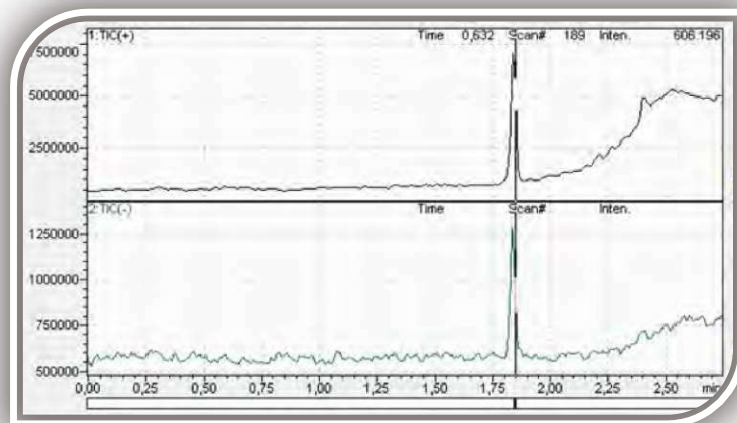
¹H-NMR



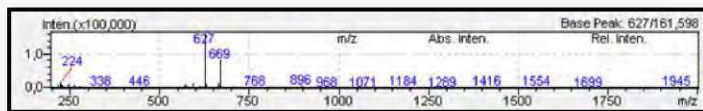
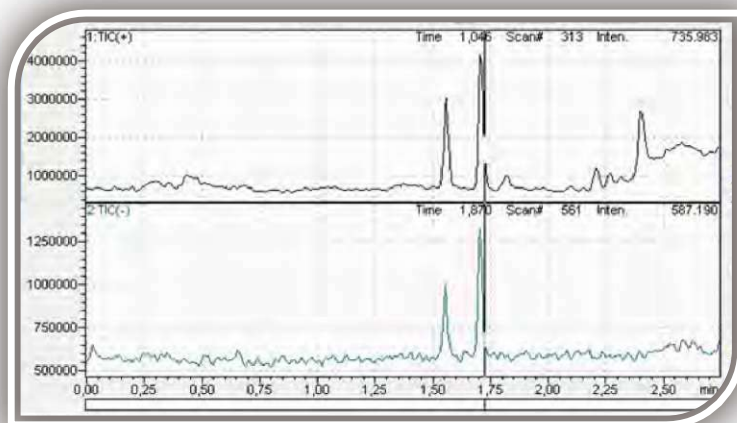
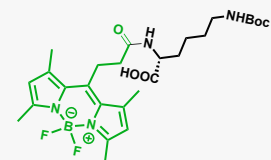
BAL077.24.ser
BODIPY-Lys-Tz

**H,H-COSY
2D-NMR**

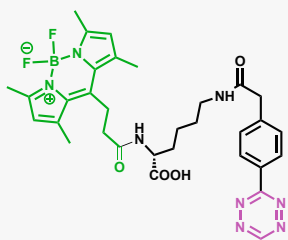


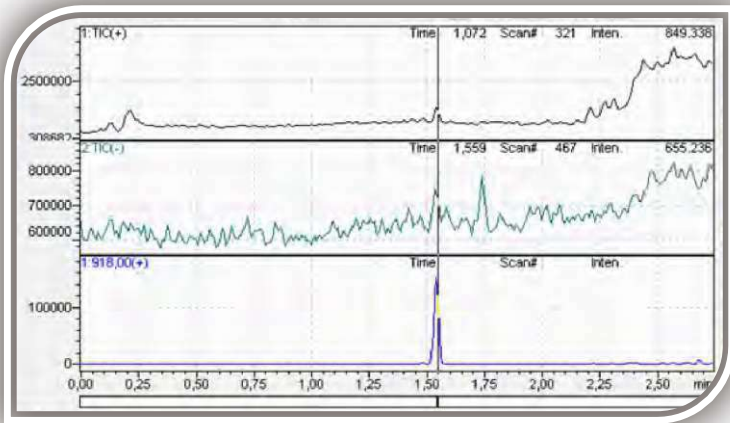


HPLC-MS

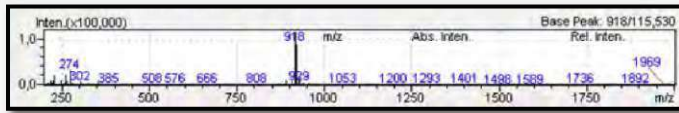
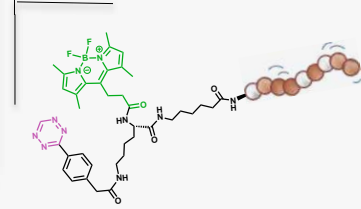


HPLC-MS

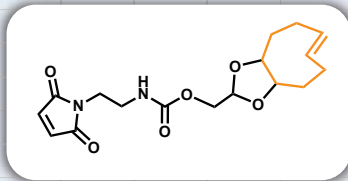




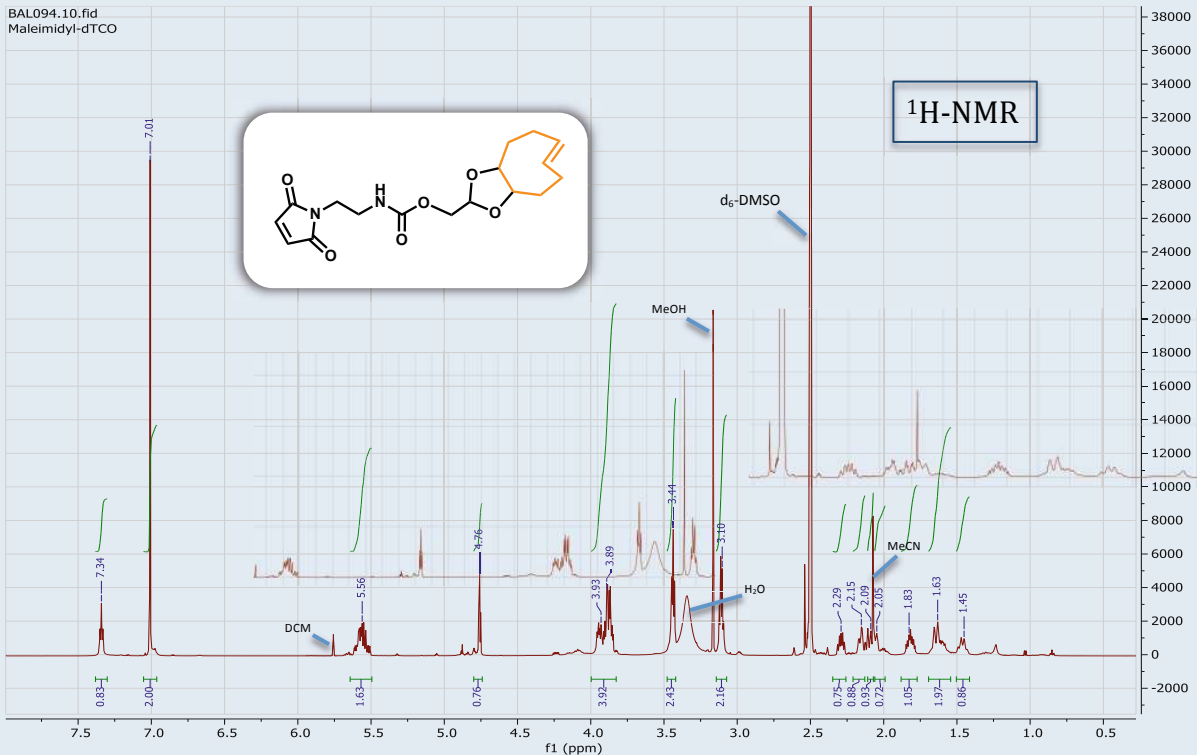
HPLC-MS

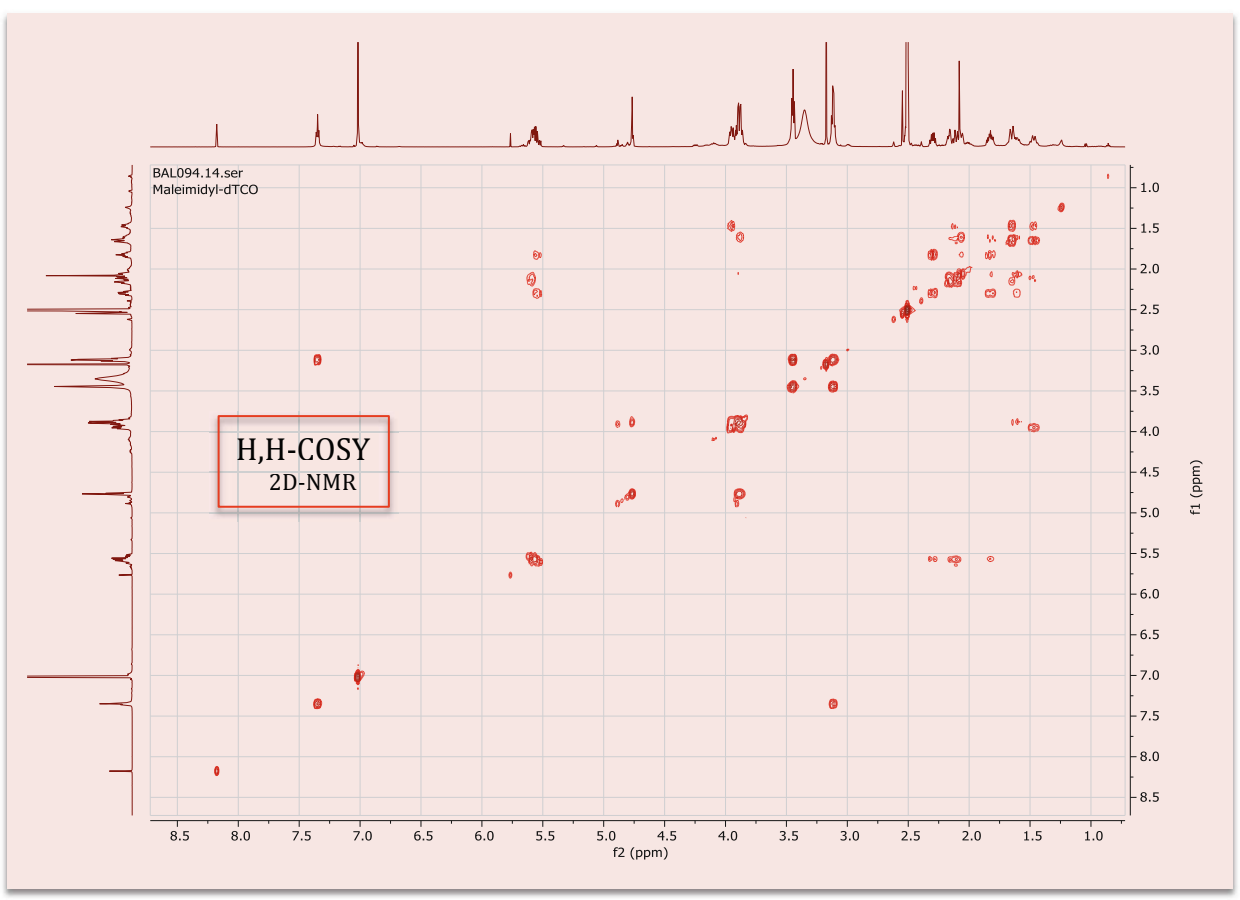
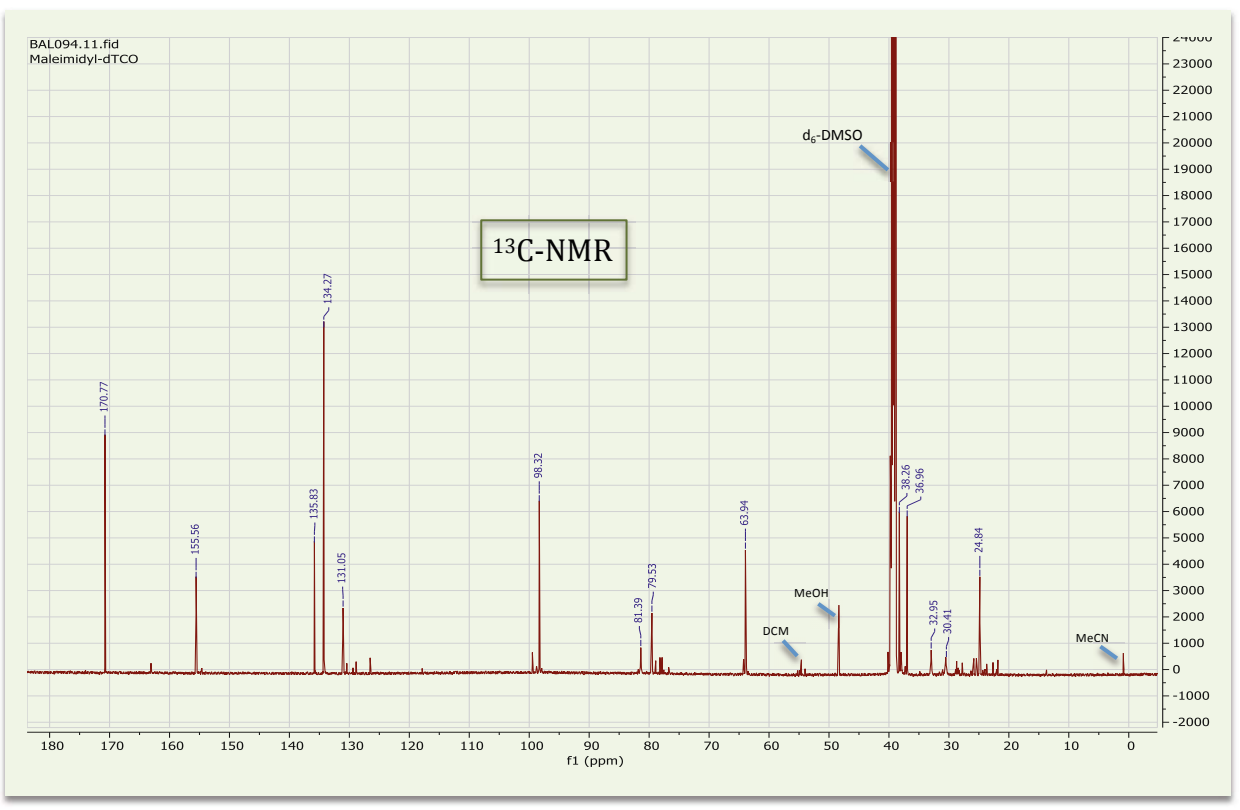


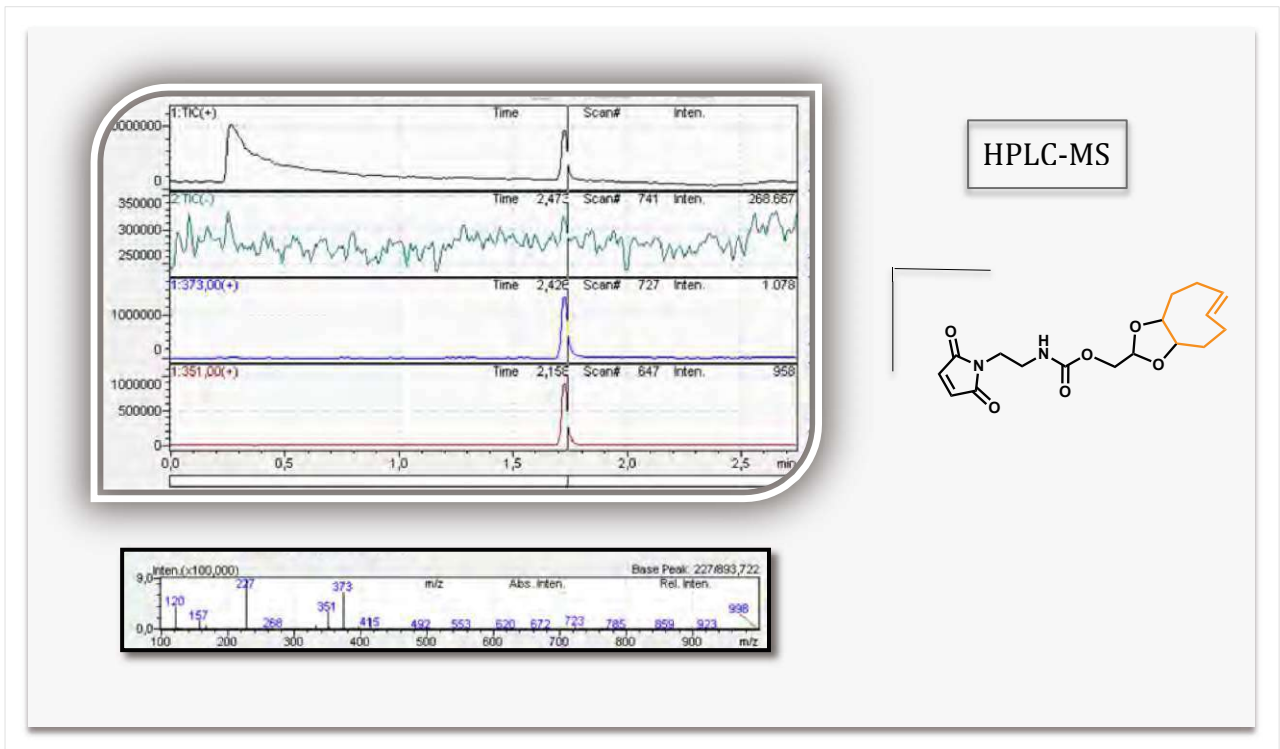
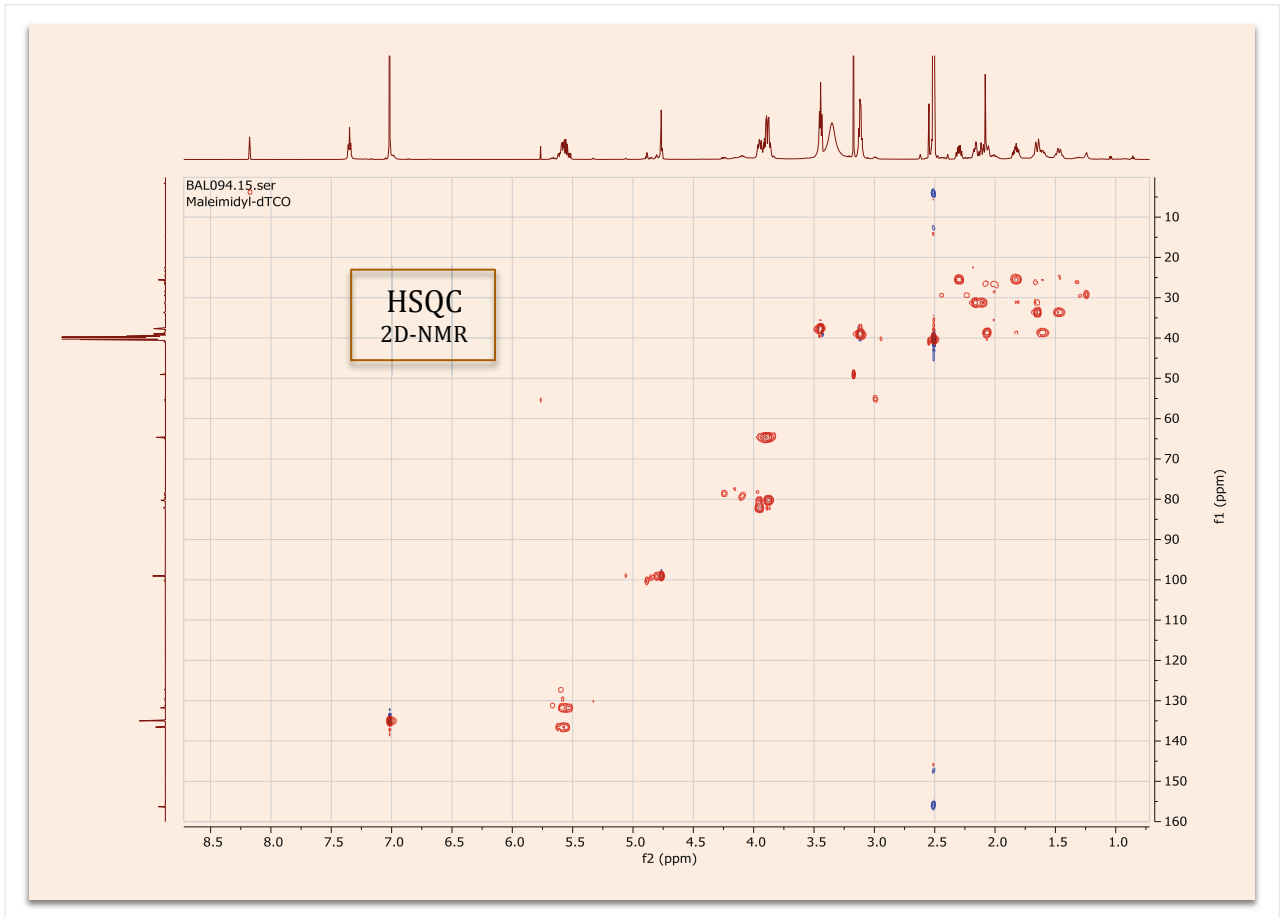
BAL094.10.fid
 Maleimidyl-dTCO

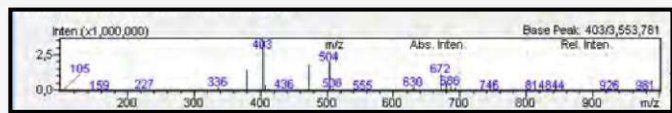
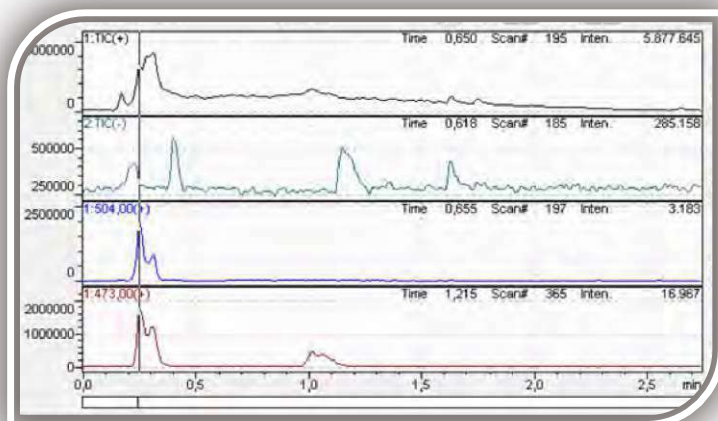


¹H-NMR

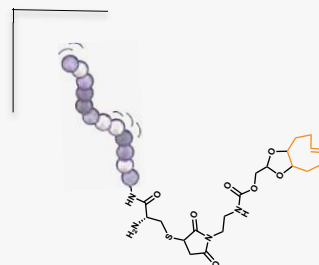








HPLC-MS



ZUM NACHDENKEN

Der Krebs ist nur in Einzelfällen gänzlich zu besiegen, denn er schafft es bedauerlicherweise immer wieder, sich an die bekämpfenden Abwehrmechanismen anzupassen, indem er mutiert. Das Immunsystem nimmt Tumorzellen generell nicht als Fremdkörper wahr und bleibt inaktiv. Zusätzlich gelingt es den Krebswucherungen auf sehr trickreiche Weise, Nährstoffvorräte der gesunden Zellen für sich umzuleiten, er ernährt sich quasi von diesen, die mehr und mehr keine oder kaum Überlebenschance wahrnehmen.

Er saugt sie somit nicht nur aus, sondern wächst unheimlich schnell aufgrund von enzymatischer Fehlsteuerung der Signaltransduktion auf molekularer Ebene! Er breitet sich in alle Richtungen aus und verteilt Tochtermetastasen, alles auf Kosten der "Normalsterblichen". Dem natürlichen Zelltod, einprogrammiert in all unseren gesunden Zellen, entweicht er nämlich gekonnt, als besitze er den Stein der Weisen. Überdies braucht er für eine Vielzahl seiner Stoffwechselfvorgänge im Gegensatz zu intakten, normalen Körperzellen keinen Sauerstoff – der Feind des Menschen lebt hauptsächlich anaerob.

REFLEXION

Elimination of cancer is only feasible in individual cases because it manages repeatedly to adjust to targeting defence mechanisms, by doing mutations. The immune system does not recognize tumor cells as foreign bodies and stays inactive. Additionally, cancerous excrescences are capable of diverting nutrient stores from healthy cells to themselves in a really cunning manner. So they are subsisting on them, which observe more and more no or hardly any chance of survival.

Therefore, cancer is not only sucking healthy cells dry, but is also growing incredibly fast due to enzymatic mismanagement of signal transduction on molecular level! It is spreading in all directions and distributing daughter metastases, at ordinary mortals' cost. Besides, tumor cells are skilfully escaping the natural cell death path, which is hardcoded in all our healthy cells, as if they are occupying the philosophers' stone. Furthermore, cancer does not need any oxygen for lots of metabolic processes, in contrast to intact, normal body cells – the enemy of human kind lives in anaerobic fashion for the most part.

Curriculum vitae



Personal Data

██████████
in Linz,
Austria

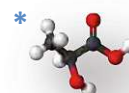
unwed
five siblings

Education

- | | |
|------------------------|---|
| Sept. 2002 – June 2010 | Bundesrealgymnasium Oberschützen Burgenland |
| Oct. 2010 – June 2011 | Community Service at Red Cross +
Paramedic Oberwart |
| Oct. 2011 – Nov. 2016 | TU Vienna Bachelor programme
Technical Chemistry Chemical Technologies and Analytics

Bachelor thesis – „ <i>Untersuchung elektrochemischer Eigenschaften dünner Schichten von Fe-, Al- und Ni-dotiertem Strontiumtitanat</i> “ |
| Nov. 2016 – June 2019 | TU Vienna Master programme
Technical Chemistry Applied Synthetic Chemistry

Diploma thesis – „ <i>Click Chemistry mediated Cell Uptake – towards triggered Auger Therapy</i> “ |



Work experience

* <https://deacademic.com/dic.nsf/dewiki/6112>

- | | |
|-------------------|--|
| September 2011 | Swarco Futurit
Software Controlling LED-display of traffic signs |
| Aug. & Sept. 2013 | Swarco Futurit
Software Controlling LED-display of traffic signs |
| September 2015 | Schaffler & Co
Chemical Laboratory Manufacturing of explosives for electric igniters |
| September 2016 | Schaffler & Co
Chemical Laboratory Manufacturing of explosives for electric igniters |
| Aug. – Sept. 2018 | Boehringer Ingelheim RCV GmbH & Co
Chemical Research Laboratory Synthesis Internship |
| April 2019 – | Boehringer Ingelheim RCV GmbH & Co
Chemical Research Laboratory Synthesis |

■ Additional qualifications

Languages German | mother language
 English | 8 years at school
 Latin | 4 years at school

Reports/certificates

Additional qualifications

Lichtbogenhandschweißen | Schutzgasschweißen | Glasblasenkurs
(plus Fortgeschrittenenkurs) | Sprengkurs

Soft Skills

Kommunikation & Rhetorik | Ökologische und gesellschaftliche
Aspekte in der Chemie | Unternehmensgründung

Free & bounded facultative subjects

Brennstoff- u. Energietechnologie | Luftreinhaltetechnik | Abwasser-
reinigung | Relativitätstheorie | Geologie u. Verkehrswegebau

Leisure activities

Soccer (SC Pinkafeld) | Basketball | Tennis | Hiking

Driving license

B, F

Vienna, 22.04.2019